Efficient Interference Cancellation Techniques for Advanced DS-CDMA Receivers

Neiyer S. Correal

Dissertation submitted to the Faculty of the
Virginia Polytechnic Institute and State University
(Virginia Tech)
in partial fulfillment of the requirements for the degree of

Doctor of Philosophy
in
Electrical Engineering

Dr. Brian D. Woerner, Chair
Dr. Ira Jacobs
Dr. Theodore S. Rappaport
Dr. Jeffrey H. Reed
Dr. Chris Beattie

July 1999
Blacksburg, Virginia

Keywords: Interference Cancellation, Multiuser Detection, CDMA,
Spread Spectrum Communications, Software Radios,
Multiple Access, Digital Radio.

Efficient Interference Cancellation Techniques for Advanced DS-CDMA Receivers

Neiyer S. Correal

(ABSTRACT)

The focus of this dissertation is the study of advanced processing techniques for multiuser interference cancellation in direct sequence code division multiple access communications. Emphasis is placed on the development of efficient techniques that are practical to implement.

The work begins with a study of several sub-optimal multiuser detection techniques under a variety of conditions. Multistage parallel interference cancellation is identified as a practical and robust approach for mitigating multiple access interference. In order to reduce the effect of biased decision statistics inherent to parallel cancellation, a low-complexity modification to parallel interference cancellation that significantly improves performance is derived. Based on this approach, two real-time DSP implementations are devised, one fully coherent and one non-coherent. Multi-symbol differential detection is then explored as an alternative for improving the performance of the non-coherent approach. Additionally, dual-antenna diversity techniques are also investigated as a means for improving performance in multipath environments.

Funded by the Defense Advanced Research Projects Agency (DARPA), the Office of Naval Research (ONR) and the MPRG Affiliates Program.

Acknowledgments

First and foremost, I would like to express thanks to my advisor Dr. Brian D. Woerner for his consistent advice, encouragement and understanding throughout my doctoral studies. Dr. Woerner's insight, kindhearted disposition, everlasting helpfulness and genuine concern for his students made working with him a memorable and pleasurable experience. I would also like to express my gratitude to my committee members for their time and counsel. I am very grateful to the MPRG faculty as well, for their encouragement and tutelage. The MPRG staff also deserves acknowledgment for their invaluable assistance and support.

Credit for this work must, of course, be shared with the people who helped me along the way. Special thanks to R. Michael Buehrer for inviting me to participate in the work that resulted in the comparative results of chapter 3, and for laying the foundations for the development of the DSP parallel interference canceller. I would also like to thank Steve Nicoloso and Francis Dominique for their invaluable input regarding DSP implementation issues. I also learned a great deal from my interactions with many Virginia Tech students, to name a few: Matt Valenti, Alan Alexander, Nitin Mangalvedhe, Paul Petrus, Rich Ertel, Don Breslin, Kai Dietze, Kim Phillips, Steve Swanchara, Tom Biedka, Keith Blankenship, Yufei Wu, Mostofa Howlader, Paolo Cardieri and Max Robert. I am also grateful to all my other friends and colleagues at the MPRG and Virginia Tech. All of you helped to create a wonderful atmosphere that promoted my personal growth.

I am very grateful to my wife Jennifer for all her love, encouragement and understanding. Thanks for always being so thoughtful, and for helping me to keep my life in context. Finally, I would like to thank my parents and my siblings for their love, sacrifice and their encouragement throughout the years. Thanks for showing me that hard work, determination, and love can make dreams come true.

This work was made possible thanks to the support of the Defense Advanced Research Projects Agency (DARPA), the Office of Naval Research (ONR), and the MPRG Industrial Partners program.

Contents

List of Figures

List of Tables

Chapter 1

Introduction

The growing need for increased capacity and improved performance is a motivating factor in the evolution of receiver structures for mobile wireless applications. Because of its favorable properties, Direct Sequence Spread Spectrum (DS-SS), a technology inherently robust to jamming and interference, is experiencing widespread adoption in wireless communications. In Code Division Multiple Access (CDMA) channels, several users attempt to simultaneously communicate a message to a common receiver, with the combined signal from all interferers often modeled as Gaussian noise, especially for large numbers of users.

A fundamental result in communications theory asserts that for communications over an additive white Gaussian noise channel, the optimal receiver corresponds to a matched filter receiver. Therefore, as long as the interference is Gaussian the optimal receiver takes the form of a correlation receiver or a filter matched to the signature sequence of the transmitter. Given the preceding facts, the inference could be drawn that in multiple access channels, a matched filter receiver should yield performance close to optimal and that the limitations observed when using this receiver are inherent to CDMA.

However, Multiple Access Interference (MAI) is not quite Gaussian and the effect of interference on the outputs of the matched filter is not independent of the desired signal. Modifications to account for these characteristics result in some minor performance improvement. A much more significant improvement results from the observation that MAI is not an unknown noise signal but

an estimable signal.

An optimal multiuser receiver for Gaussian channels was derived in [1], significantly outperforming the conventional receiver and solving the near-far problem, in which stronger users have the potential to drown out weaker ones. The computational complexity of this technique drastically limits its potential application. Multiple sub-optimal algorithms aimed at reduced complexity and maintaining good performance have been proposed. Today, implementation of advanced DS-CDMA receivers based on multiuser detection principles is becoming a reality thanks to the combination of an improved understanding of the theoretical basis of multiuser detection and advances in digital, mixed-signal, and RF technologies.

The foremost objective of this work is the development of practical interference cancellation techniques for developing prototypical advanced DS-CDMA receivers that incorporate multiuser detection principles.

The research reported in this document has contributed to several significant developments in the field of multiuser detection. Although many receivers based on joint detection principles have been proposed in digital communications and signal processing literature, cross-comparisons are not direct. In order to properly gauge the individual capabilities of these receivers and to assess their deficiencies it is beneficial to have reliable impartial comparisons of differing multiuser receivers under uniform conditions. A consequential contribution of this study is the comparative analysis of multiple multiuser receiver structures. Each multiuser receiver structure is evaluated for several conditions in multiple situations. Multiuser receiver architectures are compared in terms of performance, complexity and robustness, using identical conditions. This simulation approach provides a reliable basis for comparison. This study was instrumental in identifying parallel interference cancellation as an effective, and robust, technique suitable to practical implementation.

A more thorough analytical examination of parallel interference cancellation brought about additional results, including the derivation of closed form expressions for the decision statistics of the receiver outputs after parallel interference cancellation. This data leads to the recognition that the soft outputs after interference cancellation as biased statistics. Equations are developed that relate the bias to system parameters. It was in this newly gained knowledge that motivated the evolution to a direct modification of parallel interference cancellation that mitigates the effects of

the bias and significantly increases performance. This technique is referred to as "partial parallel interference cancellation".

The paramount contribution of this dissertation is the development of coherent and non-coherent real-time DSP-based prototypes of partial parallel interference cancellation receivers. These prototypes have the distinction of being the first working real-time receivers of their kind, granting new insights for the implementation of practical receivers for the next generation of CDMA systems.

In order to realize the aforementioned prototypes, it was necessary to employ an innovative way to carry out the required processing, reducing the computational complexity of the traditional parallel cancellation algorithm yet yielding the same results. The algorithm utilized reduces computational complexity from quadratic to linear in the number of users, a dramatic reduction in complexity that is crucial for future practical implementation of parallel interference cancellation.

In many cases when reduced complexity receiver structures are desired, non-coherent detection is an attractive alternative. The conventional approach for performing differential detection of DPSK signals concerns correlating the decision made on a particular symbol interval with that of the previous symbol interval, and making a decision based on their phase difference. This was the approach used in the practical implementation of the non-coherent interference cancellation prototype. This document also investigates non-coherent interference cancellation structures that employ increased memory at the detector and perform maximum likelihood sequence detection of the received phases. These receivers show enhanced performance in AWGN channels compared to non-coherent interference cancellation receivers that employ traditional differential detection.

Another contribution of this dissertation is the examination of combined dual antenna diversity, particularly polarization diversity, and multiuser detection for the uplink of DS-CDMA. Results indicate that polarization diversity, an approach somewhat neglected in research circles, can be a viable alternative to spatial diversity. Among the contributions of this dissertation are a simulation based comparison of the performance of various multiuser detectors with polarization diversity, and the analysis of combined polarization diversity and parallel interference cancellation considering diverse non-ideal effects.

1.1 Organization of the Document

The remainder of this dissertation is organized as follows: Chapter 2 considers spread spectrum communications and Code Division Multiple Access (CDMA), examining the operation of conventional CDMA receivers and discussing the potential benefits of advanced receivers based on multiuser detection principles.

Chapter 3 begins with an introduction to multiuser detection followed by a summary of several of the most noted approaches for multiuser detection. Next, the performance of various key multiuser algorithms is examined under a unified testbed to provide a means of comparison. The chapter concludes with a discussion of issues surrounding practical implementation of multiuser detection.

Chapter 4 presents an analysis of parallel interference cancellation, a multiuser detection technique with many desirable features for practical implementation such as low-complexity and good performance. In a parallel interference cancellation receiver, it is useful to employ the soft outputs of a matched filter bank for amplitude estimation. A bias arises in the decision statistics, however, due to imperfect estimation and interference cancellation. In this chapter, the source of the bias is examined. A partial interference cancellation scheme is proposed that mitigates the negative effects of biased estimation and significantly improves system performance.

Chapter 5 describes the real-time coherent, and non-coherent, interference cancellation receivers developed in this effort. The approach for parallel interference cancellation used in the implementation is much less complex yet mathematically equivalent to the direct implementation of the technique. Experimental results presented in this chapter confirm simulation and analytical results showing large performance gains over the conventional matched filter receiver.

Chapter 6 evaluates the performance of differentially coherent parallel interference cancellation and considers the problem of multi-symbol differential detection in multiuser scenarios. Analytical and simulation results are presented characterizing the performance in AWGN channels.

Chapter 7 examines the use of dual antenna elements for improving the performance of multiuser detectors. This chapter focuses, in particular, on combined polarization diversity and parallel interference cancellation. Simulation results indicate that by combining multiuser detection and

dual antenna diversity, the effects of MAI and fading are significantly mitigated.

Chapter 8 concludes this dissertation with a summary of research accomplishments and a discussion of future research opportunities.

Chapter 2

Code Division Multiple Access and Multiuser Detection

2.1 Introduction

Providing communications to anybody, anywhere, anytime is the goal of the next generation wireless systems. One of the challenges in achieving these goals is coping with increasing levels of interference that result from increased number of users. Due to their ability to combat interference, multiuser detection techniques have gained significant recognition in recent years as an advanced enabling technology for the next generation of wireless systems. This chapter explores the application of spread spectrum techniques for wireless communications and lays the foundations for the use of multiuser detection for improved performance.

Because of its attractive properties such as multipath rejection and graceful performance degradation in the presence of multiple access interference, spread spectrum is seeing widespread adoption in wireless communication systems. Code Division Multiple Access (CDMA) uses spread spectrum techniques to achieve efficient multiple access communications. The robustness of spread spectrum signals to interference allows multiple users to operate concurrently in the same radio frequency band. However, the effectiveness of spread spectrum for combating interference is determined by the amount of spreading bandwidth available for transmission.

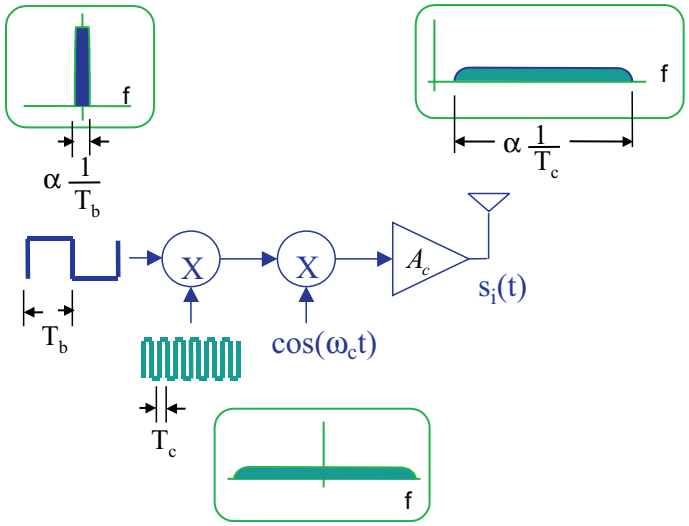

Figure 2.1: Direct sequence spread spectrum transmitter.

In CDMA, individual signature sequences that define CDMA channels are used to generate the information-bearing spread spectrum signal. The resulting signal has wide bandwidth, low power spectral density and noise-like properties [2]. Figure 2.1 shows a block diagram of a typical spread spectrum transmitter. Data is transmitted at a rate $R = 1/T_b$. A pseudo-random sequence modulates the information signal to generate the transmitted signal. The pseudo-random sequence is composed of elementary pulses of period T_c, commonly referred as chips. The bandwidth expansion ratio T_b/T_c is called the spreading gain.

Due to their random-like nature, spread spectrum signals behave as wideband noise of low power spectral density. CDMA receivers employ the signature sequence of the desired user as the key to recover the transmitted information. A block diagram of the conventional CDMA receiver is shown in Figure 2.2. Detection of the transmitted data is accomplished with a correlation demodulator driven by a synchronized replica of the signature sequence. The ability of CDMA to support multiple access operation stems from the low correlation between the signature sequences of the users.

CDMA systems have a soft capacity limit. As the number of users sharing the channel grows, the amount of interference experienced at the receiver increases, eventually degrading the received signal's quality to unacceptable levels. Figure 2.3 depicts the situation at the receiver. A plot of

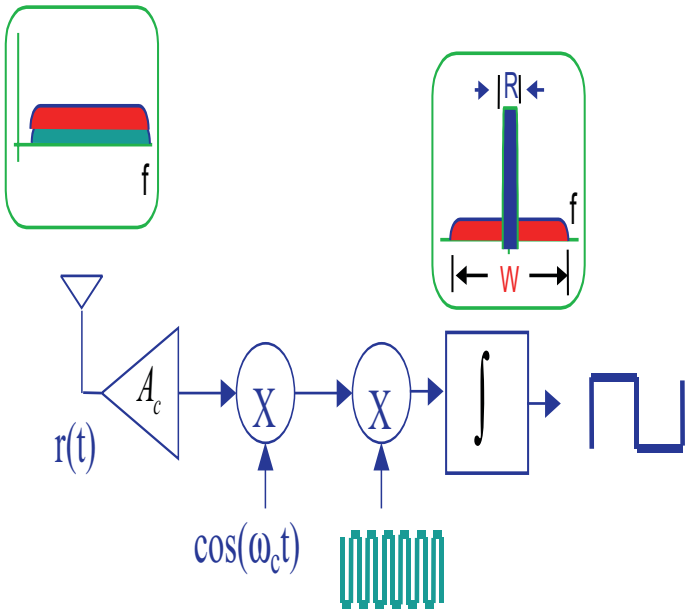

Figure 2.2: Conventional CDMA receiver.

probability of error as a function of the number of users is displayed in Figure 2.4. The number of users that can be supported depends on the amount of interference considered acceptable for a desired Quality of Service (QoS). The QoS is based on E_b/I_o where E_b is the bit energy and I_o is the interference power spectral density measured in $Watts/Hz$.

Given a required E_b/I_o, an approximate estimate of the number of users that can be supported by a conventional CDMA system can be derived as follows [2, 3]: The signal to interference ratio at which individual signals are received is given by:

$$\frac{S}{I} = \frac{S}{I_{ic} + I_{oc}}, \tag{2.1}$$

where I_{ic} accounts for the interference within the cell, and I_{oc} represents the contribution of the out-of-cell interference. Assuming operation in the presence of $K-1$ equal-power interferers, the signal to interference ratio at the receiver is expressed as:

$$\frac{S}{I} = \frac{S}{S(K-1) + I_{oc}}. \tag{2.2}$$

Assuming that interference may be modeled as approximately Gaussian [2], the number of users

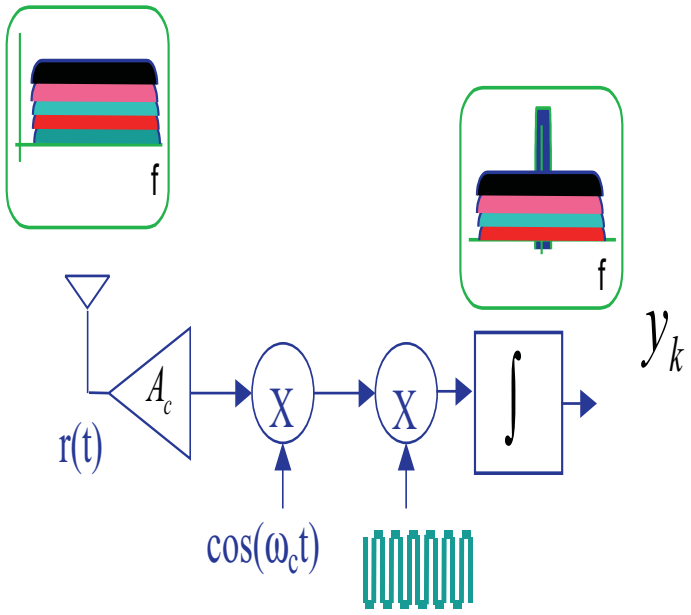

Figure 2.3: Multiple access interference at the receiver.

supported in a CDMA system is computed from the previous equation to be:

$$K = \frac{I - I_{oc}}{S} + 1. \tag{2.3}$$

Expressing the signal to interference ratio as:

$$\frac{S}{I} = \frac{E_b/T}{I_o/T_c}. \tag{2.4}$$

where T is the symbol period, and T_c is the chip period permits solving for S:

$$S = \frac{E_b I/T}{I_o/T_c}. \tag{2.5}$$

Substituting the previous expression for S into Equation (2.3) yields:

$$K = \frac{1 - \frac{I_{oc}}{I}}{\frac{E_b}{I_o} \times \frac{T_c}{T}} + 1. \tag{2.6}$$

The ratio $N = \frac{T_c}{T}$ corresponds to the spreading gain of the system. The number of users that can be supported by the system is therefore:

$$\begin{aligned} K &= \frac{N}{\frac{E_b}{I_o}(1 + \frac{I_{ic}}{I_{oc}})} + 1 \\ &= \frac{N}{\frac{E_b}{I_o}(1 + \eta)} + 1. \end{aligned} \tag{2.7}$$

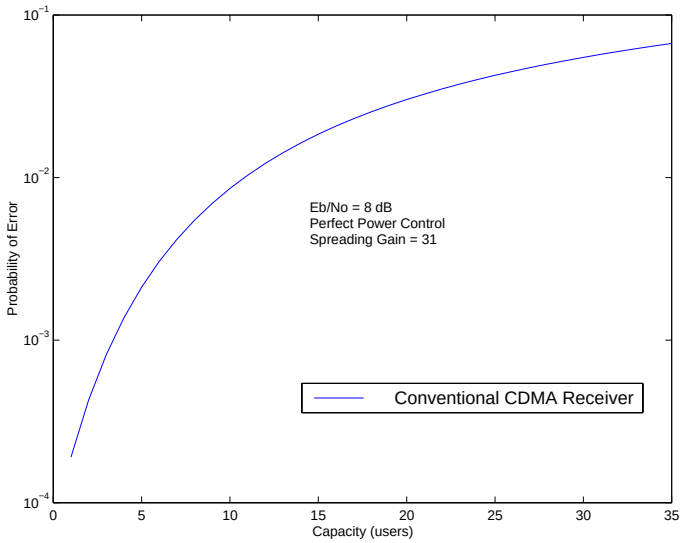

Figure 2.4: Probability of bit error vs. E_b/N_o for the conventional receiver.

where $\eta \simeq 0.6$ is typically used to characterize the ratio of intra-cell to out-of-cell interference.

Other techniques such as sectorized antennas and voice monitoring may be applied to improve the capacity of CDMA systems. Taking into account some of the current interference mitigation tactics, the average number of conversations per base station supportable by a CDMA system are condensed in the following more general formula [4]:

$$C = \left(\frac{W/R}{E_b/N_o}\right)\left(\frac{F_{sectors}F_{speech}}{F_{power}F_{outage}F_{cells}}\right), \tag{2.8}$$

where W is the chip rate, R is the source rate, $F_{sectors}(\sim 2.4)$ reflects the interference reduction achieved in a cell with three sectors [2], $F_{speech}(\sim 2)$ accounts for decreased interference with voice inactivity, $F_{power}(\sim 1.2)$, $F_{outage}(\sim 1.1)$, and $F_{cells} = 1 + \frac{I_{ic}}{I_{oc}} \sim (\ 1.6)$ typifies the effect of out-of-cell interference.

In addition to the performance degradation experienced when numerous users share the channel, CDMA receivers suffer from what is commonly termed the near-far problem. If interfering signals are received with a much larger power than the one desired, they have the potential of overwhelming the desired user with non-Gaussian interference. This undesired behavior is illustrated in Figure 2.5, which shows the probability of error as a function of the difference in signal to noise ratios of the desired user and an interferer. Current CDMA systems circumvent this problem through the

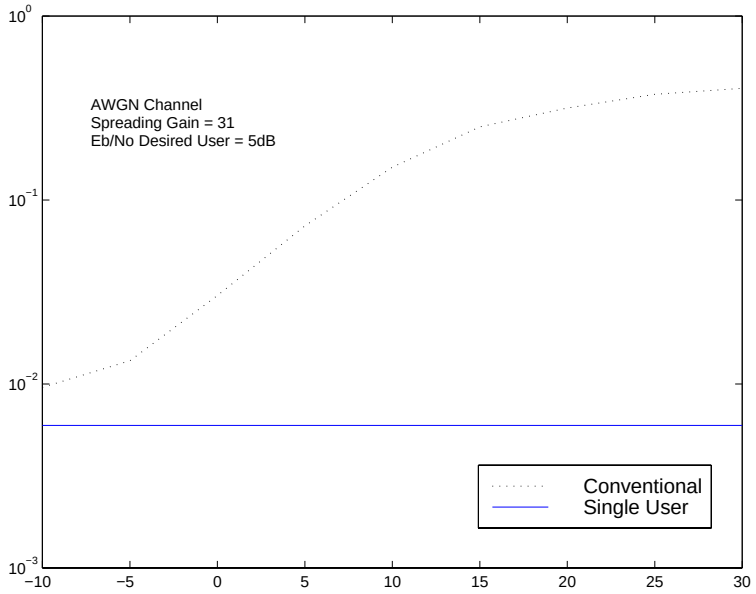

Figure 2.5: Probability of error vs. difference in SNR between the desired user and an interferer.

use of tight power control loops, the goal being equal received powers for all users.

As demonstrated, the overall capacity of CDMA systems is limited by interference. In a multiple access channel, a larger capacity region can be achieved by using a decoder that jointly processes the information received from all the transmitters [5]. Multiuser detectors reduce the multiple access interference experienced at the receiver. Therefore, they have the potential to increase the capacity of CDMA systems. The capacity improvements are dictated by the degree of interference suppression achieved by the multiuser detector.

In single-cell cases, ideal multiuser detection creates an equivalent of a single-user channel, removing all interference other than background noise. In the multi-cell case, one possible scenario is that the multiuser detector focuses only on interference from users in the same cell while neglecting the out-of-cell interferers. An upper limit to the capacity improvements achievable with multiuser detection is computed assuming the multiuser detector's ability to cancel all the interference within the cell. In this case, the amount of effective interference reduces from $I_{ic} + I_{oc}$ to I_{oc}, which results in a capacity increase of $(1 + \eta)/\eta$. Applying the popularly accepted value of $\eta = 0.6$ results in an improvement on the order of 2.7 times over conventional CDMA systems. Figure 2.6 illustrates the

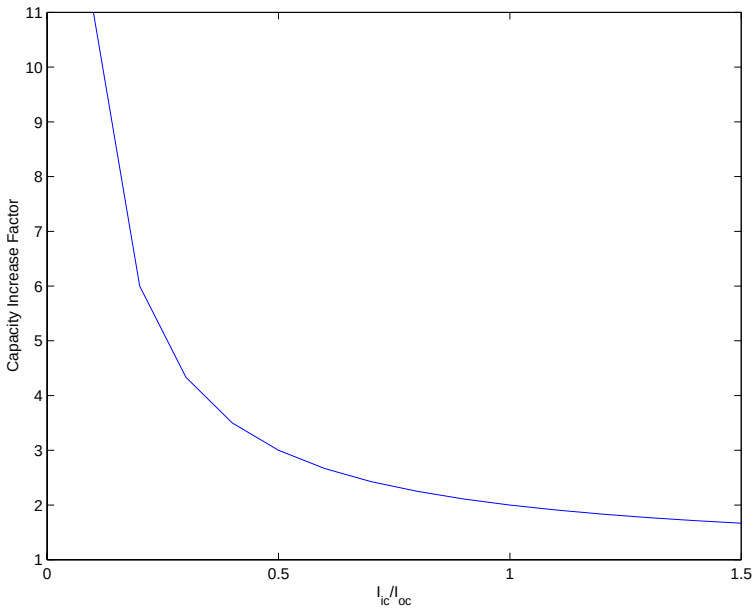

Figure 2.6: Capacity improvement limits for multiuser detection.

factor of improvement achievable with multiuser detection in a multi-cell scenario as a function of the ratio of in-cell to out-of-cell interference η.

A more favorable scenario would occur if multiuser detection is not restricted to interferers within the cell. In this case, significant advantages are obtained by also taking into account the strongest out-of-cell interferers. In [6] analytical and simulation results estimate that selective interference cancellation of strong out-of-cell interferers can potentially result in a capacity increase of 20 to 40%.

A socio-economic law, known as Metcalfe's law, states that the value of a communications network grows as the square of the number of users of the network [7]. Figure 2.7 illustrates the relative increase in value of a communications network with ideal multiuser detection with respect to the conventional receiver, as a function of η. For $\eta = 0.6$, Metcalfe's law conjectures a seven-fold increase in value. It is important to keep in mind, however, that in practical scenarios, the performance of multiuser receivers can be potentially constrained by several factors such as parameter estimation errors, uncancelled interference, the amount of energy not captured by the rake receiver's fingers, and computational complexity.

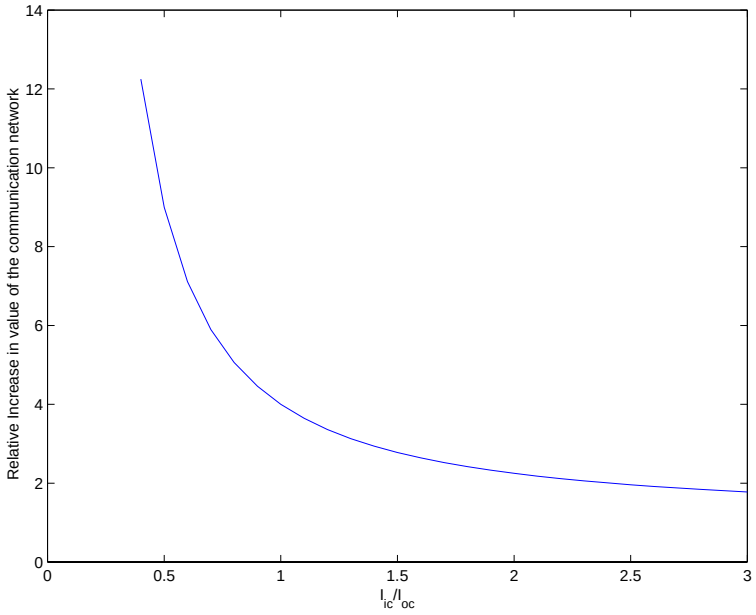

Figure 2.7: Increase in value of a CDMA system with multiuser detection according to Metcalfe's law.

In this chapter, the basic principles associated with CDMA have been described. For a more detailed treatment, the reader is referred to [2, 8]. The purpose of this chapter is to highlight the potential benefits of using multiuser detection for a cellular CDMA system. In the next section, multiuser detection is investigated in greater depth.

Chapter 3

Multiuser Detection - Comparison of Multiuser Techniques

3.1 Introduction

Multiuser detection deals with the development and application of joint demodulation and interference cancellation techniques for improved detection of a desired set of digital signals in the presence of multiple access interference, intersymbol interference and noise.

The conventional approach for demodulating DS-CDMA signals is to employ a correlation demodulator matched to the signature sequence of the desired user. This approach is optimal for the case of single-user transmissions in AWGN channels and orthogonal synchronous multiuser communications. In a multiple access channel, network information theory indicates that a larger capacity region can be achieved by using a decoder that jointly processes the information received from all the transmitters [5]. Thus, improved performance can be obtained (sacrificing low complexity) by exploiting, rather than neglecting, the inherent structure of the multiple access interference.

Multiuser detection for DS-CDMA has been an area of considerable interest in the research community due to the significant performance gains that may be potentially obtained through the use of sophisticated receivers that exploit the intrinsic structure of the Multiple Access Interference

(MAI). Multiuser receivers address the problem of demodulating digital signals confronted with MAI in a multiuser environment.

This chapter focuses on implementation issues for advanced DS-CDMA structures based on multiuser detection principles. Section 3.2 presents a general system model for DS-CDMA communications, followed by a summary of various approaches for multiuser detection in section 3.3. Section 3.4 presents practical considerations for the implementation of multiuser receivers.

3.2 Multiple Access Model

We use a system model similar to the one used in [9], where the received baseband signal from user k is defined as a binary phase modulated waveform:

$$s_k(t) = \sqrt{P_k} a_k(t) b_k(t) e^{j\theta_k} \tag{3.1}$$

where P_k is the k^{th} user's received signal power, $a_k(t)$ and $b_k(t)$ are the spreading and data waveforms respectively, and θ_k is the received phase of the k^{th} user relative to some reference phase. Due to the asynchronous nature of the system uplink, the received signal is

$$r(t) = \sum_k s_k(t - \tau_k) + n(t) \tag{3.2}$$

where τ_k is the time delay parameter that accounts for the time of arrival of the k^{th} user's signal, and n(t) represents the additive white Gaussian noise experienced at receiver.

The set of sufficient statistics can be shown to be the full set of matched filter outputs $\mathbf{y}$ where the filters are matched to each user's spreading code. In terms of the complex envelope, the vector of decision metrics is

$$\mathbf{z} = e^{-j(\mathbf{\Theta})}\mathbf{y} \tag{3.3}$$

where the i^{th} matched filter output of the k^{th} user is the $((i-1)K+k)^{\text{th}}$ element of the vector $\mathbf{y}$, $\mathbf{\Theta}$ is a $KN_b \times KN_b$ diagonal matrix where the diagonal elements $\theta_{j,j}$ are the phases of the i^{th} bit of the k^{th} user and $j = (i-1)K + k$, K is the number of users in the system, $e^{-j(\mathbf{\Theta})}$ is a diagonal matrix, N_b is the number of bits in the sequence under consideration and the elements of the vector

$\mathbf{y}$ are defined as:

$$y_{(i-1)K+k} = \int_{(i-1)T+\tau_k}^{iT+\tau_k} r(t)a_k(t-\tau_k)dt \tag{3.4}$$

where τ_k is the time delay parameter that accounts for the time of arrival of the k^{th} user's signal.

In matrix form we represent the set of matched filter outputs as

$$\mathbf{y} = \mathbf{RW}e^{j\mathbf{\Theta}}\mathbf{b} + \mathbf{n} \tag{3.5}$$

where $\mathbf{R}$ is a $KN_b \times KN_b$ matrix

$$\mathbf{R} = \begin{pmatrix} \mathbf{H(0)} & \mathbf{H(-1)} & 0 & \cdots & 0 \\ \mathbf{H(1)} & \mathbf{H(0)} & \mathbf{H(-1)} & & \vdots \\ 0 & \mathbf{H(1)} & \mathbf{H(0)} & \ddots & 0 \\ \vdots & & \ddots & \ddots & \mathbf{H(-1)} \\ 0 & \cdots & 0 & \mathbf{H(1)} & \mathbf{H(0)} \end{pmatrix} \tag{3.6}$$

and the $(k,l)^{\text{th}}$ element of the $K \times K$ matrix $\mathbf{H}$(i) is defined by

$$h_{k,l}(i) = \int_{-\infty}^{-\infty} a_k(t-\tau_k)a_l(t+iT-\tau_l)dt, \tag{3.7}$$

$\mathbf{W}$ is a $KN_b \times KN_b$ diagonal matrix of the square root of the received user energies, defined similar to $\mathbf{\Theta}$, $\mathbf{b}$ is a KN_b length vector with the $j = ((i-1)K+k)^{\text{th}}$ element equal to the i^{th} data symbol of the k^{th} user, and $\mathbf{n}$ is a complex vector of colored noise samples at the matched filter outputs. If the users are numbered such that $\tau_1 < \tau_2 < ... < \tau_K$, then $\mathbf{H(1)}$ will be an upper triangular matrix with zeros along the diagonal, $\mathbf{H}(-1) = \mathbf{H}^T(1)$ and $\mathbf{H}(i) = 0 \ \forall |i| > 1$.

3.3 Multiuser Detection Architectures

There has been extensive theoretical research in the area of multiuser detection in the past decade. Today the fundamental principles of operation of these structures are well understood. This section summarizes several of the most noted multiuser structures for DS-CDMA and describes their operation.

3.3.1 Early Multiuser Detectors

The desire to overcome the limitations due to interchannel and intersymbol interference in high speed digital transmissions over multi-wire cables played a key role in the development of early receiver structures that simultaneously compensated for these disturbances. One of the earliest receiver structures to evidence multiuser detection principles was derived in [10]. This zero-forcing structure, consisting of multiple arrays of matched filters, tapped delay lines and summing circuits, was successfully used for the multidimensional equalization of binary signals transmitted over a four wire cable at a rate of 5 Mbps.

Generalization of maximum likelihood sequence estimation to digital signals experiencing interchannel interference and intersymbol interference in Gaussian noise via vector versions of the Viterbi algorithm [11], or alternatively the Ungerboek algorithm [12], was presented in [13]. Here it was also shown that the outputs of arrays of filters matched to the impulse responses at each output to each possible input of the system were sufficient statistics for estimating the received sequence.

The optimal receiver for asynchronous DS-CDMA channels in Additive White Gaussian Noise is a maximum-likelihood sequence estimator. One of the earliest papers that explored a solution to the problem of optimum multiuser detection in asynchronous DS-CDMA channels and noted the similarity between multiuser interference and a shift register process that can be optimally decoded using the Viterbi algorithm is [14].

3.3.2 Conventional Receiver

The conventional receiver corresponds to a bank of matched filters, where each filter is matched to the signature sequence of the desired user. Figure 3.1 presents a block diagram of the conventional DS-CDMA receiver. For proper operation the conventional receiver requires knowledge of the desired user's signature sequence and accurate synchronization with the arriving signal.

For the sake of simplicity, let us consider a two user synchronous system, in matrix notation the outputs of the matched filters are:

$$\begin{bmatrix} y_1 \\ y_2 \end{bmatrix} = \begin{bmatrix} 1 & R_{1,2} \\ R_{1,2} & 1 \end{bmatrix} \begin{bmatrix} \sqrt[2]{P_1} & 0 \\ 0 & \sqrt[2]{P_2} \end{bmatrix} \begin{bmatrix} b_1 \\ b_2 \end{bmatrix} + \begin{bmatrix} z_1 \\ z_2 \end{bmatrix}, \tag{3.8}$$

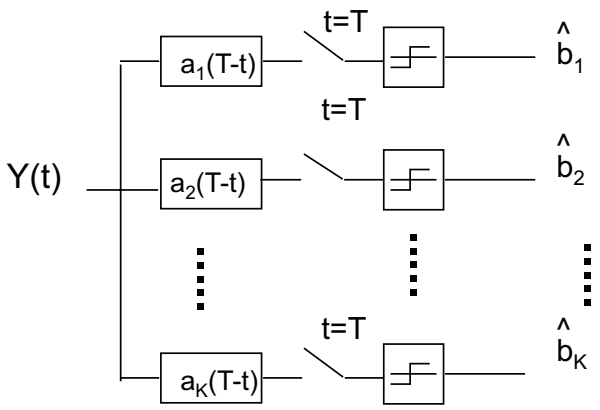

Figure 3.1: Block diagram of the conventional receiver.

where $\mathbf{z}$ is a colored Gaussian noise vector with covariance matrix $N_o/2\mathbf{R}$. The previous matrix equation can be written as:

$$\begin{aligned} y_1 &= \sqrt[2]{P_1}b_1 + R_{1,2}\sqrt[2]{P_2}b_2 + z_1 \\ y_2 &= \sqrt[2]{P_2}b_2 + R_{1,2}\sqrt[2]{P_1}b_1 + z_2 \end{aligned} \tag{3.9}$$

If the multiple access interference terms did not exist, either because $\sqrt[2]{P_k} = 0$ $(k = 1, 2)$ (single user case) or because $R_{1,2} = 0$ (orthogonal signature sequences), then performance would be optimal since the matched filter maximizes the signal to noise ratio at the output of the receiver.

MAI can significantly degrade performance of the conventional receiver, as can be inferred from Equations 3.9 by considering the effect of the cross-term $R_{k,j}\sqrt[2]{P_k}b_k$. If one user is much stronger than the other, it can potentially drown out the weaker user and corrupt its estimated data. In current CDMA systems this undesirable behavior is minimized via tight power control loops and the use of spreading sequences with good crosscorrelation properties.

In the more general case, the decision statistics at the output of the matched filter for the i^{th} bit of user k correspond to:

$$Z_{k,i} = \int_{(i-1)T+\tau_k}^{iT+\tau_k} r(t)a_k(t-\tau_k)cos(w_c t + \phi_k(t))dt, \tag{3.10}$$

where $\phi_k(t)$ and τ_k are the phase and the time delay of the k^{th} user respectively.

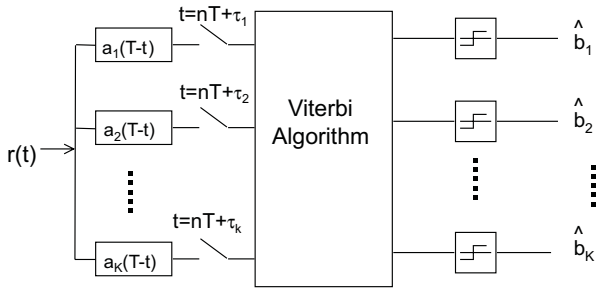

Figure 3.2: Block diagram of the jointly optimal receiver.

3.3.3 Optimal Receiver

The optimal receiver for asynchronous CDMA channels in AWGN corresponds to a maximum-likelihood sequence detector. This detector requires knowledge of the spreading codes, the timing of the users, and the received amplitudes of the users.

For the synchronous case, finding the most likely sequence corresponds to a basic combinatorial issue that could in principle be tackled by an exhaustive search type of solution. However, a dynamic programming solution is more efficient and refined.

The optimum asynchronous multiuser receiver for Gaussian channels was formally derived in [1]. It consists of a bank of matched filters that produce the decision statistics of equation (3.5), followed by a dynamic programming algorithm of the Viterbi type that computes the most likely path in a trellis diagram with 2^{K-1} states per layer, and time varying state transitions. Figure 3.2 shows a block diagram of the jointly optimal receiver. Despite its enormous complexity, this receiver is valuable not only as a theoretical feat but also as a point of reference for comparing the performance of suboptimal detectors.

The problem of maximum likelihood sequence detection can be casted in the following form: Given the received amplitudes from all possible received signals,

$$\hat{S}(t) = s(t, \mathbf{b}) \tag{3.11}$$

find the hypothesis that minimizes:

$$\int (r(t) - s(t, \mathbf{b}))^2 dt \tag{3.12}$$

i.e. find the sequence that minimizes the energy of the residual signal.

This is equivalent to finding the sequence that maximizes:

$$L[\mathbf{B},\mathbf{t}] \quad = \quad 2\int r(t)s(t,\mathbf{b})dt - \int s(t,\mathbf{b})^2 dt \tag{3.13}$$

A straightforward approach based on combinatorial optimization would have a recklessly large computational complexity. Instead, computation can be performed in terms of a path metric λ that is computed based on the bits in the current and the previous interval. The effect of the bits in the subsequent interval is accounted for by the path metric computed at the next signaling interval.

$$2\int r(t)s(t,\mathbf{b})dt - \int s(t,\mathbf{b})^2 dt = \sum \lambda_k(y_k, \hat{b}_k, \hat{b}_{k-1}) \tag{3.14}$$

The form of Equation (3.14) indicates that this process can be modeled as a finite length shift-register process whose most likely state sequence can be efficiently computed with the Viterbi algorithm.

In the interest of simplicity, this discussion will focus on a two user system. For this system let us define an input bit vector $\mathbf{b}$ as:

$$\mathbf{b} \quad = \quad \begin{pmatrix} \hat{b}_1 \\ \hat{b}_2 \\ \vdots \\ \vdots \\ \hat{b}_{2N_b-1} \\ \hat{b}_{2N_b} \end{pmatrix} = \begin{pmatrix} \hat{b}_0^1 \\ \hat{b}_0^2 \\ \vdots \\ \vdots \\ \hat{b}_{N_b}^1 \\ \hat{b}_{N_b}^2 \end{pmatrix} \tag{3.15}$$

and a matched filter output vector $\mathbf{y}$ as:

$$\mathbf{y} \quad = \quad \begin{pmatrix} y_1 \\ y_2 \\ \vdots \\ \vdots \\ y_{2N_b-1} \\ y_{2N_b} \end{pmatrix} = \begin{pmatrix} y_0^1 \\ y_0^2 \\ \vdots \\ \vdots \\ y_{N_b}^1 \\ y_{N_b}^2 \end{pmatrix} \tag{3.16}$$

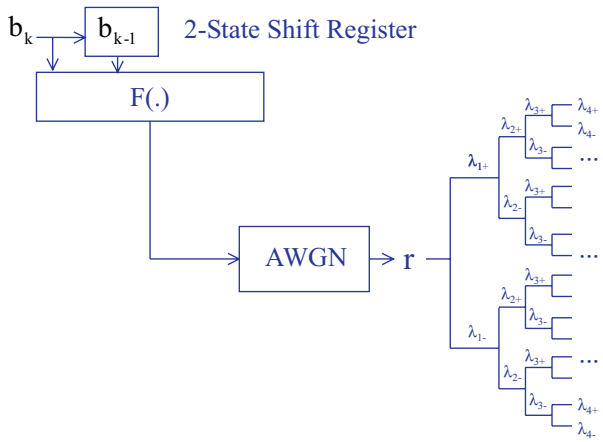

Figure 3.3: Shift register process model of asynchronous multiple access.

With these definitions, the multiple access communication system can then be accurately modeled as a 2-state shift register process with inputs from **b** as depicted in Figure 3.3.

Computation of the metrics of Equation (3.14) is readily accomplished, since:

$$\begin{aligned} \lambda_k(y_k, \hat{b}_k, \hat{b}_{k-1}) &= P_k y_k \hat{b}_k - \sqrt[2]{P_k P_{k-1}} b_k \hat{R}_{2,1} b_{k-1}, \text{ k odd} \\ &= P_k y_k \hat{b}_k - \sqrt[2]{P_k P_{k-1}} b_k R_{2,1} b_{k-1}, \text{ k even}, \end{aligned} \tag{3.17}$$

where $R_{2,1} = \int_0^\tau a_2(t-\tau)a_1(t)dt$ and $\hat{R}_{2,1} = \int_\tau^T a_2(t-\tau)a_1(t)dt$ for $0 \leq \tau \leq T$ and τ is the delay between the two users.

Calculation of the total metric is performed by adding the local metrics as each bits arrives. This procedure is shown in Figure 3.4 for the case of unit power received signals.

In the K-user case, the multiple access system can be characterized as a shift register process with $2^{(K-1)}$ storage elements. Determination of the most likely sequence of data is performed, as with the two user case, by determining the path which maximizes the decision metric in the trellis. The performance of the jointly optimal multiuser detector is very similar to that of the single user case for high enough signal to noise ratios.

A minimum bit-error-rate multiuser detector can be implemented using a framework similar to that

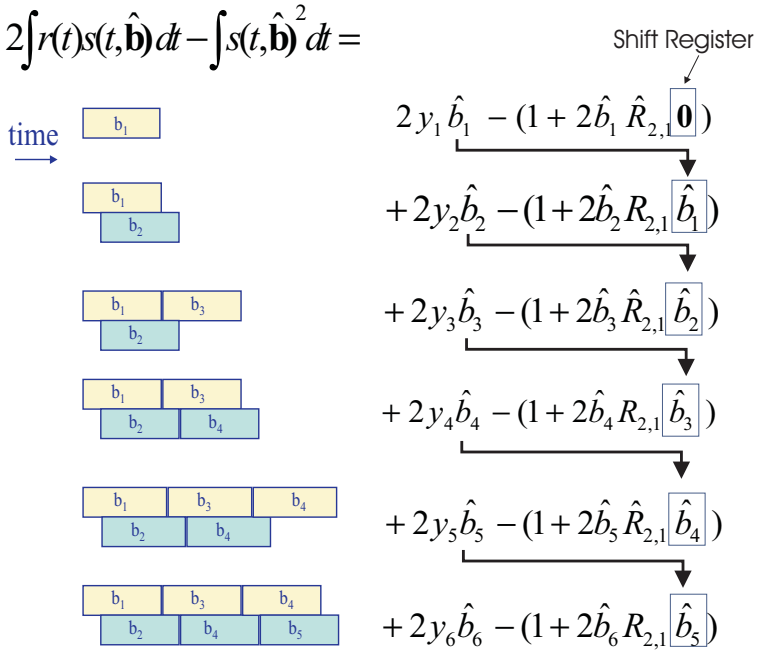

Figure 3.4: Efficient computation of the metrics for maximum likelihood sequence estimation.

used for the jointly optimum detector. In this case the solution is based on a forward-backward dynamic programming algorithm [15]. The reason why the individulally optimal and the jointly optimal approaches are not identical is the fact that the user bits are not independent of each other when conditioned on the observed waveform. The computational complexity of this approach is significantly higher than that of the jointly optimum receiver. For reasonably high signal to noise ratios the performance of the jointly optimal receiver and the minimum bit-error rate detector are likely to converge [15].

3.3.4 Decorrelator

This approach, also proposed in [14] and analyzed in [16], operates to eliminate the MAI in a manner analogous to the way a zero forcing equalizer eliminates Inter Symbol Interference (ISI). A linear transformation $\mathbf{R}^{-1}$ that corresponds to the inverse of the channel matrix is applied to the matched filter bank outputs $\mathbf{y}$ in an attempt to cancel the interference resulting from cross-correlations among the signature sequences. For the case of phase aligned users, bit decisions are

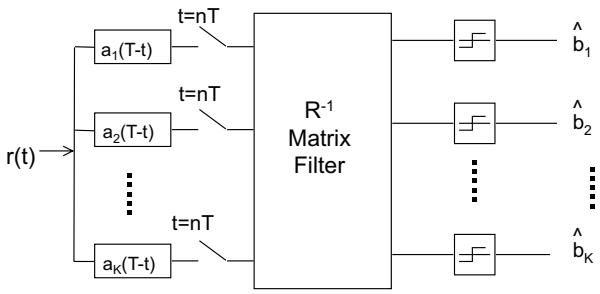

Figure 3.5: Block diagram of the decorrelator.

computed as:

$$\hat{\mathbf{b}} \quad = \quad sgn[\hat{\mathbf{y}}], \tag{3.18}$$

where

$$\hat{\mathbf{y}} \quad = \quad \mathbf{Wb} + \mathbf{R^{-1}z} \tag{3.19}$$

From these equations we can see that the noise terms are no longer independent. Figure 3.5 show a block diagram of the decorrelator.

For clarity, let us consider a two user synchronous system. Equation 3.19 can be written as:

$$\begin{bmatrix} \hat{y}_1 \\ \hat{y}_2 \end{bmatrix} \quad = \quad \begin{bmatrix} \sqrt[2]{P_1} & 0 \\ 0 & \sqrt[2]{P_2} \end{bmatrix} \begin{bmatrix} b_1 \\ b_2 \end{bmatrix} + \begin{bmatrix} \frac{1}{1-R_{1,2}^2} & \frac{-R_{1,2}}{1-R_{1,2}^2} \\ \frac{-R_{1,2}}{1-R_{1,2}^2} & \frac{1}{1-R_{1,2}^2} \end{bmatrix} \begin{bmatrix} z_1 \\ z_2 \end{bmatrix}. \tag{3.20}$$

In an ideal noiseless situation, the solution is directly obtained when the channel is inverted via $\mathbf{R^{-1}}$. Furthermore, in the presence of noise this approach is still effective. However, the correlation between noise samples creates a noise enhancement effect that can degrade performance, particularly at low SNR. In this particular example, since $|R_{1,2}| < 1$, one can directly see that the power of the noise increased from $N_0/2$ to $N_o/\left(2(1-R_{1,2}^2)\right)$.

With a discrete time model, the discrete time transfer function of a decorrelating detector can be obtained by inverting the discrete-time channel function [15]:

$$\mathbf{S}^{-1}(z) = [\mathbf{R^T}[1]z + \mathbf{R}[0] + \mathbf{R}[1]z^{-1}]^{-1} \tag{3.21}$$

Although noncausal, this alternate representation provides a representation of the receiver as a digital filter which can be approximated using a tapped delay line.

An interesting property of the decorrelator is that it is the solution to the problem of maximum likelihood sequence detection for unknown received amplitudes.

From all the possible data sequences and received amplitudes

$$\hat{S}(t) = s(t, \hat{\mathbf{b}}, \hat{\mathbf{A}}) \tag{3.22}$$

choose the hypothesis that minimizes:

$$\int (r(t) - s(t, \hat{\mathbf{b}}, \hat{\mathbf{A}}))^2 dt. \tag{3.23}$$

The maximum likelihood amplitude estimate is given by:

$$\hat{\mathbf{W}} = |\mathbf{R}^{-1}\mathbf{Y}|. \tag{3.24}$$

The decorrelator has a very desirable feature in that it does not require knowledge of the users' received energies. Another important characteristic of the decorrelator is that it can be decentralized. Demodulation of each user can be performed independently and thus can be viewed as matched filter detection with a modified filter bank [15].

3.3.5 Linear Minimum Mean-Square Error Receiver

This receiver, initially proposed in [17], corresponds to the linear transformation of the matched filter outputs $\mathbf{My} = \hat{\mathbf{y}}$ that minimizes the mean-square error between the ideal noiseless multiuser waveform and the one reconstructed via the linear transformation $E\{\|\mathbf{Wb} - \hat{\mathbf{y}}\|^{\mathbf{2}}\}$. The solution to this minimization problem is given by $\mathbf{M} = (\mathbf{R} + (\mathbf{N_o}/\mathbf{2})\mathbf{W}^{-\mathbf{2}})^{-\mathbf{1}}$ [15]. The MMSE receiver exploits a-priori knowledge of the received energies using $\mathbf{M}$ as a decorrelating transformation. The operation of the MMSE detector can be viewed as offering a balance between interference cancellation and noise enhancement. An advantage of the MMSE receiver is that the linear transformation $\mathbf{M}$ always exists even when $\mathbf{R}^{-\mathbf{1}}$ is singular. Figure 3.6 illustrates a block diagram of the MMSE detector.

For the synchronous two user case MMSE detection corresponds to:

$$\begin{bmatrix} \hat{y}_1 \\ \hat{y}_2 \end{bmatrix} = (\frac{2\sqrt[2]{P_2} + N_o}{N_o}\frac{2\sqrt[2]{P_1} + N_o}{N_o} - R_{1,2}^2)^{-1} \begin{bmatrix} \frac{2\sqrt[2]{P_2}+N_o}{N_o} & -R_{1,2} \\ -R_{1,2} & \frac{2\sqrt[2]{P_1}+N_o}{N_o} \end{bmatrix} \begin{bmatrix} y_1 \\ y_2 \end{bmatrix}, \tag{3.25}$$

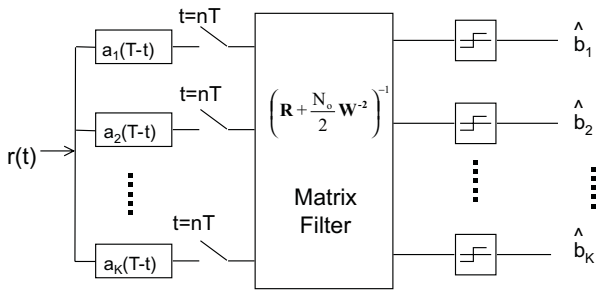

Figure 3.6: Block diagram of the MMSE detector.

where $\mathbf{y} = \mathbf{RWb} + \mathbf{z}$.

In the asynchronous case, the MMSE has a discrete time transfer function given by [15]:

$$[\mathbf{R}^T[1]z + \mathbf{R}[0]\frac{No}{2}\mathbf{W}^{-2} + \mathbf{R}[1]z^{-1}]^{-1}. \tag{3.26}$$

This transfer function is non-causal and has an infinite length response. It can , however, be realized by truncating the observation window to a length that causes minimum degradation.

The MMSE receiver lends itself to adaptive implementation. One would expect that an adaptive implementation would require knowledge not only of the signature sequence of the users of interest but also off all users in the system. Adaptive approaches based on stochastic gradient techniques, using fractionally spaced structures, have been used in the implementation of MMSE [18]. When the LMS is used for adaptation, convergence speed depends on the eigenvalue spread. Convergence speed thus suffers degradation in near-far situations.

Blind demodulation is possible using principles similar to those used in linearly constrained minimum variance filtering [19]. In [20], a canonical representation of linear multiuser detectors consisting of a sum of two orthogonal components, one of them chosen as the signature sequence of the desired user, is used to demonstrate that MMSE demodulation is equivalent to minimum output variance detection. Since minimization of the variance at the output of the receiver does not require knowledge of the transmitted data, anchored blind adaptation becomes possible.

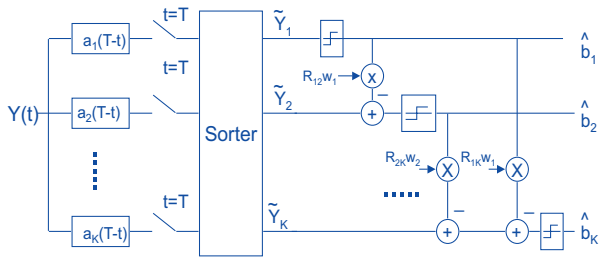

Figure 3.7: Block diagram of the successive interference cancellation receiver.

3.3.6 Successive Interference Cancellation

In this technique [21, 22], estimation and interference cancellation is performed one user at a time in order of decreasing received energies. Interference cancellation is achieved by subtracting from the received signal an estimate of the multiple access interference generated by users with higher received energies than that of user k, the user currently being demodulated. A block diagram of the successive interference cancellation receiver is presented in Figure 3.7.

The input to the matched filter for user k is computed according to:

$$\hat{r}_k(t) = r(t) - \sum_{j=1}^{k-1} \hat{s}(t), \tag{3.27}$$

improved estimates for the kth user's data bit are obtained by using the enhanced signal $\hat{r}_k(t)$ instead of $r(t)$:

$$Z_{k,i} = \int_{(i-1)T+\tau_k}^{iT+\tau_k} \hat{r}_k(t) a_k(t-\tau_k) cos(w_c t + \phi_k(t)) dt, \tag{3.28}$$

where $\phi_k(t)$ is the phase of the k^{th} user.

Let's consider a two user synchronous system. After sorting, the strongest user is demodulated first. Its thresholded decision statistic corresponds to:

$$\hat{b}_1 \quad = \quad \text{sgn}(\sqrt[2]{P_1} b_1 + \sqrt[2]{P_2} R_{1,2} b_2 + z_1), \tag{3.29}$$

this bit decision is then used in an attempt to cancel the MAI from the second user:

$$\hat{b}_2 \quad = \quad \text{sgn}\{\sqrt[2]{P_2} b_2 + \sqrt[2]{P_1} R_{1,2} (b_1 - \hat{b}_1) + z_2\}, \tag{3.30}$$

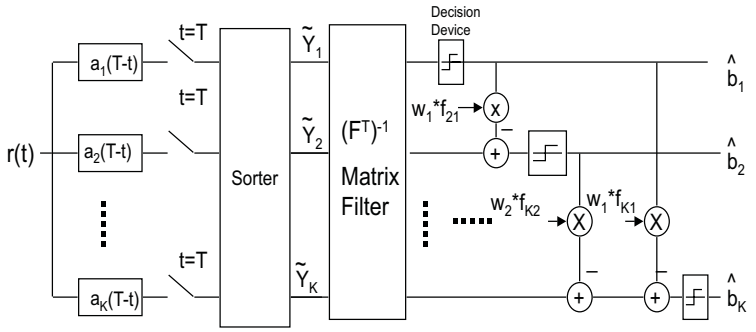

Figure 3.8: Block diagram of the decision feedback receiver.

note that if $b_1 = \hat{b}_1$ then user 2 does not experience MAI from user 1. In these equations we have assumed perfect knowledge of the received amplitudes, when in practice they would have to be estimated.

3.3.7 Decision Feedback

In this receiver, previous decisions are used together with current statistics to estimate the current output bits [23, 24]. Users are ranked in order of decreasing received power levels. A Cholesky decomposition $\mathbf{R} = \mathbf{F^T F}$ of the correlation matrix ($\mathbf{F}$ is lower triangular) is used to obtain two linear transformations: A forward filter that eliminates multiuser interference due to future inputs $\mathbf{G} = (\mathbf{F^T})^{-1}$, and a feedback filter $\mathbf{B} = (\mathbf{F} - \mathbf{diag}(\mathbf{F}))$ that uses previously bit decisions to eliminate MAI provided that feedback data is correct. Figure 3.8 shows a block diagram of a decision feedback multiuser receiver.

For the strongest user, the decorrelator and the decision feedback receivers are identical. For weaker users the decision feedback strategy tends to outperform the decorrelator.

For simplicity let us consider a three user synchronous system. Using the Cholesky decomposition of the matrix $\mathbf{R}$ the decision statistics can be written in terms of $\mathbf{F}$ as:

$$\hat{\mathbf{y}} \quad = \quad \mathbf{F}^T\mathbf{F}\mathbf{W}\mathbf{b} + \mathbf{z}, \tag{3.31}$$

which corresponds to:

$$\begin{bmatrix} y_1 \\ y_2 \\ y_3 \end{bmatrix} = \begin{bmatrix} f_{1,1} & f_{2,1} & f_{3,1} \\ 0 & f_{2,2} & f_{3,2} \\ 0 & 0 & f_{3,3} \end{bmatrix} \begin{bmatrix} f_{1,1} & 0 & 0 \\ f_{2,1} & f_{2,3} & 0 \\ f_{3,1} & f_{3,2} & f_{3,3} \end{bmatrix} \mathbf{W} \begin{bmatrix} b_1 \\ b_2 \\ b_3 \end{bmatrix} + \begin{bmatrix} z_1 \\ z_2 \\ z_3 \end{bmatrix}, \tag{3.32}$$

Applying the forward filter $\mathbf{F}^{T\,-1}$ to the matched filter outputs yields:

$$\hat{\mathbf{y}} = (\mathbf{F}^T)^{-1}\hat{\mathbf{y}} = (\mathbf{F}^T)^{-1}\mathbf{F}^T\mathbf{F}\mathbf{W}\mathbf{b} + (\mathbf{F}^{\mathbf{T}})^{-\mathbf{1}}\mathbf{z} \tag{3.33}$$

The filtered outputs correspond to:

$$\hat{y}_1 = f_{1,1}w_{1,1}b_1 + n_1 \tag{3.34}$$

$$\hat{y}_2 = f_{2,2}w_2b_2 + f_{2,1}w_1b_1 + n_2 \tag{3.35}$$

$$\hat{y}_3 = f_{3,3}w_3b_3 + f_{3,2}w_2b_2 + f_{3,1}w_1b_1 + n_3 \tag{3.36}$$

Since the strongest user does not experience MAI, it is demodulated first.

$$\hat{b}_1 = \mathrm{sgn}(\hat{y}_1), \tag{3.37}$$

this bit decision is used to cancel the MAI from the second user:

$$\begin{aligned} \hat{b}_2 &= \mathrm{sgn}\{\hat{y}_2 - f_{2,1}w_1\hat{b}_1\} \\ \hat{b}_2 &= \mathrm{sgn}\{f_{2,2}w_2b_2 + f_{2,1}w_1(b_1 - \hat{b}_1) + n_2\}, \end{aligned} \tag{3.38}$$

subsequently, all previous decisions are used in an attempt to cancel the MAI for the weakest user:

$$\begin{aligned} \hat{b}_3 &= \mathrm{sgn}\{\hat{y}_3 - f_{3,2}w_2\hat{b}_2 - f_{3,1}w_1\hat{b}_1\} \\ \hat{b}_3 &= \mathrm{sgn}\{f_{3,3}w_3b_3 + f_{3,2}w_2(b_2 - \hat{b}_2) + f_{3,1}w_1(b_1 - \hat{b}_1) + n_3\}, \end{aligned} \tag{3.39}$$

The hard decisions of the decision feedback detector can be thus written in matrix notation as:

$$\begin{aligned} \hat{\mathbf{b}} &= \mathrm{sgn}\{\hat{\mathbf{y}} - \mathbf{B}\mathbf{b}\} \\ \hat{\mathbf{b}} &= \mathrm{sgn}\{(\mathbf{F}^{\mathbf{d}}\mathbf{W}\mathbf{b}) + (\mathbf{F} - \mathbf{F}^{\mathbf{d}})\mathbf{W}(\mathbf{b} - \hat{\mathbf{b}})\} \end{aligned} \tag{3.40}$$

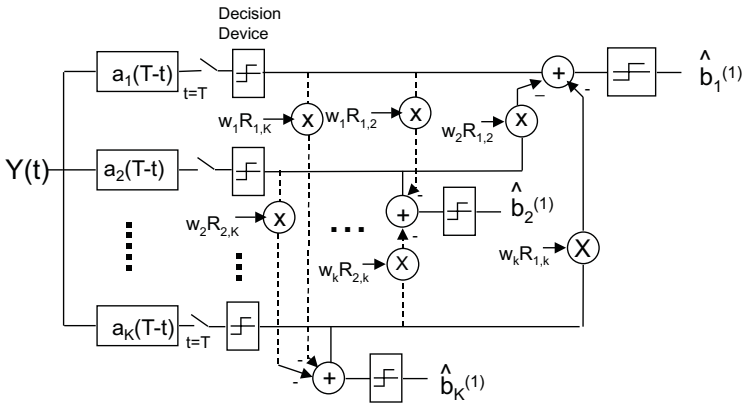

Figure 3.9: Parallel interference cancellation receiver.

3.3.8 Multistage Parallel Interference Cancellation

This type of receiver, initially proposed in [25, 26], uses an iterative approach in which estimation, re-modulation, and cancellation of interference from other users, is performed in parallel for each user. Improved estimates are then obtained from each user's enhanced signal which exhibits reduced interference. Figure 3.9 displays the block diagram of a parallel interference cancellation receiver.

Multistage parallel interference cancellation was formulated in [25] as the iterative suboptimum solution of Equation (3.13) under the assumption that the at stage $m+1$, the i^{th} bit of user k is computed as the value that maximizes the log-likelihood function when all other bits are substituted by their estimates from the m^{th} stage:

$$\hat{b}_{i,m+1}^{(k)} \quad = \quad \arg\{\max_{b_i^{(j)}=\hat{b}_{i,m}^{(j)}} [L(\mathbf{B}, \mathbf{r}(\mathbf{t}))]\}. \tag{3.41}$$

This is equivalent to reconstructing the individual user signals using the bit estimates of the previous iteration. Then, for every user, subtracting out from the received waveform the estimated MAI caused by the remaining users, and finally computing a new decisions from the user's "reduced MAI" waveform.

To better illustrate this approach, let us consider a two user system. The first stage of the receiver corresponds, as customary, to the conventional receiver:

$$\hat{b}_1^{(s=0)} \quad = \quad \mathrm{sgn}(\sqrt[2]{P_1} b_1 + \sqrt[2]{P_2} R_{1,2} b_2 + z_1)$$

$$\hat{b}_2^{(s=0)} = \mathrm{sgn}(\sqrt[2]{P_2}b_2 + \sqrt[2]{P_1}R_{1,2}b_1 + z_2) \tag{3.42}$$

these tentative bit decisions are then used in the first stage of interference cancellation in an attempt to cancel MAI:

$$\begin{aligned}\hat{b}_1^{(s=1)} &= \mathrm{sgn}\{\sqrt[2]{P_1}b_1 + \sqrt[2]{P_2}R_{1,2}(b_2 - \hat{b}_2^{(s=0)}) + z_1\} \\ \hat{b}_2^{(s=1)} &= \mathrm{sgn}\{\sqrt[2]{P_2}b_2 + \sqrt[2]{P_1}R_{1,2}(b_1 - \hat{b}_1^{(s=0)}) + z_2\},\end{aligned} \tag{3.43}$$

this expression can be readily generalized to multiple stages of interference cancellation as follows:

$$\begin{aligned}\hat{b}_1^{(s=m+1)} &= \mathrm{sgn}\{\sqrt[2]{P_1}b_1 + \sqrt[2]{P_2}R_{1,2}(b_2 - \hat{b}_2^{(s=m)}) + z_1\} \\ \hat{b}_2^{(s=m+1)} &= \mathrm{sgn}\{\sqrt[2]{P_2}b_2 + \sqrt[2]{P_1}R_{1,2}(b_1 - \hat{b}_1^{(s=m)}) + z_2\},\end{aligned} \tag{3.44}$$

In practice, minor performance improvements are experienced after $\sim$ 3 stages of interference cancellation.

There are two approaches for performing subtractive interference cancellation, a wideband despread/respread approach that involves signal reconstruction prior to interference cancellation, and a postdetection approach which uses the cross-correlations between users and the decision statistics to reconstruct the interference components after detection. As shown in Appendix A, both approaches are theoretically equivalent. When the crosscorrelations do not change rapidly, postdetection cancellation can be significantly faster. In a practical system, however, the wideband approach is simpler to implement.

Several multistage receivers, including the earliest ones, use hard decision devices and require extrinsic estimates of the received amplitudes for estimation of the received signals. Alternatively, the soft outputs of the demodulators can be used to provide joint estimates of the received symbols and energies [27, 28]. Soft non-linear functions,such as the hyperbolic tangent can also be used at the outputs of the matched filters. Appendix B motivates their use.

Significant performance gains have been obtained by performing partial rather than complete cancellation of the estimated MAI as in [25], where the degree of cancellation varies with the stage s of cancellation and system loading K [28, 29].

In this approach, the received signal used for detection of user k at stage s is defined as:

$$\hat{r}_k^{(s)}(t) = r(t) - \sum_{j \neq k} C_j^{(s)} \hat{s}_j^{(s)}(t), \tag{3.45}$$

where the signal $\hat{s}_j^{(s)}(t)$ corresponds to the estimated reconstructed signal for user j at stage s and $C_j^{(s)}$ is the partial-cancellation multiplicative factor for user j at stage s. Improved estimates are obtained from this signal via correlation with the signature sequence of user k

$$z_{k,i}^{(s)} = \frac{1}{T} \int_{(i-1)T+\tau_k}^{iT+\tau_k} \hat{r}_k^{(s)}(t) a_k(t-\tau_k) e^{-j\theta_k} dt. \tag{3.46}$$

Similar ideas have also been used in [30] to derive a multistage receiver structure based on maximum likelihood considerations and uses hyperbolic tangent soft decision functions. In [31] these principles have been used in the development of a decorrelating parallel interference canceller.

3.3.9 Comparison of Alternative Techniques

Early studies in multiuser detection helped lay the theoretical foundations for the field. The majority of the performance studies of sub-optimal receivers have been performed via computer simulations under idealized and non-uniform conditions.

In order to fairly compare the capabilities of different multiuser structures, it becomes necessary to conduct a simulation campaign using a common set of parameters. In addition, it is also necessary to include non-ideal situations into analysis and simulations to assess their impact on system performance.

Using a common simulation test bed, the aforementioned sub-optimal multiuser detectors have been compared under different channel conditions for randomly generated codes [9]. Figure 3.10 shows analytical and simulated capacity curves in terms of probability of error vs. number of users K for various sub-optimal receiver architectures. The multistage parallel partial interference cancellation approach uses 2 stages of cancellation and a common partial cancellation multiplicative factor of 0.5. This graph is a clear example of the significant performance improvements that can be obtained under idealized conditions by using advanced multiuser receiver structures.

The performance of the receivers for slow flat Rayleigh fading is presented in Figure 3.11. This figure shows that in this type of situation, all of the multiuser receivers significantly outperform

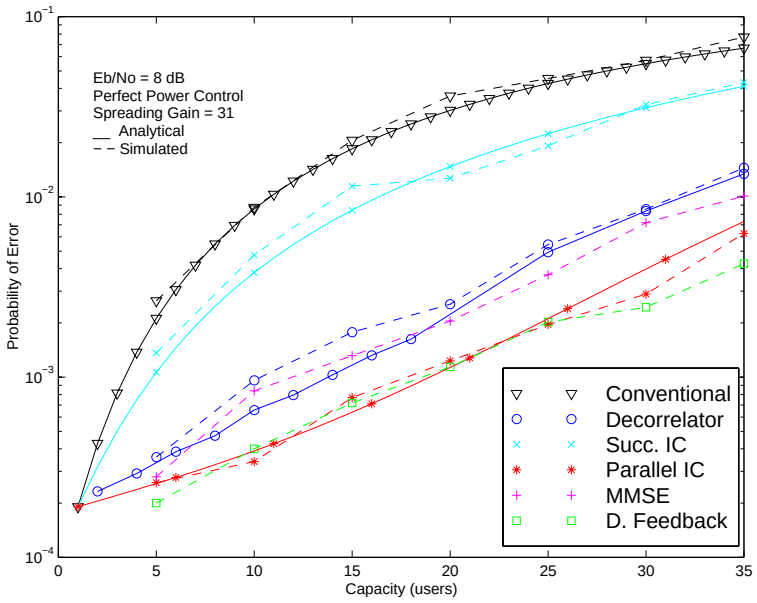

Figure 3.10: Probability of error vs. Number of users with perfect power control ($E_b/N_o = 8$ dB and processing gain $= 31$).

the conventional receiver. Today's second generation DS-CDMA systems equipped with powerful forward error correction codes operate at a $E_b/(N_o + I_o) \approx 7$ dB for non-coherent reverse link and $E_b/(N_o + I_o) \approx 5$ dB for the coherent forward link [32]. The curves in Figure 3.11 also indicate that for practical E_b/N_o the performance of the multiuser receivers is highly comparable to the single user bound.

Figure 3.12 shows the performance degradation in near-far channels of these sub-optimal receivers. In this case there are three users in an AWGN channel. The probability of error for users 1 and 2 is plotted as the power of user 3 is varied from 10 dB below the signal power of the users of interest to 30 dB above. The parallel interference cancellation approach is not strictly near-far resistant. However, this figure indicates that all the receivers display significant robustness to the near-far problem for reasonable power differences. The near-far performance of the multistage approach can be improved by performing selective cancellation, i.e., not canceling weaker users with unreliable estimates.

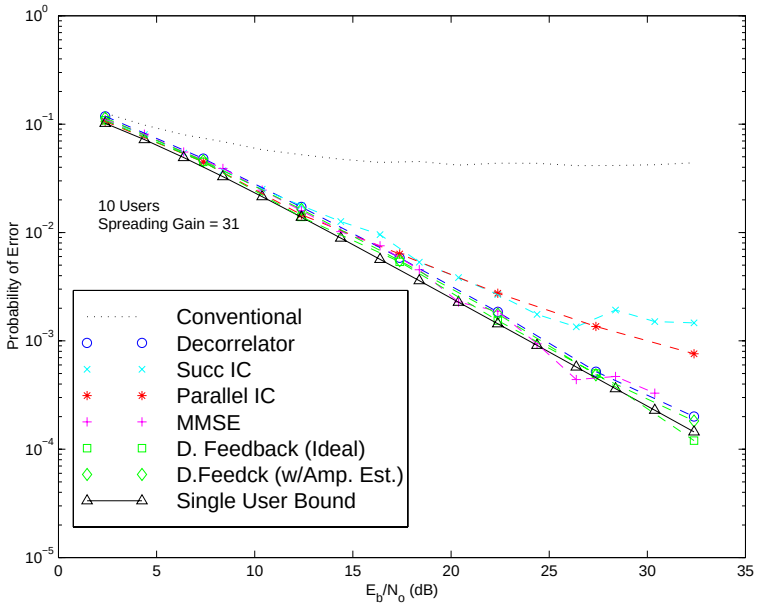

Figure 3.11: Probability of error vs. Number of users for flat Rayleigh fading (10 users and processing gain = 31).

3.4 Practical Implementation Issues

This section explores some of the key implementation issues for the development of practical CDMA multiuser receivers, begining with a consideration of the computational complexity of several proposed multiuser receivers. Several techniques for multiuser parameter estimation are reported, and issues regarding imperfect parameter estimation, quantization and finite precision are discussed subsequently.

3.4.1 Computational Complexity

One of the main issues affecting the selection of a multiuser architecture for practical implementation is complexity. In this section several of the most notable approaches to multiuser detection are analyzed in terms of their computational complexity. In order to compare computational complexity of different multiuser receivers the asymptotic time complexity per bit decision (TCB) will be used. TCB corresponds to the time required by the decision algorithm to select the received

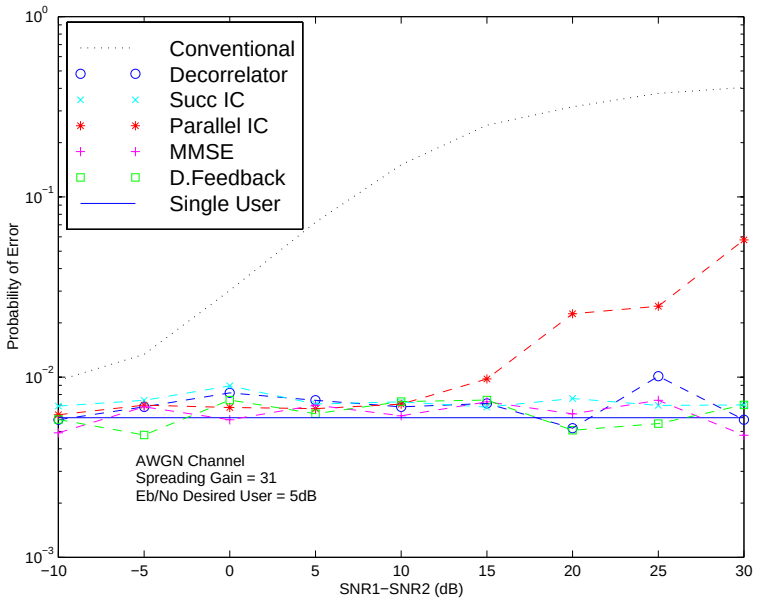

Figure 3.12: Performance degradation in near/far channels ($\overline{E_b/N_o} = 5$ dB and processing gain = 31).

sequence, divided by the number of transmitted bits (as the number of transmitted bits tends to infinity) [1]. A TCB of $p(x)$ is usually denoted as $O(f(x))$ when for sufficiently large x there exists a constant k such that $f(x) \leq kp(x)$.

The optimal receiver for asynchronous CDMA channels in AWGN is a maximum-likelihood sequence estimator. An early paper that explored a solution to the problem of optimum multiuser detection in asynchronous DS-CDMA channels is [14]. By deriving the relationship between the observation vector and the transmitted symbols in an asynchronous DS-CDMA system, and noting that this relationship is analogous to the input-output relations of a linear finite-state machine corresponding to a rate 1 convolutional encoder, Schneider conjectured that an optimal receiver could be implemented as a maximum-likelihood sequence estimator with 2^{2K} states and $O(8^K)$ time complexity per bit (TCB).

The optimum multiuser detector for Gaussian channels was formally derived in [1]. It consists of a bank of matched filters followed by a dynamic programming algorithm of the Viterbi type. Reduction in complexity is obtained by exploiting that every user's symbol only overlaps with two

symbols of every other user in the system. This fact, evidenced in the triple-diagonal structure of the matrix $\mathbf{R}$, simplifies sequential computation of the log-likelihood function. In this case, the number of states are 2^{K-1} and thus the time complexity per bit is $O(2^K)$. The main drawback of the optimum receiver is its computational complexity, which is exponential in the number of users, precluding its use in most practical applications.

Schneider's work also proposed the idea of applying a linear transformation to the matched filters outputs for cancellation of the co-channel interference. The main complication in the implementation of this receiver is the computation of the decorrelating transformation $\mathbf{R^{-1}}$. Direct matrix inversion results in a TCB that is $O(K^3)$. Although approximate implementation in the form of a receiver composed of digital tapped delay lines is possible, the computational complexity remains high, especially for high mobility systems where the cross-correlation relationships between multiple users change rapidly. In [33], a low complexity approximation of $\mathbf{R^{-1}} = (\mathbf{I} - \mathbf{S})^{-1}$ by $\mathbf{I} + \mathbf{S}$ is proposed. This technique requires relatively low cross correlations among all users, since part of the interference is not canceled. Iterative techniques for inversion of the tri-diagonal decorrelating matrix having a complexity of $0(K^2)$ per iteration have been proposed in [34].

Direct implementation of the MMSE receiver faces the same complexity limitations encountered by the decorrelator. However, the MMSE can be more readily computed based on adaptive algorithms that avoid direct matrix inversion [35]. A blind adaptive technique that does not require training sequences and requires as little information as the conventional receiver has been derived in [20]. The moderate complexity of the gradient adaptation algorithm together with the advantages of blind adaptation, make this approach attractive.

A successive interference cancellation approach that requires the transmitter powers to follow a geometric distribution was proposed in [21]. The idea is to assign the user powers so that all users have basically the same BER. Successive cancellation has been further studied in [36, 22]. The time complexity per bit of the basic algorithm is $O(K)$. However, the serial approach to interference cancellation requires ranking of the users according to the received powers, an operation that has a complexity proportional to $K \log_2(K)$.

Selective cancellation has also been proposed as an alternative to reducing the complexity of the successive cancellation. The impact of limiting the number of canceled users in successive interfer-

ence cancellation is considered in [36]. In [37] performance is improved, with increased complexity, by using a group partitioning approach that combines state sequence estimation via a Viterbi algorithm with successive cancellation.

Implementation of a decision feedback detector involves sorting of the users according to their received energies, generation of the forward filter using a Cholesky decomposition of the matrix $\mathbf{R}$, and an inversion of the resulting triangular matrix plus forward/feedback filtering. The combination of all these involved tasks translates into an $O(K^3)$ TCB.

The multistage parallel interference cancellation scheme for multiuser detection has an $O(K)$ time complexity per bit decision and a fixed decoding delay. For every user the basic process of parallel interference cancellation entails estimation, regeneration and subtraction of multiple access interference. The inherent parallel nature of the algorithm can be easily exploited in a multiprocessing environment where several processors can work together to solve a large, computationally complex task. This makes the parallel cancellation approach extremely attractive, since by exploiting parallelism, the computational burden on a single processor can be lowered in comparison to direct implementation of the successive cancellation approach [9].

Another approach that has been proposed for multiuser detection is the use of neural networks. A neural net based multiuser receiver that results in similar decision regions as the decorrelating detector was studied in [38]. The use of radial basis functions (RBF) networks was explored in [39]. A disadvantage of this scheme is that, even though training of neural networks can be performed off-line, for systems with good performance these networks tend to have a hardware complexity which is exponential in the number of users. For a more thorough analysis of computational complexity of multiuser receivers, the reader is referred to [9].

3.4.2 Parameter Estimation

Multiuser parameter estimation is essential to the development of practical structures that employ multiuser detection principles. In general, the timing of the received waveforms, the received amplitudes, and the carrier phases (for coherent implementations) are parameters that need to be accurately estimated and tracked for successful multiuser demodulation.

3.4.2.1 Synchronization

Once the multiple access signal arrives at the receiver, synchronization is necessary in order to effectively despread and demodulate the desired user's signal. There are two main components to code synchronization: coarse acquisition and tracking. In the acquisition phase, the receiver's code is brought into coarse alignment with the received signal. Once synchronization to within a chip period is achieved, the receiver enters a tracking phase during which it refines and maintains the alignment between the locally generated code and the spreading code embedded in the received signal.

Acquisition schemes can be classified as non-coherent or coherent, based on whether or not despreading occurs prior to carrier recovery. In most spread spectrum receivers, carrier recovery is usually achieved using conventional phase-locked loops after code acquisition. With coherent techniques it is assumed that the receiver will be able to accurately estimate the received phase and resolve Doppler related frequency uncertainties, a difficult task in a mobile multiple-access scenario.

Most synchronization methods are based on measuring the correlation between the received signal and a locally generated copy of the spreading sequence. Another approach originally proposed in [40] and later modified in [41] is based on coherent detection of n consecutive chips of the received sequence, where n is the length of the generator shift register. The detected symbols are loaded into the shift-register generator as an initial state. If the chips are correctly detected, then synchronization is achieved. In high SNR situations this technique has the advantage of rapid acquisition.

One of the most commonly used techniques for synchronization is a non-coherent approach that can be implemented via active correlation with a local replica of the code that slips in phase with respect to the received signal. The signal from the correlator is square-law envelope detected. When code synchronization occurs, the input signal to a pre-detection filter collapses from a wideband noise-like signal into a narrowband signal. The energy at the output of this filter can be sensed via a variety of techniques. A detector with a fixed integration time is the simplest approach, with enhanced performance achieved by using successive integration tests in what is known as a multiple dwell approach [8].

In [42] several parallel acquisition schemes for asynchronous direct sequence spread spectrum communications, including the optimal estimation scheme, have been analyzed. The optimal scheme, maximizes the a posteriori probability that the estimate is within the pull-in range of the code tracking loop. This is done by locating and computing the function's multiple local maxima, and choosing the one that produces the largest value as the estimate. This involves computation of the correlation between the received signal and phase shifted replicas of it, and the evaluation of multiple exponential and error functions. Due to the high level of complexity of the optimal scheme, suboptimal schemes, which are much easier to implement, have also been proposed [43].

The acquisition performance of a noncoherent parallel acquisition scheme for the uplink of a mobile DS-CDMA system has been studied in [44]. This study, which considered several practical conditions, suggests that system capacity based on an acquisition based criterion can be lower than that based on post-acquisition probability of error.

Another approach for synchronization is based on matched-filter synchronization techniques [45]. This type of approach uses a bandpass filter that is matched to a segment of the spreading sequence. The matched filter is used to signal a sequence generator when the segment to which it is matched has been received. Matched filter synchronizers allow significant reductions of synchronization time.

A code tracking mechanism is necessary after initial acquisition to refine and maintain proper code-phase alignment with the received signal. Closed-loop tracking techniques such as early-late gate loops are commonly used for code tracking. Tau-dither and delay-lock [46] are two common configurations in use. Tracking is also necessary to correct code-phase drifts due to offsets in the clock generators between the transmitter and the receiver. Detailed descriptions of several acquisition and tracking techniques can be found in [47, 8, 48].

Interference cancellation approaches can be used to enhance acquisition within DS-CDMA systems. Acquisition using serial and parallel interference cancellation approaches were proposed in [49, 50]. The parallel technique allows faster synchronization than the serial approach at the expense of increased complexity. Interference cancellation based synchronization approaches fit naturally into a multiuser detection scenario. The multistage parallel interference cancellation and the successive interference cancellation approach can directly take advantage of these techniques as the signals required for synchronization are readily available. A recursive delay estimator based on parallel

interference cancellation using early-late delayed-locked loop principles was proposed in [51]. In this case, the system uses three parallel correlators spaced one sample apart. The filtered outputs of the correlators are used to determine the timing estimate for the next bit interval.

In [52] an analysis is performed of the improvement in the mean acquisition time when using a multistage architecture in the synchronization process. By using the residual signal after cancellation of all active users, the multistage parallel interference cancellation receiver was able to reduce the mean acquisition time and the probability of false alarm in a multiuser environment.

Another issue studied in [52] deals with the effect of unsynchronized users on the BER performance of synchronized users. Since interference cancellation can only be performed on synchronized users, the system can potentially experience the near-far problem in the presence of non-acquired users. For a four stage parallel cancellation receiver, simulations showed that one unsynchronized user with 6 dB higher power than the synchronized users caused over a 10% drop in capacity at a BER of 10^{-3}. A possible solution is to have new users transmit with low powers during call initiation so as to reduce their negative effect on synchronized users. Adaptive power control issues for systems with multiuser receivers have been studied in [53].

3.4.2.2 Quantifying the Effects of Timing and Phase Errors

Most studies in multiuser detection presuppose that the receiver has attained perfect timing and carrier phase synchronization with the various transmitters and disregard the effect of tracking errors. A practical wireless system will have to deal with the effects of imperfect code synchronization, oscillator instability, phase jitter, dynamic evolution of the network and propagation channel uncertainties.

Another assumption that is often found in the literature is that of perfectly coherent demodulation. Even with extremely stable frequency sources, imperfect phase estimation is likely to occur in a practical coherent multiuser system. Since a practical system is likely to experience timing and phase misalignments, it is necessary to quantify the effect that these types of errors will have on system performance.

The effects of timing and phase errors on the performance of the optimal detector as well as a

2 user multistage parallel cancellation detector were investigated in [54]. With timing errors, the maximum likelihood receiver suffered a greater relative degradation in performance than the parallel cancellation approach. It was also observed that if phase errors become large, the parallel canceller can outperform the maximum likelihood sequence estimator. These results suggest that linear detectors are more robust to channel estimation errors than exponentially complex detectors, an observation that has also been made for single user channels with intersymbol interference.

The degradation of the near-far performance of the decorrelator due to timing synchronization errors under the assumption of perfect phase estimates has been studied in [55]. Results show that synchronization errors lead to inaccurate interference cancellation and intersymbol interference, thus causing degradation of the near-far robustness and bit error rate performance of the decorrelating detector. An alternate delay independent decorrelating structure that requires the delay error to be less than a chip has been proposed in [56].

The effect of synchronization tracking errors on the BER performance of the successive interference cancellation approach and the conventional detector in AWGN was studied via analysis and simulation in [57]. Tracking errors were modeled as independent identically (IID) distributed zero-mean normal random variables and all users were phase-aligned. Simulation results in AWGN for a system with $N = 31$ indicate that for small standard deviations of the tracking errors ($\sigma \approx 0.2T_c$) the successive interference cancellation approach still provides significant performance improvements.

In the case of the multistage parallel interference cancellation approach, analytical and simulation studies of the effects of phase jitter and timing misalignment errors were investigated in [58]. This work shows that even though synchronization errors affect the performance of the parallel interference cancellation approach more significantly than a conventional receiver, the parallel cancellation approach still outperforms the conventional receiver in the presence of reasonable phase and timing errors.

The impact of synchronization errors in the performance of several multiuser detection algorithms has been studied via simulation in [9]. In this study it is assumed that acquisition has been successfully accomplished and tracking errors are IID zero-mean Gaussian random variables. Figure 3.13 shows the effect of synchronization errors in flat Rayleigh fading for various multiuser receivers. This graph shows that synchronization errors are more consequential for the decorrelator, the

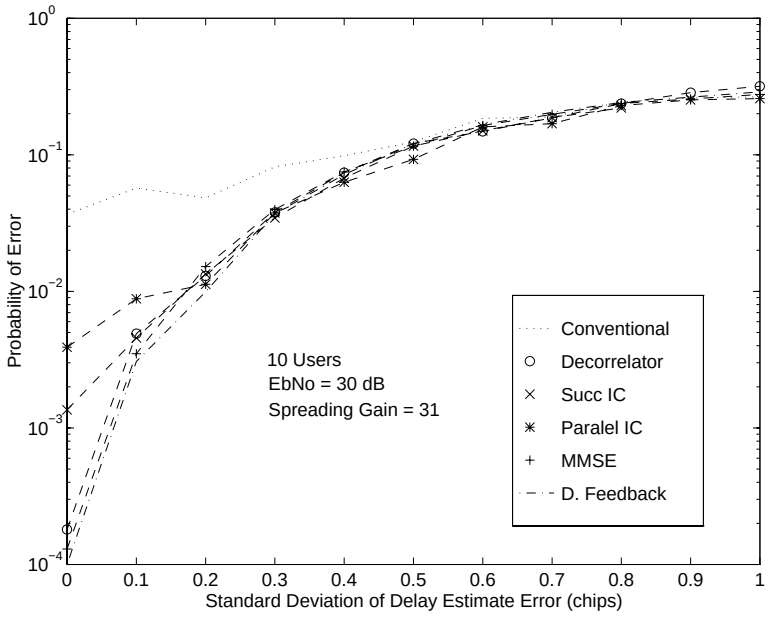

Figure 3.13: Probability of error vs. Standard deviation of synchronization errors in a flat Rayleigh fading channel ($\overline{E_b/N_o} = 30$ dB, processing gain = 31, K=10).

MMSE and the decision feedback receivers.

Synchronization errors cause imperfect MAI cancellation and thus affect the near-far performance of the multiuser detectors. Figure 3.14 shows the effect of tracking errors on the near-far performance of various receivers for a system with two users and one interferer, as the power of the interferer varies from 10 dB below to 30 dB above the power of the desired users. In this case the standard deviation of the estimation error is $\sigma = 0.1T_c$. Comparison of these results with those of Figure 3.12 clearly show how imperfections in the timing estimates can severely alter very desirable features of these receivers.

Phase estimation with a known test sequence using the outputs of the In-phase and Quadrature decision statistics in a multistage parallel cancellation receiver was explored in [59]. The combination of time averaging and interference cancellation was found to improve the quality of the estimates. Pilot symbol aided coherent detection has also been studied in [60]. Use of a pilot channel in the uplink is anticipated for the third generation personal communications systems.

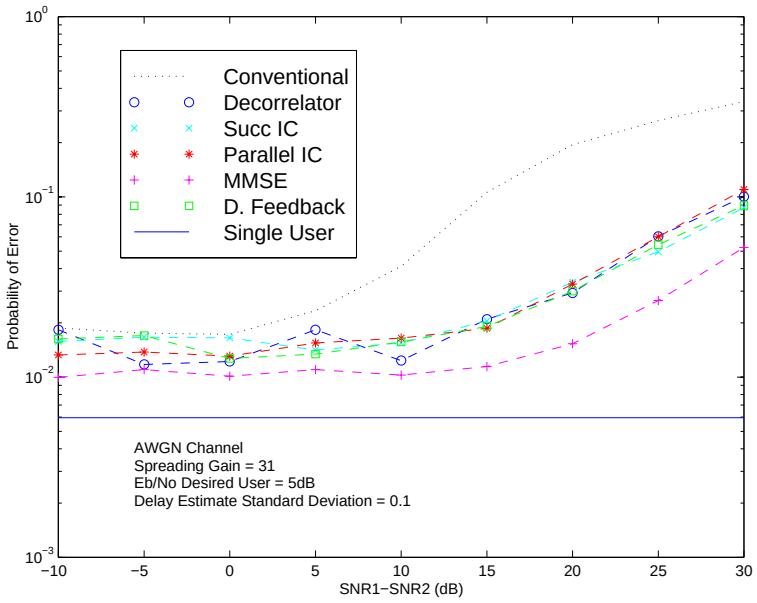

Figure 3.14: Probability of error vs. Difference in powers between the desired user and one interferer.(Standard deviation of estimation error $\sigma = 0.1T_c$, $\overline{E_b/N_o}$= 30 dB, processing gain = 31, K=10

3.4.2.3 Non-coherent Multiuser Detection

In many applications, it is impractical to use a pilot signal or a training sequence. An alternate approach that avoids the need for phase estimation and simplifies the receiver architecture is non-coherent detection. The problem of non-coherent multiuser demodulation of differentially phase-shift keyed DS-CDMA signals over AWGN was addressed in [61], where an optimally near-far resistant bilinear decorrelating detector was proposed.

A differentially coherent multipath RAKE decorrelating detector that uses equal gain combining was studied in [62]. The performance of this detector is studied via simulation for a two-user case and $N = 127$. The relative performance of the coherent and the differentially coherent approach showed similar degradations to those in single-user channels.

The basic idea of these differentially encoded PSK receivers is that interference suppression is performed separately in the in-phase and quadrature arms. Decision statistics are obtained by projecting the current decision statistic onto the previous one and then looking at the phase of the

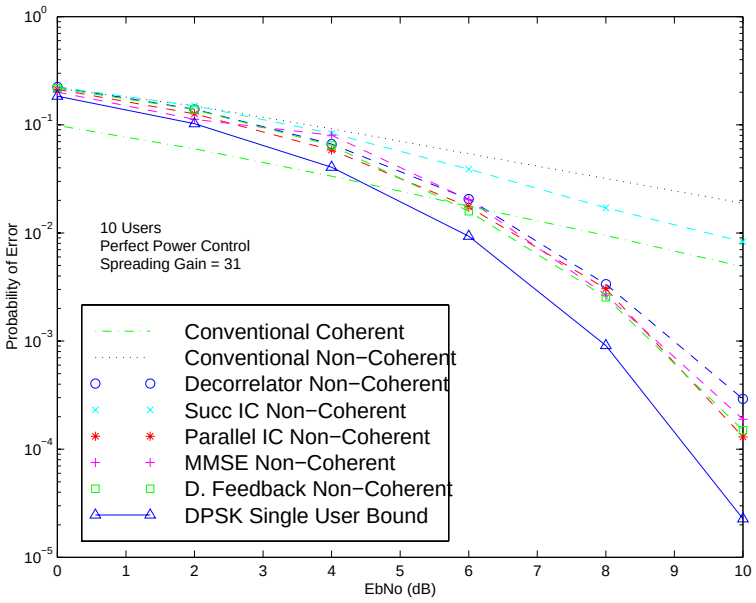

Figure 3.15: Probability of error vs. E_b/N_o for various differentially coherent multiuser receivers in an AWGN channel with perfect power control. (Processing gain = 31, K=10).

resulting complex value $Z_n = Y_n Y_{n-1}^*$.

The performance of differentially coherent multiuser receivers in AWGN channels with perfect power control as a function of E_b/N_o is illustrated in Figure 3.15. This figure indicates that the differentially coherent receivers show the same trends as the fully coherent versions. The performance of the differentially coherent successive interference canceller is lower than that of the partial parallel interference canceller, the MMSE receiver, the decision feedback receiver and the decorrelator. For modest system loads, the differentially coherent receivers show around a 3-db degradation with respect to their ideal coherent counterparts.

The performance of the differentially coherent multiuser receivers in slow flat Rayleigh fading is presented in Figure 3.16. As this figure indicates, in flat Rayleigh fading channels, differentially coherent multiuser receivers provide significant performance improvements when compared to a differentially coherent multiuser receiver. By compensating for multiple access interference, the performance of these multiuser receivers approach that of a single user with differentially coherent detection. Imperfect interference cancellation results in degraded performance of the subtractive

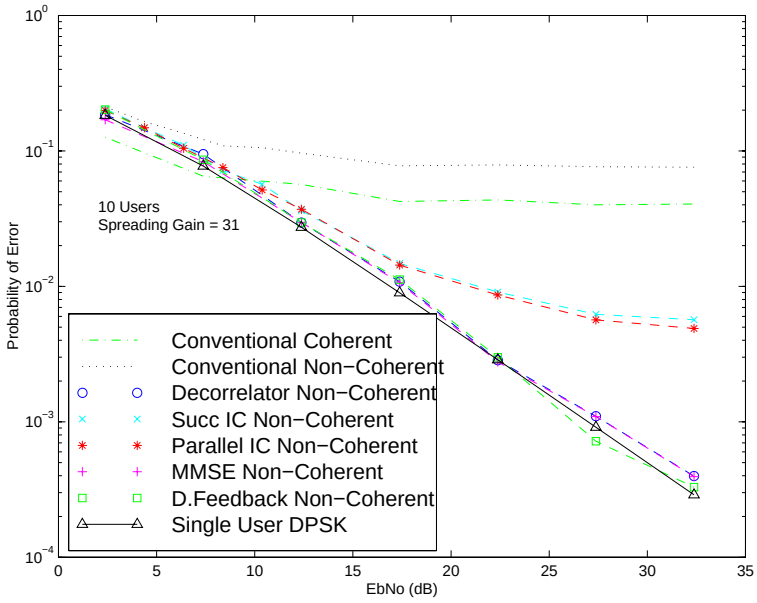

Figure 3.16: Probability of error vs. E_b/N_o for various differentially coherent multiuser receivers in Flat Rayleigh Fading channels. (Processing gain = 31, K=10).

interference cancellation when compared to the linear receivers. Although the MMSE and Decision Feedback receivers have perfect knowledge of the fading coefficients, at high SNRs their performance is practically identical to the decorrelator.

The effects of timing errors for differentially coherent multiuser detection in AWGN can be observed in Figure 3.17. This figure shows that timing errors are more critical for linear multiuser receivers than for subtractive interference receivers. This graph also shows that differentially coherent multiuser receivers are very sensitive to timing inaccuracies. A similar trait has been observed in the fully coherent case.

The performance of the noncoherent receivers in the Near/Far situations is illustrated in Figure 3.18. There are two interferers, one with equal power to the desired user, and one with a power which varies from 10dB below the desired user to 30dB above. The performance of the differentially coherent receivers resembles that observed for their coherent counterparts, with the parallel interference canceller being the most sensitive to near/far conditions.

Another alternative for non-coherent detection is based on the approach used in the reverse link

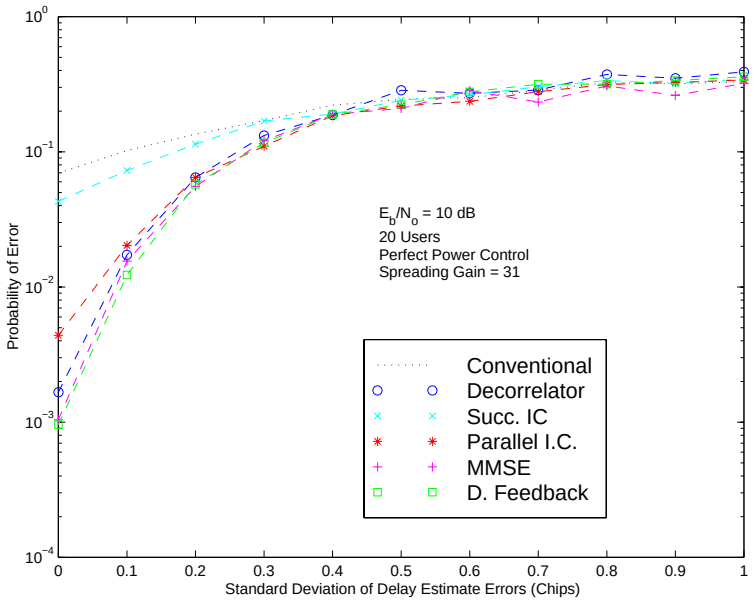

Figure 3.17: Differentially coherent multiuser detector probability of error vs. standard deviation of synchronization errors in AWGN channels.

of IS-95. M-ary orthogonal modulation and OQPSK are used to avoid the need for a pilot signal. The performance of a non-coherent successive interference cancellation approach with multipath combining based on M-ary orthogonal modulation was explored in [22].

The degradation effects due to frequency errors have been quantified for the conventional receiver in [2]. It is shown that as long as the product $N\Delta f T_c$ is relatively small, little degradation is experienced. For advanced receivers, the use of highly accurate oscillators is an obvious solution to problems related to carrier-frequency offsets. Today, base stations of an IS-95 CDMA system maintain their carrier frequency within $\pm 5 \times 10^{-8}$ of the CDMA frequency assignment [63]. Minor frequency offsets may also be managed by a multiuser receiver as long as the offsets are such that most of the despread signal falls within the bandwidth of the postcorrelation filter. Further work is needed to analyze the full effect of frequency errors in the performance of multiuser detection strategies.

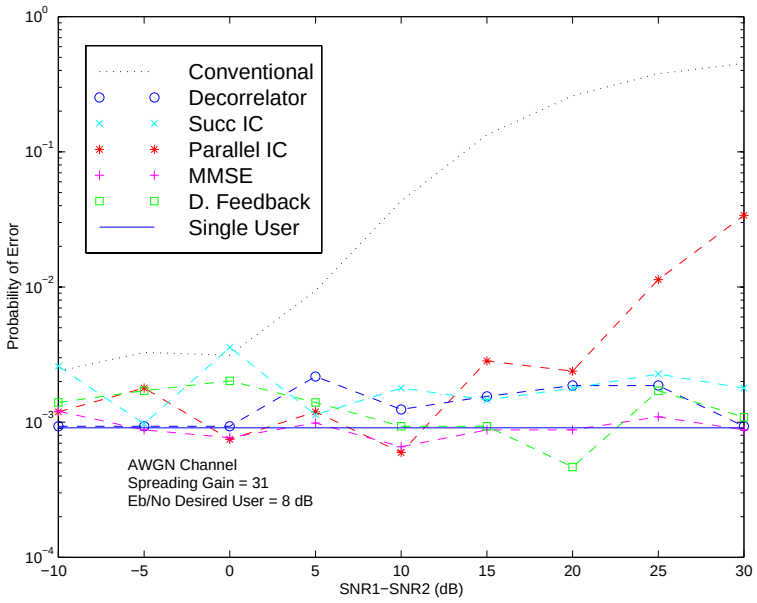

Figure 3.18: Performance degradation of non-coherent receivers in near/far channels ($\overline{E_b/N_o}$=8dB and processing gain = 31)

3.4.2.4 Amplitude Estimation

As opposed to the decorrelating detector, which does not require amplitude information, most multiuser detection algorithms require accurate estimation of the received signal energies. Several approaches have been proposed with varying degrees of complexity.

Maximum likelihood parameter estimation using a test sequence was explored in [64]. This approach is not practical in many situations due to its high complexity and throughput reductions. An adaptive approach that uses a tree-search algorithm and has a complexity of $O(K^2)$ per decoded bit was presented in [65]. A correlation estimator, that averages out unknown parameters was introduced in [66]. The performance of these type of estimators in the presence of time-varying parameters needs to be further studied however.

A reduced-complexity sequential detection-estimation approach for amplitude estimation is proposed in [67]. An alternate approach that exploits cyclostationarity for joint estimation of amplitudes, phases and delays has been presented in [68]. Adaptive joint estimation of symbol and

individual amplitudes and phases via an extended Kalman filter or an RLS approach has been studied in [69].

In [70] an algorithm based on Gauss-Seidel iterations is proposed for implementing an approximation to the maximum likelihood approach to joint data and amplitude estimation. The channel attenuation coefficients are computed using the Expectation Maximization (EM) algorithm. The estimated channel attenuation coefficients were found to be accurate in the sense that they did not cause noticeable degradation in the performance of the receiver.

A drawback of several previously mentioned algorithms is the high level of complexity required for their implementation. In order to minimize the complexity of amplitude estimation in multiuser receivers, the soft outputs of a matched filter bank can be directly used for amplitude estimation. A simple way to reduce the noise variance of the correlation estimates is to average the amplitude estimates over a number of successive bits. For time-varying channels, the coherence time of the channel needs to be taken into consideration for determining an appropriate number of bits for averaging [59].

The performance of parallel interference cancellation with amplitude estimation has been analyzed in [59]. Results show small degradation with soft cancellation and amplitude averaging.

The performance of various multiuser receivers has been compared for practical amplitude and phase estimation in slow Rayleigh fading. The subtractive interference cancellation receivers generate their channel estimates from a moving average over 10 consecutive soft decision statistics. The remaining receivers use in-phase and quadrature estimates provided by a decorrelator. The subtractive interference receivers experience a slight degradation due to imperfect cancellation caused by the amplitude mismatch. For the remaining receivers, the amplitude estimates provided by the decorrelator are satisfactory and do not reduce performance significantly. Figure 3.19 illustrates the performance of the multiuser receivers with amplitude and phase estimation.

In multistage interference cancellation, it was shown in [29] that matched filter soft amplitude estimation leads to biased estimates. However, in a multistage scenario, partial cancellation can be used to reduce the bias at the first stage. In subsequent stages, the bias rapidly decreases and the amplitude estimates improve from stage to stage as the number of stages increases above one.

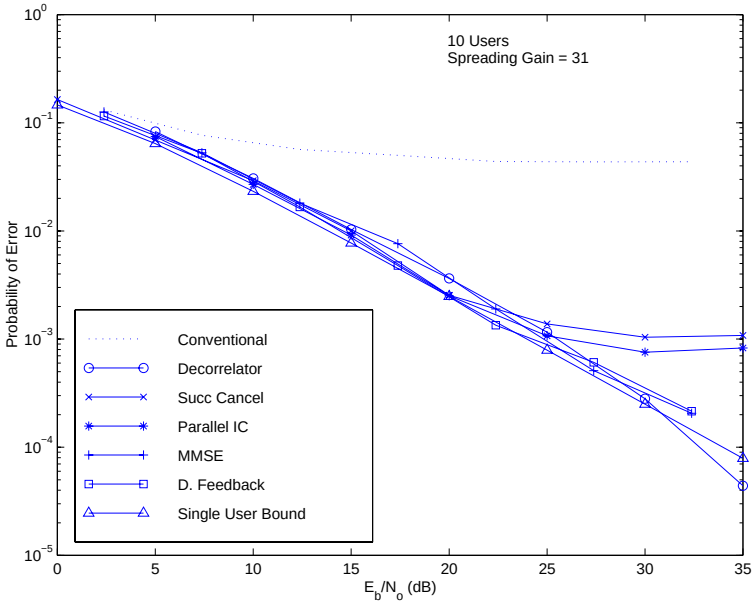

Figure 3.19: Probability of error vs. E_b/N_o for flat Rayleigh fading with amplitude and phase estimation (10 users, processing gain = 31, 10 symbol average channel estimate)

In [51] the use of parallel interference cancellation adaptive channel attenuation estimation filters is investigated. These filters not only proved better than moving average estimators, but also outperformed other multiuser based adaptive amplitude estimators.

3.4.3 Quantization Effects

Arithmetic operations such as addition and multiplication are at the core of the algorithms used in advanced multiuser receivers. Because of this, the performance of the algorithms, and the receivers, can be heavily influenced by the word-length and the type of arithmetic used by the system. Floating-point arithmetic simplifies algorithmic development and has a wider dynamic range than fixed-point. Fixed-point solutions, however, do not necessarily sacrifice performance. In addition fixed-point hardware is significantly faster and cheaper than floating-point.

It is therefore necessary to evaluate the effect of fixed-point arithmetic on the performance of multiuser detection techniques. The performance of a fixed point implementation of the multistage

parallel interference cancellation technique was investigated analytically and via simulations in [52]. Results show that the multistage implementation performs with little degradation with as few as eight bits of precision provided that the received signal $r(t)$ has a limited dynamic range.

Finite precision decorrelating structures have been considered in [71]. For moderate channel occupancies and slowly varying multiuser interference, optimal finite precision decorrelating detectors seem to perform very closely as their infinite precision counterparts. However, they appear not to be feasible for rapidly varying multiuser situations due to the complexity involved in finding the required optimal user sequences.

The performance degradation of the MMSE receiver due to quantization has been explored in [72]. Results show that finite word-lengths have a detrimental effect in the overall performance of this receiver, especially for heavy loads. For suitably short word-lengths, the MMSE can even perform poorer than the conventional receiver.

Word-length optimization at the algorithmic level can reduce the hardware complexity and improve the speed and power consumption of a digital transceiver, especially for highly integrated IC solutions. A design methodology that allows the evaluation of the effects of word-length on system performance and complexity for communication systems is presented in [73].

3.5 Conclusions

Multiuser detection has the potential of significantly improving the performance of DS-CDMA systems. Due to the prohibitively large computational complexity of optimal multiuser detection, several alternative sub-optimal receivers have been developed. For practical implementation of multiuser detection, subtractive interference cancellation receivers are favored due to their lower complexity, effectiveness, and robust performance.

Comparative studies described in this document indicate that the enhancement in capacity obtained with multistage partial parallel interference cancellation is one of the highest among suboptimal receivers. Furthermore, in systems using power control, the capacity of parallel interference cancellation is significantly superior to that of the successive approach. Due to its inherent parallel

structure, parallel interference cancellation can be readily implemented with multiple processing structures working in parallel.

A significant drawback of successive interference cancellation is its demodulation latency, which grows linearly with the number of users, with potential adverse effects. Another drawback of this technique is the practical complexity involved in implementing the mechanism that regularly sorts the users according to their received powers.

Due to its low complexity, higher capacity, lower latency, and robustness, multistage partial parallel interference cancellation is the preferred technique for practical implementation of goals described in this document.

Chapter 4

Soft Cancellation

For practical implementation, multistage parallel interference cancellation is an attractive approach, both in terms of performance and computational complexity [9], as well as its robustness to moderate phase jitter and synchronization errors [58].

In order to minimize the complexity of an interference cancellation receiver, a matched filter bank is commonly used at each stage for estimation of the transmitted bits and received signal energies. Regeneration and complete subtraction of the estimated MAI is then performed to reduce the interference affecting each user.

In 1996, Michael Buehrer, then a senior PhD student at Virginia Tech, found that his individual simulation results for a direct implementation of parallel interference cancellation were significantly poorer than those expected according to the analytical expression for capacity derived in [74], especially at high loads. My own independently written simulations confirmed his findings.

We conjectured that the brute force parallel canceller did not behave as assumed in the derivation of this analytical expression. Michael Buehrer's insight to investigate the statistical properties of the decision statistics was key in solving the problem. His histograms showed that the decision statistics after interference cancellation were biased, and that the amount of bias was proportional to the number of users. Simultaneously, it became apparent that by subtracting only part of the estimated interference we could make our simulation results approximate the analytical results. Histograms showed a reduction in the bias of the decision statistics after partial cancellation.

By focusing on the statistical properties of the underlying signature sequences, I was able to explain analytically the source of the bias and to characterize its dependence on the number of users and the spreading gain. Based on these results Pascal Renucci, a Masters Student at Virgina Tech, found an analytical solution to the problem of optimizing the soft cancellation factor for a single stage receiver [75].

This chapter introduces a derivation of the source of the bias and an efficient technique for mitigating the effects of the bias and increasing performance. The proposed technique lends itself to practical real-time DSP implementation. Section 4.1 describes the CDMA system model. Section 4.2 presents the source of the bias, and in section 4.3 an effective, yet simple, technique that mitigates the effects of the bias and significantly enhances system performance is described. Simulation results are presented comparing the performance of the direct implementation with that of the proposed technique

4.1 System Model

This section describes the DS-CDMA multiple access model used in this derivation, which is similar to the model described in [76].
The k^{th} user's received signal has the form:

$$s_k(t-\tau_k) \quad = \quad \sqrt{2P_k}b_k(t-\tau_k)a_k(t-\tau_k)\cos(\omega_c t+\phi_k), \tag{4.1}$$

where P_k is the received signal power of the k^{th} user, $a_k(t)$ and $b_k(t)$ are the spreading and data waveforms respectively (assume rectangular pulses for both, a spreading gain of N chips per bit, and completely random spreading waveforms); τ_k is a time delay that accounts for the asynchronous nature of the system uplink and the arrival times of the different multipath components; ϕ_k is the received phase of the k^{th} user, relative to some arbitrary reference phase. Note that while typical developments of multiuser algorithms assume code-on-pulse spreading (the code period equals the symbol period), interference cancellation does not require it, since for each symbol interference cancellation can be directly implemented at the chip level. Commercial DS-CDMA systems such as IS-95 typically use long PN spreading codes, thus making the algorithm practical for these systems.

The received signal $r(t)$ is given by:

$$r(t) = \sum_{k=1}^{K} s_k(t - \tau_k) + n(t), \tag{4.2}$$

where K is the number of users, and there is a single noise source $n(t)$ from a common front end. The decision metrics $Z_{k,i}^{(s+1)}$ for the i^{th} bit of the k^{th} user after s stages of cancellation for an S-stage parallel cancellation scheme can be expressed as:

$$Z_{k,i}^{(s+1)} = \int_{iT+\tau_k}^{(i+1)T+\tau_k} \hat{r}_k^{(s)}(t) a_k(t - \tau_k) \cos(\omega_c t + \phi_k) dt, \tag{4.3}$$

where the received signal $\hat{r}_k^{(s)}(t)$ at stage s is estimated according to:

$$\hat{r}_k^{(s)}(t) = r(t) - \sum_{j=1}^{K} \hat{s}_j^{(s)}(t), \tag{4.4}$$

and the signal $\hat{s}_j^{(s)}(t)$ corresponds to the estimated signal of user j at stage s. This signal is reconstructed according to:

$$\hat{s}_k^{(s)}(t) \quad = \quad \frac{2}{T} a_k(t - \tau_k) \cos(\omega_c t + \phi_k) \sum_{i=-\infty}^{\infty} \left| Z_{k,i}^{(s)} \right| b_{k,i}^{(s)} p_{_T}(t - iT - \tau_k). \tag{4.5}$$

where $b_{k,i}^{(s)}$ is the i^{th} bit estimate for user k at stage s, and $p_{_T}(t)$ is a unit pulse function of duration T equal to the bit period. The bit estimates $b_{k,i}^{(s)}$ are computed by thresholding the decision metrics.

$$b_{k,i}^{(s)} = sgn[Z_{k,i}^{(s)}]. \tag{4.6}$$

4.2 Analysis of Bias in the Decision Statistics

In this section, the decision statistic for the direct parallel interference cancellation structure is derived. From the derivation, it becomes apparent that a bias in the the decision statistics due to MAI ans imperfect cancellation exists.

In a direct implementation of multistage parallel interference cancellation, estimates of each user's received signal are computed at each stage in parallel by attempting to *completely* subtract out the estimated MAI from all other users from the received signal. Improved estimates can then be obtained from each of the updated user signals with reduced MAI. This process can be repeated iteratively in multiple stages.

One of the major concerns in practical implementations of multiuser receivers is computational complexity. In our implementation, a bank of matched filters is used, at each stage, for soft joint estimation of the transmitted bits and the received signal amplitudes in order to lessen the overall complexity of the multistage parallel cancellation receiver. Complete subtraction of the estimated MAI reduces the multiple access interference affecting each user. A side benefit of this approach is its analytical tractability.

The performance of the soft-decision approach can be improved further by using a moving average estimator for the received amplitudes, where the length of the window is determined by the coherence time of the channel [59]. Use of separate adaptive channel estimation algorithms can lead to enhanced performance. In [51], adaptive channel estimation filters significantly improve the quality of the channel coefficient estimates with moderate additional complexity.

As shown below, straightforward implementation of parallel interference cancellation based on complete subtraction results in biased decision statistics. The bias has its strongest effect on the decision statistics in the first stage of interference cancellation. In subsequent stages of cancellation, the influence of the bias diminishes. However, if this bias leads to incorrect cancellation at the first stage, the residual effects of these errors may be observed at subsequent stages.

For clarity, first consider a two user ($K = 2$) system with no multipath. The path subscript l is then omitted to simplify notation. Since only relative delays and phases are important, set $\phi_1 = 0$, $\tau_1 = 0$, $\phi_2 = \phi$, and $\tau_2 = \tau$. Following the notation of [77, 78], the decision statistic at stage $s = 1$ (i.e. before any interference cancellation) for $b_i^{(1)}$, the i^{th} bit of user 1 is:

$$Z_{1,i}^{(s=1)} = T\sqrt{\frac{P_1}{2}}b_i^{(1)} + \sqrt{\frac{P_2}{2}}\cos(\phi)[b_{i-1}^{(2)}R_{2,1}(\tau) + b_i^{(2)}\hat{R}_{2,1}(\tau)] + \eta_i^{(1)}, \tag{4.7}$$

where,

$$\eta_i^{(k)} = \int_{iT+\tau_k}^{(i+1)T+\tau_k} n(t)a_k(t-\tau_k)cos(\omega_c t + \phi_k)dt, \tag{4.8}$$

and $R_{2,1}(\tau)$ and $\hat{R}_{2,1}(\tau)$ are the continuous-time partial cross-correlation functions of the first and the second signature sequences defined by $R_{k,i}(\tau) = \int_0^\tau a_k(t-\tau)a_i(t)dt$ and $\hat{R}_{k,i}(\tau) = \int_\tau^T a_k(t-\tau)a_i(t)dt$ for $0 \leq \tau \leq T$. Figure 4.1 illustrates these definitions.

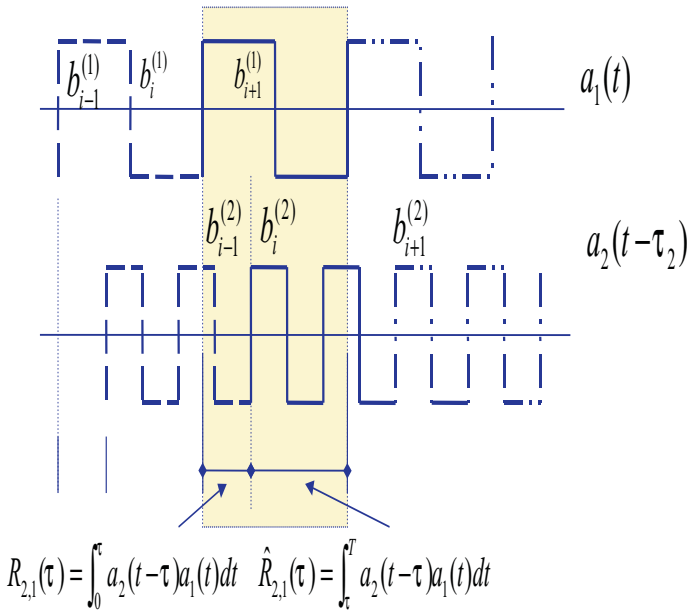

Figure 4.1: Asynchronous waveforms for a two-user channel.

Similarly, for user 2 at stage $s = 1$ the decision statistic is given by:

$$Z_{2,i}^{(s=1)} = T\sqrt{\frac{P_2}{2}}b_i^{(2)} + \sqrt{\frac{P_1}{2}}\cos(\phi)[b_i^{(1)}\hat{R}_{2,1}(\tau) + b_{i+1}^{(1)}R_{2,1}(\tau)] + \eta_i^{(2)}. \tag{4.9}$$

At stage 2, the estimated signal for user 2 obtained via equation (4.5), is subtracted from the received signal $r(t)$ to form a new estimated received signal for user 1 at stage 2. Using equation (4.3) to compute the decision statistic for user 1 at stage 2 leads to the expression:

$$Z_{1,i}^{(2)} = Z_{1,i}^{(1)} - \frac{\cos(\phi)}{T}\left[Z_{2,i-1}^{(1)}R_{2,1}(\tau) + Z_{2,i}^{(1)}\hat{R}_{2,1}(\tau)\right]. \tag{4.10}$$

Substituting into (4.10) the expression for the decision statistics of users 1 and 2 from equations (4.7) and (4.9), and canceling common terms, one obtains:

$$\begin{aligned} Z_{1,i}^{(2)} = T\sqrt{\frac{P_1}{2}}b_i^{(1)} - \frac{\cos^2(\phi)}{T}\sqrt{\frac{P_1}{2}}\Big[&b_{i-1}^{(1)}\hat{R}_{2,1}(\tau)R_{2,1}(\tau) + \\ &b_i^{(1)}R_{2,1}^2(\tau) + b_i^{(1)}\hat{R}_{2,1}^2(\tau) + b_{i+1}^{(1)}R_{2,1}(\tau)\hat{R}_{2,1}(\tau)\Big] + \\ &\eta_i^{(1)} - \frac{\cos(\phi)}{T}\left[\eta_{i-1}^{(2)}R_{2,1}(\tau) + \eta_i^{(2)}\hat{R}_{2,1}(\tau)\right]. \end{aligned} \tag{4.11}$$

Conditioning on $b_i^{(1)}$ and taking the expected value of the decision statistic, yields:

$$E\{Z_{1,i}^{(2)}|b_i^{(1)}\} = T\sqrt{\frac{P_1}{2}}b_i^{(1)} - \sqrt{\frac{P_1}{2}}b_i^{(1)}E\{\frac{\cos^2(\phi)}{T}\}E\{(R_{2,1}^2(\tau) + \hat{R}_{2,1}^2(\tau))\}. \quad (4.12)$$

For random sequences $E\{(R_{2,1}(\tau)\hat{R}_{2,1}(\tau)\} \cong 0$, therefore the expectation $E\{(R_{2,1}^2(\tau) + \hat{R}_{2,1}^2(\tau))\}$ in equation (4.12) can be expressed as $E\{(R_{2,1}(\tau) + \hat{R}_{2,1}(\tau))^2\}$. Equation (4.12) can be formulated as:

$$E\{Z_{1,i}^{(2)}|b_i^{(1)}\} = T\sqrt{\frac{P_1}{2}}b_i^{(1)} - \sqrt{\frac{P_1}{2}}b_i^{(1)}E\{\frac{\cos^2(\phi)}{T}\}E\{(R_{2,1}(\tau) + \hat{R}_{2,1}(\tau))^2\}. \quad (4.13)$$

To evaluate this expression, note that $E\{(R_{2,1}(\tau) + \hat{R}_{2,1}(\tau))^2\}$ corresponds to the variance of $\int_0^T a_2(t-\tau)a_1(t)dt$ for a pair of randomly selected sequences since $R_{2,1}(\tau) + \hat{R}_{2,1}(\tau) = \int_0^T a_2(t-\tau)a_1(t)dt$, and $E\{(R_{2,1}(\tau) + \hat{R}_{2,1}(\tau))\} \cong 0$. The variance of this random variable (normalized for rectangular chips of period $T_c = 1$) has been shown to equal $2N/3$ using the underlying discrete cross-correlation functions [78, 79], and modeling interference as a white noise process passing through a tandem combination of two filters matched to each other [2].

Using this result and normalizing for $T_c = 1$, Equation (4.13) becomes:

$$E\{Z_{1,i}^{(2)}|b_i^{(1)}\} = N\sqrt{\frac{P_1}{2}}b_i^{(1)}\left[1 - \frac{1}{3N}\right]. \quad (4.14)$$

Since the estimates of the interfering signals are correlated with the desired user's power and bit value, a bias is produced when they are used to reconstruct and remove the interference.

For the two user case, Equation (4.14) shows a bias of $(-1/3N)$ in the mean of the decision statistics. Extension of this result to a K-user system is straightforward. For K independent users with random signature sequences, following a similar approach one obtains:

$$E\{Z_{1,i}^{(2)}|b_i^{(1)}\} = N\sqrt{\frac{P_1}{2}}b_i^{(1)}\left[1 - \frac{(K-1)}{3N}\right]. \quad (4.15)$$

From this equation, the bias in the mean increases linearly with system loading and is inversely proportional to the processing gain N. Similar behavior is also seen in the synchronous case [28]. However, most analyses, including our previous work [58, 74], assume independence between stages. Since the estimates of the interfering signals are correlated with the desired user's power and bit value, a bias is produced when they are used to remove the interference.

4.3 Mitigation of Bias through use of Partial Interference Cancellation

In this section we propose a simple yet effective way to mitigate the effect of the bias and improve performance of a parallel multistage interference cancellation receiver.

A simple yet effective way to mitigate the effect of the bias and improve the performance of a parallel multistage interference cancellation receiver is based on multiplying the channel gain estimates before signal reconstruction by a partial-cancellation factor $0 \leq C_K^{(s)} \leq 1$ that varies with the stage of cancellation s and system loading K. In this case, the decision metric of Equation (4.5) becomes:

$$\hat{s}_j^{(s)}(t) = \frac{2C_K^{(s)}}{T} a_j(t) \cos(\omega_c t + \phi_j) \sum_{i=-\infty}^{\infty} Z_{j,i}^{(s)} p_T(t - iT). \tag{4.16}$$

This can also be interpreted as modifying the complete cancellation scheme of Equations (4.4) and (4.5) to include the partial-cancellation factor $C_K^{(s)}$ as follows:

$$\hat{r}_k^{(s)}(t) = r(t) - C_K^{(s)} \sum_{j \neq k} \hat{s}_j^{(s)}(t), \tag{4.17}$$

Multiplicative factors less than one for interference cancellation have also been used in the derivation of an iterative approach based on maximum likelihood considerations [28, 30], mentioned in [80], and attributed to the general unreliability of the estimates at early stages.

An analysis similar to that used earlier in this section shows that the expected value of the decision statistics of the partial interference cancellation approach is given by:

$$E\{Z_{1,i}^{(2)} | b_i^{(1)}\} = N\sqrt{\frac{P_1}{2}} b_i^{(1)} \left[1 - \frac{C_K^{(2)}(K-1)}{3N}\right]. \tag{4.18}$$

The effect of the partial-cancellation factor on the mean and the variance of the decision statistics for a two stage parallel cancellation receiver with $C_K^{(2)} = 0.5$ can be seen in Figure 4.2 and Figure 4.3 respectively. The beneficial effects of partial-cancellation become apparent from a comparison with the full cancellation approach.

When $Z_{k,i}^{(s)}$ is an unbiased estimate, it has been shown in [74] employing the standard Gaussian approximation, that in an AWGN channel the analytical bit error performance of the multistage

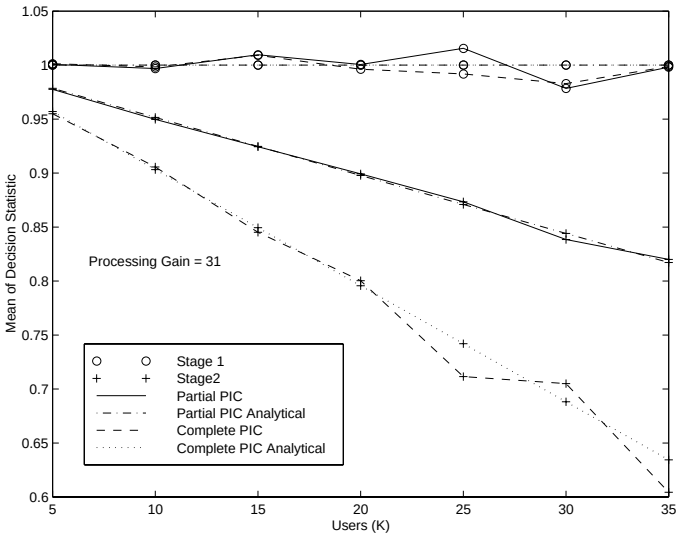

Figure 4.2: Analytical and simulation results for the mean of the decision statistics for a two stage receiver using complete cancellation, and the proposed partial cancellation technique with $C_K^{(2)} = 0.5$. ($N = 31$, $N_o = 0$).

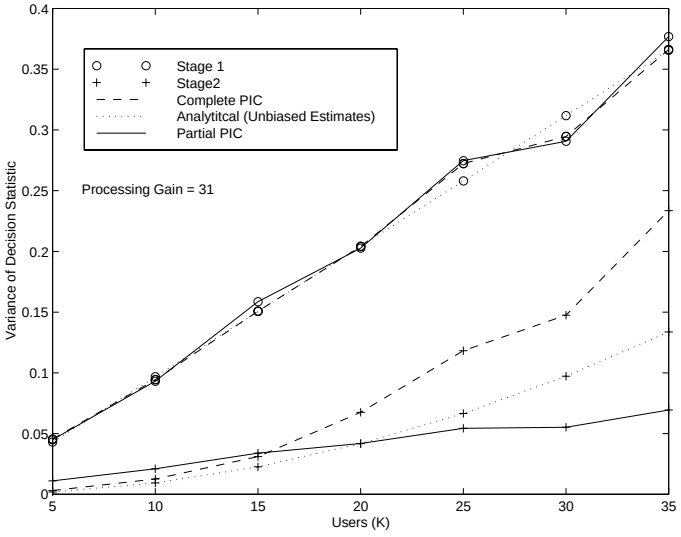

Figure 4.3: Variance of the decision statistics for the complete cancellation and the proposed partial interference cancellation technique. Simulation and analytical results (assuming unbiased estimation) for a two stage receiver with $C_K^{(2)} = 0.5$ ($N = 31$, $N_o = 0$).

parallel cancellation approach for user k at stage s for BPSK is:

$$P_k^{(s)}(E) = Q\left(\left[\frac{1}{2E_b/N_o}\left(\frac{1-\left(\frac{K-1}{3N}\right)^s}{1-\frac{K-1}{3N}}\right)+\frac{1}{(3N)^s}\right.\right.$$
$$\left.\left.\times\left(\frac{(K-1)^s-(-1)^s}{K}\frac{\sum_{j\neq k}P_j}{P_k}+(-1)^s\right)\right]^{-1/2}\right), \tag{4.19}$$

where K is the number of users and N is the processing gain.

Figure 4.4 shows the probability of bit error vs. the number of users K (with random spreading codes) for the complete-cancellation approach, the partial-cancellation approach, and the analytical results for the case of unbiased estimation. For these simulations, a sub-optimal implementation of the partial cancellation approach was employed. In it, the partial cancellation receiver uses a single constant partial-cancellation factor for the first stage of cancellation (in this case $C_K^{(2)} = 0.5$) and in the following stages performs complete cancellation. The justification for this approach is that after the first stage of cancellation, the estimates are much more reliable. Thus in stages $s > 2$, bias mitigation is practically unnecessary.

Comparison of the capacity curves show that use of the proposed receiver structure results in significant performance improvements over the full parallel cancellation approach. In fact, the results for the third stage of the proposed receiver are very close to those that would be obtained with unbiased estimation. The significant improvements in capacity offered by the partial cancellation approach are evident.

Another example of enhanced in performance offered by the partial-cancellation technique over the complete-cancellation implementation is observed in Figure 4.5.

Both receivers make use of Rake receivers and maximal ratio combining. The channel is a 2-ray frequency selective Rayleigh fading channel with parameters taken from measurement data presented in [81], and correspond to one strong main path and a weak second path ($\sigma_1 = 0.93$ and $\sigma_2 = 0.28$, $E\{r_i^2\} = 2\sigma_i^2$). The partial-cancellation factor for the second stage is 0.5 and the third stage performs complete cancellation. Figure 4.5 shows that for these conditions, two stages of the partial-cancellation technique provide better performance than three stages of the direct approach. Also, after three stages of interference cancellation, the simplified partial-cancellation technique achieves about one order-of-magnitude improvement in BER compared to the direct

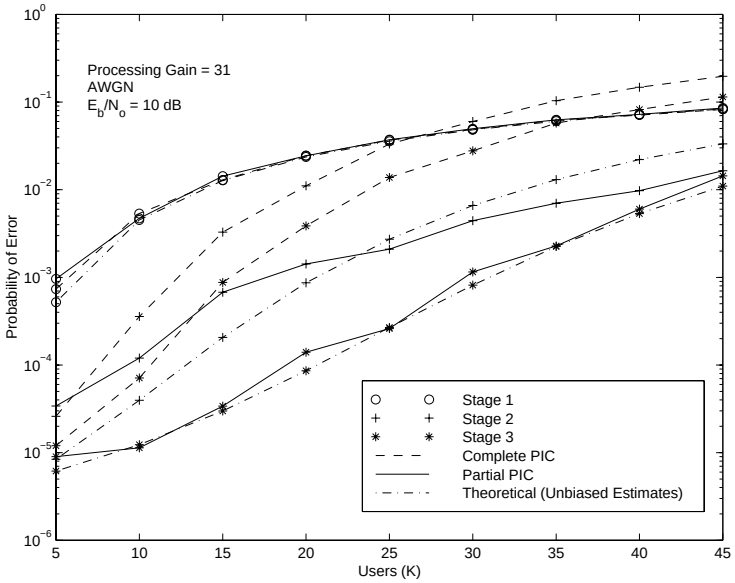

Figure 4.4: Simulated probability of bit error vs. number of users K for the complete parallel cancellation and the partial parallel interference cancellation approach used in the DSP implementation ($E_b/N_o = 10$ dB, and $N = 31$, with $C_K^{(2)} = 0.5$ and $C_K^{(3)} = 1$).

implementation .

In many situations, the near-far effect can be a limiting factor of a DS-CDMA receiver's performance. In order to analyze the near-far resistance of the proposed technique, performance is examined for three desired users in the presence of a fourth user whose power varies from 20 dB below the power of the desired users to 30 dB above. Figure 4.6 shows that over a wide range of power disparities, the proposed scheme shows near-far robustness. It is also interesting to note that even though the near-far resistance of the second stage of the proposed receiver is inferior to that of direct interference cancellation, in stage three the proposed scheme reaps the benefits of bias-mitigation and outperforms the direct approach.

Until now, we have assumed that the receiver structure under study achieves and maintains perfect symbol synchronization during operation. In a more realistic scenario, however, this assumption does not hold and the decision statistics are adversely affected by clock instabilities, propagation channel uncertainties and movement of the radios. Figure 4.7 shows the effect of delay estimation errors on the performance of the proposed receiver. The estimation error is assumed to be a

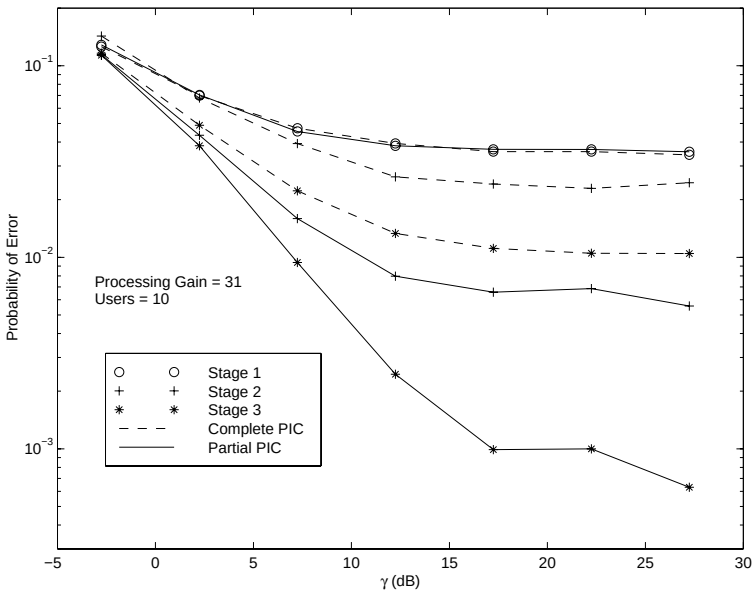

Figure 4.5: BER vs. Average E_b/N_o comparison between complete cancellation and partial cancellation (with $C_K^{(2)} = 0.5$ and $C_K^{(3)} = 1$) for a 2-ray frequency selective Rayleigh fading channel ($\sigma_1 = 0.93$ and $\sigma_2 = 0.28$, $N = 31$).

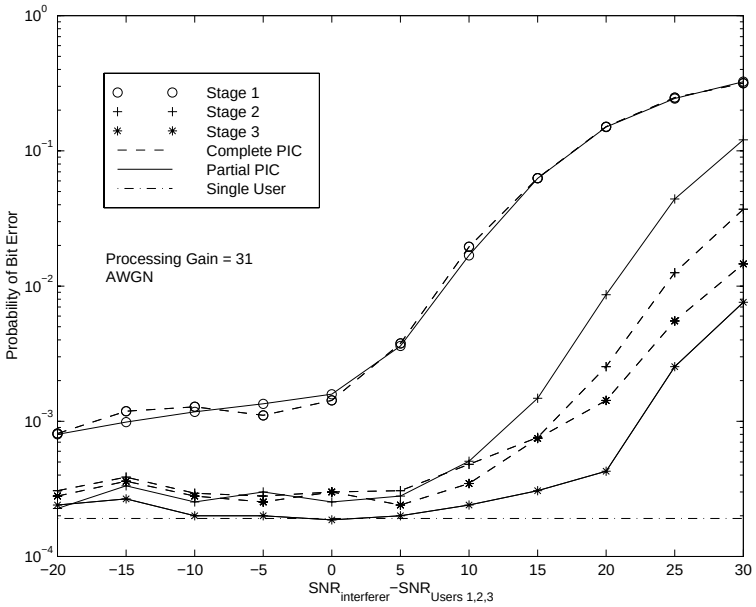

Figure 4.6: BER performance degradation in near-far AWGN channels (3 users with $\overline{E_b/N_o} = 8$ dB, 1 interferer with varying power. $C_K^{(2)} = 0.75$ and $C_K^{(3)} = 1$, $N = 31$).

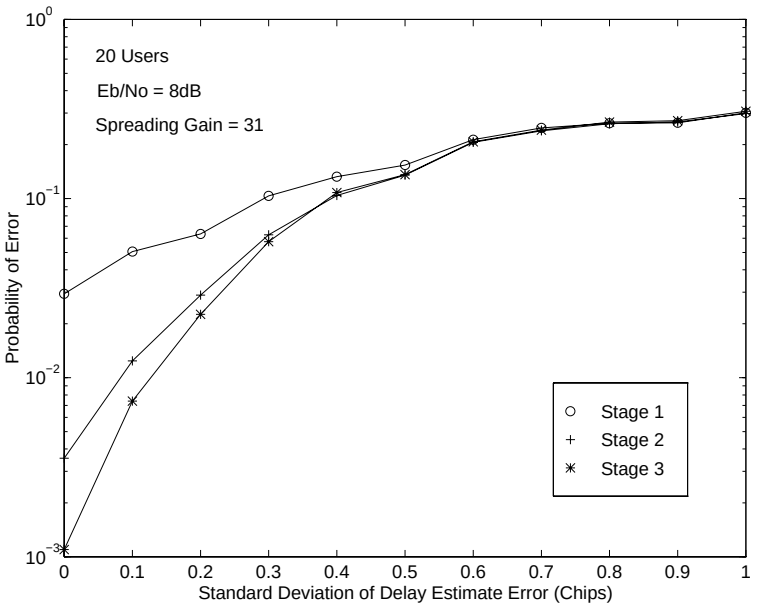

Figure 4.7: Effects of symbol timing synchronization errors on system performance for partial cancellation in AWGN channels ($C_K^{(2)} = 0.5$, $C_K^{(3)} = 1$ and $N = 31$).

Gaussian random variable of zero mean and a given standard deviation measured in fractions of a chip. The simulation results indicate that the proposed receiver structure displays robustness to moderate synchronization and timing errors. A more detailed analysis of the effects of timing and phase synchronization errors for the multistage parallel cancellation approach is given in [58].

Another attractive feature of the proposed receiver structure is that it lends itself to differentially coherent implementation. In this case, the need for phase estimation and tracking is avoided. Processing is performed on the in-phase and quadrature components of the received signal. Decisions are made on the estimates produced by projecting the current complex-valued decision statistic onto the previous one.

4.4 Conclusions

In this chapter we have identified a bias in the decision statistics for a direct implementation of the parallel interference cancellation approach. A very simple technique is proposed to mitigate

the negative effects produced by the bias. The proposed technique shows near-far robustness and provides significant improvements in CDMA system performance over the direct implementation of parallel interference cancellation.

Chapter 5

Hardware Implementation of Interference Cancellation

Implementation of advanced DS-CDMA receivers based on multiuser detection principles is becoming a reality thanks to the combination of an improved understanding of the theoretical basis of multiuser detection and advances in digital, mixed-signal, and RF technologies. In the previous chapter, the source of the bias was explicitly recognized and a partial interference cancellation scheme that reduces the negative effects of biased estimation and significantly improves system performance was proposed. In this chapter, a practical real-time algorithm that significantly reduces the implementation complexity of the parallel cancellation scheme without sacrificing performance is derived. To facilitate a software radio implementation, the signal processing complexity of the approach is characterized.

The real-time processing algorithm is tested via software implementation on a general purpose floating-point DSP. The hardware test setup is described and the results are presented and compared with simulation and analytical results. The experimental results confirm the simulation and analytical results, showing large performance gains over the conventional matched filter.

The intent is to develop a practical implementation of an advanced DS-CDMA receiver based on multiuser detection principles. In chapter 3, the performance of several major receiver structures for a variety of situations and channel conditions have been examined. Comparative performance

and computational complexity results based on theoretical and simulation analyses are presented in [9]. Figure 3.10 shows the probability of bit error vs. the number of users K for several multiuser detection schemes. For a practical implementation, the multistage parallel interference cancellation approach of [25] is attractive in terms of performance, computational complexity, and robustness to moderate phase jitter and synchronization errors [58].

Part of the power in the software radio concept is that it allows innovative algorithms and their implementation to be considered in an integrated manner. In this chapter, a practical real-time implementation of a coherent and a non-coherent multiuser detector based on the proposed parallel partial cancellation approach is presented along with experimental tests that confirm significant performance improvements over the conventional receiver. The austerity of the receiver enables the practical application of the joint detection principles described in this document to future commercial DS-CDMA systems. Extension to multi-sensor reception may be accomplished via integration with a flexible multi-sensor testbed. A testbed has been constructed at the MPRG that can be used to prototype adaptive antennas and may be extended for multiuser algorithm development [82]. While the work here considers only a single antenna element, the algorithms could be extended to multiple antennas.

This hardware prototype has been developed as part of the Defense Advanced Research Projects Agency (DARPA)'s Global Mobile Information Systems (GloMo) initiative [83]. This implementation is, to our knowledge, the first working prototype of the parallel interference cancellation technique, though, development activities are also underway at a number of research institutes.

Computational complexity is a primary issue that affects the selection of a multiuser detection algorithm for real-time implementation. Although subtractive interference cancellation multiuser receivers are computationally efficient in comparison to other approaches, the parallel cancellation approach can be simplified even further. This section presents a simple technique for dramatically reducing the complexity of the decision statistics in the multistage parallel interference cancellation scheme.

5.1 Coherent Implementation

Coherent detection may be used when phase estimation and tracking can be performed accurately. This is accomplished through the use of an unmodulated auxiliary pilot signal for channel estimation. In a DSP implementation employing harmonic sampling, the input RF signal is filtered and mixed down to an intermediate frequency (IF) by an analog front end. After IF sampling, a digital down-converter, such as the Analog Devices AD6620, Harris HSP50214 or GrayChip GC1012, is then used to translate the desired signal to its baseband In-phase and Quadrature (I&Q) components. For analysis and implementation of the baseband processing strategy, it is advantageous to resort to a complex-envelope representation. The baseband signal from the digital downconverters corresponds to:

$$r(t) = \sum_{k=1}^{K} s_k(t - \tau_k) + n(t), \tag{5.1}$$

where the received baseband signal from user k corresponds to a binary phase modulated waveform:

$$s_k(t) = \sqrt{P_k} a_k(t) b_k(t) e^{j\theta_k}, \tag{5.2}$$

and θ_k is the received phase of the kth user relative to some reference phase.

Using complex envelope representation, the decision statistics of Equation (3.46) (now scaled by a factor of $1/T$) may be expressed as:

$$Z_{k,i}^{(s)} \quad = \quad Y_{I_{k,i}}^{(s)} \cos(\theta_k) + Y_{Q_{k,i}}^{(s)} \sin(\theta_k), \tag{5.3}$$

where the decision metrics $Y_{I_{k,i}}^{(s)}$ and $Y_{Q_{k,i}}^{(s)}$ correspond to the I&Q outputs of a bank of matched filters for the i^{th} bit of the k^{th} user after s stages of cancellation. The In-phase and Quadrature correlation metrics can be expressed as:

$$Y_{I_{k,i}}^{(s+1)} = \frac{1}{T} \int_{(i-1)T+\tau_k}^{iT+\tau_k} \hat{r}_{I_k}^{(s)}(t) a_k(t - \tau_k) dt \tag{5.4}$$

$$Y_{Q_{k,i}}^{(s+1)} = \frac{1}{T} \int_{(i-1)T+\tau_k}^{iT+\tau_k} \hat{r}_{Q_k}^{(s)}(t) a_k(t - \tau_k) dt, \tag{5.5}$$

where the received complex-baseband signal $\hat{r}_k^{(s)}(t)$ at stage s for user k is generated by subtracting the estimated MAI from the from the received signal:

$$\hat{r}_{I_k}^{(s)}(t) = r_I(t) - \sum_{j=1, j\neq k}^{K} \hat{s}_{I_j}^{(s)}(t - \tau_j) \tag{5.6}$$

$$\hat{r}_{Q_k}^{(s)}(t) = r_Q(t) - \sum_{j=1, j\neq k}^{K} \hat{s}_{Q_j}^{(s)}(t-\tau_j). \tag{5.7}$$

Signal $\hat{s}_j^{(s)}$ corresponds to the complex-valued signal for user j at stage s, reconstructed using the decision statistic $Z_{j,i}^{(s)}$ which provides a combined estimate of the data bit and the signal amplitude:

$$\hat{s}_{I_j}^{(s)}(t) = a_j(t) \sum_{i=-\infty}^{\infty} C_j^{(s)} Z_{j,i}^{(s)} p_{_T}(t-iT)\cos(\phi_j) \tag{5.8}$$

$$\hat{s}_{Q_j}^{(s)}(t) = a_j(t) \sum_{i=-\infty}^{\infty} C_j^{(s)} Z_{j,i}^{(s)} p_{_T}(t-iT)\sin(\phi_j), \tag{5.9}$$

where $p_{_T}(t)$ is a unit pulse function of duration T equal to the bit period and $C_j^{(s)}$ is the partial-cancellation multiplicative factor used for bias mitigation. This notation allows the use of a different cancellation factor for every user to optimize system performance for different channel conditions and for unequal received powers. Derivation of the optimal partial-cancellation factor has been studied in [75].

For parallel interference cancellation, the approach described by Equations (5.6) and (5.7) is conceptually attractive since it makes the underlying idea of interference cancellation simple to understand. However this approach also entails a computational complexity of $O(K^2)$, since for each of the K users reconstruction of the MAI affecting each signal is accomplished by adding the estimated signals of the remaining $K-1$ users. As the number of users increases, the complexity of this approach grows rapidly.

In the implementation, a theoretically equivalent approach reduces the complexity of the re-estimation scheme to $O(K)$ [59]. A block diagram of this approach is shown in Figure 5.1.

The reduced complexity approach used in the DSP implementation is summarized as follows:
First, a residual signal $\tilde{r}(t)$ is created by subtracting from the received signal the sum of the estimated received signals from *all* users:

$$\tilde{r}_I^{(s)}(t) = r_I(t) - \sum_{j=1}^{K} \hat{s}_{I_j}^{(s)}(t-\tau_j) \tag{5.10}$$

$$\tilde{r}_Q^{(s)}(t) = r_Q(t) - \sum_{j=1}^{K} \hat{s}_{Q_j}^{(s)}(t-\tau_j), \tag{5.11}$$

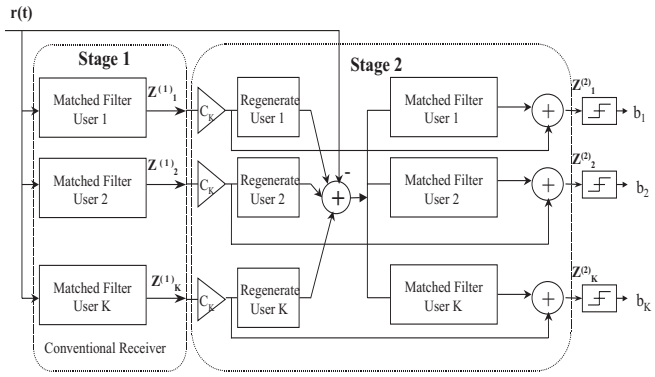

Figure 5.1: Block diagram of the coherent parallel partial interference cancellation receiver.

where $\hat{s}_{I_j}^{(s)}(t)$ and $\hat{s}_{Q_j}^{(s)}(t)$ are defined in Equations (5.8) and (5.9). With these definitions, $\hat{r}_{I_k}^{(s)}(t)$ and $\hat{r}_{Q_k}^{(s)}(t)$ correspond to:

$$\hat{r}_{I_k}^{(s)}(t) = \hat{s}_{I_k}^{(s)}(t-\tau_k) + \tilde{r}_I^{(s)}(t) \tag{5.12}$$

$$\hat{r}_{Q_k}^{(s)}(t) = \hat{s}_{Q_k}^{(s)}(t-\tau_k) + \tilde{r}_Q^{(s)}(t). \tag{5.13}$$

Substituting these expressions into Equations (5.4) and (5.5) gives:

$$Y_{I_{k,i}}^{(s+1)} = \frac{1}{T}\int_{(i-1)T+\tau_k}^{iT+\tau_k} (\hat{s}_{I_k}^{(s)}(t-\tau_k) + \tilde{r}_I^{(s)}(t))a_k(t-\tau_k)dt, \tag{5.14}$$

$$Y_{Q_{k,i}}^{(s+1)} = \frac{1}{T}\int_{(i-1)T+\tau_k}^{iT+\tau_k} (\hat{s}_{Q_k}^{(s)}(t-\tau_k) + \tilde{r}_Q^{(s)}(t))a_k(t-\tau_k)dt, \tag{5.15}$$

Substituting the definitions of Equations (5.8) and (5.9) for the reconstructed signals $\hat{s}_{I_k}^{(s)}$(t) and $\hat{s}_{Q_k}^{(s)}(t)$ of user k into the previous equations, the decision statistics after s stages of cancellation in Equations (5.14) and (5.15) reduce to:

$$Y_{I_{k,i}}^{(s+1)} = C_k^{(s)} Z_{k,i}^{(s)} \cos(\theta_k) + \frac{1}{T}\int_{(i-1)T+\tau_k}^{iT+\tau_k} \tilde{r}_I^{(s)}(t)a_k(t-\tau_k)dt \tag{5.16}$$

and

$$Y_{Q_{k,i}}^{(s+1)} = C_k^{(s)} Z_{k,i}^{(s)} \sin(\theta_k) + \frac{1}{T} \int_{(i-1)T+\tau_k}^{iT+\tau_k} \tilde{r}_Q^{(s)}(t) a_k(t-\tau_k) dt. \tag{5.17}$$

The improved decision statistics are computed according to Equation (5.3) using the decision statistics $Z_{k,i}^{(s)}$ obtained in the previous stage and a correction factor that is computed using the complex-valued residual signal $\tilde{r}(t)^{(s)}$:

$$Z_{k,i}^{(s+1)} = C_k^{(s)} Z_{k,i}^{(s)} + \mathcal{R}e \left[\int_{(i-1)T+\tau_k}^{iT+\tau_k} \tilde{r}^{(s)}(t) a_k(t-\tau_k) e^{-j\phi_k} dt \right] \tag{5.18}$$

The dramatic reduction in computational complexity over the straightforward full cancellation approach of Equations (5.6) and (5.7) stems from the fact that the residual signal is identical for all users and thus needs to be generated only once per stage.

5.2 Non-Coherent Implementation

An implementation of the proposed receiver that does not require a coherent phase reference and employs differentially encoded BPSK has also been developed. The notion of non-coherent multiuser demodulation of differentially phase-shift keyed DS-CDMA signals has been addressed in [62, 61, 84]. An alternate approach based on M-ary orthogonal modulation and OQPSK has been explored in [22]. Use of differential detection and multistage parallel interference cancellation has also been addressed in [9] where a BER performance comparison presented as well for various non-coherent multiuser receivers. Here we focus on a reduced complexity approach for practical implementation. In this receiver, the In-Phase and Quadrature decision statistics of Equations (5.4) and (5.5) are used directly for estimation of the amplitudes, symbols and relative phases of the received signals. The approach of the non-coherent implementation is similar to that of the coherent approach. A block diagram of the receiver is presented in Figure 5.2.

The received baseband signal $\hat{r}_k^{(s)}(t)$ at stage s for user k is generated by subtracting the reconstructed MAI caused by undesired users, from the received signal:

$$\hat{r}_{I_k}^{(s)}(t) = r_I(t) - \sum_{j=1, j\neq k}^{K} \hat{s}_{I_j}^{(s)}(t-\tau_j) \tag{5.19}$$

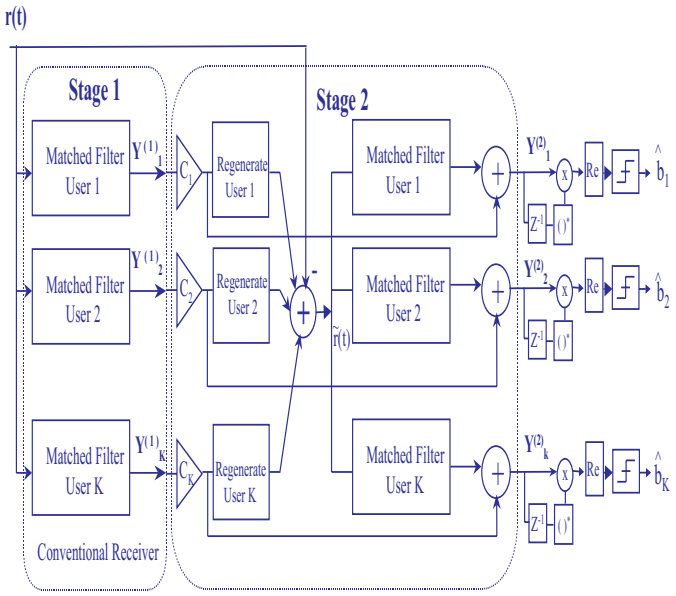

Figure 5.2: Block diagram of the differentially coherent parallel partial interference cancellation receiver.

$$\hat{r}_{Q_k}^{(s)}(t) = r_Q(t) - \sum_{j=1, j\neq k}^{K} \hat{s}_{Q_j}^{(s)}(t - \tau_j). \tag{5.20}$$

Equations (5.19) and (5.20) are introduced for the purpose of clarity. In the actual implementation of the non-coherent receiver, the previously discussed residual signal approach was also employed in order to reduce computational complexity.

The In-phase and Quadrature outputs of the matched filter bank at stage s are:

$$Y_{I_{k,i}}^{(s+1)} = \frac{1}{T} \int_{(i-1)T+\tau_k}^{iT+\tau_k} \hat{r}_{I_k}^{(s)}(t) a_k(t - \tau_k) dt \tag{5.21}$$

$$Y_{Q_{k,i}}^{(s+1)} = \frac{1}{T} \int_{(i-1)T+\tau_k}^{iT+\tau_k} \hat{r}_{Q_k}^{(s)}(t) a_k(t - \tau_k) dt. \tag{5.22}$$

In the non-coherent implementation, the In-phase and Quadrature components of the complex-valued signal $\hat{s}_j^{(s)}$ for user j at stage s, are reconstructed from the decision statistics $Y_{I_{j,i}}^{(s)}$ and $Y_{Q_{j,i}}^{(s)}$ obtained in the previous stage as follows:

$$\hat{s}_{I_j}^{(s)}(t) = a_j(t) \sum_{i=-\infty}^{\infty} C_j^{(s)} Y_{I_{j,i}}^{(s)} p_T(t - iT) \tag{5.23}$$

$$\hat{s}_{Q_j}^{(s)}(t) = a_j(t) \sum_{i=-\infty}^{\infty} C_j^{(s)} Y_{Q_{j,i}}^{(s)} p_T(t - iT), \tag{5.24}$$

where $C_j^{(s)}$ is the partial-cancellation multiplicative factor used for bias mitigation for user j. Note that information about the user's phases is embedded in the correlation metrics $Y_{I_{j,i}}^{(s)}$ and $Y_{Q_{j,i}}^{(s)}$.

Using the residual signal, the signals $\hat{r}_{I_k}^{(s)}(t)$ and $\hat{r}_{Q_k}^{(s)}(t)$ of Equations (5.19) and (5.20) can be expressed as:

$$\hat{r}_{I_k}^{(s)}(t) = \hat{s}_{I_k}^{(s)}(t - \tau_k) + \tilde{r}_I^{(s)}(t) \tag{5.25}$$

$$\hat{r}_{Q_k}^{(s)}(t) = \hat{s}_{Q_k}^{(s)}(t - \tau_k) + \tilde{r}_Q^{(s)}(t). \tag{5.26}$$

Substituting these expressions into Equations (5.21) and (5.22), and using the definitions of Equations (5.23) and (5.24), the decision statistics after s stages of cancellation are reduced to:

$$Y_{I_{k,i}}^{(s+1)} = C_k^{(s)} Y_{I_{k,i}}^{(s)} + \frac{1}{T} \int_{(i-1)T+\tau_k}^{iT+\tau_k} \tilde{r}_I^{(s)}(t) a_k(t - \tau_k) dt \tag{5.27}$$

and

$$Y_{Q_{k,i}}^{(s+1)} = C_k^{(s)} Y_{Qk,i}^{(s)} + \frac{1}{T} \int_{(i-1)T+\tau_k}^{iT+\tau_k} \tilde{r}_Q^{(s)}(t) a_k(t - \tau_k) dt. \tag{5.28}$$

Decisions are made on the estimates produced by projecting the current complex-valued decision statistic onto the previous one. The phase of the resulting complex number is then used as an estimate of the phase difference between consecutive symbols:

$$Z_{k,i}^{(s)} = \mathcal{R}e \left[Y_{k,i}^{(s)} (Y_{k,i-1}^{(s)})^* \right], \tag{5.29}$$

In terms of the complex envelope representation, the decision statistics for differential decoding are thus given by:

$$Z_{k,i}^{(s)} = Y_{I_{k,i}}^{(s)} Y_{I_{k,i-1}}^{(s)} + Y_{Q_{k,i}}^{(s)} Y_{Q_{k,i-1}}^{(s)}. \tag{5.30}$$

Thus, while the phase is implicitly estimated for cancellation, it is not used for detection. Figure 5.3 presents BER curves as a function of the number of users in AWGN, obtained via simulation for a multistage non-coherent implementation and an ideal coherent implementation.

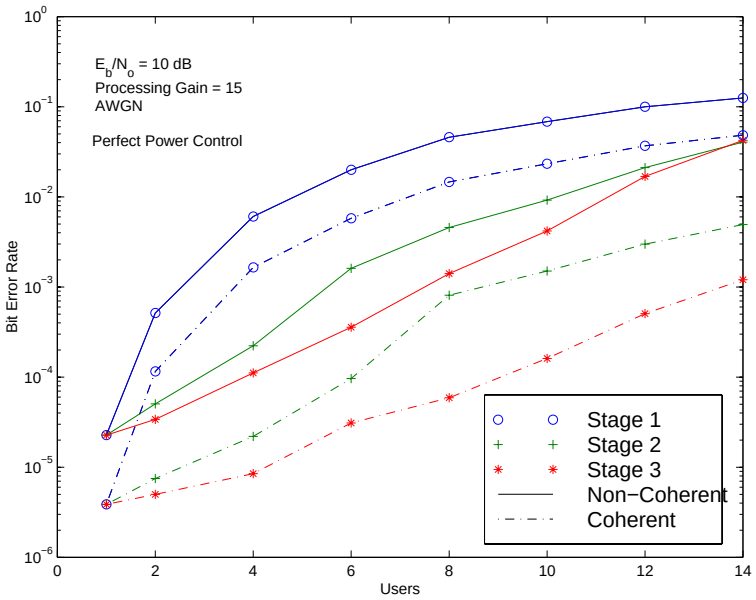

Figure 5.3: Probability of bit error vs. number of users for the non-coherent multiuser receiver, and for an ideal coherent implementation ($N = 15$, $C_k^{(1)} = 1.0$, $C_k^{(2)} = 0.75$ for loads ≤ 6 users and $C_k^{(2)} = 0.5$ for larger loads).

It is interesting to note that as the number of users increases, the relative performance of the non-coherent receiver with respect to the coherent scheme deteriorates. This can be attributed to the degradation of the inherent phase information in the decision statistics caused by increasing levels of MAI.

5.3 Computational Complexity Calculations

In order to quantify the computational complexity of the algorithms for DSP implementation, a processing engine capable of performing single-cycle multifunction operations and zero-overhead looping is assumed. In this processing architecture, multiply and add instructions as well as compute/move operations are performed in parallel in one processor cycle. It is also assumed that the processor is capable of performing multiple memory accesses per instruction cycle.

The computational complexity per bit period of the reduced-complexity algorithm can be computed

in terms of the number of users K, the spreading factor N, the number of samples per chip N_s, the number of fingers in the Rake receiver L, and the number of stages S as follows:

Complex baseband data acquisition, floating point conversion and storage require on the order of $6LNN_s$ operations. The computational burden of this task on the CPU can, however, be reduced significantly by using a separate I/O processing unit. Implementation of the correlation demodulator stage involves correlation in the I & Q arms, multiplication of the decision statistics by the conjugate of the phase, normalization by $1/(NN_s)$ and storage of the soft decision statistics. Execution of these tasks requires $2KLNN_s + 28KL$ operations.

Interference cancellation involves fetching the soft decision statistics, re-spreading the estimated user signals and subtraction of the re-spread signals from the original received signal. This requires $4KLNN_s+32KL$ operations in the case of the reduced complexity approach, and $4(K^2-K)LNN_s+32(K^2-K)L$ operations for the direct approach.

Computation of the improved decision statistics requires correlation of the residual signal with the signature sequences, normalization of the correction factors, multiplication by the conjugate of the user's phase, and addition of the correction factors to the initial decision statistics. This stage can be thought of as another correlation demodulator with computational complexity $2KLNN_s + 28KL$.

In a multistage approach, implementation of multiple stages of interference cancellation and re-estimation is achieved by cascading functional blocks that perform interference cancellation followed by re-estimation. After the desired number of cancellation stages, the final decision statistics for the L branches are computed via maximal ratio combining, an operation which requires $5KL$ operations. Transformation of the soft outputs of the combiner to hard bit decisions is accomplished in K operations.

The conventional receiver, which corresponds to a correlation demodulator, has a computational complexity of $6LNN_s + 2KLNN_s + 33KL + K$. For multistage parallel interference cancellation, the number of operations required with the reduced complexity implementation is approximately $6LNN_s + 2KLNN_s(3S-2) + 60KLS - 27KL + K$. The overall computational complexity of this approach is linear in the number of users. The computational complexity of the direct approach on the other hand corresponds to $6LNN_s + 2KLNN_sS(2K-1) + KLS(32K-4) - 4KLNN_s(K-$

Table 5.1: Estimated and measured number of processing cycles required for implementation of the main functional tasks for interference cancellation.

Task	$N_s = 4$		$N_s = 2$	
	Est.	**Meas.**	**Est.**	**Meas.**
Correlation	592	610	360	374
MAI Cancellation	1088	1103	612	622
Re-Estimation	592	624	360	382
Total	2272	2305	1332	1378

$1) - KL(32K - 37) + K$, a computational complexity that is quadratic in the number of users K.

The preceeding expressions account for the major functional tasks of the algorithm itself and do not account for phase estimation (required for coherent detection, unnecessary with the non-coherent receiver), or synchronization and tracking. Table 5.1 compares the estimated computational complexity for the major functional blocks of the reduced complexity algorithm with measures obtained from profiling sessions of the code running on our DSP platform with $N = 15$, $K = 4$, $L = 1$, $S = 2$, setting the number of samples per chip first to $N_s = 4$, and then to $N_s = 2$.

An advantage of the multistage parallel interference cancellation approach is its suitability for efficient implementation with multiple processors working concurrently. A data flow multiprocessing approach where data passes linearly from one processor to another, and each processor performs a different functional task, can be used to efficiently achieve the required high computational bandwidth. Another advantage of the data flow multiprocessing approach is that it results in a homogeneous scalable system, where the main processing structure is replicated multiple times according to the number of stages of interference cancellation desired.

Although the overall number of required processor cycles remains unchanged, the number of cycles required per processor is significantly reduced. In this case, the most computationally expensive functional task sets the limit in the processing pipeline. For comparison, assume that signal reconstruction and interference cancellation tasks are performed in a single processor, thus dictating the computational requirement of the reduced complexity multiprocessor implementation.

Figure 5.4 shows the number of processing operations per bit for implementation of the different

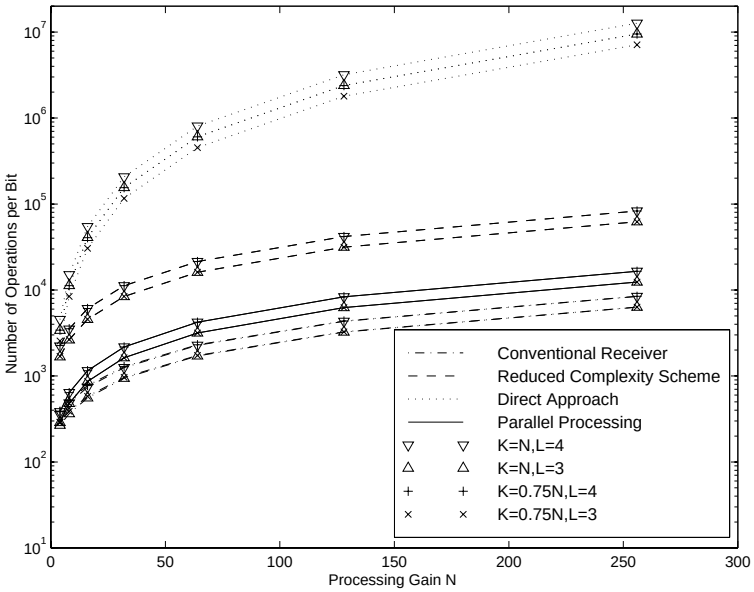

Figure 5.4: Number of operations per user bit vs. processing gain for system loads $K = 0.75N$ and $K = N$, for a receiver with an $L = 3$ and $L = 4$ Rake receiver, $N_s = 4$ samples per chip, and $S = 3$ stages of cancellation.

algorithms as a function of processing gain N for system loads of $K = 0.75N$ and $K = N$. A receiver using an $L = 3$ and $L = 4$ Rake receiver, 4 samples per chip ($N_s = 4$) and three stages of processing ($S = 3$). In this graph, the advantage of using a parallel processing technique is evident, especially for highly loaded systems with large processing gains.

When compared to the classical approach for demodulating multiple users, the proposed reduced complexity implementation does not bring about a significant increase in memory requirements. This is accomplished by using a direct bit-by-bit processing scheme as opposed to a memory intensive block processing approach. Due to the asynchronous nature of the multiple-access channel, buffering of contiguous bits is necessary to avoid overwriting useful data. The proposed algorithm has been successfully implemented using a processing strategy that requires a transitional processing buffer that only encompasses five bit epochs per interference cancellation stage, as opposed to two for the conventional receiver. Other intermediate results such as the correction factors and the intermediate decision statistics require very little additional memory and can be ignored, to a first order approximation.

5.4 Hardware Implementation

5.4.1 DSP Processing

In a DSP implementation of an advanced receiver, the input RF signal can be filtered and mixed down to an IF frequency by an analog front end. After IF sampling, a digital down-converter, such as the AD6620, HSP50214 or GC1012, can then be used to demodulate the desired signal to its baseband in-phase and quadrature components. The continuous in-phase and quadrature signal streams should then be acquired and buffered to memory by the signal processor.

Since the advanced DSP based transceiver must be able to perform all the processing operations required within the application's real time constraints, at the time of this writing it is usually necessary to resort to the use of hand coded assembly language to optimize the code for speed and size. The inefficiencies of high level language compilers make it difficult to fully implement a complex real-time algorithm using these languages. However, a compromise can be reached where only computationally intensive tasks are hand coded in assembly. The advantage of using hand coded assembly is that it allows the designer to take full advantage of the particular hardware capabilities of the processor.

Several families of digital signal processors are available in the market. With increasing support of multiprocessing, computationally intensive algorithms can now be implemented by using multiple processors working in parallel. Although many of the early signal processors were not specifically designed to be used in multiprocessor systems, new processors well suited to multiprocessing applications have become available: Analog Devices ADSP21062 SHARC, Texas Instruments TMS320C6x, TMS320C4X and TMS320C80, and Motorola's DSP96002. A comparison of these DSPs is shown in Table 5.2. In order to ensure that the DSP computational units operate efficiently, the I/O circuitry in these DSPs has been designed to support continuous high speed flows of data. A more detailed description of general DSP processing technologies can be found in [85], and of DSP applied to software radios in [86].

Field Programmable Gate Arrays (FPGA's) can also be used to build the required custom computational resources for the advanced receiver. An advantage of FPGA's is their reprogrammability,

Table 5.2: Comparison of digital signal processors suited for high speed multiprocessing.

Processor	Cycle time	Speed (MIPS)	On Chip Memory
SHARC	25 ns	40	128 Kb
C6x	5 ns	1600	1 Mb
C80	20 ns	50	50 Kb
C40	33 ns	30	2 Kb
DSP96002	50 ns	20	2 Kb

which simplifies upgrades and allows rapid-prototyping.

Combination of different technologies to implement different functions of the advanced receiver can provide significant advantages. Hybrid approaches that combine DSPs with custom ASICS and FPGAs are already being used for the implementation of conventional CDMA receivers [87].

The following section describes the baseband demodulation segments and presents a description of the RF front end developed in [82], which was developed to operate as a generic multi-sensor RF front end. First, the analog section of the multi-sensor testbed is described. Then, a practical I/Q implementation with carefully timed data streams (to allow cancellation of asynchronous multiple access signals) is described. Experimental results follow.

5.4.2 RF Front-end

A multi-sensor testbed suitable for adaptive beam-forming and multiuser detection can be implemented by combining a multi-sensor testbed such as the one developed in [82] with a baseband processing section performing multiuser detection. A block diagram of this generic multi-sensor RF front end is seen in Figure 5.5.

The analog tuner downconverts signals from an RF of 2050 MHz to an IF of 68 MHz. It has a noise figure of 4 dB, and provides 75 dB of spurious free dynamic range in a 2MHz IF bandwidth with a minimum detectable signal of -111.4 dBm.

The RF bandpass filter rejects out-of-band interference. It is desirable for this filter to have a

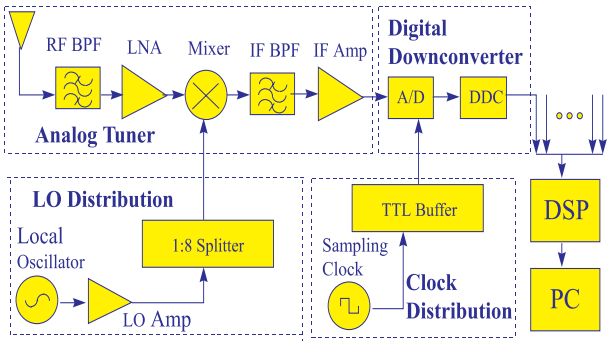

Figure 5.5: Block diagram of the multi-sensor testbed. (Reprinted from [82]).

low insertion loss and linear phase across the passband. The RF Low Noise Amplifier (LNA) increases the level of the signal before it reaches the mixer. The choice of LNA plays a key role in determining the noise figure of the receiver. Excessive gains are avoided, however, since they give rise to intermodulation and distortion in the mixing process.

Following RF amplification, the signal is mixed down to IF. A common Local Oscillator (LO)-signal drives the mixers of all the branches of the analog tuners. Selection of the mixer is important since distortion from the mixing process affects the receiver's dynamic range. Post-mixer bandpass filtering rejects undesired out-of-band signals, mixer spurious products, and RF and LO mixer-leakage.

After amplification of the analog IF signal, the IF is digitized using harmonic sampling. Several practical considerations for selecting analog to digital converters for harmonic sampling applications are presented in [88]. Once the IF signal has been digitized, digital down-converters further filter and translate the band of interest to the complex-baseband. By relieving the DSP from the processing burden of downconversion, more computational power becomes available for the tasks of estimation, interference cancellation and detection. Digital downconversion not only eliminates the need for another IF stage, but it also overcomes many of the problems related to analog downconversion and lowpass digitization. Discussion of sampling, IF processing, and digital downconversion techniques are presented in [89, 90].

5.4.3 Baseband Multiuser Demodulation Segment

In this section, the real-time asynchronous baseband multiuser-demodulation segment is described. The multiuser demodulation scheme has one stage of interference cancellation. In this system, baseband processing functions are implemented on modular Analog Devices ADSP21020 EZLAB boards. The direct sequence BPSK system has a processing gain $N = 15$, and supports an aggregate rate of 20 Kbps. As discussed in the previous section, after proper signal conditioning, the IF signal is downconverted, decimated, and filtered for baseband processing. The input to the signal processing segment is the complex-baseband multiple access data stream of Equation (5.1). Data acquisition is interrupt driven.

Since arithmetic operations such as addition and multiplication are at the core of the algorithms used in this receiver, the performance of the algorithms is influenced by the wordlength and the type of arithmetic used by the system. Fixed-point hardware is currently significantly cheaper, faster, and more power efficient than floating-point hardware. Nonetheless, following the trend in rapid prototyping, this implementation uses a 32-bit floating point processor since floating-point arithmetic simplifies algorithm development. Optimization for fixed-point can be performed from this working foundation. The performance of a fixed-point implementation of the multistage parallel interference cancelation technique has been investigated analytically and via simulations in [52].

In order to minimize the effects of timing errors, a high sampling rate is desired. On the other hand, high sampling rates increase the processing bandwidth required from the DSPs. The effects of timing errors on the performance of multistage parallel interference cancellation receivers have been studied in [58]. Analytical and simulation results indicate that multistage parallel interference cancellation receivers are fairly robust and show moderate reductions in performance due to timing errors on the order of $T_c/8$. A rate of 4 samples per chip was selected as a compromise between minimizing the negative effects of synchronization errors and timing misalignment at the receiver (keeping average timing errors below $T_c/8$), and minimizing the overall computational complexity of the implementation.

The DSP section of the receiver operates on the complex-baseband signal as it arrives, which avoids unnecessary processing delays and storage requirements associated with block processing.

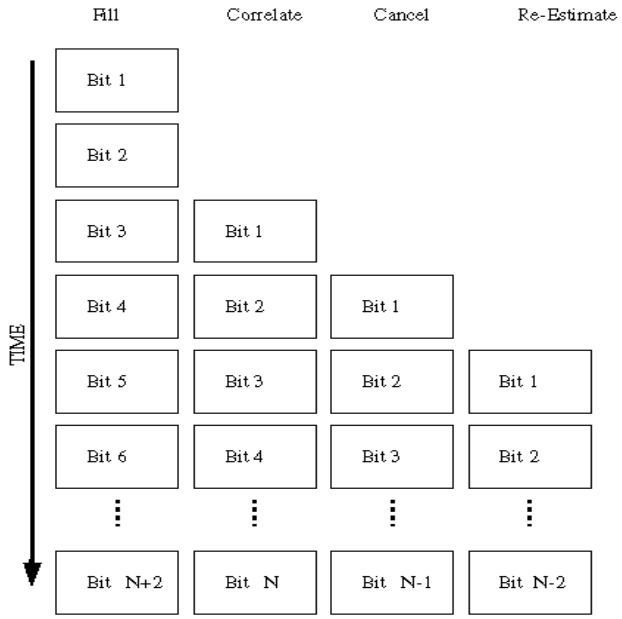

Figure 5.6: Timing/task partition diagram for the real-time implementation.

This system takes advantage of the short length of the spreading codes by using a noncoherent matched-filter approach for initial acquisition.

A coherent synchronization approach that takes advantage of the multistage architecture by using the residual signal $\tilde{r}(t)$ for improved acquisition and tracking has been studied in [91]. Since the residual signal has reduced levels of MAI, the probability of false alarm and mean acquisition time of the system are reduced. This technique will be incorporated in the receiver in the near future.

The processing can be described with the aid of the signal flow diagram in Figure 5.1 and the processing pipeline presented in Figure 5.6. Baseband processing is based on the decision metric from (5.18). Due to the asynchronous nature of the system, care must be taken in deriving the real-time processing flow.

The digital signal processing pipeline for this receiver consists of a data acquisition stage, a signal processing and interference cancellation stage and an output stage where the decision statistics are computed. The signal processing pipeline of the real time implementation can be described as follows: As the samples corresponding to bit interval $n+2$ are being collected, the signal processing section calculates the conventional receiver soft outputs for bit n, computes the residual signal $\hat{r}$

for bit $n-1$, and forms the K improved decision values for the bit interval $n-2$ [59]. If desired, the output section uses these decision statistics to estimate the transmitted data. This processing pipeline can be readily adapted to allow multiple slower processors to be used rather than a single high speed processor.

5.5 Experimental Results

In order to test the real-time baseband processing segments of the DSP based parallel interference cancellation receiver, a real-time multiple access channel emulator was developed using an ADSP21020 EZLAB board. The baseband channel emulator takes the information that the different users wish to convey to the multiuser receiver, and creates an asynchronous complex-baseband multiuser signal stream. The channel emulator allows stipulation of the desired E_b/N_o, and the relative delays and phases among users. The delays and phases, remain constant for the duration of the test. The baseband channel emulator is interfaced to the DSP baseband processing segment over the same interface that is used to receive the complex-baseband signals produced by the IF digital downconversion.

The memory requirements of this implementation are very modest due to the approach used for real-time processing. The processing buffer used for complex-baseband data collection requires $5NN_s$ words of storage. In order to take advantage of the parallel processing capabilities of the DSP, separate copies of the signature sequences were created for the in-phase and quadrature channels. This requires only $2KNN_s$ words. Storage of intermediate results, such as the decision statistics of the conventional receiver require K words. Thus the amount of memory required is a linear function of K, N and N_s. By pipelining data rather than using a packet processing approach, high latencies are avoided and memory is conserved.

A bit-error-rate tester was developed using the multiple access channel emulator. At the transmitter, a pseudorandom data stream of length $2^{31}-1$ is internally generated from which bits are assigned to the different users. The composite multiple access signal is then created and the desired level of Additive White Gaussian Noise (AWGN) is added. At the receiver, the received stream is decoded and the estimated data is compared against an internally generated reference

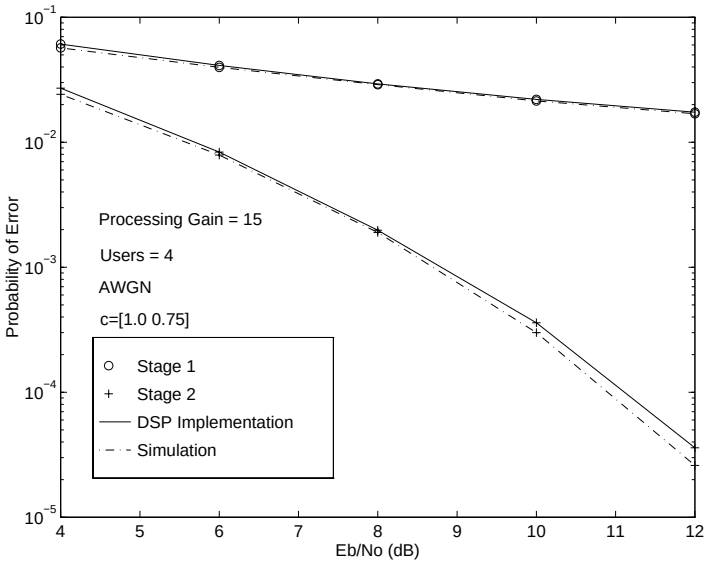

Figure 5.7: Probability of bit error vs. E_b/N_o experimental and simulation results for a single trial of the coherent receiver's DSP implementation ($N = 15$, with $C_k^{(2)} = 0.75$).

pseudorandom bit stream. The number of mismatches are measured in real-time and the measured BER is compared with those predicted by simulations. The experimental results agree with the simulations.

Figure 5.7 shows a comparison between the experimental BER from the real-time system and those predicted via simulation for a test with 4 users. Table 5.3 gives the spreading codes assigned to the users in the tests. The spreading sequences were produced by using the m-sequence generator defined by $1 + x + x^4$ and its image, in a Gold code sequence configuration. Multiple sequences are obtained by changing the offset between the initial conditions in the shift registers.

In these tests, the delays and the relative phases were kept constant. Other tests show a good fit between experimental and simulation results resembling those in Figure 5.7. Similar tests were performed for the non-coherent receiver. These experimental results also agree with those obtained via simulation.

Figure 5.8 shows BER results obtained for various trials with different delays and phases for the 4 user case with the coherent version of the receiver. This figure shows that the real-time DSP

Table 5.3: Spreading sequences used in the hardware tests of the multiuser receiver.

	Spreading Sequence
User 1	1 1 0 0 1 0 1 1 1 1 0 1 0 0 1
User 2	1 1 1 1 0 0 0 1 0 0 0 1 1 0 1
User 3	0 1 0 0 0 1 0 0 1 0 0 0 1 0 1
User 4	1 0 1 0 1 1 1 1 1 0 1 0 1 0 0

implementation of the parallel partial interference cancellation receiver provides significant gains in performance. Improvement exceeds over one order of magnitude at $E_b/N_o = 10$ dB, compared to the conventional receiver for DS-CDMA. Analytical results based on the assumption of unbiased estimation [74] give optimistic results. BER results for the non-coherent receiver for the 4 user case are presented in Figure 5.9. These results also show a consequential performance improvement.

In all these tests synchronization is performed only on user 1. Perfect knowledge of the relative delays and phases with respect to user 1 was made available to the receiver. (The non-coherent receiver was not provided with side phase information). In this paper, the effects of imperfect phase and timing estimation are not addressed. However, it has been shown analytically and via simulations that this structure is robust to phase estimation and synchronization errors [58].

Another version of the system has been successfully used to emulate the transmission of JPEG files over AWGN channels. In order to show the improved performance of the DSP implementation of the multiuser receiver, a JPEG file was jointly transmitted by 4 users. Each of the users was given one bit of the JPEG file in a round-robin fashion for transmission. At the receiver, the file was reassembled. The reconstructed JPEG file gives a sense of the average performance of the system across all users.

Figure 5.10 shows the reconstructed signal obtained from data estimated using the coherent conventional receiver for a four user system operating at an $E_b/N_o = 10$ dB. Figure 5.11 shows the JPEG file reconstructed from the estimates obtained in real-time for the coherent parallel partial interference cancellation approach.

The reconstructed signal obtained from data estimated with the non-coherent conventional receiver for 4 users and $E_b/N_o = 12$ dB is shown in Figure 5.12. The reconstructed file with the non-coherent

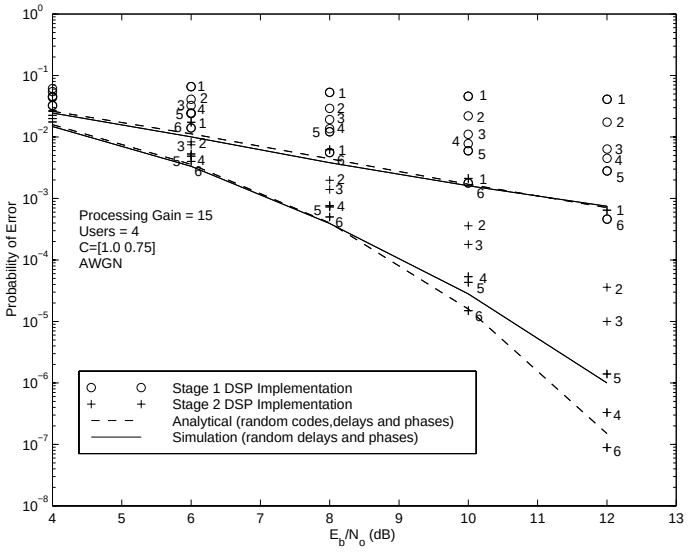

Figure 5.8: Probability of bit error vs. E_b/N_o from real-time BER measurement results for the coherent multiuser receiver, simulated curves for random delays and phases, and analytical curves assuming unbiased estimation ($N = 15$, with $C_k^{(1)} = 1.0$ and $C_k^{(2)} = 0.75$).

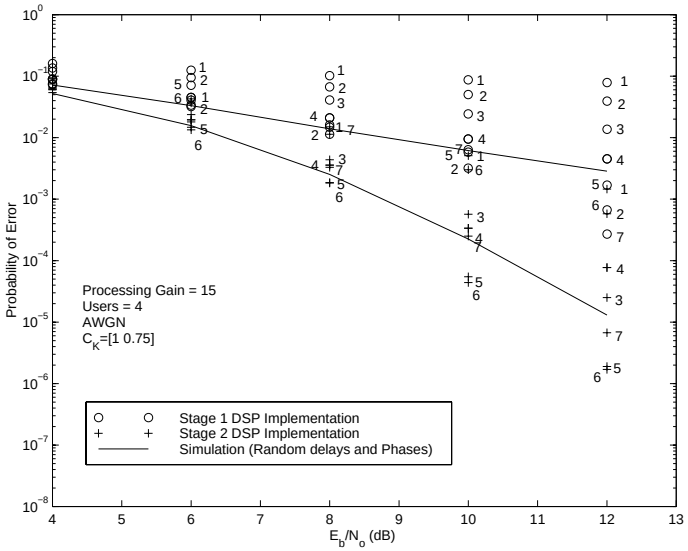

Figure 5.9: Probability of bit error vs. E_b/N_o from real-time BER measurement results for the non-coherent receiver, simulated curves for random delays and phases, and analytical curves assuming unbiased estimation ($N = 15$, with $C_k^{(1)} = 1.0$ and $C_k^{(2)} = 0.75$).

Figure 5.10: Reconstructed JPEG file from data estimated by the conventional coherent CDMA receiver ($E_b/N_o = 10$ dB, $N = 15$).

Figure 5.11: Reconstructed JPEG file from data estimated by the coherent partial parallel interference cancellation receiver ($E_b/N_o = 10$ dB, $N = 15$, with $C_k^{(1)} = 1.0$ and $C_k^{(2)} = 0.75$).

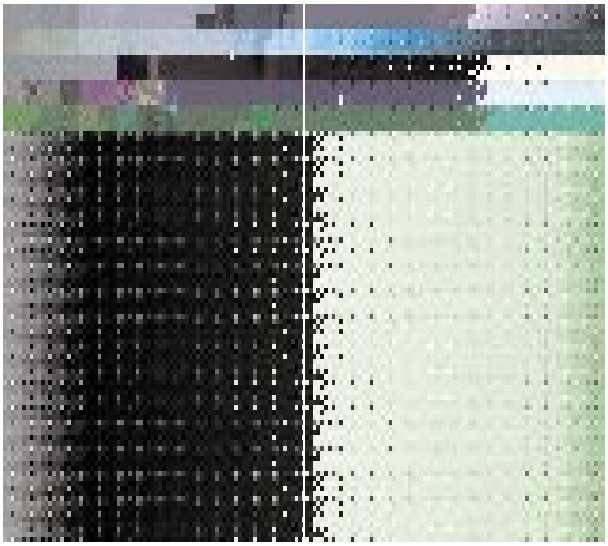

Figure 5.12: Reconstructed JPEG file from data estimated by the non-coherent receiver, processing gain = 15, 4 users and $E_b/N_o = 12$ dB.

interference cancellation receiver is indistinguishable from the one shown in 5.11

5.5.1 Summary of Other Implementation Efforts

An FPGA-based multiuser detector based on the approach described in this chapter was developed by the Mobile and Portable Radio Research Group (MPRG) and the Virginia Tech Information Systems Center (VISC) [92]. A Xilinx XC4010-based FPGA evaluation board was used to implement a multiuser transmitter. The FPGA-based multiuser receiver was developed using stream-based modular design principles. The system handles four users at a rate of 31.25 Kbit/s per user. The FPGA-based receiver testbed consists of an RF front-end, a Harris 50214 digital downconverter evaluation board, the PCI-based GigaOps G900 computing platform, and a host PC.

An FPGA-based detector featuring RAKE receivers and successive interference cancellation is under development at Rutgers University's Wireless Information Network Laboratory WINLAB [93]. The FPGA-based system uses a pipelined structure for interference cancellation and the implementation has been based on the IS-95 standard. To obtain maximum reduction of inter-cell interference the power control strategy is to assign higher powers to users close to the base-station

and lower powers to users at the border of the cell. The approach taken for this implementation is based on using COMDISCO's Signal Processing WorkSystem (SPW^{TM}) with the Hardware Design Library (HDS) and Xilinx FPGA boards. SPW simulations have been used to verify the functionality of the cancellation scheme.

Implementation efforts at CEA-LETI have focused on a dedicated integrated circuit approach. The core of the implementation is an ASIC DS-CDMA transceiver with the added functionality of signal regeneration for use with subtractive interference cancellation schemes. A board prototype that allows two stages of interference cancellation is currently under development [94].

A two-user DS-CDMA parallel interference cancellation hardware demonstrator is currently under development at the Swiss Federal Institute of Technology's communication technology laboratory [95]. The system is being designed around the single-user digital spread spectrum transceiver presented in [96]. Monte-Carlo simulations have been used to model the receiver and verify its performance.

Other studies that have explored practical implementation of multiuser detection can be summarized as follows: In [97] an experimental setup was used to study the performance of an inter-channel interference canceling structure. In this coherent two-user BPSK system, the spreading and re-spreading operations were hard-wired and regeneration of the interference replica was by-passed. Instead the reconstructed signal was emulated by adding noise to the interfering signal to simulate possible imperfections in the regeneration process. The test results were encouraging showing significant improvements in BER when employing interference cancellation.

An experiment conducted to demonstrate the feasibility of using an interference cancellation system to combat the near far problem has been presented in [98]. The experimental set-up for the two-user system used TTL logic to create the user signals which were then mixed up to RF. The composite signal was then mixed down and interference cancellation was applied. Even though this implementation did not compensate for the delay introduced by the RC low-pass filter used in the estimation of the received signal, experimental measurements showed improvements in BER and near-far resistance.

5.6 Conclusions

Recent technological advances make advanced DS-CDMA multiuser receivers practical. A real-time DSP based parallel partial interference cancellation receiver has been successfully implemented and its performance has been experimentally tested in AWGN channels. The implementation is based on a low complexity approach to interference cancellation using the decision statistics from the previous stage of cancellation, and a correction factor obtained from a residual signal that is common to all users, to generate improved estimates. This approach reduces implementation complexity from quadratic to linear in the number of users with no penalties in performance. Experimental results confirm significant performance gains over the conventional receiver. The excellent tradeoff between complexity and performance offered by the parallel partial interference cancellation technique and its similarity to the conventional receiver makes it an attractive approach for practical implementation in systems that exploit multiuser detection.

Chapter 6

Non-coherent Multiuser DS-CDMA Demodulation via Multiple-Symbol Differential Detection

Due to their simplicity, robustness and rapid synchronization capabilities, non-coherent detectors are favored for many practical applications such as packet radio. The standard approach for performing differential detection of DPSK signals is based on correlating the decision statistic for a particular symbol interval with that of the previous symbol interval, and evaluating the relative phase difference. This was the approach used in the non-coherent implementation described in section 5.2.

This section introduces a non-coherent demodulation technique that uses an observation interval encompassing multiple symbols, and investigates its application to non-coherent DS-CDMA multi-stage interference cancellation. The multi-symbol technique employed in this development is based on maximum likelihood sequence estimation of the received phases, an approach previously considered for single user differentially coherent PSK systems [99, 100], where it was demonstrated that in single user AWGN channels, multi-symbol differential PSK is capable of closing the gap between standard differential detection and coherent detection of PSK signals with differential encoding.

6.1 Single-User Multiple Symbol Differential Detection

The objective of this section is to illustrate the concept of multiple symbol differential detection. The technique is first described for a single direct sequence spread spectrum user operating in a AWGN using an approach that parallels the derivation in [99] for single user channels. Once the basic principles of multi-symbol differential detection have been demonstrated, multiple symbol differential detection will be applied to multiple access scenarios.

Let the transmitted baseband signal from a DS-SS user in an AWGN channel correspond to a phase modulated waveform, expressed in complex envelope notation:

$$s(t) = \sqrt{P}a(t)e^{j\phi(t)}, \tag{6.1}$$

where P is the transmitted signal power of the desired user, $a(t)$ is the spreading waveform, and $\phi(t) = \phi_{(i)}p_{_T}(t - iT)$, where $\phi_{(i)} \in \{2(n-1)\pi/2, n = 1, 2\}$ is the transmitted phase, and $p_{_T}(t)$ is a unit pulse function of duration T equal to the bit period. For differential transmission information is conveyed via the phase difference between consecutive symbols, allowing differential detection at the receiver.

At the receiver, the received signal is expressed as:

$$r(t) = \sqrt{P}a(t)e^{j(\phi(t)+\theta(t))} + n(t), \tag{6.2}$$

where $n(t)$ represents the complex-valued additive white Gaussian noise at the receiver, with noise density N_o, and $\theta(t)$ represents an unknown phase shift present in the received phase.

As opposed to a standard differential PSK receiver, where a decision is made according to the phase difference between two successively received symbols, the multi-symbol approach is based on observing multiple consecutive symbols, and performing maximum likelihood sequence estimation of the received phases. As in standard differential detection, the underlying assumption is that the phase offset remains virtually constant throughout the observation interval.

For a conventional matched filter demodulator, the decision statistics y are obtained by sampling the outputs of the matched filter at the appropriate symbol intervals:

$$y_{(i)} = \frac{1}{\sqrt{T}} \int_{(i-1)T}^{iT} r(t)a(t)dt. \tag{6.3}$$

the decision statistics $y_{(i)}$ for the i^{th} interval can be expressed as:

$$y_{(i)} = s_{(i)} + n_{(i)}, \tag{6.4}$$

where

$$s_{(i)} = \sqrt{E_b} e^{j\phi_{(i)}}, \tag{6.5}$$

and $\phi_{(i)} \in \{2(n-1)\pi/2, n = 1, 2\}$ is the transmitted phase, and $n_{(i)} = \int_{(i-1)T}^{iT} n(t)a(t)dt$.

In classical differential detection the decision statistic for the current interval is projected onto the previous one, and a decision is made based on the phase of the resulting complex value $y_i y_{i-1}^*$. In multiple symbol differential detection, a sliding window is used to select an observation vector $\mathbf{y}$ consisting of N_w consecutive decision statistics ($\mathbf{y} = [\mathbf{y_{(k-N_w+1)}} \mathbf{y_{(k-N_w+2)}} \cdots \mathbf{y_{(k)}}]$). The observations in $\mathbf{y}$ are used to make a jointly optimal decision. In the following, it will be assumed that $\theta(t)$ remains virtually constant throughout the N_w-symbol observation interval and will thus be referred to as θ.

In the absence of side information about the unknown phase shift θ, maximum likelihood sequence detection is achieved by finding the sequence $\mathbf{s}$ that maximizes the a posteriori probability of the observation given the signal $\mathbf{p(y|s)}$, also known as the likelihood function $L(\mathbf{s})$. In AWGN channels, the likelihood function corresponds to:

$$\begin{aligned} L(\mathbf{s}) &= \int_{-\pi}^{\pi} \mathbf{p}(\mathbf{y}|\mathbf{s}, \theta)\mathbf{p}(\theta)\mathbf{d}\theta \\ &= \int_{-\pi}^{\pi} \frac{1}{(2\pi\sigma^2)^{N_w}} \exp\left(\frac{-||\mathbf{y} - \mathbf{s}e^{j\theta}||^2}{\sigma^2}\right) p(\theta)\ d\theta. \end{aligned} \tag{6.6}$$

In order to cast the previous integral into a more revealing form, the argument of the exponential function is expressed as [99]:

$$\begin{aligned} ||\mathbf{y} - \mathbf{s}\mathbf{e}^{\mathbf{j}\theta}||^{\mathbf{2}} &= \sum_{i=0}^{N_w-1} |y_{k-i} - s_{k-i}e^{j\theta}|^2 \\ &= \sum_{i=0}^{N_w-1} (|y_{k-i}|^2 + |s_{k-i}|^2) - 2\sum_{i=0}^{N_w-1} |y_{k-i}s_{k-i}^*| cos(\theta - \alpha), \end{aligned} \tag{6.7}$$

where

$$\alpha = \arctan\left(\frac{Im\{\sum_{i=0}^{N_w-1} z_{k-i}s_{k-i}^*\}}{\Re\{\sum_{i=0}^{N_w-1} z_{k-i}s_{k-i}^*\}}\right) \tag{6.8}$$

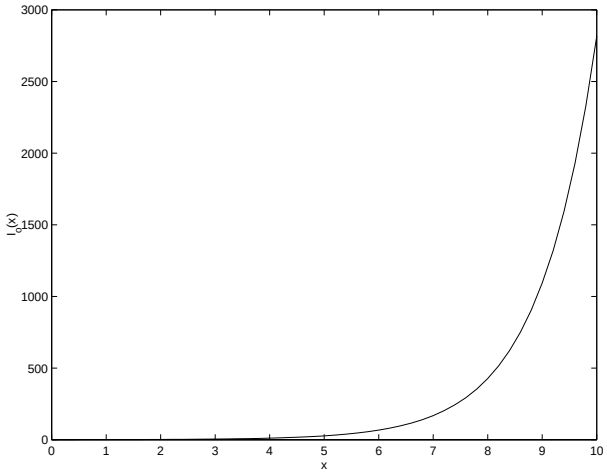

Figure 6.1: Modified zero-*th* order Bessel function of the first kind.

and

$$cos(\theta-\alpha) = cos\theta\left(\frac{\Re\{\sum_{i=0}^{N_w-1} z_{k-i}s_{k-i}^*\}}{|\sum_{i=0}^{N_w-1} z_{k-i}s_{k-i}^*|}\right) - sin\theta\left(\frac{Im\{\sum_{i=0}^{N_w-1} z_{k-i}s_{k-i}^*\}}{|\sum_{i=0}^{N_w-1} z_{k-i}s_{k-i}^*|}\right). \tag{6.9}$$

Substituting the expression of (6.7) into Equation (6.6) yields:

$$\begin{aligned} L(\mathbf{s}) &= \frac{1}{(2\pi\sigma^2)^{N_w}} \exp\left(-\frac{\sum_{i=0}^{N_w-1}|y_{k-i}|^2 + |s_{k-i}|^2}{2\sigma^2}\right) \\ &\quad \times \frac{1}{2\pi}\int_{-\pi}^{\pi} \exp\left(\frac{|\sum_{i=0}^{N_w-1} y_{k-i}s_{k-i}^*|}{\sigma^2}\right) cos(\theta-\alpha)d\theta. \end{aligned} \tag{6.10}$$

Equation (6.10) can be written in more compact form by expressing its last term as a special case of a more general family of functions: the modified Bessel functions of the first kind of order n. This family of functions, usually denoted as $I_n(x)$, is defined according to:

$$I_n(x) = \frac{1}{2\pi}\int_{2\pi} \exp(x\cos\theta)\cos n\theta \; d\theta. \tag{6.11}$$

With this definition, Equation (6.10) is expressed as:

$$L(\mathbf{s}) = \frac{1}{(2\pi\sigma^2)^{N_w}} \exp\left(-\frac{\sum_{i=0}^{N_w-1}|y_{k-i}|^2 + |s_{k-i}|^2}{2\sigma^2}\right) I_o\left(\frac{|\sum_{i=0}^{N_w-1} y_{k-i}s_{k-i}^*|}{\sigma^2}\right). \tag{6.12}$$

The received phases are estimated by finding the sequence that maximizes the likelihood function. Since for PSK all symbols have the same magnitude, the first term of Equation (6.12) can be

disregarded. Maximization of the function $I_o(x)$ is equivalent to maximization of its argument, since the modified Bessel function of the first kind of order zero $I_o(x)$, shown in Figure 6.1, is monotonically increasing with x. Therefore, maximization of the likelihood function is achieved by the sequence that maximizes:

$$\arg\left\{\max_{\mathbf{s}}\left|\sum_{i=0}^{N_w-1} y_{k-i}s_{k-i}^*\right|\right\}. \tag{6.13}$$

Substituting the value of s_{k-i} from Equation (6.5) into expression (6.13), and recalling that the information has been differentially encoded as a change-in-phase, results in:

$$\arg\left\{\max_{\phi}\left|\sum_{i=0}^{N_w-1} y_{k-i}e^{-j(\phi_{(k-(i-1))}+\Delta\phi_{(k-i)})}\right|\right\}. \tag{6.14}$$

Observing that $\phi_{(k-(i-1))} = \phi_{(k-(i-2))} + \Delta\phi_{(k-(i-1))}$, the argument of the exponential term in the previous equation can be expressed recursively according to

$$\phi_{(k-(i-1))} + \Delta\phi_{(k-i)} = \phi_{(k-N_w+1)} + \sum_{m=0}^{N_w-i-2} \Delta\phi_{(k-i-m)}. \tag{6.15}$$

The use of differential decoding affords the receiver invariance to a constant phase offset at the input, therefore a common phase offset ϕ_a can be subtracted from all the constellation points without altering the decisions. Taking ϕ_a to be ϕ_{k-N_w+1} and subtracting that common phase reduces the problem to finding the sequence of phases such that

$$\arg\left\{\max_{\phi}\left|y_{k-N_w+1} + \sum_{i=0}^{N_w-2} y_{k-i}e^{-j\sum_{m=0}^{N_w-i-2}\Delta\phi_{(k-i-m)}}\right|\right\} \tag{6.16}$$

is maximized. Note that an equivalent result is obtained by maximizing:

$$\arg\left\{\max_{\phi}\left|y_{k-N_w+1} + \sum_{i=0}^{N_w-2} y_{k-i}e^{-j\sum_{m=0}^{N_w-i-2}\Delta\phi_{(k-i-m)}}\right|^2\right\}. \tag{6.17}$$

In order to assess the degrees of improvements that can be achieved with this approach, first developed in [99], a Monte Carlo simulation of the multi-symbol approach for a single user DS-SS system was carried out. Maximum likelihood sequence detection of the received phases was based on the metric of Equation 6.16. Figure 6.2 presents simulation results of the BER performance of the differentially coherent binary PSK DS-SS system as a function of the bit energy to interference

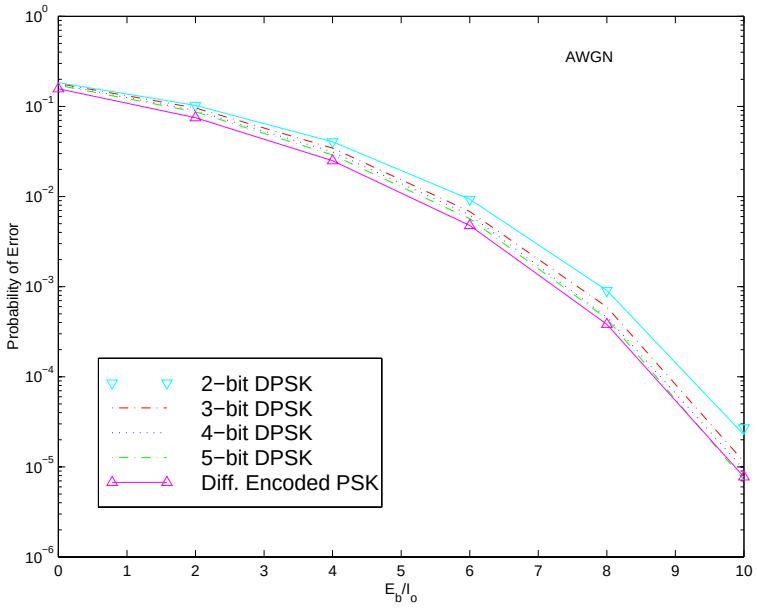

Figure 6.2: Non-coherent 2-PSK probability of error vs. E_b/I_o as a function of the observation window length.

density ratio for various observation window lengths. The results in this figure confirm those reported in [99], which showed that in single user AWGN channels, improved performance is achieved by using larger observation windows. Note that the most consequential improvement is achieved in going from standard DPSK (2-bit window) to a 3-bit observation window.

6.2 Multiuser Multiple Symbol Differential Detection

After interference cancellation, the non-coherent multiuser receiver implementation of section 5.2 uses the standard two-symbol observation approach for differential detection of the transmitted data. It is conceivable that improved performance can also be achieved for interference cancellation receivers, by extending the length of the observation window beyond two symbol intervals, and performing single user maximum likelihood sequence estimation of the received phases.

Using a complex-baseband equivalent model of the receiver, the received signal for user k at stage s, $\hat{r}_k^{(s)}(t)$, is generated by subtracting from the received signal the estimated MAI caused by the

remaining users:

$$\hat{r}_k^{(s)}(t) = r(t) - \sum_{\substack{j=1 \\ j \neq k}}^{K} \hat{s}_j^{(s)}(t - \tau_j), \tag{6.18}$$

where the complex-baseband soft outputs of the matched filter bank at stage s are:

$$y_{k,i}^{(s+1)} = \frac{1}{\sqrt{T}} \int_{(i-1)T+\tau_k}^{iT+\tau_k} \hat{r}_k^{(s)}(t) a_k(t - \tau_k) dt \tag{6.19}$$

In the proposed approach, decisions are based on determining the most likely sequence according to:

$$\arg \left\{ \max_{\phi} \left| y_{k,j-N_w+1}^{(s)} + \sum_{i=0}^{N_w-2} y_{k,j-i}^{(s)} e^{-j \sum_{m=0}^{N_w-i-2} \Delta\phi_{(j-i-m)}} \right| \right\}. \tag{6.20}$$

Simulation results displayed in Figure 6.3 show the probability of error vs. E_b/N_o for the multiuser receiver and various lengths of the observation window. These results indicate that in AWGN channels, the performance of the non-coherent multiuser detector can also be improved by using multiple symbol differential detection. Figure 6.4 illustrates the effect of multi-symbol differential detection on the capacity of a system employing interference cancellation and multi-symbol differential detection. This figure indicates that in AWGN channels significant capacity improvements are achieved via this approach. For bit error rates around 10^{-3}, the multi-symbol receivers can support four more users than the receiver employing the standard differential detection technique. It is apparent that the largest gains are achieved in going from standard differential detection ($N_w = 2$) to three observation symbols ($N_w = 3$). Figure 6.5 shows a possible implementation of the detection circuit. Note that the circuitry is roughly four times more complex than a standard differential decoding circuit. However, relative to the operations required for interference cancellation, the relative increase in complexity of the receiver is very small.

6.2.1 Probability of Error

This section extends the analytic approach of [99] for single user multiple symbol differential decoding to derive bounds on the probability of error of multi-symbol differential partial parallel interference cancellation. In this approach, an upper bound for the probability of bit error is obtained through the union bound of pairwise probabilities of error. Computation of the pairwise

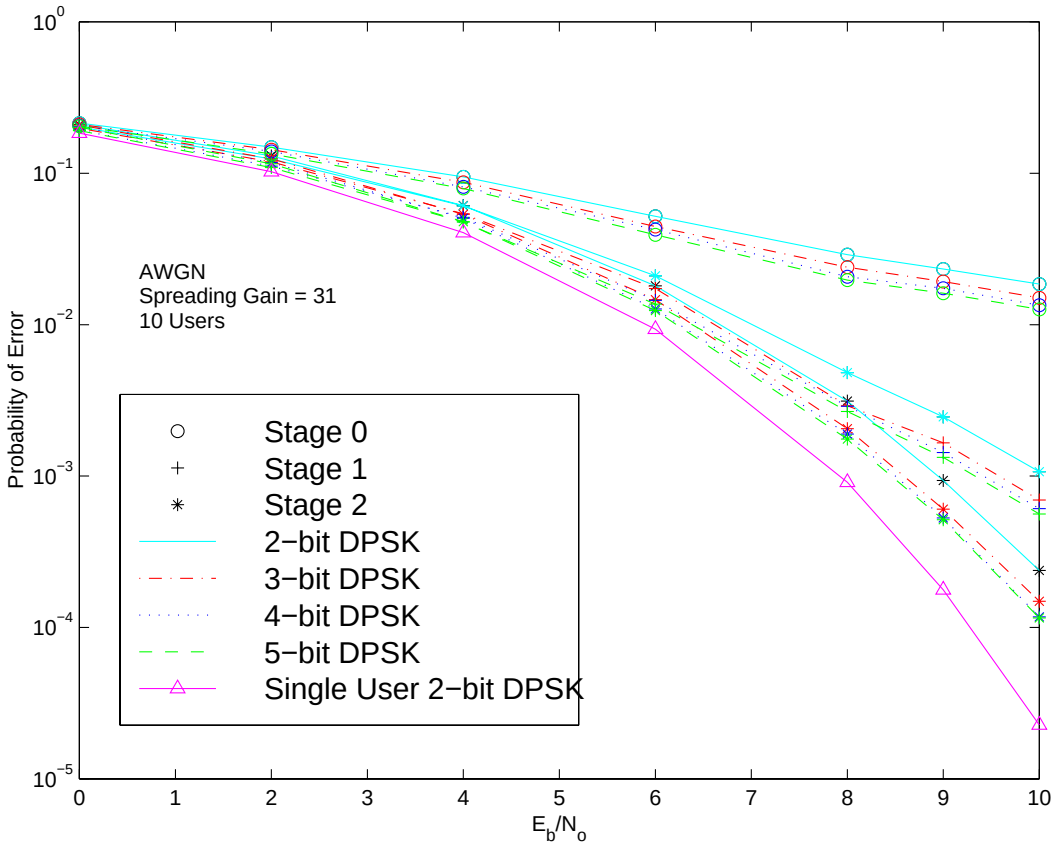

Figure 6.3: Multiuser probability of error vs. E_b/N_o as a function of the length of the observation window. Random codes, asynchronous users, spreading gain = 31, AWGN and 10 users.

error probabilities is performed using a technique developed in [101] for unified computation of the probability of error of FSK and other digital modulation techniques. Probability of error expressions for standard differential detection are obtained, with the aid of analytical results previously reported in [28], as a particular case of the more general framework of multiple symbol detection. These expressions are the differentially coherent counterparts of the ones derived in [28] for coherent PSK. Subsequently, probability of error bounds are derived for the case of $N_w = 3$, as well as asymptotic bounds for arbitrary observation lengths.

For the sake of simplicity, this analysis focuses on the synchronous case. However, note that for random signature sequences, asynchronous operation reduces the effective variance of the multiple access interference by a factor of two compared to the less favorable synchronous case [78]. There-

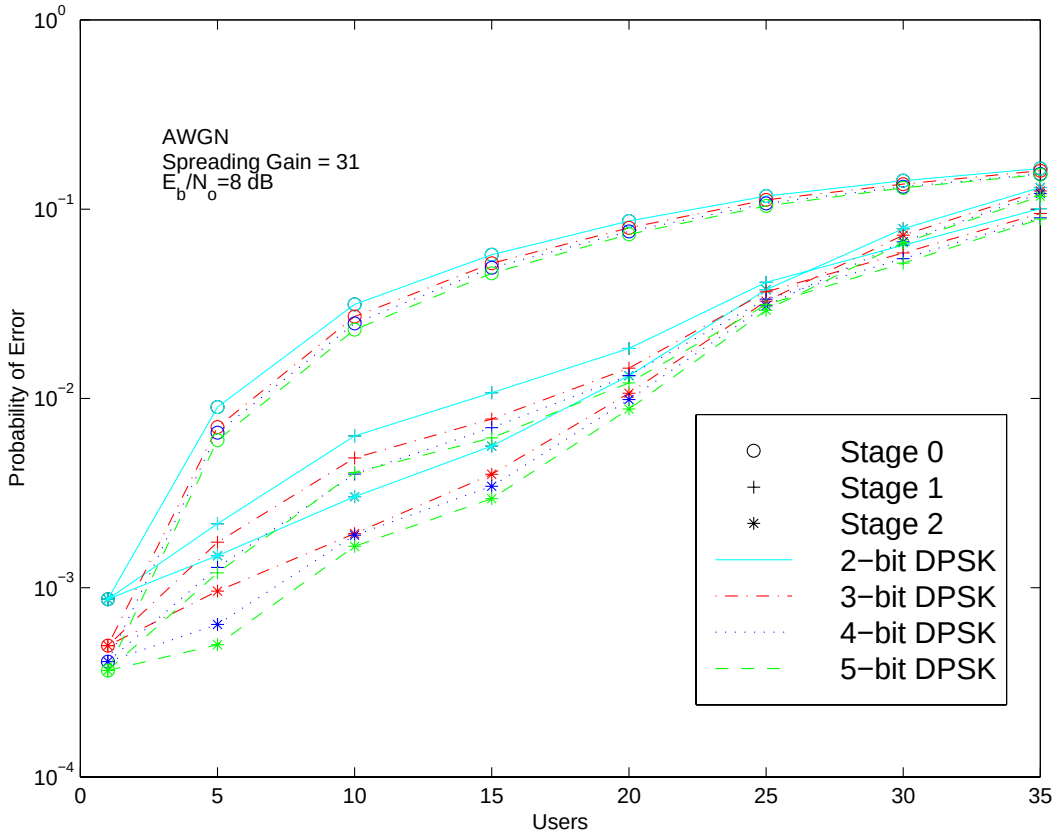

Figure 6.4: Multiuser probability of error vs. Number of users for various observation window lengths. Random codes, asynchronous users, spreading gain = 31, AWGN and $E_b/N_o = 8$ dB.

fore, the results obtained in this section give an upper bound for the probability of error of the asynchronous case as well.

As the first step in computing the pairwise error probabilities, let us represent the sequence of encoded phase transitions associated with $\mathbf{u_j}$, the $(N_w - 1)$-bit long information sequence conveyed by user j, by :

$$\mathbf{\Delta}\phi_{\mathbf{j}} \quad = \quad (\Delta\phi_{j,k}, \Delta\phi_{j,k-1}, ..., \Delta\phi_{j,k-N_w+2}), \tag{6.21}$$

and let the sequence of detected phases corresponding to the erroneously decoded information sequence $\hat{\mathbf{u}}_{\mathbf{j}}$, be represented by:

$$\mathbf{\Delta}\hat{\phi}_{\mathbf{j}} = (\Delta\hat{\phi}_{j,k}, \Delta\hat{\phi}_{j,k-1}, ..., \Delta\hat{\phi}_{j,k-N_w+2}). \tag{6.22}$$

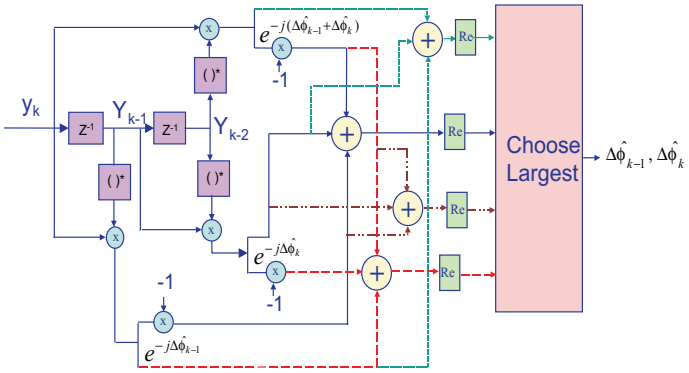

Figure 6.5: Multi-symbol detection circuit for $N_w = 3$. Adapted from [99].

Assuming equally likely symbols, the probability of bit error can be union bounded using a weighted combination of pairwise error probabilities. The probability of error is thus overbounded by:

$$P_{b,j} \leq \frac{1}{N_w - 1} \sum_{\mathbf{\Delta}\phi_\mathbf{j} \neq \mathbf{\Delta}\hat{\phi}_\mathbf{j}} w(\mathbf{u_j}, \hat{\mathbf{u}}_\mathbf{j}) Pr\{\hat{\eta}_j > \eta_j | \mathbf{\Delta}\phi_\mathbf{j}\}, \tag{6.23}$$

where $\mathbf{\Delta}\phi_\mathbf{j}$ is the reference sequence, $w(\mathbf{u_j}, \hat{\mathbf{u}}_\mathbf{j})$ is the Hamming distance between the transmitted and the estimated information sequence, and $Pr\{\hat{\eta}_j > \eta_j | \mathbf{\Delta}\phi_\mathbf{j}\}$ corresponds to the pairwise error probability of choosing $\mathbf{\Delta}\hat{\phi}_\mathbf{j}$ when $\mathbf{\Delta}\phi_\mathbf{j}$ was transmitted.

The pairwise error probability $Pr\{\hat{\eta}_j > \eta_j | \mathbf{\Delta}\phi_\mathbf{j}\}$ can be computed based on the decision rule of Equation (6.17) by assuming a Gaussian distribution for the MAI, and noting that in this case the decision rule computes the squared magnitude of a complex-valued Gaussian random variable. Let us re-write Equation (6.17) in the following form:

$$\arg \left\{ \max_{\phi} \left| \sum_{i=0}^{N_w - 1} y_{k-i} e^{\sum_{m=0}^{N_w - i - 2} \Delta\phi_{(k-i-m)}} \right|^2 \right\}, \tag{6.24}$$

and define:

$$z_1 = \sum_{i=0}^{N_w - 1} y_{1,k-i} e^{-j \sum_{m=0}^{N_w - i - 2} \Delta\phi_{1,k-i-m}}, \tag{6.25}$$

and

$$z_2 = \sum_{i=0}^{N_w - 1} y_{1,k-i} e^{-j \sum_{m=0}^{N_w - i - 2} \Delta\hat{\phi}_{1,k-i-m}}, \tag{6.26}$$

where $y_{1,k-i}$ represents the i^{th} decision statistic (soft matched filter output) of user 1 in the window of observations.

For the previous definitions, the pairwise error probability $Pr\{\hat{\eta}_j > \eta_j|\mathbf{\Delta}\phi_\mathbf{j}\}$ is equivalent to $Pr\{|z_2|^2 > |z_1|^2|\mathbf{\Delta}\phi\}$. Calculation of the pairwise probability of error will be performed based on the results reported in [101] and applied in [99] to the single user problem. In summary, the pairwise error probability can be evaluated according to [99]:

$$Pr\{|z_2|^2 > |z_1|^2\} = \frac{1}{2}[1 - Q(\sqrt{b}, \sqrt{a}) + Q(\sqrt{a}, \sqrt{b})], \tag{6.27}$$

where

$$Q(a, b) = \int_b^\infty \exp\left(-\frac{a^2 + x^2}{2}\right) I_o(ax)dx \tag{6.28}$$

is the Marcum-Q function, with arguments determined according to:

$$\left\{ \begin{array}{c} a \\ b \end{array} \right\} = \frac{1}{2N_s}\left\{\frac{S_1 + S_2 - 2|\rho|\sqrt{S_1 S_2}\cos(\theta_1 - \theta_2 + \phi)}{1 - |\rho|^2} \mp \frac{S_1 - S_2}{\sqrt{1 - |\rho|^2}}\right\}. \tag{6.29}$$

In the previous equation, S_1 and S_2 correspond to:

$$\begin{aligned} S_1 &= \frac{1}{2}|\overline{z_1}|^2 \\ S_2 &= \frac{1}{2}|\overline{z_2}|^2. \end{aligned} \tag{6.30}$$

The total noise power, N_s, is evaluated according to:

$$\begin{aligned} N_s &= \frac{1}{2}E\left\{|z_1 - \overline{z_1}|^2\right\} \\ &= \frac{1}{2}E\left\{|z_2 - \overline{z_2}|^2\right\}, \end{aligned} \tag{6.31}$$

the normalized complex noise crosscorrelation between the two random processes, ρ, is evaluated via:

$$\rho = \frac{1}{2}\frac{\overline{(z_1 - \overline{z_1})^*(z_2 - \overline{z_2})}}{\overline{|z_1 - \overline{z_1}|^2}}. \tag{6.32}$$

and the phase terms in Equation (6.29) are given by: $\theta_1 = arg\{\overline{z_1}\}$, $\theta_2 = arg\{\overline{z_1}\}$ and $\phi = arg\{\rho\}$.

6.2.1.1 Analysis for Stage 0. The Conventional Receiver

Stage 0, the conventional CDMA receiver, can be implemented with a bank of matched filters, as well as with correlation demodulators.

The focus of analysis is user 1, as customary. Equal received powers are assumed. Using notation based on [28], the i^{th} decision statistic of user 1 in the observation window, $y_{1,k-i}^{(s=0)}$, corresponds to:

$$y_{1,k-i}^{(s=0)} = \sqrt{E_b}e^{j\phi_{1,k-i}} + \sqrt{E_b}\sum_{\mu=2}^{K} R_{1,\mu}e^{j\phi_{\mu,k-i}} + n_{1,k-i}. \tag{6.33}$$

To simplify notation, the unknown phase shift at the receiver has been accounted for in $\phi_{j,k-i}$, the phase of user j at time $k-i$.

The multiple-symbol decision statistic at the output of the single user detector for user 1 , z_1, is evaluated via substitution of (6.33) into Equation (6.25):

$$\begin{aligned} z_1 &= N_w\sqrt{E_b}e^{j\phi_{1,k-N_w+1}} + \sqrt{E_b}\sum_{i=0}^{N_w-1}\sum_{\mu=2}^{K} R_{1,\mu}e^{j\phi_{\mu,k-i}-j\sum_{m=0}^{N_w-i-2}\Delta\phi_{1,k-i-m}} \\ &\quad + \sum_{i=0}^{N_w-1} n_{1,k-i}e^{-j\sum_{m=0}^{N_w-i-2}\Delta\phi_{1,k-i-m}}, \end{aligned} \tag{6.34}$$

The mean value of z_1 corresponds to:

$$\overline{z_1} = N_w\sqrt{E_b}e^{j\phi_{1,k-N_w+1}}. \tag{6.35}$$

The power in the non-random component of z_1 is computed according to Equation (6.30) and results in:

$$S_1 = \frac{1}{2}N_wE_b. \tag{6.36}$$

The mean value of z_2, as defined in Equation (6.26), can be computed as:

$$\begin{aligned} \overline{z_2} &= \sqrt{E_b}e^{j\phi_{1,k-N_w+1}}\sum_{i=0}^{N_w-1} e^{j\sum_{m=0}^{N_w-i-2}\Delta\phi_{1,k-i-m}-\Delta\hat{\phi}_{1,k-i-m}} \\ &= \sqrt{E_b}e^{j\phi_{1,k-N_w+1}}\delta, \end{aligned} \tag{6.37}$$

where the parameter δ is defined as:

$$\delta = \sum_{i=0}^{N_w-1} e^{j\sum_{m=0}^{N_w-i-2}\Delta\phi_{1,k-i-m}-\Delta\hat{\phi}_{1,k-i-m}}. \tag{6.38}$$

The power in the non-random component of z_2 is thus given by:

$$\begin{aligned} S_2 &= \frac{1}{2}|\overline{z_2}|^2 \\ S_2 &= \frac{1}{2}E_b|\delta^2|. \end{aligned} \tag{6.39}$$

According to Equation (6.31), the total noise power N_s corresponds to:

$$N_s = \frac{1}{2}E\left\{|\sum_{i=0}^{N_w-1} y_{1,k-i}e^{-j\sum_{m=0}^{N_w-i-2}\Delta\phi_{1,k-i-m}} - N_w\sqrt{E_b}e^{j\phi_{1,k-N_w+1}}|^2\right\}. \tag{6.40}$$

Substituting for $y_{1,k-i}$, given in Equation (6.33), and cancelling common terms results in:

$$\begin{aligned} N_s = \frac{1}{2}E\Bigg\{|\sqrt{E_b}\sum_{i=0}^{N_w-1}\{\sum_{\mu=2}^{K} R_{1,\mu}e^{-j\sum_{m=0}^{N_w-i-2}\phi_{\mu,k-i}-\Delta\phi_{1,k-i-m}} \\ +n_{1,k-i}\}e^{-j\sum_{m=0}^{N_w-i-2}\Delta\phi_{1,k-i-m}}|^2\Bigg\}, \end{aligned} \tag{6.41}$$

which corresponds to:

$$\begin{aligned} N_s &= \frac{1}{2}\left(E_b\sum_{i=0}^{N_w-1}E\left\{|R_{1,\mu}|^2\right\} + \sum_{i=0}^{N_w-1}E\left\{|n_{1,k-i}|^2\right\}\right) \\ &= \frac{1}{2}N_w(E_b\frac{K-1}{N} + N_o), \end{aligned} \tag{6.42}$$

since for random signature sequences, the signature crosscorrelations are random variables with zero mean and variance $E\{R^2\} = \frac{1}{N}$ [28].

The correlation coefficient, defined in Equation (6.32) can be more conveniently expressed as:

$$\rho = \frac{1}{2N_s}\overline{(z_1-\overline{z_1})^*(z_2-\overline{z_2})}, \tag{6.43}$$

replacing these variables with their underlying expressions results in:

$$\begin{aligned} \rho = \frac{1}{2N_s}E\Bigg\{\Bigg(\sum_{i=0}^{N-1} y_{1,k-i}e^{-j\sum_{m=0}^{N_w-i-2}\Delta\phi_{1,k-i-m}} - N_w\sqrt{E_b}e^{j\phi_{1,k-N_w+1}}\Bigg)^* \\ \left(\sum_{i=0}^{N-1} y_{1,k-i}e^{-j\sum_{m=0}^{N_w-i-2}\Delta\hat{\phi}_{1,k-i-m}} - \sqrt{E_b}e^{j\phi_{1,k-N_w+1}}\delta\right)\Bigg\}, \end{aligned} \tag{6.44}$$

substituting for $y_{1,k-i}$, given in Equation (6.33) yields:

$$\rho = \frac{1}{2N_s}E\left\{\sum_{i=0}^{N_w-1}\sum_{n=0}^{N_w-1}\left(\sum_{\mu=2}^{K}\sqrt{E_b}R_{1,\mu}e^{-j\sum_{m=0}^{N_w-i-2}\phi_{\mu,k-i}} + n_{1,k-i}\right)^*\right.$$

$$\times \left(\sum_{\mu=2}^{K} \sqrt{E_b} R_{1,\mu} e^{-j \sum_{m=0}^{N_w-n-2} \phi_{\mu,k-n}} + n_{1,k-n} \right) e^{j \sum_{m=0}^{N_w-i-2} \Delta\phi_{1,k-i-m} - \Delta\hat{\phi}_{1,k-n-m}} \Bigg\}, \tag{6.45}$$

after simplifying, one obtains:

$$\begin{aligned} \rho &= \frac{1}{2N_s} \sum_{i=0}^{N_w-1} E \left\{ \left(\sum_{\mu=2}^{K} E_b R_{1,\mu}^2 + |n_{1,k-i}|^2 \right) \right\} e^{j \sum_{m=0}^{N_w-i-2} \Delta\phi_{1,k-i-m} - \Delta\hat{\phi}_{1,k-n-m}} \\ &= \frac{1}{2N_s} E \left\{ \left(\sum_{\mu=2}^{K} E_b R_{1,\mu}^2 + |n_{1,k-i}|^2 \right) \right\} \delta, \end{aligned} \tag{6.46}$$

where δ is defined according to Equation (6.38).

The previous equation can be conveniently expressed as:

$$\begin{aligned} \rho &= \frac{1}{2} \frac{E\{(\sum_{\mu=2}^{K} E_b R_{1,\mu}^2 + |n_{1,k-i}|^2\} \delta}{\frac{1}{2} N_w E \left\{ (\sum_{\mu=2}^{K} E_b R_{1,\mu}^2 + |n_{1,k-i}|^2 \right\}} \\ &= \frac{\delta}{N_w}. \end{aligned} \tag{6.47}$$

Standard differential detection is equivalent to multiple symbol differential detection with $N_w = 2$ [99]. For binary signaling, the pairwise probability of error is identical to the probability of bit error. Therefore, for the particular case on binary signaling and standard differential detection:

$$\begin{aligned} \delta &= \sum_{i=0}^{N_w-1} e^{j \sum_{m=0}^{N_w-i-2} \Delta\phi_{1,k-i-m} - \Delta\hat{\phi}_{1,k-i-m}} \\ &= 1 + e^{\pm j\pi} \\ &= 0, \end{aligned} \tag{6.48}$$

since $\Delta\phi_{1,k-1} - \Delta\hat{\phi}_{1,k-1}$ evaluates to either π or $-\pi$ when an error event occurs. This result significantly simplifies the computation of the probability of bit error.

Direct evaluation of the probability of bit error for standard differential decoding ($N_w = 2$) is readily achieved by computing the pairwise probability of error according to Equation (6.27). The arguments of the Marcum-Q function, obtained by substituting the previously derived expressions for $S_1, S_2, \rho = 0$ and N_s into (6.29), evaluate to:

$$\begin{Bmatrix} a \\ b \end{Bmatrix} = \begin{Bmatrix} 0 \\ \frac{S_1}{N_s} \end{Bmatrix}. \tag{6.49}$$

Substituting the expressions for S_1 and N_s given in Equations (6.36) and (6.42), for the case $N_w = 2$, yields:

$$\left\{ \begin{array}{c} a \\ b \end{array} \right\} = \left\{ \begin{array}{c} 0 \\ 2\frac{E_b}{E_b\frac{K-1}{N}+N_o} \end{array} \right\}. \tag{6.50}$$

The pairwise probability of error for standard differential detection, computed according to Equation (6.27), is thus given by:

$$Pr\{|z_2|^2 > |z_1|^2\} = \frac{1}{2}\left[1 - Q\left(\sqrt{\frac{2E_b}{E_b\frac{K-1}{N}+N_o}}, 0\right) + Q\left(0, \sqrt{\frac{2E_b}{E_b\frac{K-1}{N}+N_o}}\right)\right]. \tag{6.51}$$

This expression can be readily evaluated by taking advantage of the following two properties of the Marcum-Q function [99]:

$$Q(a, 0) = 1 \tag{6.52}$$

$$Q(0, b) = e^{-\frac{b^2}{2}}, \tag{6.53}$$

Employing these limiting forms in Equation(6.51), and recalling that for binary constellations, the pairwise probability of symbol error equals the probability of bit error, leads to the following expression for the probability of bit error for standard differential detection:

$$P_b = \frac{1}{2}\exp\left(\frac{-E_b}{E_b\frac{K-1}{N}+N_o}\right). \tag{6.54}$$

6.2.1.2 Analysis for Stage 1 with Full Interference Cancellation

In parallel interference cancellation receivers, the decision statistics obtained in the previous stage are used in an attempt to remove the interference experienced at the current stage. As shown in appendix A, at stage one ($s = 1$), the decision statistics of stage zero ($s = 0$) can be used in combination with the crosscorrelations between user signatures to cancel the interference caused by other users.

After postdetection interference cancellation, the decision statistics of user 1 are given by:

$$y_1^{(s=1)} = y_1^{(s=0)} - \sum_{u=2}^{K} y_u^{(s=0)} R_{1,u}. \tag{6.55}$$

At stage ($s = 0$), the decision statistics for user u correspond to:

$$y_u^{(s=0)} = \sqrt{E_b}e^{j\phi_u} + \sqrt{E_b}\sum_{l\neq u}^{K} R_{u,l}e^{j\phi_l} + n_u, \tag{6.56}$$

therefore,

$$y_1^{(s=1)} = y_1^{(s=0)} - \sum_{u=2}^{K}\left(\sqrt{E_b}e^{j\theta_u} + \sum_{l\neq u}^{K}\sqrt{E_b}R_{l,u}e^{j\theta_l} + n_u\right)R_{1,u}, \tag{6.57}$$

Substituting the expression for the soft outputs of the conventional single user receiver into Equation 6.57 results in:

$$\begin{aligned} y_1^{(s=1)} &= \sqrt{E_b}e^{j\phi_1} + \sum_{l=2}^{K}\sqrt{E_b}R_{1,l}e^{j\phi_l} + n_1 \\ &\quad - \sum_{u=2}^{K}\left(\sqrt{E_b}e^{j\phi_u} + \sum_{l\neq u}^{K}\sqrt{E_b}R_{l,u}e^{j\phi_l} + n_u\right)R_{1,u}, \end{aligned} \tag{6.58}$$

cancelling common terms, one obtains:

$$y_1^{(s=1)} = \sqrt{E_b}\left[1 - \sum_{u=2}^{K}R_{1,u}^2\right]e^{j\phi_1} - \sqrt{E_b}\sum_{u=2}^{K}\sum_{\substack{l=2\\l\neq u}}^{K}R_{l,u}R_{1,u}e^{j\phi_l} + \left(n_1 - \sum_{u=2}^{K}n_uR_{1,u}\right). \tag{6.59}$$

Following, an approach similar to the one used for the conventional matched filter receiver, Equation (6.27) is employed for computing the pairwise probability of error, $Pr\{|z_2|^2 > |z_1|^2\}$, after one stage of interference cancellation. Let us define:

$$z_1^{(s=1)} = \sum_{i=0}^{N_w-1} y_{1,k-i}^{(s=1)}e^{-j\sum_{m=0}^{N_w-i-2}\Delta\phi_{1,k-i-m}}, \tag{6.60}$$

and

$$z_2^{(s=1)} = \sum_{i=0}^{N_w-1} y_{1,k-i}^{(s=1)}e^{-j\sum_{m=0}^{N_w-i-2}\Delta\hat{\phi}_{1,k-i-m}} \tag{6.61}$$

For the sake of brevity, the superscript ($s = 1$) will be dropped, being understood that the analysis focuses on the performance after one stage of interference cancellation.

Evaluation of z_1, as defined in Equation (6.60), results in:

$$\begin{aligned} z_1 &= N_w\sqrt{E_b}e^{j\phi_{1,k-N_w+1}}\left[1 - \sum_{u=2}^{K}R_{1,u}^2\right] - \sum_{i=0}^{N_w-1}\left(\sqrt{E_b}\sum_{u=2}^{K}\sum_{\substack{l=2\\l\neq u}}^{K}R_{l,u}R_{1,u}e^{j\phi_{l,k-i}}\right. \\ &\quad \left. -(n_{1,k-i} - \sum_{u=2}^{M}n_{u,k-i})R_{1,u}\right)e^{-j\sum_{m=0}^{N_w-i-2}\Delta\phi_{1,k-i-m}}. \end{aligned} \tag{6.62}$$

Its mean, $\overline{z_1}$, is given by:

$$\overline{z_1} = N_w\sqrt{E_b}\left(1-\frac{K-1}{N}\right)e^{j\phi_{1,k-N_w+1}}. \tag{6.63}$$

The power in the non-random component of z_1 corresponds to:

$$\begin{aligned} S_1 &= \frac{1}{2}|\overline{z_1}|^2 \\ &= \frac{1}{2}N_w^2E_b\left(1-\frac{K-1}{N}\right)^2. \end{aligned} \tag{6.64}$$

After interference cancellation, the noise power in Equation (6.31) is:

$$\begin{aligned} N_s = \frac{1}{2}E\Bigg\{\Big|\sum_{i=0}^{N_w-1} y_{1,k-i}e^{-j\sum_{m=0}^{N_w-i-2}\Delta\phi_{1,k-i-m}} \\ -N_w\sqrt{E_b}\left(1+\frac{K-1}{N}\right)e^{j\phi_{1,k-N_w+1}}\Big|^2\Bigg\} \end{aligned} \tag{6.65}$$

substituting for $y_{1,k-i}$, as given in (6.59), results in:

$$\begin{aligned} N_s &= \frac{1}{2}E\left\{\Big|\sqrt{E_b}\sum_{i=0}^{N_w-1}\left(\frac{K-1}{N}-\sum_{u=2}^{K}R_{1,u}^2\right)e^{j\phi_{1,k-N_w+1}}\Big|^2\right\} \\ &+E\left\{\Big|\sqrt{E_b}\sum_{i=0}^{N_w-1}\sum_{u=2}^{K}\sum_{\substack{l=2\\l\neq u}}^{K}R_{l,u}R_{1,u}e^{j\phi_{l,k-i}-j\sum_{m=0}^{N_w-i-2}\Delta\phi_{1,k-i-m}}\Big|^2\right\} \\ &+E\left\{\Big|\sum_{i=0}^{N_w-1}\left(n_{1,k-i}-\sum_{u=2}^{K}n_{u,k-i}R_{1,u}\right)e^{-j\sum_{m=0}^{N_w-i-2}\Delta\phi_{1,k-i-m}}\Big|^2\right\}. \end{aligned} \tag{6.66}$$

To facilitate analytical calculation it is useful to model the binomially distributed signature cross-correlations as independent Gaussian random variables of zero mean and variance $E\{R^2\}=\frac{1}{N}$, as in [28]. Since for Gaussian random variables $E\{x^{2k}\}=1*3*(2k-1)\sigma_x^2$, the computation of closed form analytical expressions is significantly simplified. Let us proceed to evaluate Equation (6.66), using the previously mentioned assumption.

$$\begin{aligned} N_s &= \frac{1}{2}E_b{N_w}^2\left(\frac{(K-1)^2}{N^2}-2\frac{(K-1)(K-1)}{N^2}+\frac{(K-1)(K-2)}{N^2}+3\frac{K-1}{N^2}\right) \\ &+\frac{E_b}{2}\sum_{i=0}^{N_w-1}\sum_{n=0}^{N_w-1}E\left\{\left(\sum_{u=2}^{K}\sum_{\substack{l=2\\l\neq u}}^{K}R_{l,u}R_{1,u}e^{j\phi_{l,k-i}-j\sum_{m=0}^{N_w-i-2}\Delta\phi_{l,k-i-m}}\right)^*\right. \\ &\left.\times\left(\sum_{u=2}^{K}\sum_{\substack{l=2\\l\neq u}}^{K}R_{l,u}R_{1,u}e^{j\phi_{l,k-n}-j\sum_{m=0}^{N_w-n-2}\Delta\phi_{1,K-n-m}}\right)\right\} \end{aligned}$$

$$+\frac{1}{2}E\left\{\sum_{i=0}^{N_w-1}\sum_{n=0}^{N_w-1}\left[\left(n_{1,k-i}-\sum_{u=2}^{K}n_{u,k-n}R_{1,u}\right)^{*}\left(n_{1,k-n}-\sum_{l=2}^{K}n_{u,k-n}R_{1,u}\right)\right]\right.$$
$$\left.e^{j\sum_{m=0}^{N_w-i-2}\Delta\phi_{1,k-i-m}-j\sum_{m=0}^{N_w-n-2}\Delta\phi_{1,k-n-m}}\right\}, \tag{6.67}$$

cancelling common terms yields:

$$\begin{aligned}N_s &= \frac{1}{2}E_b{N_w}^2\left(\frac{2(K-1)}{N^2}\right)\\ &\quad+\frac{E_b}{2}\sum_{i=0}^{N_w-1}\sum_{u=2}^{K}\sum_{\substack{l=2\\l\neq u}}^{K}\sum_{\substack{\mu=2\\\mu\neq u}}^{K}E\left\{R_{u,l}R_{u,\mu}R_{1,l}R_{1,\mu}\right\}\\ &\quad+\frac{1}{2}\sum_{i=0}^{N_w-1}E\{|n_{1,k-i}-\sum_{u=2}^{K}n_{u,k-i}R_{1,u}|^2\},\end{aligned} \tag{6.68}$$

expanding the second and third terms results in:

$$\begin{aligned}N_s &= \frac{1}{2}E_b{N_w}^2\left(\frac{2(K-1)}{N^2}\right)\\ &\quad+\frac{E_b}{2}\sum_{i=0}^{N_w-1}\sum_{u=2}^{K}\sum_{\substack{\mu=2\\\mu\neq u}}^{K}E\left\{R_{u,\mu}^2\right\}E\left\{R_{1,\mu}^2\right\}\\ &\quad+\frac{1}{2}\left(\sum_{i=0}^{N_w-1}E\{|n_{1,k-i}|^2\}-2\sum_{u=2}^{K}E\{n_{1,k-i}n_{u,k-i}R_{1,u}\}+\sum_{u=2}^{K}E\{|n_{u,k-i}R_{1,u}|^2\}\right)\end{aligned} \tag{6.69}$$

Since the crosscorrelations between signature sequences are assumed to be mutually independent, and there are $(K-1)(K-2)$ elements in the second term then:

$$\begin{aligned}N_s &= \frac{1}{2}E_b{N_w}^2\left(\frac{2(K-1)}{N^2}\right)\\ &\quad+\frac{E_b}{2}N_w\frac{(K-1)(K-2)}{N^2}\\ &\quad+\frac{1}{2}N_w\left(N_o-2N_o\sum_{u=2}^{K}E\{R_{1,u}^2\}+\sum_{u=2}^{K}N_oE\{|R_{1,u}|^2\}\right).\end{aligned} \tag{6.70}$$

Finally, evaluating the contribution of the background noise term as a particular case of Equation (C.10) yields:

$$\begin{aligned}N_s &= \frac{E_b}{2}{N_w}^2\left(\frac{2(K-1)}{N^2}\right)\\ &\quad+\frac{E_b}{2}N_w(K-1)(K-2)\frac{1}{N^2}\\ &\quad+\frac{N_o}{2}N_w\left(1-\frac{K-1}{N}\right)\\ &= \frac{1}{2}N_w\left(\left[E_b(K-1)\frac{2N_w+K-2}{N^2}\right]+N_o\left[1-\frac{K-1}{N}\right]\right).\end{aligned} \tag{6.71}$$

At this point, the probability of error for standard differential detection (i.e. $N_w = 2$) can be computed by substituting the expressions from (6.64) and (6.71) into Equation (6.49):

$$\left\{ \begin{array}{c} a \\ b \end{array} \right\} = \left\{ \begin{array}{c} 0 \\ \frac{2E_b\left(1+\frac{K-1}{N}\right)^2}{\left[E_b(K-1)\frac{4+K-2}{N^2}\right]+N_o\left[1-\frac{K-1}{N}\right]} \end{array} \right\} \tag{6.72}$$

And then inserting these values of a and b into Equation 6.27 yields:

$$\begin{aligned} P_b^{(s=1)} &= Pr\{|z_2|^2 > |z_1|^2\}^{(s=1)} \\ &= \frac{1}{2}\exp\left(\frac{-\frac{E_b}{N_o}\left(1-\frac{K-1}{N}\right)^2}{\left[\frac{E_b}{N_o}\frac{(K-1)(K+2)}{N^2}\right]+\left[1-\frac{K-1}{N}\right]}\right). \end{aligned} \tag{6.73}$$

In deriving the previous equation, it was assumed that the crosscorrelation terms were independent random Gaussian variables. If one drops this simplifying assumption and models the crosscorrelations as true binomially distributed random variables, a more accurate expression can be obtained at the expense of more involved mathematics [28]:

$$P_b^{(s=1)} = \frac{1}{2}\exp\left(\frac{-\frac{E_b}{N_o}\left(1-\frac{K-1}{N}\right)^2}{\left[\frac{E_b}{N_o}\frac{(K-1)}{N^2}((K+2)+\frac{K^2-5K+2}{N})\right]+\left[1-\frac{K-1}{N}+\frac{(K-1)(K-2)}{N^2}\right]}\right). \tag{6.74}$$

6.2.1.3 Analysis for Stage 2 with Full Cancellation

At the second stage of interference cancellation ($s = 2$), the decision statistics obtained at stage one ($s = 1$) are used to remove the interference caused by other users.

In the postdetection approach, the decision statistic of user 1 is computed according to:

$$y_1^{(s=2)} = y_1^{(s=0)} - \sum_{j=2}^{K} y_j^{(s=1)} R_{1,j}. \tag{6.75}$$

The decision statistic for user j at stage one ($s = 1$) corresponds to:

$$y_j^{(s=1)} = \sqrt{E_b}e^{j\phi_j} - \sqrt{E_b}\sum_{u\neq j}^{K}\sum_{l\neq j}^{K} R_{l,u}R_{j,u}e^{j\phi_l} + \left(n_j - \sum_{u\neq j}^{K} n_u R_{j,u}\right) \tag{6.76}$$

Substituting the expression for $y_j^{(s=1)}$ into Equation 6.75 results in:

$$y_1^{(s=2)} = y_1^{(s=0)} - \sum_{j=2}^{K}\left(\sqrt{E_b}e^{j\phi_j} - \sqrt{E_b}\sum_{u\neq j}^{K}\sum_{l\neq u}^{K} R_{l,u}R_{j,u}e^{j\phi_l}\right.$$

$$-\sum_{j=2}^{K}(n_j+\sum_{u\neq j}n_uR_{j,u})\Bigg)R_{1,j} \tag{6.77}$$

Substituting for $y_1^{(s=0)}$ from Equation (6.56), and cancelling the estimated multiple access contribution of the interferers results in:

$$\begin{aligned} y_1^{(s=2)} &= \sqrt{E_b}e^{j\phi_1}+ \\ &\quad +\sqrt{E_b}\sum_{j=2}^{K}\sum_{u\neq j}^{K}\sum_{l\neq u}^{K}R_{l,u}R_{j,u}R_{1,j}e^{j\phi_l} \\ &\quad +(n_1-\sum_{j=2}^{K}n_jR_{1,j}+\sum_{j=2}^{K}\sum_{u\neq j}^{K}n_kR_{j,u}R_{1,j}). \end{aligned} \tag{6.78}$$

This equation can be more conveniently written by grouping the terms that correspond to user 1 in a single term:

$$\begin{aligned} y_1^{(s=2)} &= \sqrt{E_b}\left[1+\sum_{j=2}^{K}\sum_{\substack{u=2\\u\neq j}}^{K}R_{1,u}R_{j,u}R_{1,j}e^{j\phi_1}\right]+ \\ &\quad +\sqrt{E_b}\sum_{j=2}^{K}\sum_{u\neq j}^{K}\sum_{\substack{l=2\\l\neq u}}^{K}R_{l,u}R_{j,u}R_{1,j}e^{j\phi_l} \\ &\quad +\left(n_1-\sum_{j=2}^{K}n_jR_{1,j}+\sum_{j=2}^{K}\sum_{u\neq j}^{K}n_kR_{j,u}R_{1,j}\right). \end{aligned} \tag{6.79}$$

As in the analysis of the previous two stages, let us define the following multi-symbol random variables:

$$z_1^{(s=2)}=\sum_{i=0}^{N_w-1}y_{1,k-i}^{(s=2)}e^{-j\sum_{m=0}^{N_w-i-2}\Delta\phi_{1,k-i-m}} \tag{6.80}$$

$$z_2^{(s=2)}=\sum_{i=0}^{N_w-1}y_{1,k-i}^{(s=2)}e^{-j\sum_{m=0}^{N_w-i-2}\Delta\hat{\phi}_{1,k-i-m}}. \tag{6.81}$$

Substituting the expression for $y_1^{(s=2)}$ found in Equation (6.79) into the previous equation, and taking the expected value of z_1, results in:

$$E\{z_1^{(s=2)}\}=N_w\sqrt{E_b}. \tag{6.82}$$

The power in the non-random component of z_1 is:

$$\begin{aligned} S_1^{(s=2)} &= \frac{1}{2}|\overline{z_1^{(s=2)}}|^2 \\ &= \frac{1}{2}N_w^2 E_b. \end{aligned} \tag{6.83}$$

In order to simplify the notation, in the following analysis the superscript $(s=2)$ will be dropped, with the understanding that the focus of the analysis is the second stage of interference cancellation.

At the second stage of interference cancellation, the noise power of Equation (6.31) is given by:

$$N_s = \frac{1}{2}E\left\{|\sum_{i=0}^{N_w-1} y_{1,k-i}e^{-j\sum_{m=0}^{N_w-i-2}\Delta\phi_{1,k-i-m}} - N_w\sqrt{E_b}e^{j\phi_{1,k-N_w+1}}|^2\right\}. \tag{6.84}$$

Substituting into the previous equation the expression for $y_{1,k-i}$ presented in Equation (6.79), results in:

$$\begin{aligned} N_s = \frac{1}{2}E\Bigg\{ & |N_w\sqrt{E_b}[\sum_{j=2}^{K}\sum_{\substack{u=2\\u\neq j}}^{K} R_{1,u}R_{j,u}R_{1,j}]e^{j\phi_{1,k-N_w+1}} \\ & +\sqrt{E_b}\sum_{i=0}^{N_w 1}\left(\sum_{j=2}^{K}\sum_{l=2}^{K}\sum_{\substack{u\neq j\\u\neq l}}^{K} R_{1,j}R_{j,u}R_{u,l}e^{j\phi_l}\right)e^{-j\sum_{m=0}^{N_w-i-2}\Delta\phi_{1,k-i-m}} \\ & +\sum_{i=0}^{N_w-1}(n_1 - \sum_{j=2}^{K} n_j R_{1,j} + \sum_{j=2}^{K}\sum_{u\neq j} n_u R_{j,u}R_{1,u})e^{-j\sum_{m=0}^{N_w-i-2}\Delta\phi_{1,k-i-m}}|^2\Bigg\}, \end{aligned} \tag{6.85}$$

In order to simplify the task, the crosscorrelations between signatures will be modeled as independent Gaussian random variables of zero mean and variance $E\{R^2\} = \frac{1}{N}$. Under this assumption, based on results from [28], the noise power corresponds to:

$$\begin{aligned} N_s = & \frac{1}{2}E_b N_w^2 2(K-1)(K-2)\frac{1}{N^3} \\ & +\frac{1}{2}E_b N_w \frac{5(K-1)(K^2-K+1)}{N^3} \\ & +\frac{1}{2}N_o N_w[1+\left(\frac{K-1}{N}\right)\left(1-\frac{2K-1}{N}\right)], \end{aligned} \tag{6.86}$$

At this point, the probability of error for standard differential detection ($N_w = 2$) can be computed by substituting the expressions from (6.83) and (6.86) into:

$$\begin{Bmatrix} a \\ b \end{Bmatrix} = \begin{Bmatrix} 0 \\ \frac{S_1}{N_s} \end{Bmatrix}, \tag{6.87}$$

and then employing Equation (6.27) to obtain the probability of error:

$$\begin{aligned} P_b^{(s=2)} &= Pr\{|z_2|^2 > |z_1|^2\}^{(s=2)} \\ &= \frac{1}{2}\exp\left(\frac{-E_b}{E_b\left(\frac{(K-1)(5K^2-K-3)}{N^3}\right)+N_o[1+\left(\frac{K-1}{N}\right)\left(1-\frac{2K-1}{N}\right)]}\right). \end{aligned} \tag{6.88}$$

Figure 6.6 shows a plot of the probability of bit error vs. E_b/N_o for the case of full interference cancellation. As can be seen in this figure, the analytical results are in agreement with the simulated results. For stage 1, the graph also includes a plot of the results obtained using the binomial distribution of the crosscorrelations. This figure reveals something peculiar about the performance of the full interference cancellation scheme. As predicted analytically, and confirmed by simulations, for large number of users the probability of bit error for the standard differential correlation demodulator is better than the probability of bit error after one stage of full interference cancellation.

A plot of probability of bit error vs. number of users can be observed in Figure 6.7. This figure illustrates that for small system loads, full interference cancellation is still beneficial. This figure also shows that for system loads on the order of the processing gain N, the conventional receiver outperforms the interference cancellation receivers.

6.2.2 Partial Interference Cancellation

The analysis in this section focuses on combined parallel interference cancellation and multiple symbol differential detection. Partial interference cancellation, is an attractive technique that can be used, as in Chapter 4, to overcome some of the drawbacks associated with full subtraction of the estimated interference.

6.2.2.1 Analysis of Stage 1 with Partial Interference Cancellation

In the partial interference cancellation approach, the decision statistics at stage one are obtained by partially subtracting the estimated interference caused by the remaining users:

$$y_1^{(s=1)} = y_1^{(s=0)} - C_1 \sum_{u=2}^{K} y_u^{(s=0)} R_{1,u}, \tag{6.89}$$

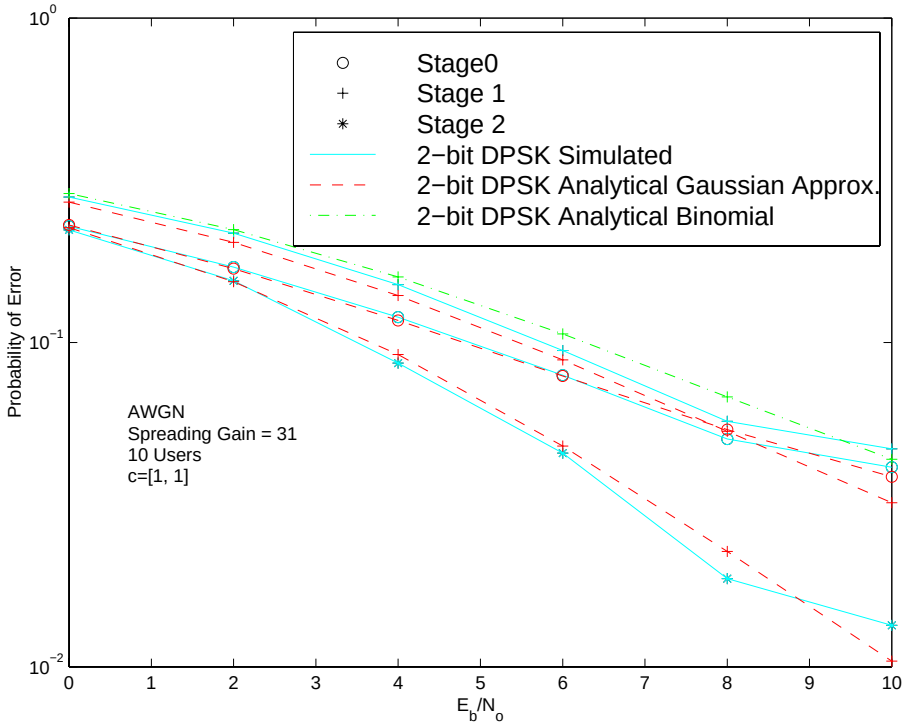

Figure 6.6: Comparison of analytical and simulated multiuser probability of error vs. E_b/N_o for full cancellation. Random codes, spreading gain = 31, AWGN and 10 synchronous users.

where C_1 is the partial cancellation factor at stage 1. Using Equation (6.33) to express the soft outputs of the conventional receiver, and cancelling like terms, gives the decision statistics after partial interference cancellation:

$$\begin{aligned} y_1^{(s=1)} &= \sqrt{E_b}e^{j\phi_1} + \sum_{l=2}^{K}\sqrt{E_b}R_{1,l}e^{j\phi_l} + n_1 \\ &\quad -C_1\sum_{u=2}^{K}\left(\sqrt{E_b}e^{j\phi_u} + \sum_{l\neq u}^{K}\sqrt{E_b}R_{l,u}e^{j\phi_l} + n_u\right)R_{1,u}. \end{aligned} \tag{6.90}$$

Factoring common terms results in:

$$\begin{aligned} y_1^{(s=1)} &= \sqrt{E_b}\left[1 - C_1\sum_{u=2}^{K}R_{1,u}^2\right]e^{j\phi_1} \\ &\quad +(1-C_1)\sum_{u=2}^{K}\sqrt{E_b}R_{1,u}e^{j\phi_u} - C_1\sqrt{E_b}\sum_{u=2}^{K}\sum_{\substack{l=2\\l\neq u}}^{K}R_{l,u}R_{1,u}e^{j\phi_l} + \left(n_1 - C_1\sum_{u=2}^{K}n_uR_{1,u}\right). \end{aligned} \tag{6.91}$$

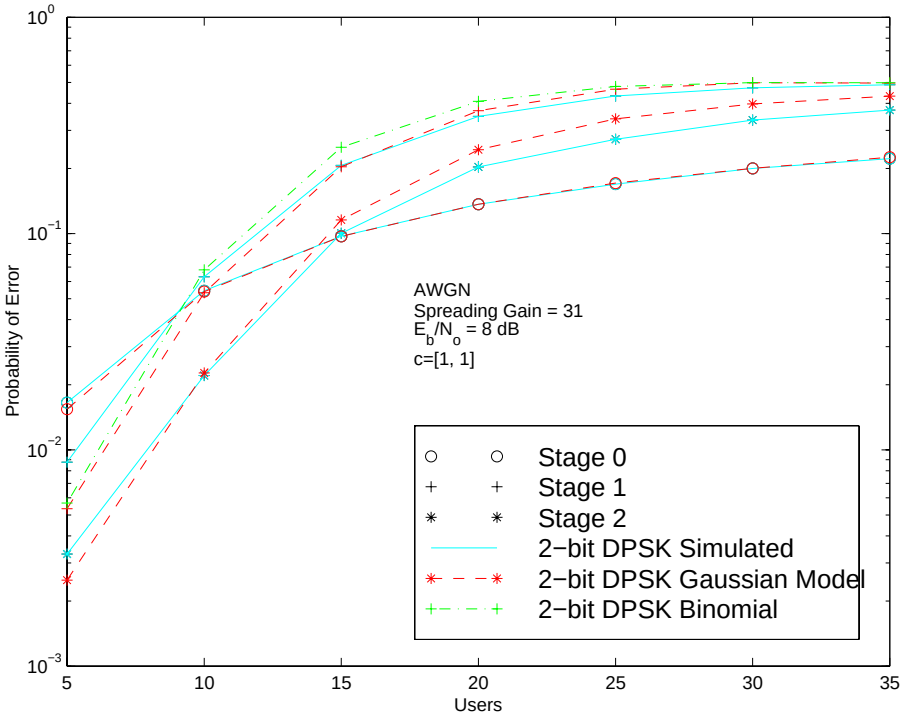

Figure 6.7: Comparison of analytical and simulated multiuser probability of error vs. number of users for full cancellation, $E_b/N_o = 8$ dB. Random codes, spreading gain = 31, AWGN and 10 users.

To compute the pairwise probability of error, $Pr\{|z_2|^2 > |z_1|^2\}$, let us define the variables z_1 and z_2 as:

$$z_1 = \sum_{k=0}^{N_w-1} y_1^{(s=1)} e^{-j\sum_{m=0}^{N_w-i-2}\Delta\phi_{1,k-i-m}}, \tag{6.92}$$

and

$$z_2 = \sum_{k=0}^{N_w-1} y_1^{(s=1)} e^{-j\sum_{m=0}^{N_w-i-2}\Delta\hat{\phi}_{1,k-i-m}}. \tag{6.93}$$

Substituting in Equation (6.92) the expression given in Equation 6.91 for $y_1^{(s=1)}$ results in:

$$\begin{aligned} z_1 = {} & N_w\sqrt{E_b}e^{j\phi_{1,k-N_w+1}}\left[1 - C_1\sum_{u=2}^{K}R_{1,u}^2\right] + \sum_{k=0}^{N_w-1}\left((1-C_1)\sum_{u=2}^{K}\sqrt{E_b}R_{1,u}e^{j\phi_u}\right. \\ & \left. -C_1\sqrt{E_b}\sum_{u=2}^{K}\sum_{\substack{l=2\\ l\neq u}}^{K}R_{l,u}R_{1,u}e^{j\phi_{l,k-i}} + (n_{1,k-i} - C_1\sum_{u=2}^{M}n_{u,k-i})R_{1,u}\right)e^{-j\sum_{m=0}^{N_w-i-2}\Delta\phi_{1,k-i-m}}, \end{aligned}$$

(6.94)

its mean, $\overline{z_1}$, corresponds to:

$$\overline{z_1} = N_w\sqrt{E_b}\left(1 - C_1\frac{K-1}{N}\right)e^{j\phi_{1,k-N_w+1}}. \tag{6.95}$$

Note that the bias in the mean has been reduced by an amount proportional to the partial cancellation factor ($0 \leq C_1 \leq 1$).

The power in the non-random component S_1 is:

$$\begin{aligned} S_1 &= \frac{1}{2}|\overline{z_1}|^2 \\ &= \frac{1}{2}N_w^2 E_b\left(1 - C_1\frac{K-1}{N}\right)^2. \end{aligned} \tag{6.96}$$

After interference cancellation, the noise power of Equation (6.31) corresponds to:

$$\begin{aligned} N_s = \frac{1}{2}E\Bigg\{\Big|\sum_{i=0}^{N_w-1} y_{1,k-i}e^{-j\sum_{m=0}^{N_w-i-2}\Delta\phi_{1,k-i-m}} \\ -N_w\sqrt{E_b}\left(1 + C_1\frac{K-1}{N}\right)e^{j\phi_{1,k-N_w+1}}\Big|^2\Bigg\}, \end{aligned} \tag{6.97}$$

substituting for $y_{1,k-i}$ as given in (6.91) results in:

$$\begin{aligned} N_s = &\frac{1}{2}E\left\{\left|\sqrt{E_b}C_1\sum_{i=0}^{N_w-1}\left(\frac{K-1}{N} - \sum_{u=2}^{K}R_{1,u}^2\right)e^{j\phi_{1,k-N_w+1}}\right|^2\right\} \\ &+\frac{1}{2}E\left\{\left|\sqrt{E_b}(1-C_1)\sum_{i=0}^{N_w-1}\sum_{u=2}^{K}\sqrt{E_b}R_{1,u}e^{j\phi_{u,k-i}-j\sum_{m=0}^{N_w-i-2}\Delta\phi_{1,k-i-m}}\right|^2\right\} \\ &+\frac{1}{2}E\left\{\left|\sqrt{E_b}C_1\sum_{i=0}^{N_w-1}\sum_{u=2}^{K}\sum_{\substack{l=2\\l\neq u}}^{K}R_{l,u}R_{1,u}e^{j\phi_{l,k-i}-j\sum_{m=0}^{N_w-i-2}\Delta\phi_{1,k-i-m}}\right|^2\right\} \\ &+\frac{1}{2}E\left\{\left|\sum_{i=0}^{N_w-1}\left(n_{1,k-i} - C_1\sum_{u=2}^{K}n_{u,k-i}R_{1,u}\right)e^{-j\sum_{m=0}^{N_w-i-2}\Delta\phi_{1,k-i-m}}\right|^2\right\}. \end{aligned} \tag{6.98}$$

Evaluation of the expectations is readily performed, by taking advantage of the fact that these expectations are very similar to the ones already evaluated for the full cancellation case.

$$\begin{aligned} N_s = &\frac{1}{2}{N_w}^2 E_b C_1^2\left(\frac{2(K-1)}{N^2}\right) \\ &+\frac{1}{2}N_w E_b(1-C_1)^2\frac{K-1}{N} \end{aligned}$$

$$+\frac{1}{2}N_w E_b C_1^2 (K-1)(K-2)\frac{1}{N^2}$$
$$+\frac{1}{2}N_w \left(N_o - 2N_o C_1 \sum_{u=2}^{K} E\{R_{1,u}^2\} + \sum_{u=2}^{K} N_o C_1^2 E\{R_{1,u}^2\} \right), \quad (6.99)$$

this equation can be directly evaluated by recalling that $E\{R_{1,u}^2\} = \frac{1}{N}$. Therefore:

$$\begin{aligned} N_s &= \frac{1}{2}{N_w}^2 E_b C_1^2 \left(\frac{2(K-1)}{N^2} \right) \\ &\quad +\frac{1}{2}N_w E_b (1-C_1)^2 \frac{K-1}{N} \\ &\quad +\frac{1}{2}N_w E_b C_1^2 (K-1)(K-2)\frac{1}{N^2} \\ &\quad +\frac{1}{2}N_w N_o \left(1 - 2C_1 \frac{K-1}{N} + C_1^2 \frac{K-1}{N} \right). \end{aligned} \quad (6.100)$$

The probability of error for the standard differential receiver ($N_w = 2$) can be computed at this point. The parameters a and b of the Marcum-Q function are given by:

$$\left\{ \begin{array}{c} a \\ b \end{array} \right\} = \left\{ \begin{array}{c} 0 \\ \frac{S_1}{N_s} \end{array} \right\}, \quad (6.101)$$

and S_1 and N_s are given in Equations (6.96) and (6.100) respectively. Substituting into (6.27) yields the pairwise error probability of choosing $\mathbf{\Delta}\hat{\phi}$ when $\mathbf{\Delta}\phi$ is transmitted. Since for $N_w = 2$ and binary signaling, the pairwise probability is equivalent to the probability of bit error, then:

$$Pr\{|z_2|^2 > |z_1|^2\}^{(s=1)} = \frac{1}{2}\exp\left(\frac{-E_b \left(1 - C_1 \frac{K-1}{N}\right)^2}{E_b \left(2C_1^2 \frac{2(K-1)}{N^2} + (1-C_1)^2 \frac{K-1}{N} + C_1^2 (K-1)\frac{K-2}{N^2} \right) + N_o \left(1 - 2C_1 \frac{K-1}{N} + C_1^2 \frac{K-1}{N} \right)} \right). \quad (6.102)$$

Or in a slightly more compact notation:

$$\begin{aligned} P_b^{(s=1)} &= Pr\{|z_2|^2 > |z_1|^2\}^{(s=1)} \\ &= \frac{1}{2}\exp\left(\frac{-E_b \left(1 - C_1 \frac{K-1}{N}\right)^2}{E_b \frac{K-1}{N} \left(C_1^2 \frac{K+2}{N} + (1-C_1)^2 \right) + N_o \left(1 - C_1 \frac{K-1}{N}(2 - C_1) \right)} \right). \end{aligned} \quad (6.103)$$

Note that for $C_1 = 1$, Equation (6.103) evaluates to (6.73), which corresponds to the probability of bit error for the full cancellation approach. For $C_1 = 0$, it evaluates to the conventional receiver.

In the previous derivation, because the user crosscorrelations were modeled as mutually independent Gaussian variables, certain consequential terms were disregarded. In reality, the signature sequence crosscorrelations are uncorrelated, but not independent, random variables.

It is shown in Appendix E of [28] that:

$$E\{R_{i,j}R_{j,m}R_{i,m}\} = \frac{1}{N^2}. \tag{6.104}$$

Taking this fact into consideration, one can augment the expressions employed in the computation of the probability of error to account for quadratic terms that arise as a result of expressions of the form of Equation 6.104.

An augmented expression for the equivalent noise power can be obtained by incorporating this knowledge into Equation (6.97). After adding the appropriate terms, this expression becomes:

$$\begin{aligned} N_s &= \frac{1}{2}{N_w}^2 E_b C_1^2 \left(\frac{2(K-1)}{N^2}\right) \\ &\quad + \frac{1}{2}N_w E_b (1-C_1)^2 \frac{K-1}{N} \\ &\quad + \frac{1}{2}N_w E_b C_1^2 (K-1)(K-2)\frac{1}{N^2} \\ &\quad - \frac{1}{2}2N_w E_b C_1 (1-C_1)\frac{(K-1)(K-2)}{N^2} \\ &\quad + \frac{1}{2}N_w N_o \left(1 - 2C_1\frac{K-1}{N} + C_1^2\left(\frac{K-1}{N} + \frac{(K-1)(K-2)}{N^2}\right)\right). \end{aligned} \tag{6.105}$$

The probability of error is given by:

$$P_b^{(s=1)} = \frac{1}{2}\exp\left(\frac{-E_b\left(1-C_1\frac{K-1}{N}\right)^2}{E_b\frac{K-1}{N}\left(C_1^2\left(\frac{K+2}{N}\right)+(1-C_1)\left((1-C_1)-2C_1\frac{(K-2)}{N}\right)\right)+N_o\left(1-C_1\frac{K-1}{N}\left(2-C_1\left(1+\frac{(K-2)}{N}\right)\right)\right)}\right). \tag{6.106}$$

Figure 6.8 shows a comparison of the analytic results produced with the augmented expression, along with simulation and analytical results using the independent Gaussian assumption for the user crosscorrelations. This figure shows that the augmented expression produces optimistic results when compared to simulation results. This is due to the fact that in addition to the quadratic terms there are consequential higher order terms that have not been accounted for.

In [28], a more accurate expression was derived for the bit-energy-to-noise spectral density ratio at stage 1. This expression is based on the analytical averages of the binomially distributed signature

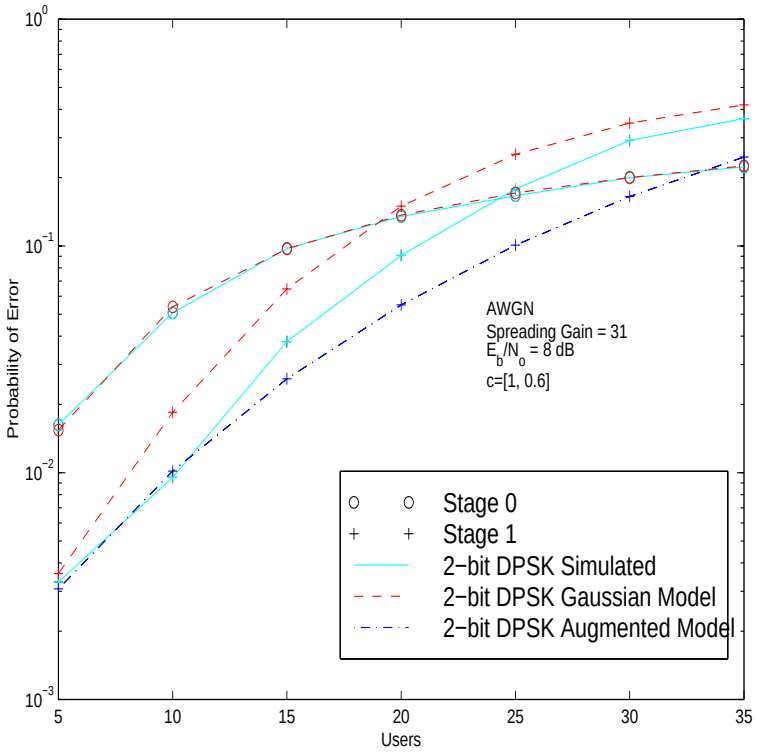

Figure 6.8: Comparison of analytical results obtained with the augmented expression and simulated results for stage 1 of the multiuser probability of error vs. E_b/N_o. Random codes, spreading gain = 31, AWGN and 10 synchronous users.

sequence crosscorrelations, and results in a more accurate formula.

$$P_b^{(s=1)} = \frac{1}{2}\exp\left(\frac{-E_b\left(1-C_1\frac{K-1}{N}\right)^2}{E_b\frac{K-1}{N}\left(C_1^2\left(\frac{K+2}{N}+\frac{K^2-5K+2}{N^2}\right)+(1-C_1)((1-C_1)-2C_1\frac{(K-2)}{N})\right)+N_o\left(1-C_1\frac{K-1}{N}(2-C_1(1+\frac{(K-2)}{N}))\right)}\right). \quad (6.107)$$

Figure 6.9 shows analytical and simulated probability of bit error curves for the differential partial parallel interference cancellation approach. This figure provides a comparison between the analytic results that result from modeling the crosscorrelations as independent Gaussian random variables and the results based on the binomial distribution for the crosscorrelations. The curve for the binomially distributed crosscorrelations is quite accurate. The Gaussian model, however, produces slightly pessimistic estimates.

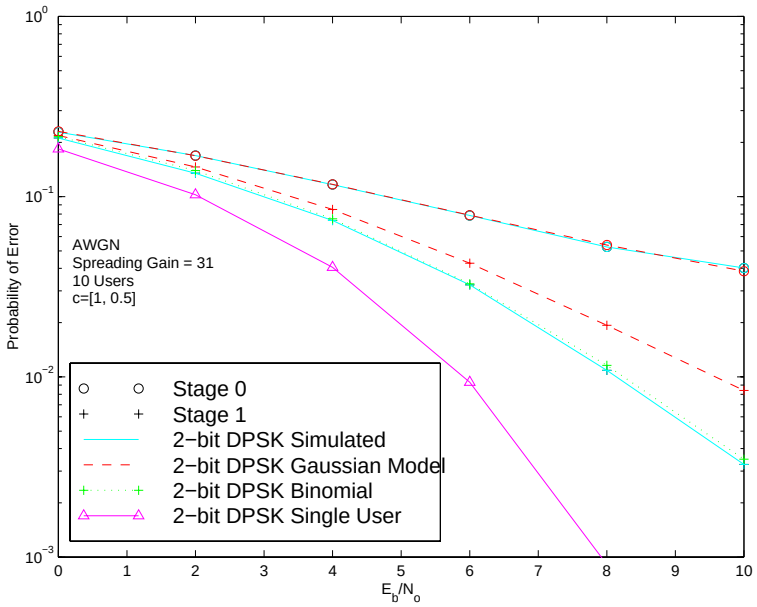

Figure 6.9: Comparison of analytical and simulated results for stage 1 of the multiuser probability of error vs. E_b/N_o. Random codes, spreading gain = 31, AWGN and 10 synchronous users.

6.2.2.2 Analysis of Stage 2 with Partial Cancellation

At the second stage of interference cancellation ($s = 2$), the decision statistics obtained in stage one ($s = 1$) are used to partially remove the interference caused by the remaining users. The decision statistic of user 1 is given by:

$$y_1^{(s=2)} = y_1^{(s=0)} - C_2 \sum_{j=2}^{K} y_j^{(s=1)} R_{1,j}, \tag{6.108}$$

where $0 < C_2 \leq 1$ is the partial cancellation factor for stage 2.

The decision statistic for user j after one stage of partial interference cancellation corresponds to:

$$\begin{aligned} y_j^{(s=1)} &= \sqrt{E_b} e^{j\phi_j} + (1 - C_1) \sum_{u \neq j}^{K} \sqrt{E_b} R_{j,u} e^{j\phi_u} \\ &\quad - C_1 \sqrt{E_b} \sum_{u \neq j}^{K} \sum_{l \neq u}^{K} R_{l,u} R_{j,u} e^{j\phi_l} + \left(n_j - C_1 \sum_{u \neq j}^{K} n_u R_{j,u} \right). \end{aligned} \tag{6.109}$$

Substituting the expression for $y_j^{(s=1)}$ into Equation 6.108 yields:

$$\begin{aligned} y_1^{(s=2)} &= y_1^{(s=0)} - C_2 \sum_{j=2}^{K} \left(\sqrt{E_b} e^{j\phi_j} + (1-C_1) \sum_{u \neq j}^{K} \sqrt{E_b} R_{j,u} e^{j\phi_u} \right. \\ &\quad \left. - C_1 \sqrt{E_b} \sum_{u \neq j}^{K} \sum_{l \neq u}^{K} R_{l,u} R_{j,u} e^{j\phi_l} + (n_j - C_1 \sum_{u \neq j}^{K} n_u R_{j,u}) \right) R_{1,j}. \end{aligned} \tag{6.110}$$

Substituting for $y_1^{(s=0)}$ from Equation (6.56), and partially cancelling the estimated multiple access contribution of the interferers results in

$$\begin{aligned} y_1^{(s=2)} &= \sqrt{E_b} e^{j\phi_1} + (1-C_2) \sum_{j=2}^{K} \sqrt{E_b} R_{1,j} e^{j\phi_j} \\ &\quad - C_2 (1-C_1) \sum_{j=2}^{K} \sum_{u \neq j}^{K} \sqrt{E_b} R_{j,u} R_{1,j} e^{j\phi_u} \\ &\quad + C_1 C_2 \sum_{j=2}^{K} \sum_{u \neq j}^{K} \sum_{l \neq u}^{K} \sqrt{E_b} R_{l,u} R_{j,u} R_{1,j} e^{j\phi_l} \\ &\quad + \left(n_1 - C_2 \sum_{j=2}^{K} n_j R_{1,j} + C_1 C_2 \sum_{j=2}^{K} \sum_{u \neq j}^{K} n_u R_{j,u} R_{1,j} \right), \end{aligned} \tag{6.111}$$

which can be dissected as:

$$\begin{aligned} y_1^{(s=2)} &= \sqrt{E_b} \left(1 - C_2 (1-C_1) \sum_{j=2}^{K} R_{1,j}^2 + C_1 C_2 \sum_{j=2}^{K} \sum_{\substack{u=2 \\ u \neq j}}^{K} R_{1,u} R_{j,u} R_{1,j} \right) e^{j\phi_1} \\ &\quad + (1-C_2) \sum_{j=2}^{K} \sqrt{E_b} R_{1,j} e^{j\phi_j} \\ &\quad - C_2 (1-C_1) \sum_{j=2}^{K} \sum_{\substack{u=2 \\ u \neq j}}^{K} \sqrt{E_b} R_{j,u} R_{1,j} e^{j\phi_u} \\ &\quad + C_1 C_2 \sqrt{E_b} \sum_{j=2}^{K} \sum_{\substack{u \neq j \\ u \neq l}}^{K} \sum_{l=2}^{K} R_{l,u} R_{j,u} R_{1,j} e^{j\phi_l} \\ &\quad + \left(n_1 - C_2 \sum_{j=2}^{K} n_j R_{1,j} + C_1 C_2 \sum_{j=2}^{K} \sum_{u \neq j}^{K} n_u R_{j,u} R_{1,j} \right). \end{aligned} \tag{6.112}$$

As its been done for the previous stages, let us define the variable z_1 as:

$$z_1 = \sum_{k=0}^{N_w - 1} y_1^{(s=2)} e^{-j \sum_{m=0}^{N_w - i - 2} \Delta\phi_{1,K-i-m}}, \tag{6.113}$$

the expected value of this variable is:

$$\overline{z_1} = N_w\sqrt{E_b}\left[1 - C_2(1-C_1)\frac{K-1}{N}\right]e^{j\phi_{1,K-N_w+1}}. \quad (6.114)$$

The power in the non-random component of z_1 is computed according to:

$$\begin{aligned} S_1^{(s=2)} &= \frac{1}{2}|\overline{z_1^{(s=2)}}|^2 \\ &= \frac{1}{2}N_w^2 E_b\left[1 - C_2(1-C_1)\frac{K-1}{N}\right]^2. \end{aligned} \quad (6.115)$$

For the sake of brevity the superscript $(s=2)$ will be dropped from the following analysis since it is understood that the analysis focuses on stage 2.

After the second stage of partial interference cancellation, the noise power in Equation (6.31) can be obtained from:

$$\begin{aligned} N_s = \frac{1}{2}E\Bigg\{|\sum_{i=0}^{N_w-1} & y_{1,k-i}e^{-j\sum_{m=0}^{N_w-i-2}\Delta\phi_{1,k-i-m}} \\ & -N_w\sqrt{E_b}\left[1 - C_2(1-C_1)\frac{K-1}{N}\right]e^{j\phi_{1,K-N_w+1}}|^2\Bigg\}. \end{aligned} \quad (6.116)$$

Substituting for $y_{1,k-i}$ from Equation (6.111) into the previous equation results in the following expression:

$$\begin{aligned} N_s = \frac{1}{2}E\Bigg\{|\sum_{i=0}^{N_w-1}\Bigg(&\sqrt{E_b}C_2\left[C_1\sum_{j=2}^{K}\sum_{\substack{u=2\\u\neq j}}^{K}R_{1,u}R_{j,u}R_{1,j} - (1-C_1)\sum_{j=2}^{K}R_{1,j}^2\right. \\ &\left.+(1-C_1)\frac{K-1}{N}\right]e^{j\phi_{1,K-N_w+1}} \\ &+(1-C_2)\sqrt{E_b}\sum_{j=2}^{K}R_{1,j}e^{j\phi_{j,k-i}}e^{-j\sum_{m=0}^{N_w-i-2}\Delta\phi_{1,k-i-m}} \\ &-C_2(1-C_1)\sum_{j=2}^{K}\sum_{\substack{u=2\\u\neq j}}^{K}\sqrt{E_b}R_{j,u}R_{1,j}e^{j\phi_{u,k-i}}e^{-j\sum_{m=0}^{N_w-i-2}\Delta\phi_{1,k-i-m}} \\ &+C_1C_2\sqrt{E_b}\sum_{j=2}^{K}\sum_{\substack{u\neq j\\u\neq l}}^{K}\sum_{l=2}^{K}R_{l,u}R_{j,u}R_{1,j}e^{j\phi_{l,k-i}}e^{-j\sum_{m=0}^{N_w-i-2}\Delta\phi_{1,k-i-m}} \\ &+(n_{1,k-i} - C_2\sum_{j=2}^{K}n_{j,k-i}R_{1,j} + C_1C_2\sum_{j=2}^{K}\sum_{u\neq j}^{K}n_{u,k-i}R_{j,u}R_{1,j})e^{-j\sum_{m=0}^{N_w-i-2}\Delta\phi_{1,k-i-m}}\Bigg)|^2\Bigg\}. \end{aligned} \quad (6.117)$$

Evaluation of this expression is simplified by modeling the crosscorelations between user signatures as independent Gaussian random variables of zero mean and variance $1/N$.

Noticing the similarities between the expression of Equation (6.85) and Equation (6.117) for the second stage of full cancellation, and employing Equation (C.10) for the background noise, allows evaluation of the equivalent noise power:

$$\begin{aligned} N_s &= \frac{1}{2}N_w^2 E_b C_2^2 \left[C_1^2\left(2\frac{(K-1)(K-2)}{N^3}\right)+(1-C_1)^2\left(\frac{2(K-1)}{N^2}\right)\right] \\ &+\frac{1}{2}N_w E_b (1-C_2)^2\frac{K-1}{N} \\ &+\frac{1}{2}N_w E_b C_2^2(1-C_1)^2(K-1)(K-2)\frac{1}{N^2} \\ &+\frac{1}{2}N_w E_b (C_1C_2)^2\frac{5(K-1)(K^2-K+1)}{N^3} \\ &+\frac{1}{2}N_w E_b 2(1-C_2)C_1C_2\frac{(K-1)(2K-1)}{N^2} \\ &+\frac{1}{2}N_w N_o\left[1+C_2\left(\frac{K-1}{N}\right)\left(C_2+2C_1-2+C_1(C_1C_2-2)\frac{2K-1}{N}\right)\right]. \end{aligned} \quad (6.118)$$

Evaluation of the probability of bit error for standard differential detection is feasible at this point. For standard differential detection, the parameters a and b required in Equation (6.27) correspond to:

$$\left\{\begin{array}{c} a \\ b \end{array}\right\} = \left\{\begin{array}{c} 0 \\ \frac{S_1}{N_s} \end{array}\right\}, \quad (6.119)$$

and S_1 and N_s are given in Equations (6.118) and (6.115) respectively.

According to Equation (6.27), the resulting expression for the probability of error is:

$$P_b^{(s=2)} = \frac{1}{2}\exp\left(\frac{-E_b[1-C_2(1-C_1)\frac{K-1}{N}]^2}{\begin{array}{c} E_b\left(2C_2^2\left[C_1^2\left(2\frac{(K-1)(K-2)}{N^3}\right)+(1-C_1)^2\left(\frac{2(K-1)}{N^2}\right)\right]+(1-C_2)^2\frac{K-1}{N}+\right. \\ \left. C_2^2(1-C_1)^2\frac{(K-1)(K-2)}{N^2}+(C_1C_2)^2\frac{5(K-1)(K^2-K+1)}{N^3}+2(1-C_2)C_1C_2\frac{(K-1)(2K-1)}{N^2}\right) \\ +N_o\left[1+C_2\left(\frac{K-1}{N}\right)\left(C_2+2C_1-2+C_1C_2(C_1-2)\frac{2K-1}{N}\right)\right] \end{array}}\right). \quad (6.120)$$

Note that this formula evaluates to Equation (6.88) for the full cancellation case (i.e., when both C_1 and C_2 equal to one).

For stage 2, using the independent Gaussian model for the crosscorrelations yields slightly pessimistic results. Augmenting the expressions to account for the fact that the signature sequence crosscorrelations are not independent more accurate results can be obtained. This can however become very involved. A very simple modification to the previous expression that accounts for the non-independence of the cross-correlations in the numerator will be used. Using the result of Equation (6.104), one can modify Equation (6.114) to account for the non-zero term

$$E\{C_1C_2\sqrt{E_b}\sum_{j=2}^{K}\sum_{\substack{u=2\\u\neq j}}^{K}R_{1,u}R_{j,u}R_{1,j}e^{j\phi_1}\} \;=\; C1C2\sqrt{E_b}\frac{(K-1)(K-2)}{N^2}. \tag{6.121}$$

The power in the non-random component of z_1 then becomes:

$$\begin{aligned} S_1^{(s=2)} &= \frac{1}{2}|\overline{z_1^{(s=2)}}|^2 \\ &= \frac{1}{2}N_w^2E_b\left[1-C_2(1-C_1)\frac{K-1}{N}+C1C2\frac{(K-1)(K-2)}{N^2}\right]^2. \end{aligned} \tag{6.122}$$

Using this expression in the evaluation of the probability of error results in:

$$\begin{aligned} P_b^{(s=2)} = \frac{1}{2}\exp\Bigg(&\frac{-E_b[1-C_2(1-C_1)\frac{K-1}{N}+C1C2\frac{(K-1)(K-2)}{N^2}]^2}{E_b\left(2C_2^2\left[C_1^2\left(2\frac{(K-1)(K-2)}{N^3}\right)+(1-C_1)^2\left(\frac{2(K-1)}{N^2}\right)\right]+(1-C_2)^2\frac{K-1}{N}\;+\right.}\\ &\left.\frac{}{C_2^2(1-C_1)^2\frac{(K-1)(K-2)}{N^2}+(C_1C_2)^2\frac{5(K-1)(K^2-K+1)}{N^3}+2(1-C_2)C_1C_2\frac{(K-1)(2K-1)}{N^2}\right)}\\ &\frac{}{+N_o\left[1+C_2\left(\frac{K-1}{N}\right)\left(C_2+2C_1-2+C_1C_2(C_1-2)\frac{2K-1}{N}\right)\right]}\Bigg). \end{aligned} \tag{6.123}$$

A comparison of simulation and analytical results is presented in Figure 6.10. This figure indicates that at low E_b/N_os the analytical results obtained using the Gaussian assumption are very close to the simulated ones. However, at higher values of E_b/N_o, it gives rather pessimistic results. For stage 1, the curve based on the binomial distribution is quite accurate. The augmented expression, is closer to the simulated results, however there is still significant disagreement.

Simulation and analytical curves of probability of bit error as a function of the number of users are shown in Figure 6.11. This figure shows the curves based on the independent Gaussian assumption provide slightly pessimistic results. The curve based on the augmented expression, gives a better estimate of the capacity of the system. For stage 1, the expression that uses the binomial

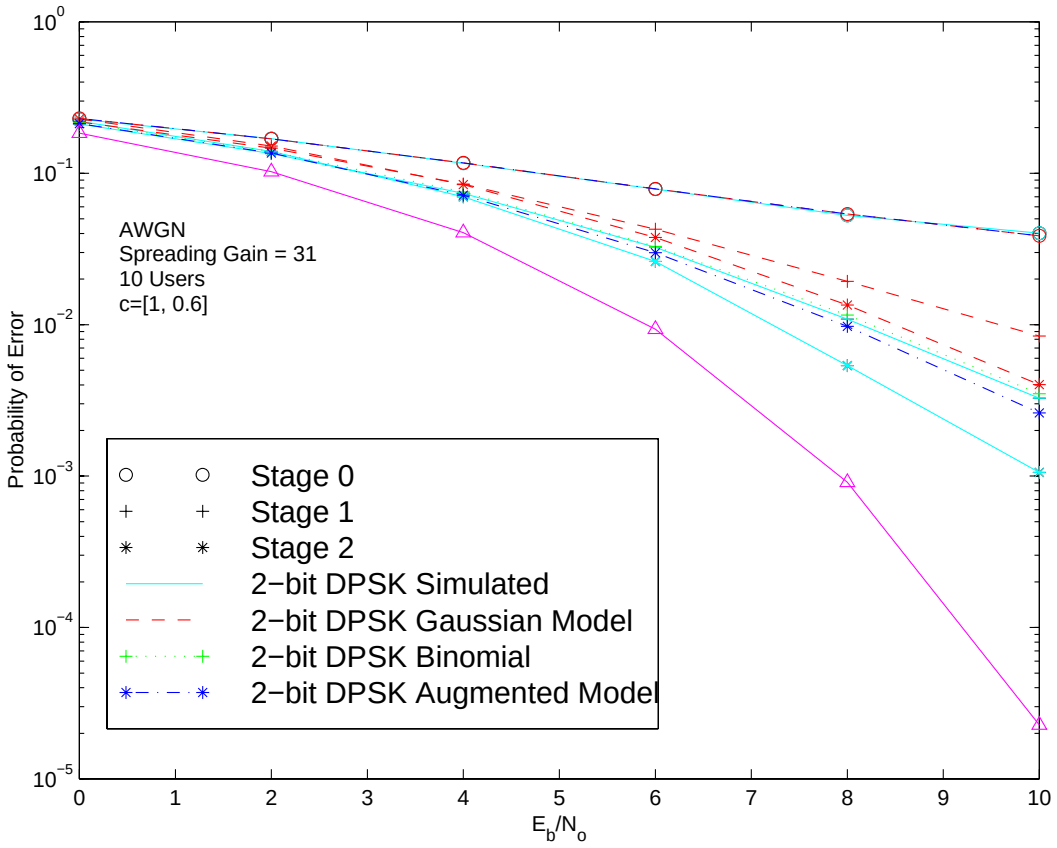

Figure 6.10: Comparison of analytical and simulated results for the probability of error vs. E_b/N_o at stages 0, 1 and 2 of the of the partial cancellation receiver. Random codes, spreading gain = 31, AWGN and 10 synchronous users.

distribution is very close to the simulated results. This indicates that it is very important to take into consideration the statistical properties of the binomially distributed crosscorrelations when accurate modeling is required.

6.2.3 Probability of Error for Multiple Symbol Detection

In the previous section, closed form expressions were obtained for the probability of error with standard differential decoding. This section extends the analytical results to larger window lengths employing the approach used in [99] for the single user case. Taking into consideration that most

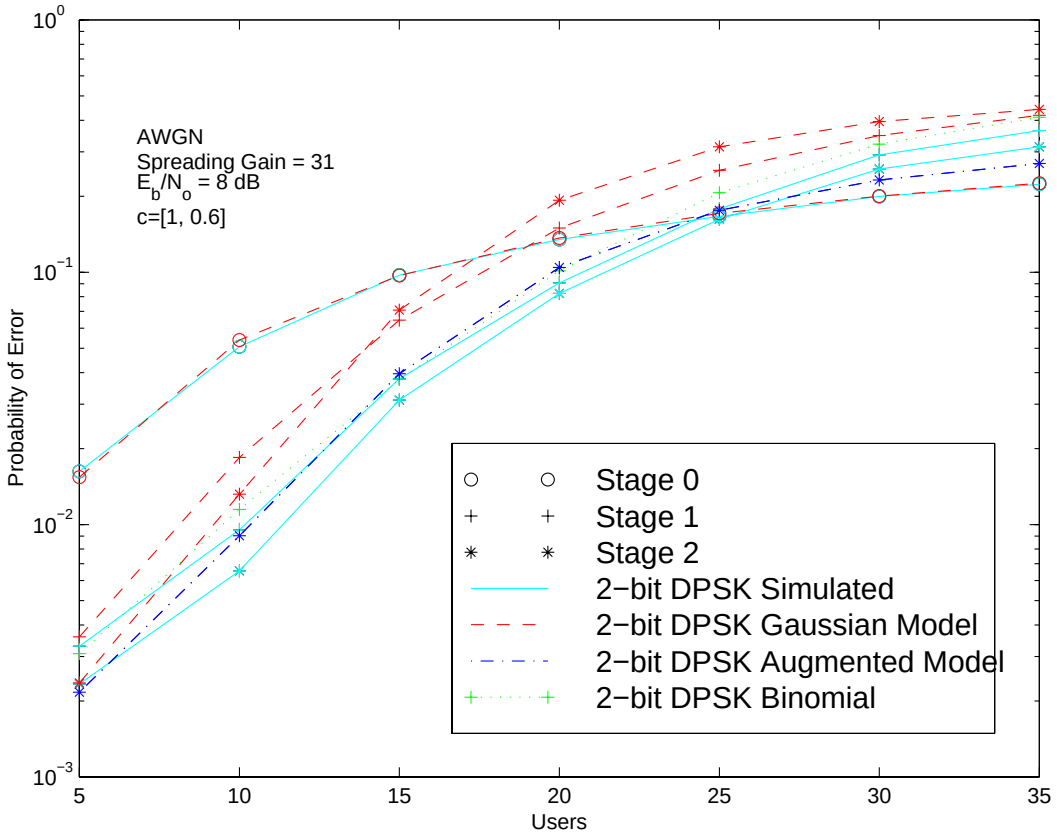

Figure 6.11: Comparison of analytical and simulated results for the probability of error vs. number of users for stages 0, 1 and 2 of the partial cancellation receiver. Random codes, spreading gain = 31, AWGN, synchronous users, and $E_b/N_o = 8$ dB.

of the improvements are obtained by extending the observation interval to $N_w = 3$ symbols, and because of its analytical tractability, the analysis initially focuses on the three-symbol memory case. Asymptotic bounds are then provided for larger observation lengths.

As in the previous section, the probability of bit is upper bounded according to the union bound:

$$P_{b,j} \leq \frac{1}{N_w - 1} \sum_{\mathbf{\Delta}\phi_\mathbf{j} \neq \mathbf{\Delta}\hat{\phi}_\mathbf{j}} w(\mathbf{u_j}, \hat{\mathbf{u}}_\mathbf{j}) Pr\{|z_2|^2 > |z_1|^2 | \mathbf{\Delta}\phi_\mathbf{j}\}, \tag{6.124}$$

where,

$$Pr\{|z_2|^2 > |z_1|^2 | \mathbf{\Delta}\phi_\mathbf{j}\} = \frac{1}{2}[1 - Q(\sqrt{b}, \sqrt{a}) + Q(\sqrt{a}, \sqrt{b})], \tag{6.125}$$

Table 6.1: Hamming distance between input sequences for $N_w = 3$ and binary signaling. (Adapted from [99])

$\Delta\phi_{1,k} - \Delta\hat{\phi}_{1,k}$	$\Delta\phi_{1,k-1} - \Delta\hat{\phi}_{1,k-1}$	$w(\mathbf{u_j}, \hat{\mathbf{u}}_\mathbf{j})$	δ
0	π	1	-1
π	0	1	1
π	π	2	1

and

$$\left\{ \begin{array}{c} a \\ b \end{array} \right\} = \frac{1}{2N_s} \left\{ \frac{S_1 + S_2 - 2|\rho|\sqrt{S_1 S_2}\cos(\theta_1 - \theta_2 + \phi)}{1 - |\rho|^2} \mp \frac{S_1 - S_2}{\sqrt{1 - |\rho|^2}} \right\}, \tag{6.126}$$

and $\theta_1 = arg\{\overline{Z_1}\}$, $\theta_2 = arg\{\overline{Z_1}\}$ and $\phi = arg\{\rho\}$.

6.2.3.1 Analysis for Stage 0

In order to compute the pairwise probability of error, the Hamming distance between the transmitted information sequence and the erroneously decoded sequence is required. As illustrated in Table 6.1, for $N_w = 3$ the Hamming distance between $\mathbf{u_j}$ and $\hat{\mathbf{u}}_\mathbf{j}$ takes on two possible values, 1 or 2.

The arguments a and b of Equation (6.126) correspond to:

$$\left\{ \begin{array}{c} a \\ b \end{array} \right\} = \frac{N_w^2 E_b}{4N_s} \left\{ 1 \mp \sqrt{1 - |\rho^2|} \right\}, \tag{6.127}$$

and were computed from S_1, S_2 and ρ as derived in Appendix D.

Equation (6.124) can be used in the derivation of an upper bound for the probability of error at stage 0 for $N_w = 3$. The union bound is derived by computing the possible pairwise probabilities of error according to Equation (6.125) with arguments a and b given in (6.127) and weighting them by their Hamming distance, given in Table 6.1. The resulting upper bound corresponds to:

$$P_b \leq \left[1 - Q\left(\sqrt{\frac{E_b}{E_b \frac{K-1}{N} + N_o} \left(\frac{3}{2} + \sqrt{2} \right)}, \sqrt{\frac{E_b}{E_b \frac{K-1}{N} + N_o} \left(\frac{3}{2} - \sqrt{2} \right)} \right) \right.$$

$$+Q\left(\sqrt{\frac{E_b}{E_b\frac{K-1}{N}+N_o}\left(\frac{3}{2}-\sqrt{2}\right)},\sqrt{\frac{E_b}{E_b\frac{K-1}{N}+N_o}\left(\frac{3}{2}+\sqrt{2}\right)}\right)\Bigg] \tag{6.128}$$

Numerical evaluation can be used to compute the resulting probability of error. However, a notion of the improvements that can be achieved by going to a 3-symbol observation window can be obtained by evaluating the bit error probability for large values of energy to interference ratios. An expression characterizing this asymptotic performance can be computed based the asymptotic expression for the pairwise probability of error of Equation (E.11):

$$Pr\{\hat{\eta}>\eta\} = \frac{1}{2\sqrt{\frac{\pi E_b}{(E_b\frac{K-1}{N}+N_o)}}}\left(\frac{N_w+|\delta|}{|\delta|(N_w-|\delta|)}\right)^{1/2}\exp\left(-\frac{E_b}{E_b\frac{K-1}{N}+N_o}\left(\frac{N_w-|\delta|}{2}\right)\right). \tag{6.129}$$

Evaluation of the previous expression for $N_w = 3$, together with the results of Table 6.1 allows computation of the probability of bit error of Equation (6.124) as:

$$P_b \leq \frac{2\sqrt{2}}{\sqrt{\pi\frac{E_b}{E_b\frac{K-1}{N}+N_o}}}\left[\frac{1}{2}\exp\left(-\frac{E_b}{E_b\frac{K-1}{N}+N_o}\right)\right]. \tag{6.130}$$

Note that for $K = 1$, this expression evaluates to the one derived in [99] for the single user case.

Comparison of Equations (6.130) and (6.54) shows that for large energy to interference ratios, the amount of improvement that can be achieved by going to a 3-symbol observation window is bounded by:

$$\frac{2\sqrt{2}}{\sqrt{\pi\frac{E_b}{E_b\frac{K-1}{N}+N_o}}}. \tag{6.131}$$

The asymptotic performance for arbitrary values of N_w can be obtained by noticing that in the evaluation of the probability of bit error, given in Equation (6.124), the dominant terms correspond to those error events with the highest asymptotic pairwise probability of error. Following the approach of [99] for the single user channel, from Equation (E.8) it is apparent that the prevalent terms correspond to sequences having the smallest argument for the exponential function, or equivalently, those sequences for which $|\delta|$ is largest. According to the definition of δ given in Equation (6.38), the largest value of δ is achieved by estimated sequences $\hat{\mathbf{u}}_\mathbf{j}$ whose $\mathbf{\Delta}\hat{\phi}_\mathbf{j}$ only differs in one symbol from $\mathbf{\Delta}\phi_\mathbf{j}$.

For these sequences $N-|\delta|$ achieves a minimum given by:

$$\begin{aligned}\min(N-|\delta|) &= N-|\delta|_{max} \\ &= N-|N-1+e^{\Delta\phi_k-\Delta\hat{\phi}_k}|, \end{aligned} \tag{6.132}$$

for the particular case of binary antipodal signaling, all the vectors are co-linear and therefore :

$$\begin{aligned}\min(N-|\delta|) &= N-|N-2| \\ &= 2. \end{aligned} \tag{6.133}$$

Having found the value of the dominant argument of the exponential function in Equation (E.11), the next step is to find the weight enumerator (number of occurrences) of the dominant sequences.

The situations that yield $|\delta|_{max}$ are described in Appendix B of [99], where it is shown that for binary signaling:

$$\sum_{\mathbf{\Delta}\hat{\phi}\neq\mathbf{\Delta}\phi_\mathbf{j}} w(\hat{\mathbf{u}},\mathbf{u}) = \left\{ \begin{array}{c} 2(N_w-1);\ N_w>2 \\ 1;\ N_w=2 \end{array} \right\} \tag{6.134}$$

Employing the previous results for evaluation of Equation (6.124), and noticing that $(N_w-|\delta|_{max})|\delta|_{max}$ equals N_w-2, results in an expression for the asymptotic bit error rate performance for large energy to interference ratios and arbitrary values of N_w:

$$P_b \leq \frac{2}{\sqrt{\pi\frac{E_b}{E_b\frac{K-1}{N}+N_o}}}\left(\frac{N_w-1}{N_w-2}\right)^{1/2}\left[\frac{1}{2}\exp\left(-\frac{E_b}{E_b\frac{K-1}{N}+N_o}\right)\right]. \tag{6.135}$$

Note that for very large values of E_b

$$\frac{E_b}{E_b\frac{K-1}{N}+N_o} \rightarrow \frac{N}{K-1} \tag{6.136}$$

In order to achieve an asymptotically large energy to interference ratio, it is also necessary that the ratio between the number of interferers and the spreading gain to be sufficiently small.

6.2.3.2 Analysis for Stage 1

The pairwise probability of error for $N_w=3$ is computed in a manner similar to the one used for stage 0. The arguments of the Marcum-Q function required for the computation of the probability

of error are given in Equation (D.39). Incorporating into this equation the expression for the effective noise power of Equation (6.100) yields:

$$\left\{ \begin{array}{c} a \\ b \end{array} \right\} = \frac{E_b \left(1 - C_1 \frac{K-1}{N}\right)^2 \left\{ N_w^2 \mp N_w \sqrt{N_w^2 - |\delta|^2} \right\}}{2E_b N_w \left(N_w C_1^2 \left(\frac{2(K-1)}{N^2} \right) + (1-C_1)^2 \frac{K-1}{N} + C_1^2 (K-1)(K-2) \frac{1}{N^2} \right) + \overline{N_o \left(1 - 2C_1 \frac{K-1}{N} + C_1^2 \frac{K-1}{N}\right)}}. \tag{6.137}$$

Equation (6.124), along with the results of Table 6.1, are used to derive an upper bound to the probability of bit error for a three symbol observation interval ($N_w = 3$):

$$P_b \leq [1 - Q(\sqrt{b}, \sqrt{a}) + Q(\sqrt{a}, \sqrt{b})]. \tag{6.138}$$

The values of a and b for the full cancellation case are computed from Equation (6.137) setting $C_1 = 1$. Substituting the resulting expressions into Equation (6.138) results in:

$$\begin{aligned} P_b \leq & \left[1 - Q\left(\sqrt{\frac{E_b (1 - \frac{K-1}{N})^2}{E_b \frac{(K-1)(K+4)}{N^2} + N_o \left(1 - \frac{K-1}{N}\right)}} \times \left[\sqrt{\left(\frac{3}{2} + \sqrt{2}\right)}, \sqrt{\left(\frac{3}{2} - \sqrt{2}\right)} \right] \right) \right. \\ & \left. + Q\left(\sqrt{\frac{E_b (1 - \frac{K-1}{N})^2}{E_b \frac{(K-1)(K+4)}{N^2} + N_o \left(1 - \frac{K-1}{N}\right)}} \times \left[\sqrt{\left(\frac{3}{2} - \sqrt{2}\right)}, \sqrt{\left(\frac{3}{2} + \sqrt{2}\right)} \right] \right) \right]. \end{aligned} \tag{6.139}$$

For partial interference cancellation, the bound for the probability of bit error for N_w=3 is given by:

$$\begin{aligned} P_b \leq & \left[1 - Q\left(\sqrt{\xi \left(\frac{3}{2} + \sqrt{2}\right)}, \sqrt{\xi \left(\frac{3}{2} - \sqrt{2}\right)}] \right) \right. \\ & \left. + Q\left(\sqrt{\xi \left(\frac{3}{2} - \sqrt{2}\right)}, \sqrt{\xi \left(\frac{3}{2} + \sqrt{2}\right)} \right) \right], \end{aligned} \tag{6.140}$$

where

$$\xi = \frac{E_b \left(1 - C_1 \frac{K-1}{N}\right)^2}{E_b \left(3C_1^2 \left(\frac{2(K-1)}{N^2}\right) + (1-C_1)^2 \frac{K-1}{N} + C_1^2 (K-1)(K-2) \frac{1}{N^2}\right) + N_o \left(1 - 2C_1 \frac{K-1}{N} + C_1^2 \frac{K-1}{N}\right)} \tag{6.141}$$

denotes the effective energy to interference ratio at the receiver.

A comparison of the simulated results and the analytical bounds for $N_w = 3$ and full interference cancellation ($C_1 = 1$) is illustrated in Figure 6.12. A comparison for partial interference cancellation

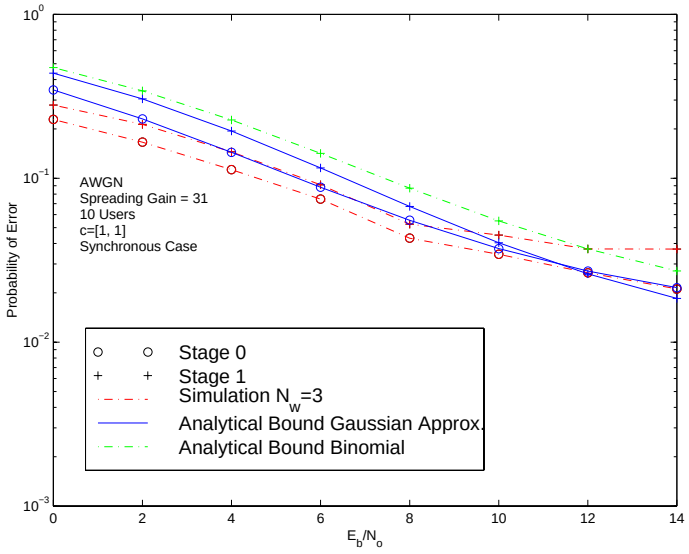

Figure 6.12: Analytical bounds for BER performance of full interference cancellation with $N_w = 3$. Random codes, spreading gain = 31, AWGN and 10 synchronous users.

is presented in Figure 6.13. The Marcum-Q function was computed numerically using the following alternate expressions [102]:

$$Q(\beta u, \beta) = \frac{1}{2\pi} \int_{-\pi}^{\pi} \left[\frac{1 + u \sin\theta}{1 + 2u \sin\theta + u^2} \right] \exp\left(-\frac{\beta^2}{2} [1 + 2u \sin\theta + u^2] \right) d\theta, \quad 0 \leq u < 1 \qquad (6.142)$$

and

$$Q(\alpha, \alpha u) = 1 + \frac{1}{2\pi} \int_{-\pi}^{\pi} \left[\frac{u^2 + u \sin\theta}{1 + 2u \sin\theta + u^2} \right] \exp\left(-\frac{\alpha^2}{2} [1 + 2u \sin\theta + u^2] \right) d\theta, \; 0 \leq u < 1. \qquad (6.143)$$

For the full cancellation approach, at stage 0, the bound obtained using the independent Gaussian model for the crosscorrelations between signature sequences produces a very good approximation to the simulated performance. For stage 1, the bound that employs on the expression based on the binomial distribution of the crosscorrelations, holds for $E_b/N_o \leq 10$dB . The bound based on the independent Gaussian model is tighter but it only holds for $E_b/N_o \leq 8$dB. For stage 0 of the partial cancellation approach, the bound based on the Gaussian model produces a good approximation to the simulated results. For stage 1, the bound obtained using the binomial expression holds for $E_b/N_o \leq 11$dB. As expected, it gives a closer approximation to the probability of error than the approximation based on the Gaussian assumption.

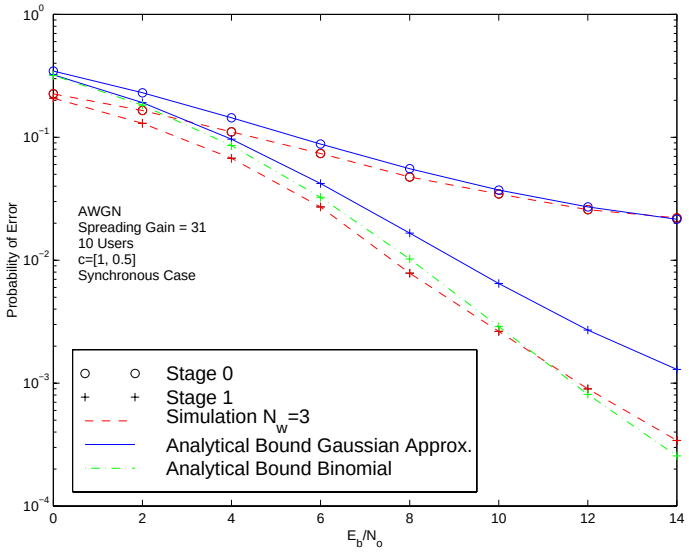

Figure 6.13: Analytical bounds for BER performance of partial interference cancellation with $N_w = 3$. Random codes, spreading gain = 31, AWGN and 10 users.

6.3 Detection of differentially encoded PSK signals using the Viterbi algorithm

In the multiple symbol approach presented in the previous sections, demodulation is performed block by block with a one-symbol block overlap. An alternative approach might be to create a sliding window of symbols for observation. This alternative approach is analogous to the well-known Viterbi algorithm for maximum likelihood sequence detection [103]. This section explores the relationship of this approach to the multiple symbol differential approach of [99].

A block, $[y_{k-N_w+1}, y_{k-N_w+2}, ..., y_k]$, corresponding to N_w consecutive decision statistics is observed, subsequently, maximum likelihood sequence estimation of the received phases is performed based on the following metric:

$$\arg\left\{\max_{\phi}\left|\sum_{i=0}^{N_w-1} y_{k-i}e^{-j\sum_{m=0}^{N_w-i-2}\Delta\phi_{(k-i-m)}}\right|^2\right\}. \tag{6.144}$$

Expanding and cancelling common terms, an equivalent decision rule is obtained:

$$\arg\left\{\max_{\phi}\Re\{\sum_{i=1}^{N_w-1}\sum_{\mu=1}^{i}y_{k-N_w+1+i}y^*_{k-N_w+1+i-\mu}e^{-j\sum_{m=0}^{\mu-1}\Delta\phi_{(k-N_w+1+i-m)}}\}\right\}. \tag{6.145}$$

As an example, let us consider the case $N_w = 3$. In this case, Equation (6.145) reduces to:

$$\arg\left\{\max_{\phi}\Re\{y_k y^*_{k-2}e^{-j(\Delta\phi_k+\Delta\phi_{k-1})}+y_k y^*_{k-1}e^{-j\Delta\phi_k}+y_{k-1}y^*_{k-2}e^{-j\Delta\phi_{k-1}}\}\right\}. \tag{6.146}$$

The structure of a detector that computes this metric and selects the most likely sequence is presented on Figure 6.5.

A reduced complexity structure can be obtained by truncating the inner summation in Equation (6.145) to a length of Λ [100]. After truncation, the reduced complexity structure operates on the following metric:

$$\arg\left\{\max_{\phi}\Re\{\sum_{i=1}^{N_w-1}\sum_{\mu=1}^{\Lambda}y_{k-N_w+1+i}y^*_{k-N_w+1+i-\mu}e^{-j\sum_{m=0}^{\mu-1}\Delta\phi_{(k-N_w+1+i-m)}}\}\right\}, \tag{6.147}$$

where the parameter Λ controls the performance and the complexity of the detection approach.

For the case of $\Lambda = 2$, the reduced complexity approach corresponds to:

$$\arg\left\{\max_{\phi}\Re\{\sum_{i=1}^{N_w-1}y_{k-N_w+1+i}e^{-j\Delta\phi_{k-N_w+i+1}}(y_{k-N_w+i-1}e^{j\Delta\phi_{k-N_w+i}}+y_{k-N_w+i})^*\}\right\}. \tag{6.148}$$

Based on the previous expression, let us define the branch metrics λ according to:

$$\lambda_{k-N_w+1+i} = \Re\left\{y_{k-N_w+1+i}e^{-j\Delta\phi_{k-N_w+i+1}}(y_{k-N_w+i-1}e^{j\Delta\phi_{k-N_w+i}}+y_{k-N_w+i})^*\right\}. \tag{6.149}$$

The reduced complexity approach of Equation (6.148) can be expressed in terms of the branch metrics λ as:

$$\arg\left\{\max_{\phi}\sum_{i=1}^{N_w-1}\lambda_{k-N_w+1+i}\right\}, \tag{6.150}$$

The sequence $\boldsymbol{\Delta}\phi$ that maximizes the sum of path metrics can be expediently found using the Viterbi algorithm as in [104]. A block diagram of the detector is shown in Figure 6.14.

In the Viterbi algorithm [103], the trellis diagram is employed for the computation of the sequence with the highest path metric. For $\Lambda = 2$, the trellis diagram is illustrated in Figure 6.15. At time

$t = k - N_w + 1 + i$ there are two states $\Delta\phi_{k-N_w+1+i} = 0$ and $\Delta\phi_{k-N_w+1+i} = \pi$, which represent a change in phase at the $k - N_w + 1 + i$th signaling interval. After computing the survivors for all the nodes, an estimate of the transmitted sequence is obtained by tracing back through the trellis.

Figure 6.16 shows simulation results for the single user case for standard differential detection, multiple symbol differential decoding with $N_w = 3$, as well as for the reduced complexity approach based on the Viterbi algorithm.

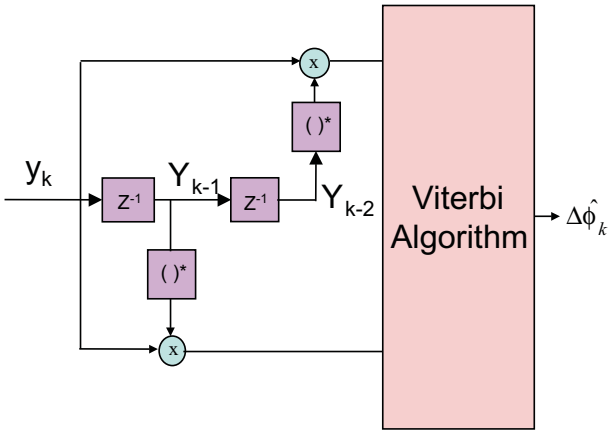

Figure 6.14: Block diagram for demodulation with the Viterbi Algorithm

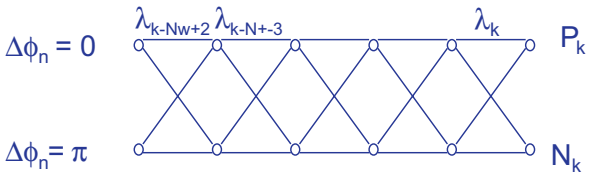

Figure 6.15: Trellis diagram for Viterbi decoding of DPSK

Note that even though the branch metric used in Viterbi-decoding differential detection uses what seems to be a simpler front end that the one used in block multi-symbol detection with $N = 3$, Viterbi decoding uses a sliding window approach that results in improved performance.

A simulation based comparison of the Viterbi decoding differential detection and full complexity block multi-symbol detection with $N_w = 3$ was performed in order to estimate the benefits afforded by the sliding window approach used in Viterbi decoding. Figure 6.16 shows probability of bit

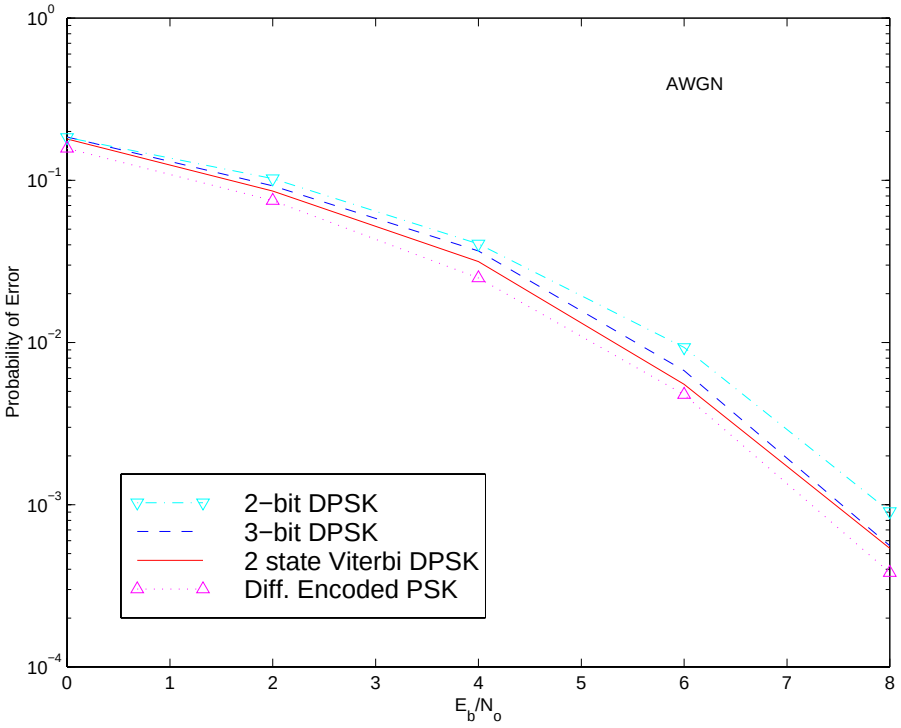

Figure 6.16: Comparison of single user probability of error vs. E_b/N_o for Viterbi decoding, and block oriented multi-symbol detection. Random codes, spreading gain = 31, AWGN and RRC filter $\rho = 0.22$.

error vs. E_b/N_o curves for the single user DS-SS case in AWGN. All receivers operated on the same decision statistics to detect the transmitted data. This figure confirms the results for Viterbi decoding of differential PSK reported in [104].

Figure 6.17 shows probability of bit error curves for the conventional receiver and parallel partial interference cancellation receivers with Viterbi-decoding differential detection. These curves indicate that Viterbi-decoding differential detection can also be used in non-coherent multiuser detectors to provide enhanced performance in AWGN channels. In this case, as shown in the capacity curves of Figure 6.18, the performance of the Viterbi decoding approach is almost identical to that of the multi-symbol case for $N_w = 4$.

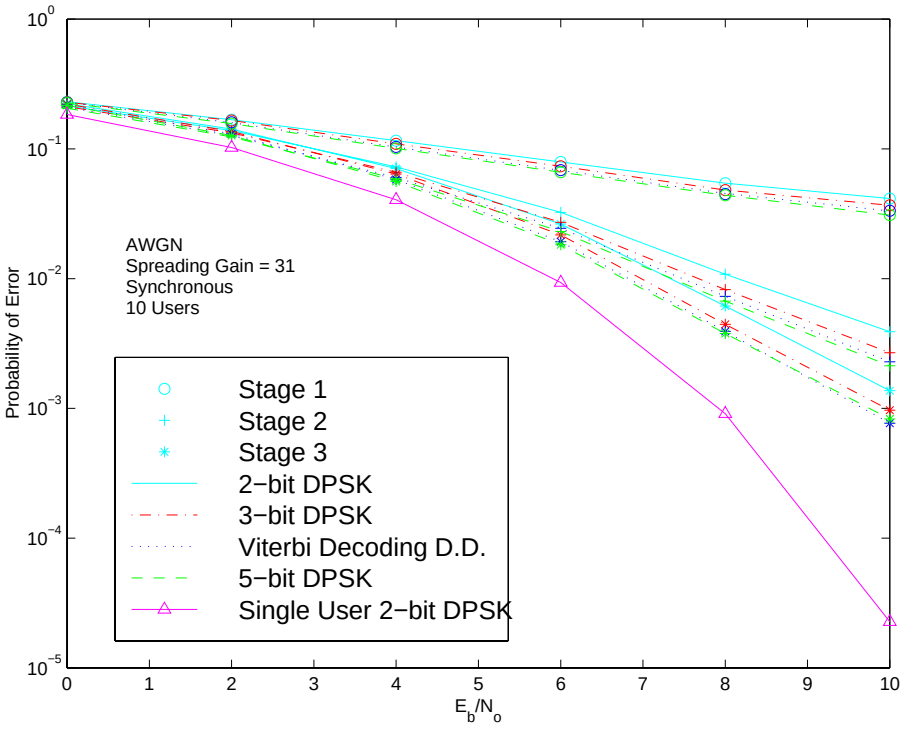

Figure 6.17: Probability of error vs. E_b/N_o for Viterbi decoding, and block oriented multi-symbol detection. Random codes, synchronous users, spreading gain = 31, c=[1, 0.5], AWGN and 10 users.

6.4 Conclusions

In AWGN channels, improved demodulation of DPSK signals can be achieved by increasing the memory at the receiver beyond one symbol and performing multiple symbol differential detection. It is assumed that the phase offset remains virtually constant throughout the observation interval. In many practical applications, this assumption is likely to hold for small observation window lengths. Most of the benefits of multiple symbol detection of differentially encoded signals were achieved by increasing the memory at the receiver to only three symbols. Differentially coherent parallel interference cancellation receivers based on multiple symbol differential detection have been developed and show enhanced performance. Bounds on the probability of bit error have been obtained for $N_w = 3$. An attractive low alternative to block multiple symbol detection, Viterbi-decoding differential detection, produced improvements similar to those obtained with block detection and $N_w = 4$.

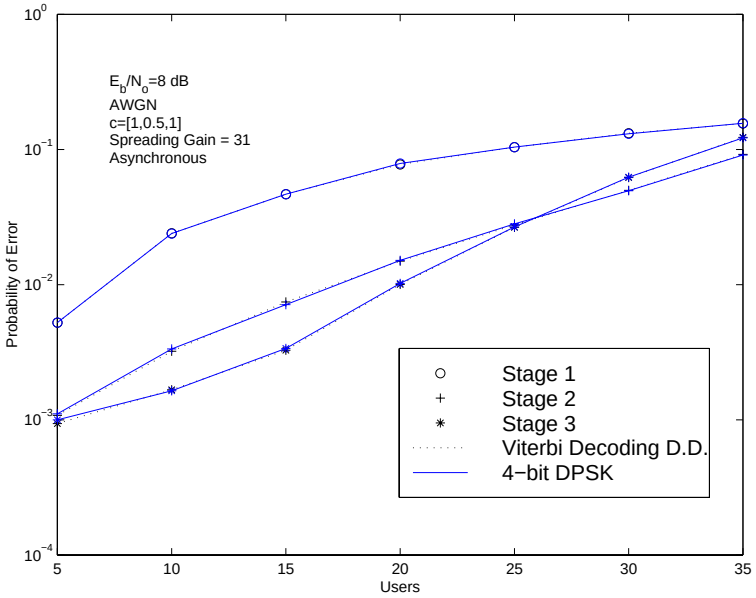

Figure 6.18: Probability of error vs. Number of users for Viterbi decoding and block oriented multi-symbol detection with $N_w = 4$, $E_b/N_o = 8$ dB, asynchronous users and spreading Gain=31.

Chapter 7

Diversity Techniques for Multiuser Detection

In conventional asynchronous DS-CDMA multiple access systems, multiuser interference hinders detection and causes the near-far effect, a problem currently mitigated through the use of accurate power control. In chapter 3, parallel interference cancellation [25], successive interference cancellation [22], and linear Minimum Mean Square Error (MMSE) detection [17] were shown to be attractive approaches for practical implementation of advanced receivers based on joint detection principles.

In digital wireless systems, multipath fading also degrades performance. It manifests itself as a reduction in the effective carrier-to-interference ratio experienced by the received signal. In mobile applications, multipath causes deep fades and large amplitude variations in the received signal. Diversity reception is a useful approach for combating the harmful effects of fading [105]. Diversity schemes exploit the availability of partly-independent versions of the signal at the receiver. The use of combined diversity reception and multiuser detection has been studied for various joint detection schemes in [106, 107]. Among diversity techniques, spatial diversity is one of the most investigated approaches. However, polarization diversity, an attractive alternative, has received rather meager attention to date.

The polarization of an electromagnetic wave is a description of the motion of the tip of the in-

stantaneous electric field vector with respect to time at a fixed point in space [108]. Polarization diversity reception is one of several methods which can be used for diversity reception. In mobile environments, the inclined orientation of the transmitter antenna and the cross-polarization due to multipath give rise to quasi-independent signals that can be directly used in a two branch polarization diversity scheme. Experimental test results have found polarization diversity to be an effective alternative to spatial diversity at the base station [109, 110, 111]. Despite its attractive properties, relatively limited attention has been focused toward this approach.

Polarization diversity has various attractive features. First, it does not require the large antenna spacings required by spatial diversity to significantly improve the quality of the received signals. This has the potential of simplifying base station deployment. Second, due to multiple reflections and scattering, a significant amount of the transmitted energy is transposed to a polarization state orthogonal to that of the transmitting antenna. Polarization diversity allows the receiver to take advantage of the energy received in the co-polarized and cross-polarized states.

This chapter evaluates via simulation the potential benefits of incorporating multiuser detection and polarization diversity to the uplink of a DS-CDMA mobile communications system. Section 7.1 introduces a system model for DS-CDMA communications with polarization diversity. Section 7.2 presents simulation results for the conventional receiver, the MMSE detector, the multistage partial parallel interference canceller and the successive interference cancellation receiver. Following, the performance of the partial parallel interference cancellation scheme is analyzed in more detail.

7.1 System Model for Polarization Diversity

This section presents a mathematical model for the uplink of a DS-CDMA system, and a description of the proposed receiver. The transmitted baseband signal from user k is defined as a binary phase modulated waveform:

$$s_k(t) = \sqrt{2P_k}a_k(t)b_k(t) \tag{7.1}$$

where P_k is the k^{th} user's received signal power, and $a_k(t)$ and $b_k(t)$ are the spreading and data waveforms, respectively.

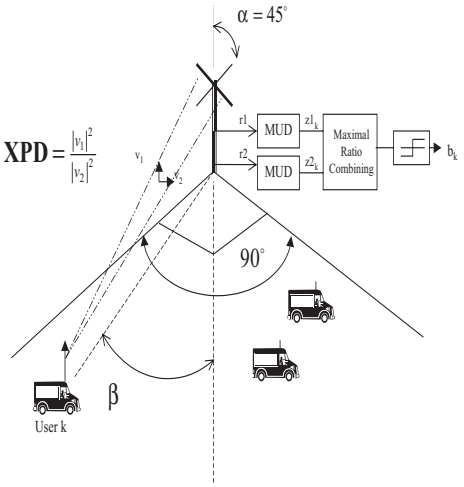

Figure 7.1: System geometry and block diagram of the combined polarization diversity and multiuser detection approach

Modeling of polarization diversity is based on the model presented in [110]. For simplicity, it will be assumed that the wireless channel corresponds to a slow flat fading channel, and that the mobile units transmit in the vertical polarization state. The transmitted signal is received by a base station polarization diversity antenna employing orthogonal slant 45° linear polarizations. Channel induced rotation of the polarization state causes the received signal at the base station to have a vertical, and a horizontal polarization component. Figure 7.1 shows the geometry of the system.

For slow flat fading channels, the horizontally and vertically polarized components of the received signal can be expressed as:

$$x_k(t) = \varrho_{h,k}(t) s_k(t) \cos(w_c t + \theta_{h,k}(t)) \tag{7.2}$$

$$y_k(t) = \varrho_{v,k}(t) s_k(t) \cos(w_c t + \theta_{v,k}(t)) \tag{7.3}$$

Where $\varrho_{h,k}(t)$ and $\varrho_{v,k}(t)$ are the channel attenuation coefficients in the horizontal and vertical components respectively. Initially, it will be assumed that $\varrho_{v,k}(t)$ and $\varrho_{h,k}(t)$ have completely uncorrelated Rayleigh distributions; $\theta_{v,k}(t)$ and $\theta_{h,k}(t)$ represent the relative carrier phase of user k, and are modeled as having independent uniform distributions. These assumptions are supported by measurements in [111, 110], where it was reported that the signal envelopes present very low

correlation coefficients and the phases are uniformly distributed. It is also assumed that the receiver compensates for shadowing effects via an automatic power control mechanism.

The relative amplitude of $\varrho_{v,k}(t)$ with respect to $\varrho_{h,k}(t)$ is characterized by the cross-polarization discrimination (XPD) of the propagation path between the mobile and the base station. XPD is the ratio of the signal level at the output of a receiving antenna that is co-polarized to the transmitting antenna to the output of a receiving antenna of the same gain but nominally orthogonally polarized to the transmitting antenna [108]. In this paper we take the vertical and the horizontal components as the co-polarized and cross-polarized states respectively.

Following the approach of [110], at the polarization diversity antenna elements V_1 and V_2, the received signal corresponding to user k is:

$$\begin{aligned} v_{1,k}(t) &= x_k(t)\sin\alpha\cos\beta + y_k(t)\cos\alpha \\ v_{2,k}(t) &= -x_k(t)\sin\alpha\cos\beta + y_k(t)\cos\alpha, \end{aligned} \tag{7.4}$$

where α is the inclination angle of the antenna elements with respect to the vertical, and β is the offset angle of the mobile from the main beam direction of the diversity antenna. In this study the receiver uses a slant 45 antenna ($\alpha = 45^\circ$).

The received signals can be expressed in terms of their envelope and phase as:

$$\begin{aligned} v_{1,k}(t) &= R_{1,k}(t)s_k(t)\cos(w_c t + \phi_{1,k}(t)) \\ v_{2,k}(t) &= R_{2,k}(t)s_k(t)\cos(w_c t + \phi_{2,k}(t)), \end{aligned} \tag{7.5}$$

at the polarization diversity antenna elements, due to multiple access, the received signal corresponds to the combination of the individual signals from all the mobile users, and can be expressed as:

$$\begin{aligned} r_1(t) &= \sum_{k=1}^{K} v_{1,k}(t-\tau_k) + n_1(t) \\ r_2(t) &= \sum_{k=1}^{K} v_{2,k}(t-\tau_k) + n_2(t), \end{aligned} \tag{7.6}$$

where K is the number of users, and τ_k denotes the relative delay of user k, which accounts for the asynchronous nature of the system uplink. The background noise affecting the received signals is

represented by $n_1(t)$ and $n_2(t)$. The multiuser receiver structures under study act on the signals received by each diversity branch and produce soft branch decision statistics. Improved bit decisions are obtained from post-detection processing via maximum ratio combining of the decision statistics from the polarization diversity branches.

The multistage interference cancellation receiver, takes advantage of the 2-branch diversity available from the slant 45 antenna elements. In this receiver, the first stage of processing corresponds to two conventional receivers, which are implemented as a bank of correlation demodulators, each operating on the received signal from one diversity branch.

For interference cancelation, at stage s, an estimate of the received signal for each active user is computed by partially subtracting out from the received signal the estimated multiple access interference (MAI) caused by the remaining users. The estimated signal, at stage s, after MAI cancellation can be expressed as:

$$\begin{aligned} \hat{r}_{1,k}^{(s)}(t) &= r_1(t) - C_k^{(s)} \sum_{j \neq k} \hat{v}_{1,j}^{(s)}(t) \\ \hat{r}_{2,k}^{(s)}(t) &= r_2(t) - C_k^{(s)} \sum_{j \neq k} \hat{v}_{2,j}^{(s)}(t), \end{aligned} \tag{7.7}$$

where $C_k^{(s)}$ is the partial-cancellation multiplicative factor for user k, its value is selected based on the operating conditions of the system [75]. The estimated received signals at the diversity elements for user j at stage s are reconstructed from the estimates of the previous stage according to:

$$\begin{aligned} \hat{v}_{1,j}^{(s)}(t) &= \tfrac{2}{T} a_j(t) \cos(w_c t + \phi_{1,j}(t)) \sum_{i=-\infty}^{\infty} Z_{1,j,i}^{(s-1)} p_T(t - iT) \\ \hat{v}_{2,j}^{(s)}(t) &= \tfrac{2}{T} a_j(t) \cos(w_c t + \phi_{2,j}(t)) \sum_{i=-\infty}^{\infty} Z_{2,j,i}^{(s-1)} p_T(t - iT), \end{aligned} \tag{7.8}$$

where $p_T(t)$ is a unit pulse function of duration T equal to the bit period.

The decision statistics at stage s for user k are obtained from the signals $\hat{r}_{1,k}^{(s)}(t)$ and $\hat{r}_{2,k}^{(s)}(t)$ via correlation with the desired user's signature sequence:

$$\begin{aligned} Z_{1,k,i}^{(s)} &= \int_{(i-1)T+\tau_k}^{iT+\tau_k} \hat{r}_{1,k}^{(s)}(t) a_k(t - \tau_k) \cos(w_c t + \phi_{1,j}(t)) dt \\ Z_{2,k,i}^{(s)} &= \int_{(i-1)T+\tau_k}^{iT+\tau_k} \hat{r}_{2,k}^{(s)}(t) a_k(t - \tau_k) \cos(w_c t + \phi_{2,j}(t)) dt. \end{aligned} \tag{7.9}$$

The process starts with the conventional receiver, setting $\hat{r}_{1,k}^{(0)}(t) = r_1(t)$ and $\hat{r}_{2,k}^{(0)}(t) = r_2(t)$. For each bit, the soft outputs of the conventional receivers are used as the $Z_{1,k,i}^{(1)}$ and $Z_{2,k,i}^{(1)}$ for signal reconstruction. The reconstructed signals $\hat{v}_{1,j}^{(1)}(t)$ and $\hat{v}_{2,j}^{(1)}(t)$ are used for interference cancellation. After interference cancellation, improved decision statistics are obtained from the signals $\hat{r}_{1,k}^{(1)}(t)$ and $\hat{r}_{2,k}^{(1)}(t)$. The entire process is repeated for several stages. At each stage better estimates are produced for each user, allowing more effective interference cancellation and better data detection. Enhanced bit decisions are obtained for every user from post-detection diversity through maximum ratio combining of the soft decision statistics provided by the multistage interference canceller on each individual polarization diversity branch.

7.2 Simulation Results for Various Practical Multiuser Receivers

This section presents the results of the simulation study. In these Monte Carlo simulations, the signals in the horizontal and vertical polarization states were modeled as uncorrelated with Rayleigh distributed envelopes. For narrowband CDMA systems, this is a reasonable assumption. Wideband CDMA systems however, experience a reduction of the Rayleigh fading effect [112, 113] that would make this assumption pessimistic.

Perfect isolation between antennas was assumed, and the effects of the antenna beam pattern were not considered. In these simulations, γ_1 represents the average E_b/N_o received in the vertical state.

Mobiles, with random relative delays and carrier phase offsets, communicate with a base station over a slow flat fading channel with normalized fading rate $F_dT = 0.0113$, where F_d is the maximum Doppler shift and T is the symbol duration. Modulation is BPSK, and the spreading sequences correspond to random codes of length $N = 31$. Symbol and carrier synchronization are assumed to be ideal.

At the base station, 90° sectors were used in order to limit the amount of correlation between the received signals at the polarization diversity antenna elements to less that 0.6. From the theoretical results in [110], this can be accomplished by limiting the angle between the mobiles and the antenna β to be in the range $-45^\circ \leq \beta \leq 45^\circ$. In our simulations, users were assumed to have a uniform angular distribution over the 90° sector. Perfect isolation of the diversity antenna elements was

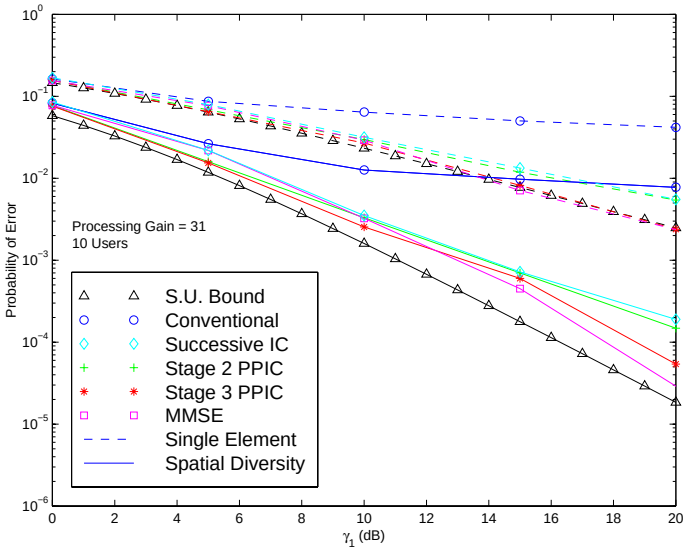

Figure 7.2: Single antenna element and dual spatial diversity probability of error vs. γ_1 results for the conventional, the PPIC, SIC and MMSE receivers, for slow flat Rayleigh fading, $XPD = 0$ dB, mobile speeds of 100 Km/h, data rate of 16 Kbps and processing gain = 31.

also assumed.

For amplitude estimation, the PPIC and SIC cancellers use directly the soft outputs of a bank of matched filters, and the MMSE receiver uses the amplitude estimates from a decorrelator. Perfect estimation and tracking of the user delays and phases was assumed. The partial cancellation factors for the PPIC were computed according to [75].

Figure 7.2 shows the probability of bit error vs. γ_1 (γ_1 is the E_b/N_o in the vertical state) for the conventional receiver, and the multiuser receivers under study. Two cases are considered: when a single vertical antenna element is used, and the case of ideal dual spatial diversity where the signals at the receive antennas are uncorrelated. The spatial diversity antennas are assumed to be vertically oriented. The channel corresponds to a slow flat Rayleigh fading channel. This figure shows that in flat-fading channels, significant improvements in performance can be obtained by using dual spatial diversity with the conventional receiver as well as with the three multiuser detectors under consideration.

This simulation results show that the PPIC receiver with a single stage of interference cancellation

yields results close to the successive cancellation approach. When a second stage of interference cancellation and estimation was used for PPIC, the PPIC receiver slightly outperformed the successive interference canceller. The linear MMSE receiver outperformed the PPIC and the SIC receivers, and its performance was very close to the single user bound for both single element and dual spatial diversity.

Figure 7.3 plots system performance in terms of bit error rate vs. γ_1 for a receiver employing a single antenna element, and for a receiver employing the polarization diversity scheme under study. These results indicate that when $XPD = 0$ dB, polarization diversity offers comparable improvements to those that can be obtained from dual spatial diversity for both the conventional and multiuser receivers.

For values of $XPD \neq 0$ dB, the performance of the polarization diversity scheme degrades compared to dual spatial diversity. Experimental measurements of the cross-polarization discrimination coefficient report an average XPD value in urban areas of 6 dB [110]. Figure 7.4 shows the probability of bit error vs. γ_1 for $XPD = 6$ dB. The dual diversity bound corresponds to the maximal ratio combining bound for two independent Rayleigh fading signals with unequal amplitudes ($XPD = 6$ dB) [102]. Despite the reduction in performance experienced when compared to the $XPD = 0$ dB case, polarization diversity still provides significant benefits to all four DS-CDMA receivers.

Figure 7.5 shows the probability of bit error as a function of the number of users in the system, for a single antenna element, and for polarization diversity with $XPD = 0$ dB. For this value of XPD, the results for polarization diversity and dual spatial diversity are similar. These curves indicate that the capacity of a DS-CDMA system can be significantly increased by combining dual antenna diversity and multiuser detection.

Figure 7.6 shows capacity curves for $XPD = 6$ dB. Comparison of this figure with Figure 7.5 confirms that systems employing polarization diversity experience a degradation in performance when $XPD \neq 0$. This characteristic can be attributed to the difference in mean signal levels in the horizontal and vertical states, which effectively reduces diversity gain. Nevertheless, polarization diversity still provides significant performance improvements over a receiver equipped with a single antenna element. Further improvements may be obtained, with higher complexity, by combining spatial and polarization diversity at the receiver.

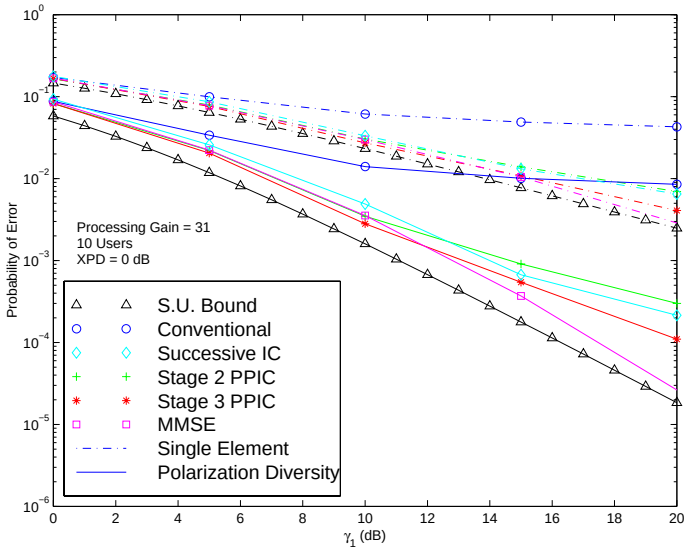

Figure 7.3: Single antenna element and polarization diversity probability of error vs. γ_1 results for the conventional, the PPIC, SIC and MMSE receivers, for slow flat Rayleigh fading, $XPD = 0$ dB, mobile speeds of 100 Km/h, data rate of 16 Kbps and processing gain = 31.

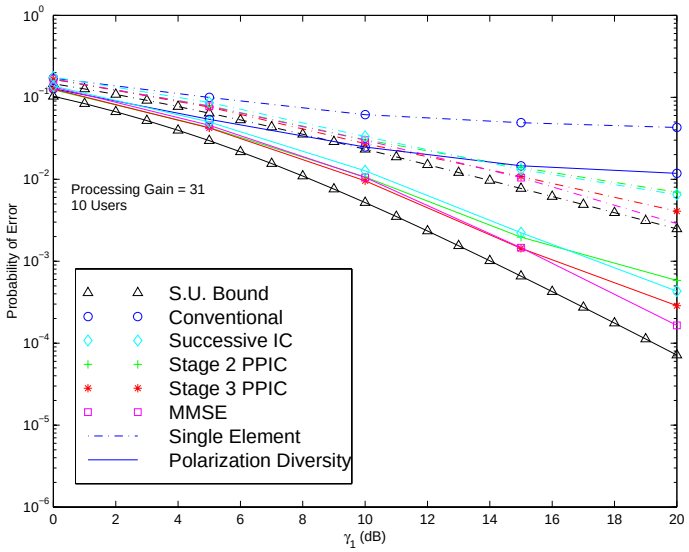

Figure 7.4: Single antenna element and polarization diversity probability of error vs. γ_1 results for the conventional, the PPIC, SIC and MMSE receivers, for slow flat Rayleigh fading, $XPD = 6$ dB, mobile speeds of 100 Km/h, data rate of 16 Kbps and processing gain = 31.

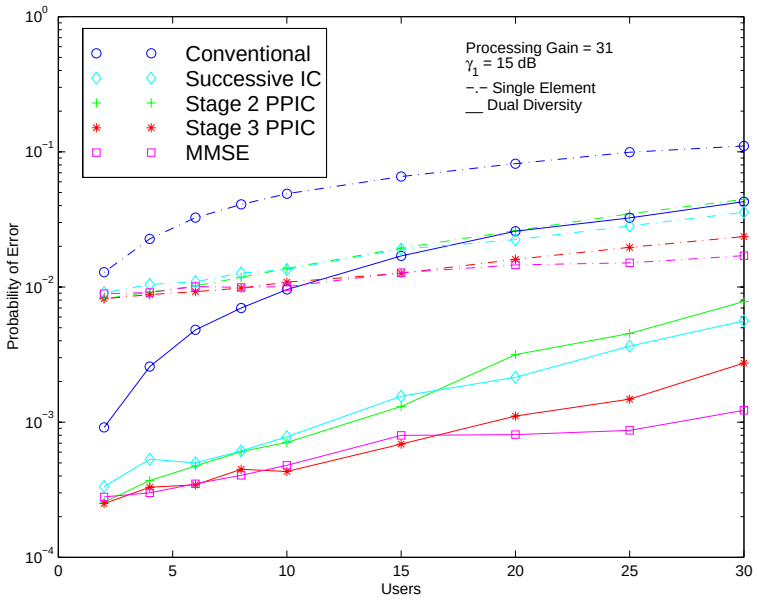

Figure 7.5: Probability of bit error vs. number of users for the conventional receiver and the multiuser receivers, with and without polarization diversity. Slow flat Rayleigh fading, average $\gamma_1 = 15$ dB, mobile speeds of 100 Km/h and a data rate of 16 Kbps. Processing Gain $= 31$ and $XPD = 0$ dB.

7.2.1 Polarization Diversity for Multistage Partial Parallel Interference Cancellation

In this section, we present error probability results for the asynchronous case obtained via baseband simulation of the conventional and the multistage cancellation receiver, with and without diversity.

Figure 7.7 shows probability of error vs. γ_1 (E_b/N_o measured in the vertical state) curves for a receiver that combines multistage interference cancellation and polarization diversity, and for a single element receiver with multistage interference cancellation. These results illustrate that polarization diversity significantly improves the performance of DS-CDMA receivers. The performance improvements are even more significant when one compares the results for the conventional receiver without polarization diversity with those for the multistage receiver with polarization diversity.

The performance of a polarization diversity scheme depends on the XPD induced by the propagation path between the mobiles and the base station. Figure 7.8 shows the BER performance of the polarization diversity multistage receiver as a function of γ_1 for several XPD values. The

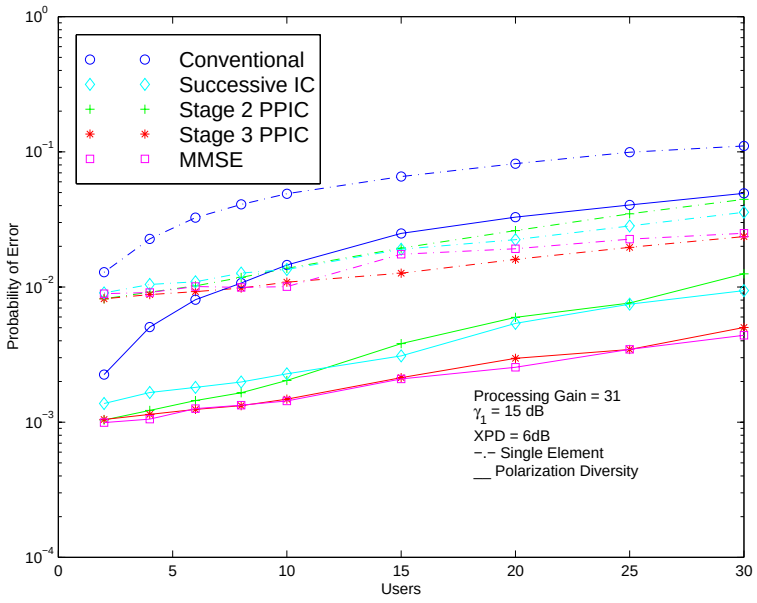

Figure 7.6: Probability of bit error vs. number of users for the conventional and the multiuser receivers, with and without polarization diversity. Slow flat Rayleigh fading, average $\gamma_1 = 15$ dB, mobile speeds of 100 Km/h and a data rate of 16 Kbps. Processing Gain $= 31$ and $XPD = 6$ dB.

performance of the conventional receiver without diversity is also shown for comparison. Recall that an XPD value of 0 dB corresponds to equal signal energy being received in the horizontal and vertical components. As XPD deviates from 0, the effectiveness of polarization diversity diminishes since the strongest branch tends to dominate. Field measurements in [110] have reported an average XPD of 6 dB for urban areas. However, XPD values close to zero have however also been reported [114]. In any case, as illustrated in this figure, even for an XPD of 9 dB, the proposed interference cancellation receiver with polarization diversity offers significant improvements over the conventional CDMA receiver.

Up to this point we have simulated the signals in the horizontal and vertical components as completely uncorrelated. Field measurements indicate that the horizontal and vertical components have a low, yet non-zero correlation coefficient [110]. Figure 7.9 shows the performance of the polarization diversity system when the correlation coefficient equals 0, 0.2 and 0.4, for an urban area with $XPD = 6$ dB. The diversity bound corresponds to maximal ratio combining for $XPD = 6$ dB. These results indicate that as long as the cross-correlation coefficient remains low, a situation

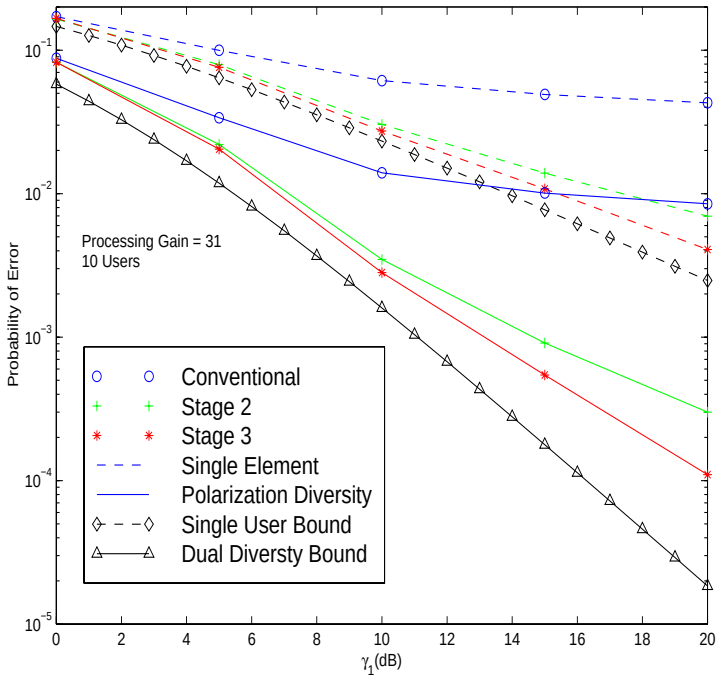

Figure 7.7: Probability of error vs. γ_1 for a multistage interference cancellation receiver with and without polarization diversity for flat Rayleigh fading with normalized fading rate $F_dT = 0.0113$, $XPD = 0$ dB, 10 users and processing gain = 31.

that measurements support [110, 111], performance is not affected significantly.

In order to quantify the improvements in system capacity that the combined approach would provide over a single-element conventional CDMA receiver, simulations were performed for XPD = 0 and 6 dB with various system loads. The probability of error as a function of the number of users in the system is presented in Figure 7.10. This figure indicates that polarization diversity has the potential of substantially improving the capacity of the conventional receiver. The capacity improvements that are achieved by a system that combines multiuser detection and polarization diversity are significantly larger, thus making the combined approach attractive.

A comparison of the performance of the multistage receiver when using polarization diversity, and when ideal spatial diversity is used instead, can be observed Figure 7.11. This figure shows the probability of error vs. γ_1 for XPD = 1 and 6 dB, when $\rho = 0.2$. This graph indicates that for an $XPD \sim 1$ dB (as measured in [114]) two-branch polarization diversity can produce performance

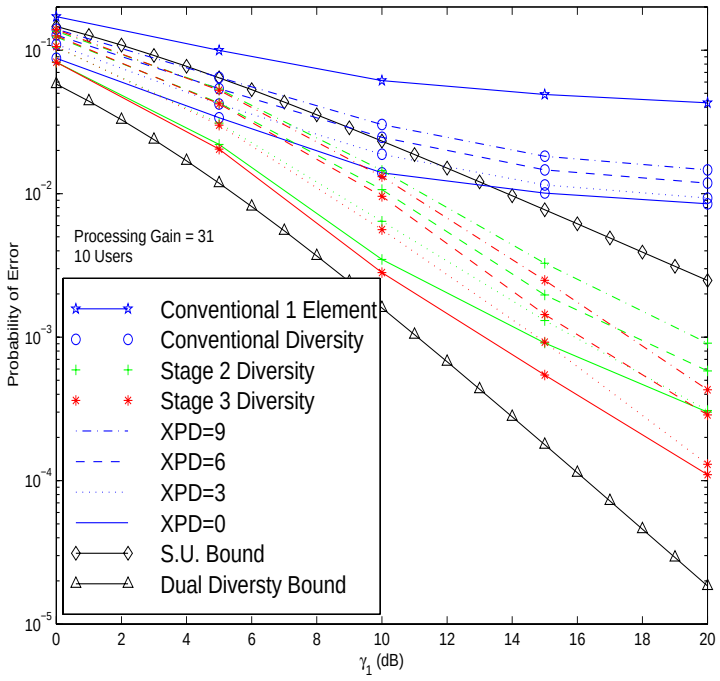

Figure 7.8: Probability of error vs. γ_1 for a multistage interference cancellation receiver with polarization diversity for various XPDs. Flat Rayleigh fading with normalized fading rate $F_dT = 0.0113$, 10 users and processing gain = 31.

improvements very similar to those obtainable with a two-branch spatial diversity scheme. For the case of XPD = 6 dB [110], spatial diversity seems to be superior although polarization diversity still provides significant gains and has the advantage of simple installation.

7.3 Conclusions

In this section, advanced receiver architectures for the uplink of a DS-CDMA system that employ multiuser detection and dual antenna diversity have been examined. Simulation results indicate that by combining multistage interference cancellation and dual antenna diversity, the effects of MAI and flat fading can be significantly mitigated. The proposed receivers achieve significant performance gains over the conventional single element DS-CDMA receiver. Simulation results show that for $XPD \approx 0$ dB, the performance of polarization diversity is comparable to that of dual

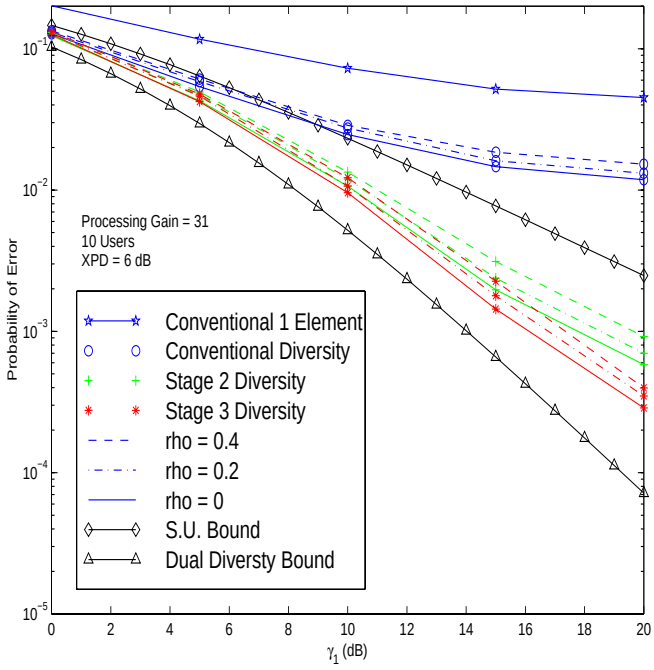

Figure 7.9: Probability of error vs. γ_1 for a multistage interference cancellation receiver with polarization diversity for several values of the correlation coefficient ρ. Flat Rayleigh fading with normalized fading rate $F_dT = 0.0113$ and $XPD = 6$ dB, 10 users, processing gain = 31.

spatial diversity for DS-CDMA communications. For $XPD \neq 0$ dB the performance of polarization diversity decreases but still provides significant gains over a receiver with no diversity.

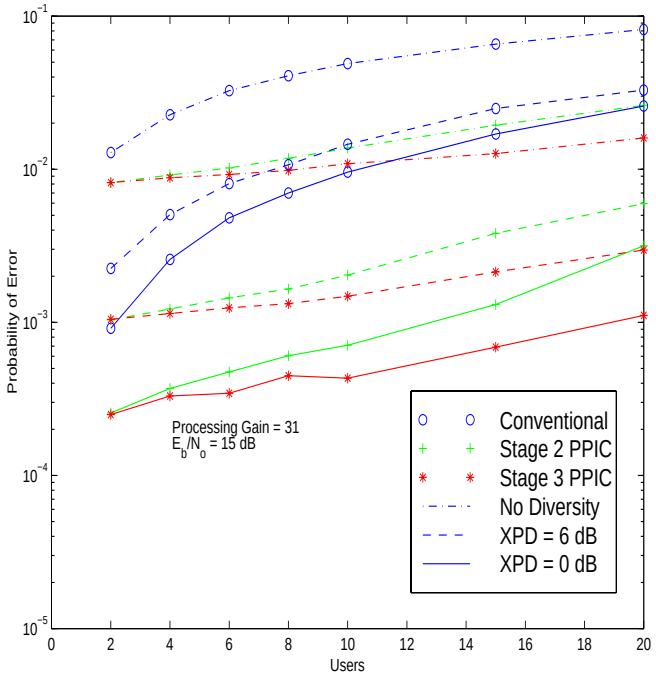

Figure 7.10: Probability of error vs. number of users for a multistage interference cancellation receiver with and without polarization diversity for XPD = 0 and 6 dB. Flat Rayleigh fading $F_dT = 0.0113$, average $\gamma_1 = 15$ dB, 10 users, and processing gain = 31.

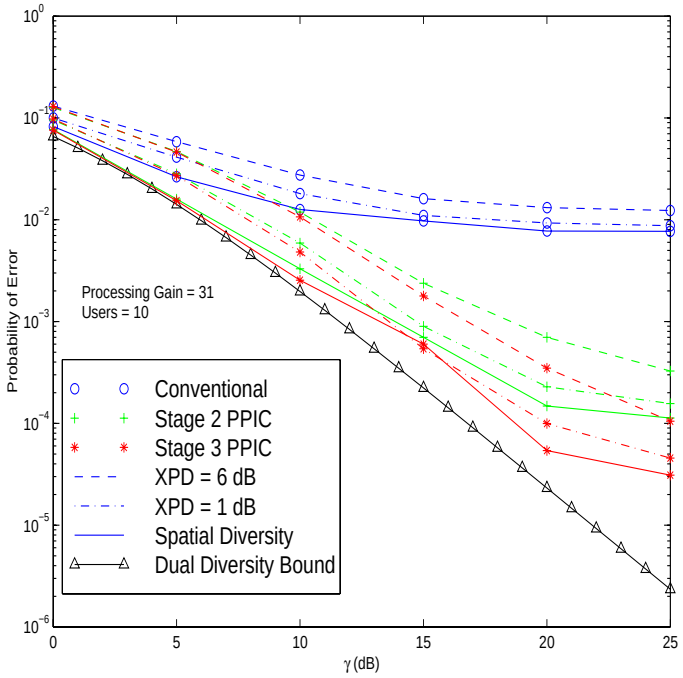

Figure 7.11: Probability of error vs. γ_1 comparison for a multistage interference cancellation receiver with ideal dual spatial diversity, and with polarization diversity for XPD = 1 dB and XPD = 6 dB; $\rho = 0.2$. Flat Rayleigh fading, $F_dT = 0.0113$, 10 users and processing gain = 31.

Chapter 8

Summary and Future Work

The research reported in this dissertation focuses on the development of practical and effective techniques for multiuser interference cancellation in CDMA systems.

Chapter 2 of this dissertation introduced the reader to spread spectrum and multiple access communications. Following, the introduction, multiuser detection was proposed as a viable enabling technology for improving the capacity of the next generation of wireless communication systems. It was shown, however, that capacity improvements are dictated by the degree of interference supression achieved by the multiuser detector.

Chapter 3 reported on a comparison of the major multiuser detection techniques under a variety of ideal and non-ideal situations. Coherent and non-coherent versions of the most noted multiuser receivers were considered. Results indicate that in AWGN and fading channels, multiuser detection affords significant improvements over the conventional receiver. Multiuser receivers also displayed robustness to disparities in received powers, which hinder performance of the conventional receiver. Performance gains decline, however, in the presence of delay estimation errors. This provides indication that acquisition and synchronization are a very important in the design of multiuser detectors. In terms of computational complexity, direct implementation of linear receivers is too complex due to matrix inversion. Because of their low complexity and robustness, subtractive interference cancellation receivers appear best suited to practical implementation, particularly parallel interference cancellation. Among its advantages over successive interference cancellation are: no

requirement for user sorting according to received powers, reduced latency, and compatibility with parallel processing.

In Chapter 4, a detailed analysis of the decision statistics after interference cancellation was presented. The analysis established that the use of soft decisions for joint estimation of the received amplitudes and the transmitted bits results in biased decision statistics. An analytical derivation was presented, uncovering the source of the bias and characterizing its dependence on the number of users and the spreading gain. Subsequently, partial interference cancellation was identified as a very effective low-complexity approach for mitigating the effect of the bias and improving performance over the typical full cancellation scheme.

The practical implementation of multiuser receivers based on the partial interference cancellation approach was the focus of chapter 5. Two real-time DSP based implementations were presented and their complexity was characterized. At the core of the development is a technique that reduces complexity from quadratic to linear in the number of users, yet yields identical results to traditional parallel cancellation. As an alternative to coherent reception, a differentially coherent structure was developed and implemented. The resulting receiver obviates the need for phase estimation, simplifying the implementation. The reported experimental results for the interference cancellers show significant improvements in bit error rate over the conventional receiver.

The combination of parallel interference cancellation and multiple symbol differential detection is investigated in Chapter 6. This chapter shows, analytically and via simulation, that significant performance improvements are achieved in AWGN channels by increasing the memory at the receiver and performing maximum likelihood sequence estimation of the received phases. It was observed that most of the improvements are obtained by increasing the memory to three symbols. Expressions describing the performance of parallel interference cancellation with traditional differential detection were obtained, as a particular case of the more general multiple symbol detection approach. A low complexity technique that uses the Viterbi algorithm for improved differential detection was also studied. Simulation results show improved performance over traditional differential detection and block multiple symbol detectors of comparable complexity.

Chapter 7 reports on a simulation study of polarization diversity for various practical DS-CDMA multiuser receivers in flat Rayleigh fading. Simulation results show that enhanced performance

is achievable through combined multiuser detection and dual antenna diversity. The performance of the diversity receivers was investigated for different values of cross-polarization discrimination (XPD). For low values of XPD, the performance proved close to that achieved with dual spatial diversity. For larger values XPD, performance improvements were still afforded, however, performance was reduced in comparison to spatial diversity. This simulation study indicates that significant capacity improvements are afforded by combining polarization diversity reception and multiuser detection at the base station

8.1 Future Work

There are various avenues for future research associated with the work performed in this dissertation:

1. In parallel interference cancellation receivers, cancellation can be *soft*, where the decision statistics at the output of the matched filter bank are used for joint estimation of the transmitted bits and amplitudes, or *hard*, where the full signal is reconstructed using hard data bit decisions and separately derived amplitude estimates. Since accurate signal reconstruction is essential for interference cancellation, future work will involve the development of improved practical methods for amplitude and phase estimation.

2. Coding techniques can be used to significantly improve the performance of multiple access spread spectrum systems in AWGN and fading channels. Most work to date in the area of multiuser detection and interference cancellation separates the analysis of multiuser detection from that of error control, with most results focusing mainly on performance in the uncoded case. Iterative techniques, which offer superior performance than convolutional coding at a higher complexity, seem to fit well in the framework of multi-stage interference cancellation. Iterative techniques such as the ones used in decoding of Turbo codes may be further expanded so that information is shared between users at every stage of cancellation to achieve improved performance.

3. The work in this document has focused on binary modulation. Expanding the results to

include QPSK and DQPSK would be a useful development. Extending the practical implementations of the parallel interference cancellation receivers to operate with 4-ary PSK is inviting, since QPSK and DQPSK provide higher throughput with relatively low additional complexity.

4. Multiuser receivers have the potential of becoming a powerful tool for improving the performance of the next generation of wireless DS-CDMA systems. However, implementation of an advanced CDMA receiver for emerging 3^{rd} generation standards offers new challenges and several issues that must be addressed. Due to new features encountered in these schemes such as QPSK multi-rate/multi-code operation and double layered spreading, new techniques need to be devised.

5. Another aspect of future work deals with interaction with smart antenna systems. There are several issues that arise when smart antennas and interference cancellation work in unison. For example, it is not completely clear what the best approach is in combining the decision statistics that result from multiuser detection on separate beams, and optimizing the process of interference cancellation and beam forming. It is also very likely that at their onset, third generation systems will employ switched beam systems rather that fully adaptive arrays. It is thus also important to investigate practical methods for interference cancellation and switched beam arrays to be coupled together.

6. Results for the single user case suggest that performance improvements of multiple symbol differential detection for differentially encoded PSK receivers are likely to be more significant for D-QPSK than for DPSK. It would be advantageous to expand the results obtained for the binary case to differentially encoded QPSK systems emplying multiuser detection.

Appendix A

A Postdetection Approach for Interference Cancellation

This appendix illustrates the postdetection method for performing parallel interference cancellation. Mathematically, this approach is equivalent to the predetection wideband approach. A closed form iterative solution is also derived for the decision statistics after interference cancellation.

The input signal to the matched filter receiver can be represented as:

$$r(t) = \sum_{k=1}^{K} \sqrt{P_k} b_k a_k(t-\tau_{k,l}) e^{j\theta_k t} + n(t), \tag{A.1}$$

The outputs of the matched filter bank for the i^{th} bit of user k at stage 0, $y_k^i(0)$, correspond to the decision statistics of the conventional receiver:

$$y_k^i(0) = \frac{1}{T} \int_{(i-1)T+\tau_k}^{T+\tau_k} r(t) a_k(t-\tau_{k,l}), \tag{A.2}$$

These observables can be expressed in terms of the elements of the cross-correlation matrix $\mathbf{R}$ as:

$$\begin{aligned} y_k^i(0) = & \sum_{l=k+1}^{K} \sqrt{P_l^{i-1}} b_l^{i-1} R_{k,l}(1) e^{j\theta_l^{i-1}} + \sum_{\substack{l=1 \\ l\neq k}}^{K} \sqrt{P_l^i} b_l^i R_{k,l}(0) e^{j\theta_l^i} \\ & + \sqrt{P_k^i} b_k^i R_{k,k}(0) e^{j\theta_k^i} + \sum_{l=1}^{k-1} \sqrt{P_l^{i+1}} b_l^{i+1} R_{k,l}(-1) e^{j\theta_l^{i+1}}, \end{aligned} \tag{A.3}$$

where

$$R_{k,l}(i) = \int_{-\infty}^{\infty} a_k(t-\tau_k)a_l(t+iT-\tau_l)dt. \tag{A.4}$$

Taking the expected value of the observables condition on a particular transmitted bit yields:

$$E\{y_k^i(0)|b_k^i\} = \sqrt{P_k^i}b_k^i R_{k,k}(0)e^{j\theta_k^i}. \tag{A.5}$$

The transmitted bit is recovered via an inverse complex rotation of the observable, in this case:

$$E\{y_k^i(0)e^{-j\theta_k^i}|b_k^i\} = \sqrt{P_k^i}b_k^i, \tag{A.6}$$

which yields the desired polarity.

At the m^{th} stage of interference cancellation, the decision statistics correspond to:

$$y_k^i(m) = \frac{1}{T}\int_{(i-1)T+\tau_k}^{T+\tau_k} (r(t) - \sum_{\substack{j=1 \\ j\neq k}} \hat{r}_j(t))a_k(t-\tau_{k,l}), \tag{A.7}$$

These decision statistics can be expressed in terms of the mutual crosscorrelations, and the estimated bits and amplitudes:

$$\begin{aligned} y_k^i(m+1) &= \frac{1}{T}\int_{(i-1)T+\tau_k}^{T+\tau_k} r(t)a_k(t-\tau_{k,l})dt - \sum_{l=k+1}^{K} \sqrt{\hat{P}_{l,m}^{i-1}}\hat{b}_{l,m}^{i-1}R_{k,l}(1)e^{j\theta_l^{i-1}} \\ &\quad -[\sum_{l=1}^{K} \sqrt{\hat{P}_{l,m}^{i}}\hat{b}_{l,m}^{i}R_{k,l}(0)e^{j\theta_l^{i}} - \sqrt{\hat{P}_{k,m}^{i}}\hat{b}_{k,m}^{i}R_{k,k}(0)e^{j\theta_k^{i}}] \\ &\quad -\sum_{l=1}^{k-1} \sqrt{\hat{P}_{l,m}^{i+1}}\hat{b}_{l,m}^{i+1}R_{k,l}(-1)e^{j\theta_l^{i+1}}, \end{aligned} \tag{A.8}$$

Noticing that $y_j^i(m) = \sqrt{\hat{P}_j^i}\hat{b}_{j,m}^i e^{j\theta_k^i}$, the previous equation can be written as:

$$\begin{aligned} y_k^i(m+1) &= y_k^0(m+1) - [\sum_{l=k+1}^{K} y_l^{i-1}(m)R_{k,l}(1) \\ &\quad -\sum_{l=1}^{K} y_l^i(m)R_{k,l}(0) + y_k^i(m)R_{k,k}(0) \\ &\quad -\sum_{l=1}^{k-1} y_l^i(m+1)R_{k,l}(-1)], \end{aligned} \tag{A.9}$$

At stage m, let us define the observation vector $\mathbf{Y}(m)$ as:

$$\mathbf{Y}(m) = \begin{pmatrix} Y_1(m) \\ Y_2(m) \\ \vdots \\ \vdots \\ Y_{K*N_b-1}(m) \\ Y_{K*N_b}(m) \end{pmatrix} = \begin{pmatrix} y_1^1(m) \\ \vdots \\ y_K^1(m) \\ \vdots \\ y_1^1(m) \\ \vdots \\ y_K^{N_b}(m) \end{pmatrix} \tag{A.10}$$

Equation (A.9) can then be written as:

$$\begin{aligned} \mathbf{Y}(m) &= \mathbf{Y}(0) - \mathbf{R}\mathbf{Y}(m-1) + \text{diag}\{\mathbf{R}\}\mathbf{Y}(m-1) \\ \mathbf{Y}(m) &= \mathbf{Y}(0) - (\mathbf{R}-\mathbf{I})\mathbf{Y}(m-1) \\ \mathbf{Y}(m) &= \mathbf{Y}(0) - \tilde{\mathbf{R}}\mathbf{Y}(m-1) \end{aligned} \tag{A.11}$$

where

$$\mathbf{R} = \begin{pmatrix} \mathbf{R(0)} & \mathbf{R(-1)} & 0 & \cdots & 0 \\ \mathbf{R(1)} & \mathbf{R(0)} & \mathbf{R(-1)} & & \vdots \\ 0 & \mathbf{R(1)} & \mathbf{R(0)} & \ddots & 0 \\ \vdots & & \ddots & \ddots & \mathbf{R(-1)} \\ 0 & \cdots & 0 & \mathbf{R(1)} & \mathbf{R(0)} \end{pmatrix} \tag{A.12}$$

and $\tilde{\mathbf{R}} = (\mathbf{R} - \mathbf{I})$.

The implications of this derivation are two-fold. First, It shows that computation of the decision statistics via the despread/re-spread wideband approach is entirely equivalent that with the post-detection approach. Second, it presents parallel interference cancellation as an iterative process whose convergence can be analyzed. The results of this derivation were initially used to confirm the feasibility of a postdetection approach. In [115] a parallel approach was used to show that the parallel interference cancellation detector converges to the decorrelating detector as the number of stages grows to infinity. For the sake of completeness, let us solve the iterative relation of Equation (A.11):

$$\begin{aligned} \mathbf{Y}(m) &= \mathbf{Y}(0) - \tilde{\mathbf{R}}\mathbf{Y}(m-1) \\ &= \mathbf{Y}(0) - (\tilde{\mathbf{R}} - \tilde{\mathbf{R}}^2 + \tilde{\mathbf{R}}^3 - \tilde{\mathbf{R}}^4 + \tilde{\mathbf{R}}^5 - \cdots)\mathbf{Y}(0) \\ &= (\mathbf{I} - \tilde{\mathbf{R}} + \tilde{\mathbf{R}}^2 - \tilde{\mathbf{R}}^3 + \tilde{\mathbf{R}}^4 - \tilde{\mathbf{R}}^5 + \cdots)\mathbf{Y}(0) \end{aligned} \tag{A.13}$$

In the limit, as $m \rightarrow \infty$ the previous summation converges to

$$\begin{aligned} \mathbf{Y}(m) &= (\tilde{\mathbf{R}} + \mathbf{I})^{-1}\mathbf{Y}(0) \\ \mathbf{Y}(m) &= \mathbf{R}^{-1}\mathbf{Y}(0) \end{aligned} \tag{A.14}$$

Which corresponds to the decorrelating detector.

Appendix B

Non-linear Decision Functions for Improved DS-CDMA Demodulation

The use of non-linear decision functions can be motivated by considering the problem of non-linear mean square estimation of the transmitted data sequence in a single user direct sequence spread spectrum channel ([15] Problem 6.1).

In the single user case, the received baseband signal corresponds to a binary phase modulated waveform:

$$r(t) = \sqrt{P}a(t) \sum_{i=-\infty}^{\infty} b_i p_{_T}(t) + n(t) \tag{B.1}$$

where P is the received signal power, $a(t)$ is the spreading waveform, b_i corresponds to the i^{th} transmitted bit, and $p_{_T}(t)$ is a unit pulse function of duration T equal to the bit period.

Non-linear mean square estimation of the transmitted data involves finding the function $g(r(t))$ of the received signal $r(t)$ that minimizes the mean squared error:

$$MSE = E\{[b_i - g(r(t))]^2\} \tag{B.2}$$

In order to find the optimal non-linear function, it is advantageous to express the mean square error as a conditional density expected value:

$$MSE = E\{E\{[b_i - g(r(t))]^2 \ |r(t) \ \}\}. \tag{B.3}$$

Since the inner expectation always has a positive value, the minimum is achieved by minimizing:

$$E\{[b_i - g(r(t))]^2 \ |r(t)\ \} = \int_{-\infty}^{\infty} [b_i - g(r(t))]^2 f_{b_i}(b_i \ |r(t)\ ) db_i \tag{B.4}$$

In this formula, $g(r(t))$ corresponds to a constant, therefore minimization is achieved when

$$\begin{aligned} g(r(t)) &= E\{[b_i \ |r(t)\ \} \\ &= \int_{-\infty}^{\infty} b f_{b_i}(b_i \ |r(t)\ ) db_i. \end{aligned} \tag{B.5}$$

Since b_i is a discrete random variable:

$$f_{b_i}(b_i \ |r(t)\ ) = P[b_1 = -1 \ |r(t)\ ]\delta(b+1) + P[b_1 = 1 \ |r(t)\ ]\delta(b-1). \tag{B.6}$$

The a posteriori probability $P[b_1 = -1 \ |r(t)\ ]$ can be computed from Bayes formula and the likelihood functions as:

$$P[b_1 = -1 \ |r(t)\ ] = \frac{1}{1 + \frac{e^{\frac{-1}{\sigma^2}\int_{(i-1)T}^{T}(r(t)+\sqrt{P}a(t))^2 dt}}{e^{\frac{-1}{\sigma^2}\int_{(i-1)T}^{T}(r(t)-\sqrt{P}a(t))^2 dt}}}, \tag{B.7}$$

where σ^2 is the variance of the noise $n(t)$.

Using the previous two expressions, we can write Equation B.6 as:

$$g(r(t)) = \frac{1}{1 + e^{\frac{-2\sqrt{P}y}{\sigma^2}}} - \frac{1}{1 + e^{\frac{2\sqrt{P}y}{\sigma^2}}} \tag{B.8}$$

where $y = \int_{(i-1)T}^{T} r(t)a(t)dt$ is the output of the matched filter demodulator.

After some simple algebraic manipulations, it can be shown that the optimum nonlinear mean square estimator corresponds to:

$$\begin{aligned} g(r(t)) &= \frac{e^{\frac{\sqrt{P}y}{\sigma^2}} - e^{\frac{-\sqrt{P}y}{\sigma^2}}}{e^{\frac{\sqrt{P}y}{\sigma^2}} + e^{\frac{-\sqrt{P}y}{\sigma^2}}} \\ &= \tanh(\frac{\sqrt{P}y}{\sigma^2}). \end{aligned} \tag{B.9}$$

Appendix C

Background Noise Variance in Parallel Interference Cancellation

In order to make the derivation of a closed form expression more manageable, the crosscorrelations between signature sequences will be modeled as independent Gaussian random variables of zero mean and variance $E\{R^2\} = \frac{1}{N}$. The Gaussian assumption, allows high order moments of the crosscorrelations between signature sequences to be expressed solely in terms of the first and second moments. In particular, the fact that for Gaussian random variables $E\{x^{2k}\} = 1 * 3 * (2k-1)\sigma_x^2$ will be particularly useful.

Let us define:

$$\Upsilon = E\left\{\left((n_1 - C_2\sum_{j=2}^{K} n_j R_{1,j} + C_1C_2\sum_{j=2}^{K}\sum_{\kappa\neq j}^{K} n_\kappa R_{j,\kappa}R_{1,j}\right)^2\right\} \tag{C.1}$$

This can be expressed as:

$$\begin{aligned}\Upsilon &= E\{n_1^2\} - 2C_2E\{\sum_{j=2}^{K} n_1 n_j R_{1,j}\} + 2C_1C_2E\{\sum_{j=2}^{K}\sum_{\kappa\neq j}^{K} n_1 n_\kappa R_{j,\kappa}R_{1,j}\} \qquad \text{(C.2)}\\ &\quad + C_2^2E\{(\sum_{j=2}^{K} n_j R_{1,j})^2\} - 2C_1C_2^2E\{(\sum_{j=2}^{K} n_j R_{1,j})(\sum_{j=2}^{K}\sum_{\kappa\neq j}^{K} n_\kappa R_{j,\kappa}R_{1,j})\}\\ &\quad + (C_1C_2)^2E\{(\sum_{j=2}^{K}\sum_{\kappa\neq j}^{K} n_\kappa R_{j,\kappa}R_{1,j})^2\} \qquad \text{(C.3)}\end{aligned}$$

It is convenient to separately analyze each one of the individual terms in the previous equation. The first term, represents the background noise variance:

$$\begin{aligned} \Upsilon_1 &= E\{n_1^2\} \\ &= N_o. \end{aligned} \tag{C.4}$$

The contribution of the second term corresponds to:

$$\begin{aligned} \Upsilon_2 &= -2C_2 E\{\sum_{j=2}^{K} n_1 n_j R_{1,j}\} \\ &= 2C_2 \sum_{j=2}^{K} E\{n_1 n_j R_{1,j}\} \\ &= -2C_2 N_o E\{R_{1,j}^2\} \\ &= -2C_2 N_o \frac{K-1}{N} \end{aligned} \tag{C.5}$$

The third term corresponds to:

$$\begin{aligned} \Upsilon_3 &= 2C_1 C_2 E\{\sum_{j=2}^{K} \sum_{\kappa \neq j}^{K} n_1 n_\kappa R_{j,\kappa} R_{1,j}\} \\ &= 2C_1 C_2 E\{\sum_{j=2}^{K} n_1 n_1 R_{1,j}^2\} \\ &= 2C_1 C_2 N_o \frac{K-1}{N} \end{aligned} \tag{C.6}$$

The fourth term can be evaluated directly:

$$\begin{aligned} \Upsilon_4 &= C_2^2 E\{(\sum_{j=2}^{K} n_j R_{1,j})^2\} \\ &= C_2^2 \sum_{j=2}^{K} E\{n_j^2\} E\{R_{1,j}^2\} \\ &= C_2^2 N_o \frac{K-1}{N} \end{aligned} \tag{C.7}$$

The contribution of the fifth term can be evaluated as follows:

$$\begin{aligned} \Upsilon_5 &= -2C_1 C_2^2 E\{(\sum_{j=2}^{K} n_j R_{1,j})(\sum_{j=2}^{K} \sum_{\kappa \neq j}^{K} n_\kappa R_{j,\kappa} R_{1,j})\} \\ &= -2C_1 C_2^2 E\{(\sum_{\mu=2}^{K} n_\mu R_{1,\mu})(\sum_{j=2}^{K} \sum_{\substack{\kappa=2 \\ \kappa \neq j}}^{K} n_\kappa R_{j,\kappa} R_{1,j} + \sum_{j=2}^{K} n_1 R_{1,j}^2)\} \end{aligned}$$

$$
\begin{aligned}
&= -2C_1C_2^2E\{\sum_{j=2}^{K}\sum_{\substack{\kappa=2\\ \kappa\neq j}}^{K} n_j n_\kappa R_{1,j}R_{j,\kappa}R_{1,j} + \sum_{\substack{\mu=2\\ \mu\neq j}}^{K}\sum_{j=2}^{K} n_1 n_\mu R_{1,\mu}R_{1,j}^2 + \sum_{j=2}^{K} n_1 n_j R_{1,j}R_{j,1}^2\} \\
&= -2C_1C_2^2N_o\left[\frac{(K-1)(K-2)}{N^2} + \frac{3(K-1)}{N^2} + \frac{(K-1)(K-2)}{N^2}\right] \qquad \text{(C.8)}
\end{aligned}
$$

The final term Υ_6 corresponds to:

$$
\begin{aligned}
\Upsilon_6 &= (C_1C_2)^2E\{(\sum_{j=2}^{K}\sum_{\kappa\neq j}^{K} n_\kappa R_{j,\kappa}R_{1,j})^2 \\
&= (C_1C_2)^2E\left\{(\sum_{j=2}^{K}\sum_{\substack{\kappa=2\\ \kappa\neq j}}^{K} n_\kappa R_{j,\kappa}R_{1,j} + \sum_{j=2}^{K} n_1 R_{j,1}^2)^2\right\} \\
&= (C_1C_2)^2[E\{(\sum_{j=2}^{K}\sum_{\substack{\kappa=2\\ \kappa\neq j}}^{K} n_\kappa R_{j,\kappa}R_{1,j})^2\} + E\{\sum_{\mu=2}^{K}\sum_{j=2}^{K} n_1^2 R_{j,1}^2 R_{1,\mu}^2\}] \\
&= (C_1C_2)^2N_o\left[\frac{(K-1)(K-2)}{N^2} + E\{\sum_{j=2}^{K} n_1^2 R_{j,1}^4\} + E\{\sum_{\substack{\mu=2\\ \mu\neq j}}^{K}\sum_{j=2}^{K} n_1^2 R_{j,1}^2 R_{1,\mu}^2\}\right] \\
&= (C_1C_2)^2N_o\left[\frac{(K-1)(K-2)}{N^2} + \frac{3(K-1)}{N^2} + \frac{(K-1)(K-2)}{N^2}\right] \qquad \text{(C.9)}
\end{aligned}
$$

Adding Υ_1 through Υ_6 yields the desired expression:

$$
\begin{aligned}
\Upsilon &= N_o\left[1 + \frac{K-1}{N}(-2C_2 + 2C_1C_2 + C_2^2) - 2C_1C_2\frac{K-1}{N}\left(\frac{2(K-2)+3}{N}\right)\right. \\
&\quad \left. +(C_1C_2)^2\frac{K-1}{N}\left(\frac{2(K-2)+3}{N}\right)\right] \\
&= N_o\left[1 + C_2\frac{K-1}{N}\left(C_2 + 2C_1 - 2 + C_1C_2(C_1-2)\frac{2K-1}{N}\right)\right]. \qquad \text{(C.10)}
\end{aligned}
$$

Appendix D

Computing the Marcum-Q Function Arguments for Pairwise Probability of Error Calculations

This appendix considers the problem of finding the arguments a and b of the Marcum-Q function employed in the computation of the pairwise error probabilities. The approach used in the derivation, is based on the work of [99] for the single user problem.

The pairwise error probability can be expressed as:

$$Pr\{|z_2|^2 > |z_1|^2\} = \frac{1}{2}[1 - Q(\sqrt{b}, \sqrt{a}) + Q(\sqrt{a}, \sqrt{b})] \tag{D.1}$$

where

$$Q(a, b) = \int_b^\infty \exp\left(-\frac{a^2 + x^2}{2}\right) I_o(ax)dx \tag{D.2}$$

is the marcum Q function, and a and b correspond to [101]:

$$\left\{ \begin{array}{c} a \\ b \end{array} \right\} = \frac{1}{2N_s}\left\{\frac{S_1 + S_2 - 2|\rho|\sqrt{S_1 S_2}\cos(\theta_1 - \theta_2 + \phi)}{1 - |\rho|^2} \mp \frac{S_1 - S_2}{\sqrt{1 - |\rho|^2}}\right\}. \tag{D.3}$$

D.1 Stage 0

The values of a and b in Equation(D.3) can be computed based on the results presented in Equations (6.36),(6.39) and (6.47). Substituting these values in Equation (D.3) one obtains:

$$\left\{ \begin{array}{c} a \\ b \end{array} \right\} = \frac{1}{2N_s} \left\{ \frac{\frac{E_b(N_w^2+|\delta|^2)}{2} - 2|\rho|\sqrt{N_w^2 E_b^2 |\delta|^2/4}}{1-|\rho|^2} \mp \frac{\frac{E_b}{2}(N_w^2 - |\delta|^2)}{1-|\rho|^2} \right\}. \tag{D.4}$$

Using the fact that at stage 0 $|\rho| = |\delta|/N_w$, the previous equation can be written as:

$$\left\{ \begin{array}{c} a \\ b \end{array} \right\} = \frac{1}{2N_s} \left\{ \frac{\frac{E_b N_w^2(1+|\rho|)}{2} - E_b N_w |\rho||\delta|}{1-|\rho|^2} \mp \frac{\frac{E_b N_w^2}{2}(1-|\rho|^2)}{\sqrt{1-|\rho|^2}} \right\}. \tag{D.5}$$

simplifying, one obtains:

$$\left\{ \begin{array}{c} a \\ b \end{array} \right\} = \frac{E_b N_W^2}{4N_s} \left\{ 1 \mp \sqrt{1-|\rho|^2} \right\}. \tag{D.6}$$

Expressing the previous equation in terms of δ results in:

$$\left\{ \begin{array}{c} a \\ b \end{array} \right\} = \frac{E_b}{4N_s} \left\{ N_w^2 \mp N_w \sqrt{N_w^2 - |\delta|^2} \right\}. \tag{D.7}$$

D.2 Stage 1

For stage 1 of full cancellation:

$$z_1^{(s=1)} = \sum_{i=0}^{N_w-1} y_{1,k-i}^{(s=1)} e^{-j\sum_{m=0}^{N_w-i-2} \Delta\phi_{1,k-i-m}} \tag{D.8}$$

$$z_2^{(s=1)} = \sum_{i=0}^{N_w-1} y_{1,k-i}^{(s=1)} e^{-j\sum_{m=0}^{N_w-i-2} \Delta\hat{\phi}_{1,k-i-m}}, \tag{D.9}$$

where

$$y_1^{(s=1)} = \sqrt{E_b}\left[1 - \sum_{u=2}^{K} R_{1,u}^2\right] e^{j\phi_1} - \sqrt{E_b}\sum_{u=2}^{K}\sum_{\substack{l=2 \\ l\neq u}}^{K} R_{l,u}R_{1,u}e^{j\phi_l} + \left(n_1 - \sum_{u=2}^{K} n_u R_{1,u}\right). \tag{D.10}$$

Substituting, one obtains:

$$z_1 = N_w\sqrt{E_b}e^{j\phi_{1,K-N_w+1}}\left[1-\sum_{u=2}^{K}R_{1,u}^2\right]-\sum_{i=0}^{N_w-1}\left(\sqrt{E_b}\sum_{u=2}^{K}\sum_{\substack{l=2\\l\neq u}}^{K}R_{l,u}R_{1,u}e^{j\phi_{l,k-i}}\right.$$
$$\left.+(n_{1,k-i}-\sum_{u=2}^{M}n_{u,k-i})R_{1,u}\right)e^{-j\sum_{m=0}^{N_w-i-2}\Delta\phi_{1,k-i-m}}, \quad \text{(D.11)}$$

the mean of z_1 is readily computed to be:

$$\overline{z_1} = N_w\sqrt{E_b}\left(1-\frac{K-1}{N}\right)e^{j\phi_{1,k-N_w+1}}. \quad \text{(D.12)}$$

Now, z_2 corresponds to:

$$z_2 = \sum_{i=0}^{N_w-1}\sqrt{E_b}e^{j\phi_{1,K-N_w+1}}\left[1-\sum_{u=2}^{K}R_{1,u}^2\right]e^{-j\sum_{m=0}^{N_w-i-2}\Delta\phi_{1,K-i-m}-\Delta\hat{\phi}_{1,k-i-m}} \quad \text{(D.13)}$$
$$-\sum_{i=0}^{N_w-1}\left(\sqrt{E_b}\sum_{u=2}^{K}\sum_{\substack{l=2\\l\neq u}}^{K}R_{l,u}R_{1,u}e^{j\phi_{l,k-i}}+(n_{1,k-i}-\sum_{u=2}^{M}n_{u,k-i})R_{1,u}\right)e^{-j\sum_{m=0}^{N_w-i-2}\Delta\hat{\phi}_{1,k-i-m}},$$

the mean of z_2 evaluates to:

$$\overline{z_2} = \sum_{i=0}^{N_w-1}\sqrt{E_b}\left(1-\frac{K-1}{N}\right)e^{j\phi_{1,K-N_w+1}}e^{-j\sum_{m=0}^{N_w-i-2}\Delta\phi_{1,k-i-m}-\Delta\hat{\phi}_{1,k-i-m}}$$
$$= \sqrt{E_b}\left(1-\frac{K-1}{N}\right)e^{j\phi_{1,K-N_w+1}}\delta \quad \text{(D.14)}$$

The power in the non-random component of z_1 is given by:

$$S_1 = \frac{1}{2}|\overline{z_1}|^2$$
$$= \frac{1}{2}N_w^2E_b\left(1-\frac{K-1}{N}\right)^2 \quad \text{(D.15)}$$

The power in the non-random component of z_2 is:

$$S_2 = \frac{1}{2}|\overline{z_2}|^2$$
$$= \frac{1}{2}E_b\left(1-\frac{K-1}{N}\right)^2|\delta|^2 \quad \text{(D.16)}$$

The crosscorrelation between processes, ρ, is given by:

$$\rho = \frac{1}{2}\frac{\overline{(z_1-\overline{z_1})^*(z_2-\overline{z_2})}}{\overline{|z_1-\overline{z_1}|^2}}, \quad \text{(D.17)}$$

Substituting the previously found expressions for $z_1, z_2, \overline{z_1}$ and $\overline{z_2}$ into the preceeding equation yields:

$$\begin{aligned}
\rho &= \frac{1}{2N_s} E \Bigg\{ \Bigg[\sum_{i=0}^{N_w-1} \Bigg(\sqrt{E_b}[1 - \sum_{u=2}^{K} R_{1,u}^2] e^{j\phi_{1,k-i}} - \sqrt{E_b} \sum_{u=2}^{K} \sum_{\substack{l=2 \\ l \neq u}}^{K} R_{l,u} R_{1,u} e^{j\phi_{l,k-i}} \\
&\quad + (n_{1,k-i} - \sum_{u=2}^{K} n_{u,k-i} R_{1,u}) \Bigg) e^{-j\sum_{m=0}^{N_w-i-2} \Delta\phi_{1,k-i-m}} - \sqrt{E_b} \left(1 - \frac{K-1}{N}\right) e^{j\phi_{1,K-N_w+1}} \Bigg]^* \\
&\quad \Bigg[\sum_{i=0}^{N_w-1} \Bigg(\sqrt{E_b}[1 - \sum_{u=2}^{K} R_{1,u}^2] e^{j\phi_{1,k-i}} - \sqrt{E_b} \sum_{u=2}^{K} \sum_{\substack{l=2 \\ l \neq u}}^{K} R_{l,u} R_{1,u} e^{j\phi_{l,k-i}} + (n_{1,k-i} \\
&\quad - \sum_{u=2}^{K} n_{u,k-i} R_{1,u}) \Bigg) e^{-j\sum_{m=0}^{N_w-i-2} \Delta\hat{\phi}_{1,k-i-m}} - \sqrt{E_b} \left(1 - \frac{K-1}{N}\right) e^{j\phi_{1,K-N_w+1}} \delta \Bigg] \Bigg\}, \qquad \text{(D.18)}
\end{aligned}$$

Cancelling common terms, this equation becomes:

$$\begin{aligned}
\rho &= \frac{1}{2N_s} E \Bigg\{ \sum_{i=0}^{N_w-1} \sum_{n=0}^{N_w-1} \Bigg[\sqrt{E_b} \left(\frac{K-1}{N} - \sum_{u=2}^{K} R_{1,u}^2 \right) e^{\phi_{1,k-i}} \qquad \text{(D.19)} \\
&\quad - \sqrt{E_b} \sum_{u=2}^{K} \sum_{\substack{l=2 \\ l \neq u}}^{K} R_{l,u} R_{1,u} e^{j\phi_{l,k-i}} + (n_{1,k-i} - \sum_{u=2}^{K} n_{u,k-i} R_{1,u}) \Bigg]^* \\
&\quad \times \Bigg[\sqrt{E_b} \left(\frac{K-1}{N} - \sum_{u=2}^{K} R_{1,u}^2 \right) e^{\phi_{1,k-n}} - \sqrt{E_b} \sum_{u=2}^{K} \sum_{\substack{l=2 \\ l \neq u}}^{K} R_{l,u} R_{1,u} e^{j\phi_{l,k-n}} \\
&\quad (n_{1,k-n} - \sum_{u=2}^{K} n_{u,k-n} R_{1,u}) \Bigg] e^{-j\sum_{m=0}^{N_w-i-2} \Delta\phi_{1,k-i-m} - \Delta\hat{\phi}_{1,k-n-m}} \Bigg\}, \qquad \text{(D.20)}
\end{aligned}$$

which can be reduced to:

$$\begin{aligned}
\rho &= \frac{1}{2N_s} E \Bigg\{ E_b | \frac{K-1}{N} - \sum_{u=2}^{K} R_{1,u}^2 |^2 + E_b | \sum_{u=2}^{K} \sum_{\substack{l=2 \\ l \neq u}}^{K} R_{l,u} R_{1,u} |^2 + | n_{1,k-n} \\
&\quad - \sum_{u=2}^{K} n_{u,k-n} R_{1,u} |^2 \Bigg\} \delta \\
&= \frac{\delta}{N_w}. \qquad \text{(D.21)}
\end{aligned}$$

Substituting the expressions from Equations (D.15), (D.16) and (D.21) into Equation (D.3) yields:

$$\begin{Bmatrix} a \\ b \end{Bmatrix} = \frac{1}{2N_s} \left(\frac{1}{2} E_b (1 - \frac{K-1}{N})^2 \right) \left\{ \frac{(N_w^2 + |\delta|^2) - 2|\delta|^2}{1 - |\rho|^2} \right\} \mp \frac{N_w^2 - |\rho|^2}{\sqrt{1 - |\rho|^2}} \qquad \text{(D.22)}$$

Using the fact that $\rho = \frac{\delta}{N_w}$, this equation simplifies to:

$$\left\{ \begin{array}{c} a \\ b \end{array} \right\} = \frac{E_b \left(1 - \frac{K-1}{N}\right)^2}{4N_s} \left\{ N_w^2 \mp N_w \sqrt{N_w^2 - |\delta|^2} \right\}. \tag{D.23}$$

D.2.0.1 Stage 1 Partial Interference Cancellation

The decision variables z_1 and z_2 are given by:

$$z_1^{(s=1)} = \sum_{i=0}^{N_w-1} y_{1,k-i}^{(s=1)} e^{-j\sum_{m=0}^{N_w-i-2} \Delta\phi_{1,k-i-m}} \tag{D.24}$$

$$z_2^{(s=1)} = \sum_{i=0}^{N_w-1} y_{1,k-i}^{(s=1)} e^{-j\sum_{m=0}^{N_w-i-2} \Delta\hat{\phi}_{1,k-i-m}}, \tag{D.25}$$

where

$$\begin{aligned} y_1^{(s=1)} &= \sqrt{E_b}\left[1 - C_1 \sum_{u=2}^{K} R_{1,u}^2\right] e^{j\phi_1} \\ &\quad + (1 - C_1) \sum_{u=2}^{K} \sqrt{E_b} R_{1,u} e^{j\phi_u} - C_1 \sqrt{E_b} \sum_{u=2}^{K} \sum_{\substack{l=2 \\ l \neq u}}^{K} R_{l,u} R_{1,u} e^{j\phi_l} + \left(n_1 - C_1 \sum_{u=2}^{K} n_u R_{1,u}\right). \end{aligned} \tag{D.26}$$

The crosscorrelation between processes ρ is given by:

$$\rho = \frac{1}{2} \frac{\overline{(z_1 - \overline{z_1})^* (z_2 - \overline{z_2})}}{\overline{|z_1 - \overline{z_1}|^2}}, \tag{D.27}$$

where the variable z_1 corresponds to:

$$\begin{aligned} z_1 &= N_w \sqrt{E_b} e^{j\phi_{1,K-N_w+1}} \left[1 - C_1 \sum_{u=2}^{K} R_{1,u}^2\right] + \sum_{k=0}^{N_w-1} \left((1 - C_1) \sum_{u=2}^{K} \sqrt{E_b} R_{1,u} e^{j\phi_u} \right. \\ &\quad \left. - C_1 \sqrt{E_b} \sum_{u=2}^{K} \sum_{\substack{l=2 \\ l \neq u}}^{K} R_{l,u} R_{1,u} e^{j\phi_{l,k-i}} + (n_{1,k-i} - C_1 \sum_{u=2}^{M} n_{u,k-i}) R_{1,u} \right) e^{-j\sum_{m=0}^{N_w-i-2} \Delta\phi_{1,K-i-m}}, \end{aligned} \tag{D.28}$$

and its mean is given by:

$$\overline{z_1} = N_w \sqrt{E_b} \left(1 - C_1 \frac{K-1}{N}\right) e^{j\phi_{1,K-N_w+1}}. \tag{D.29}$$

The power in the non-random component, S_1, is given by:

$$\begin{aligned} S_1 &= \frac{1}{2} |\overline{z_1}|^2 \\ &= \frac{1}{2} N_w^2 E_b \left(1 - C_1 \frac{K-1}{N}\right)^2 \end{aligned} \tag{D.30}$$

The variable z_2 evaluates to:

$$z_2 = \sqrt{E_b}e^{j\phi_{1,K-N_w+1}}\left[1-C_1\sum_{u=2}^{K}R_{1,u}^2\right]\delta+\sum_{k=0}^{N_w-1}\left((1-C_1)\sum_{u=2}^{K}\sqrt{E_b}R_{1,u}e^{j\phi_u}\right. \tag{D.31}$$
$$\left.-C_1\sqrt{E_b}\sum_{u=2}^{K}\sum_{\substack{l=2\\l\neq u}}^{K}R_{l,u}R_{1,u}e^{j\phi_{l,k-i}}+(n_{1,k-i}-C_1\sum_{u=2}^{M}n_{u,k-i})R_{1,u}\right)e^{-j\sum_{m=0}^{N_w-i-2}\Delta\hat{\phi}_{1,k-i-m}},$$

and its mean evaluates to:

$$\overline{z_2} = \sqrt{E_b}\left(1-C_1\frac{K-1}{N}\right)e^{j\phi_{1,K-N_w+1}}\delta, \tag{D.32}$$

The power in the non-random component S_2 is given by:

$$\begin{aligned} S_2 &= \frac{1}{2}|\overline{z_2}|^2 \\ &= \frac{1}{2}E_b\left(1-C_1\frac{K-1}{N}\right)^2|\delta|^2 \end{aligned} \tag{D.33}$$

The crosscorrelation factor ρ can be expressed in terms of the expressions for $z_1, z_2, \overline{z_1}$ and $\overline{z_2}$:

$$\rho = \frac{1}{2N_s}E\left\{\left[\sum_{i=0}^{N-1}\left(\sqrt{E_b}[1-C_1\sum_{u=2}^{K}R_{1,u}^2]e^{j\phi_{1,k-i}}-C_1\sqrt{E_b}\sum_{u=2}^{K}\sum_{\substack{l=2\\l\neq u}}^{K}R_{l,u}R_{1,u}e^{j\phi_{l,k-i}}\right.\right. \tag{D.34}$$
$$\left.+(1-C_1)\sum_{u=2}^{K}\sqrt{E_b}R_{1,u}e^{j\phi_u,k-i}+(n_{1,k-i}-C_1\sum_{u=2}^{K}n_{u,k-i}R_{1,u})\right)e^{-j\sum_{m=0}^{N_w-i-2}\Delta\phi_{1,k-i-m}}$$
$$-\sqrt{E_b}\left(1-\frac{K-1}{N}\right)e^{j\phi_{1,K-N_w+1}}\Bigg]^*\Bigg[\sum_{i=0}^{N-1}\Bigg(\sqrt{E_b}[1-C_1\sum_{u=2}^{K}R_{1,u}^2]e^{j\phi_{1,k-i}}$$
$$-C_1\sqrt{E_b}\sum_{u=2}^{K}\sum_{\substack{l=2\\l\neq u}}^{K}R_{l,u}R_{1,u}e^{j\phi_{l,k-i}}+(1-C_1)\sum_{u=2}^{K}\sqrt{E_b}R_{1,u}e^{j\phi_u,k-i}+(n_{1,k-i}$$
$$\left.\left.-C_1\sum_{u=2}^{K}n_{u,k-i}R_{1,u})\right)e^{-j\sum_{m=0}^{N_w-i-2}\Delta\hat{\phi}_{1,k-i-m}}-\sqrt{E_b}\left(1-\frac{K-1}{N}\right)e^{j\phi_{1,K-N_w+1}}\delta\right]\right\},$$

this expression can be expressed as:

$$\rho = \frac{1}{2N_s}E\left\{\sum_{i=0}^{N_w-1}\sum_{n=0}^{N_w-1}\left(\sqrt{E_b}C_1\left[\frac{K-1}{N}-\sum_{u=2}^{K}R_{1,u}^2\right]e^{j\phi_{1,k-i}}+(1-C_1)\sum_{u=2}^{K}\sqrt{E_b}R_{1,u}e^{j\phi_u,k-i}\right.\right.$$
$$\left.-C_1\sqrt{E_b}\sum_{u=2}^{K}\sum_{\substack{l=2\\l\neq u}}^{K}R_{l,u}R_{1,u}e^{j\phi_{l,k-i}}+(n_{1,k-i}-C_1\sum_{u=2}^{K}n_{u,k-i}R_{1,u})\right)^*\left(\sqrt{E_b}C_1\left[\frac{K-1}{N}\right.\right.$$

$$-\sum_{u=2}^{K} R_{1,u}^2\Bigg] e^{j\phi_{1,k-n}} + (1-C_1)\sum_{u=2}^{K}\sqrt{E_b}R_{1,u}e^{j\phi_{u},k-n} - C_1\sqrt{E_b}\sum_{u=2}^{K}\sum_{\substack{l=2\\l\neq u}}^{K} R_{l,u}R_{1,u}e^{j\phi_{l,k-n}}$$
$$+(n_{1,k-n} - C_1\sum_{u=2}^{K} n_{u,k-n}R_{1,u})\Bigg) e^{j\sum_{m=0}^{N_w-n-2}\Delta\phi_{1,k-i-m}-\Delta\hat{\phi}_{1,k-n-m}}\Bigg\}, \tag{D.35}$$

which corresponds to:

$$\rho = \frac{1}{2N_s}E\Bigg\{\sum_{i=0}^{N_w-1}\Bigg(\Bigg(\sqrt{E_b}C_1\left[\frac{K-1}{N}-\sum_{u=2}^{K}R_{1,u}^2\right]\Bigg)^2 + \Bigg((1-C_1)\sum_{u=2}^{K}\sqrt{E_b}R_{1,u}\Bigg)^2 \tag{D.36}$$
$$+\Bigg(C_1\sqrt{E_b}\sum_{u=2}^{K}\sum_{\substack{l=2\\l\neq u}}^{K}R_{l,u}R_{1,u}\Bigg)^2 + |n_{1,k-i} - C_1^2\sum_{u=2}^{K}n_{u,k-i}R_{1,u}|^2\Bigg)\Bigg\}$$

With the aid of Equation (6.98), this expression can be reduced to:

$$\rho = \frac{\delta}{N_w}. \tag{D.37}$$

Note that the full interference cancellation case, and the conventional receiver are special cases of the partial interference canceller with $C_1 = 1$ and $C_1 = 0$ respectively.

Substituting the expressions from Equations (D.30) and (D.33) into Equation (D.3) yields:

$$\left\{\begin{array}{c} a \\ b \end{array}\right\} = \frac{1}{2N_s}\left(\frac{1}{2}E_b(1-C_1\frac{K-1}{N})^2\right)\left\{\frac{(N_w^2+|\delta|^2)-2|\delta|^2}{1-|\rho|^2}\right\} \mp \frac{N_w^2-|\delta|^2}{\sqrt{1-|\rho|^2}}, \tag{D.38}$$

given the fact that $\rho = \frac{\delta}{N_w}$, this equation simplifies to:

$$\left\{\begin{array}{c} a \\ b \end{array}\right\} = \frac{E_b\left(1-C_1\frac{K-1}{N}\right)^2}{4N_s}\left\{N_w^2 \mp N_w\sqrt{N_w^2-|\delta|^2}\right\} \tag{D.39}$$

Appendix E

Asymptotic Pairwise Probability of Error Calculations for Parallel Partial Interference Cancellation

This appendix uses the approach of [**?**] to find asymptotic expressions for the pairwise probability of error.

The pairwise error probability can be expressed as:

$$Pr\{\hat{\eta} > \eta\} \quad = \quad \frac{1}{2}[1 - Q(\sqrt{b}, \sqrt{a}) + Q(\sqrt{a}, \sqrt{b})]. \tag{E.1}$$

For large arguments of the Marcum-Q functions, this pairwise probability of error can be approximated as [99]:

$$Pr\{\hat{\eta} > \eta\} \quad = \quad \frac{1}{2}\left[\frac{1}{\sqrt{b}-\sqrt{a}}\left(\sqrt{\frac{\sqrt{a/b}}{2\pi}} + \sqrt{\frac{\sqrt{b/a}}{2\pi}}\right) \times \exp\left(-\frac{(\sqrt{b}-\sqrt{a})^2}{2}\right)\right] \tag{E.2}$$

Substituting in the previous equation the expressions for a and b obtained in Appendix D Equation

(D.39) results in:

$$\begin{aligned} Pr\{\hat{\eta} > \eta\} &= \frac{1}{2\sqrt{\frac{\pi E_b N_w (1-C_1\frac{K-1}{N})^2}{4N_s}}\left(\sqrt{N_w - \sqrt{N_w^2 - |\delta|^2}} - \sqrt{N_w + \sqrt{N_w^2 - |\delta|^2}}\right)} \\ &\times \left[\left(\frac{N_w - \sqrt{N_w^2 - |\delta|^2}}{N_w + \sqrt{N_w^2 - |\delta|^2}}\right)^{1/4} + \left(\frac{N_w + \sqrt{N_w^2 - |\delta|^2}}{N_w - \sqrt{N_w^2 - |\delta|^2}}\right)^{1/4}\right] \\ &\times \exp\left\{-\frac{E_b N_w (1-C_1\frac{K-1}{N})^2}{4N_S}\right. \\ &\times \left.\left(\frac{N_w + \sqrt{N_w^2 - |\delta|^2} - 2\sqrt{N_w^2 - N_w^2 + |\delta|^2} + N_w - \sqrt{N_w^2 - |\delta|^2}}{2}\right)\right\} \end{aligned} \quad \text{(E.3)}$$

Simplifying the argument of the exponential function and expressing the second term of the previous equation in the form of $a = \sqrt{(a^2)}$, as a step to achieve further simplification, yields:

$$\begin{aligned} Pr\{\hat{\eta} > \eta\} &= \frac{1}{2\sqrt{\frac{\pi E_b N_w (1-C_1\frac{K-1}{N})^2}{4N_s}}} \times \left(\frac{1}{\left(\sqrt{N_w - \sqrt{N_w^2 - |\delta|^2}} - \sqrt{N_w + \sqrt{N_w^2 - |\delta|^2}}\right)^2}\right)^{1/2} \\ &\times \left[\left(\frac{N_w - \sqrt{N_w^2 - |\delta|^2}}{N_w + \sqrt{N_w^2 - |\delta|^2}}\right)^{1/4} + \left(\frac{N_w + \sqrt{N_w^2 - |\delta|^2}}{N_w - \sqrt{N_w^2 - |\delta|^2}}\right)^{1/4}\right] \\ &\times \exp\left(-\frac{E_b N_w (1-C_1\frac{K-1}{N})^2}{4N_s}(N_w - |\delta|)\right), \end{aligned} \quad \text{(E.4)}$$

Squaring the second term and simplifying, one obtains:

$$\begin{aligned} Pr\{\hat{\eta} > \eta\} &= \frac{1}{2\sqrt{\frac{\pi E_b N_w (1-C_1\frac{K-1}{N})^2}{4N_s}}} \times \left(\frac{1}{2(N_w - |\delta|)}\right)^{1/2} \\ &\times \left[\left(\frac{N_w - \sqrt{N_w^2 - |\delta|^2}}{N_w + \sqrt{N_w^2 - |\delta|^2}}\right)^{1/4} + \left(\frac{N_w + \sqrt{N_w^2 - |\delta|^2}}{N_w - \sqrt{N_w^2 - |\delta|^2}}\right)^{1/4}\right] \\ &\times \exp\left(-\frac{E_b N_w (1-C_1\frac{K-1}{N})^2}{4N_s}(N_w - |\delta|)\right), \end{aligned} \quad \text{(E.5)}$$

Multiplying and dividing the first fraction in the third factor of the previous equation by $N_w - \sqrt{N_w^2 - |\delta|^2}$, and the second fraction by $N_w + \sqrt{N_w^2 - |\delta|^2}$ results in:

$$\begin{aligned} Pr\{\hat{\eta} > \eta\} &= \frac{1}{2\sqrt{\frac{\pi E_b N_w (1-C_1\frac{K-1}{N})^2}{4N_s}}} \times \left(\frac{1}{2(N_w - |\delta|)}\right)^{1/2} \end{aligned}$$

$$\times \left[\sqrt{\frac{N_w - \sqrt{N_w^2 - |\delta|^2}}{|\delta|}} + \sqrt{\frac{N_w + \sqrt{N_w^2 - |\delta|^2}}{|\delta|}} \right]$$
$$\times \exp\left(-\frac{E_b N_w (1 - C_1 \frac{K-1}{N})^2}{4N_s} \left(N_w - |\delta| \right) \right), \tag{E.6}$$

Expressing the third factor in the form of $a = \sqrt{(a^2)}$, allows further simplification of the previous expression:

$$\begin{aligned} Pr\{\hat{\eta} > \eta\} &= \frac{1}{2\sqrt{\frac{\pi E_b N_w (1 - C_1 \frac{K-1}{N})^2}{2N_s}}} \times \left(\frac{1}{2(N_w - |\delta|)} \right)^{1/2} \left[\frac{2(N_w + |\delta|)}{|\delta|} \right]^{1/2} \\ &\quad \times \exp\left(-\frac{E_b N_w (1 - C_1 \frac{K-1}{N})^2}{4N_s} \left(N_w - |\delta| \right) \right) \end{aligned} \tag{E.7}$$

Finally, the pairwise probability of error is given by:

$$Pr\{\hat{\eta} > \eta\} = \frac{1}{2\sqrt{\frac{\pi E_b N_w (1 - C_1 \frac{K-1}{N})^2}{2N_s}}} \left(\frac{N_w + |\delta|}{|\delta|(N_w - |\delta|)} \right)^{1/2} \exp\left(-\frac{E_b N_w (1 - C_1 \frac{K-1}{N})^2}{2N_s} \left(\frac{N_w - |\delta|}{2} \right) \right). \tag{E.8}$$

according to Equation (6.100), N_s corresponds to:

$$\begin{aligned} N_s &= \frac{1}{2} N_w \left[N_w E_b C_1^2 \left(\frac{2(K-1)}{N^2} \right) + E_b (1 - C_1)^2 \frac{K-1}{N} + E_b C_1^2 (K-1)(K-2) \frac{1}{N^2} \right. \\ &\quad \left. + N_o \left(1 - 2C_1 \frac{K-1}{N} + C_1^2 \frac{K-1}{N} \right) \right]. \end{aligned} \tag{E.9}$$

Substituting this expression into Equation(E.8) one obtains:

$$\begin{aligned} Pr\{\hat{\eta} > \eta\} &= \frac{\left(\frac{N_w + |\delta|}{|\delta|(N_w - |\delta|)} \right)^{1/2}}{2\sqrt{\frac{\pi E_b (1 - C_1 \frac{K-1}{N})^2}{E_b \left(N_w C_1^2 \left(\frac{2(K-1)}{N^2} \right) + (1 - C_1)^2 \frac{K-1}{N} + C_1^2 (K-1)(K-2) \frac{1}{N^2} \right) + N_o \left(1 - 2C_1 \frac{K-1}{N} + C_1^2 \frac{K-1}{N} \right)}}} \\ &\quad \times \exp\left(-\frac{E_b (1 - C_1 \frac{K-1}{N})^2}{E_b \left(N_w C_1^2 \left(\frac{2(K-1)}{N^2} \right) + (1 - C_1)^2 \frac{K-1}{N} \right) + N_o \left(1 - 2C_1 \frac{K-1}{N} + C_1^2 \frac{K-1}{N} \right)} \left(\frac{N_w - |\delta|}{2} \right) \right). \end{aligned} \tag{E.10}$$

Recall that this expression only holds for large values of the arguments of the underlying Marcum-Q function and thus places restrictions on the values of certain parameters such as the number of users,

observation length and processing gain. Multi-symbol differential reception with no interference cancellation corresponds to a special case of this expression with $C_1 = 0$. In this case Equation (E.10) becomes a generalization of Equation (36) in [99] for the multiuser scenario:

$$Pr\{\hat{\eta} > \eta\} = \frac{1}{2\sqrt{\frac{\pi E_b}{(E_b\frac{K-1}{N}+N_o)}}}\left(\frac{N_w+|\delta|}{|\delta|(N_w-|\delta|)}\right)^{1/2}\exp\left(-\frac{E_b}{E_b\frac{K-1}{N}+N_o}\left(\frac{N_w-|\delta|}{2}\right)\right).$$

The complete interference cancellation case corresponds to $C_1 = 1$. In this particular case, the pairwise probability of error corresponds to:

$$\begin{aligned} Pr\{\hat{\eta} > \eta\} = & \frac{1}{2\sqrt{\frac{\pi E_b(1-\frac{K-1}{N})^2}{E_b\frac{(K-1)(K-2+2N_w)}{N^2}+N_o\left(1-\frac{K-1}{N}\right)}}}\left(\frac{N_w+|\delta|}{|\delta|(N_w-|\delta|)}\right)^{1/2} \\ & \times\exp\left(-\frac{E_b(1-\frac{K-1}{N})^2}{E_b\frac{(K-1)(K-2+2N_w)}{N^2}+N_o\left(1-\frac{K-1}{N}\right)}\left(\frac{N_w-|\delta|}{2}\right)\right). \end{aligned} \quad \text{(E.11)}$$

Bibliography

[1] S. Verdu. Minimum probability of error for asynchronous gaussian multiple access channels. *IEEE Trans. Inform. Theory*, IT-32(1):85–96, January 1986.

[2] A.J. Viterbi. *CDMA- Principles of Spread Spectrum Communication*. Addison-Wesley, 1995.

[3] W.C.Y Lee. *Mobile Communications Engineering*. Mc Graw Hill, 2nd edition, 1997.

[4] D. J. Goodman. *Wireless Personal Communications Systems*. Addison-Wesley, 1997.

[5] A. J. GoldSmith. Multiuser capacity of cellular time-varying channels. In *Asilomar Conference on Signals, Systems and Computers*, pages 83–88, 1994.

[6] P. Agashe and B.D. Woerner. Analysis of interference cancellation for a multicellular CDMA environment. *IEEE International Symposium on Personal, Indoors and Mobile Radio Communications*, pages 747–752, 1995.

[7] H. V. Poor and G. W. Wornell, editors. *Wireless Communications - Signal Processing perspectives*. Prentice Hall, 1998.

[8] M. K. Simon, J. K. Omura, R. A. Scholtz, and B. K. Levitt. *Spread Spectrum Communications Handbook*. McGraw Hill, 1994.

[9] R.M. Buehrer, N.S Correal, and B.D. Woerner. A comparison of multiuser receivers for cellualr CDMA. *Proc., IEEE GLOBECOM*, pages 1571–1577, November 1996.

[10] W. Van Etten. An optimum linear receiver for multiple channel digital transmission systems. *IEEE Trans. Commun.*, 23(8):828–834, August 1975.

[11] G. D. Forney. Maximum-likelihood sequence estimation of digital sequences in the presence of intersymbol interference. *IEEE Trans. Inform. Theory*, IT-18:363–378, May 1972.

[12] G. Ungerboek. Adaptive maximum-likelihood receiver for carrier-modulated data-transmission systems. *IEEE Trans. Commun.*, COM-22:624–636, 1974.

[13] W. Van Etten. Maximun likelihood receiver for multiple channel transmission systems. *IEEE Transactions on Communications*, COM-24(2):276–283, February 1976.

[14] K.S. Schneider. Optimum detection of code division multiplexed signals. *IEEE Transactions on Aerospace and Electronic Systems*, AES-15(1), January 1979.

[15] S. Verdu. *Multiuser Detection.* Cambridge Press, 1998.

[16] R. Lupas and S. Verdu. Linear multiuser detectors for synchronous Code-Division Multiple-Access channels. *IEEE Transactions on Information Theory*, 35(1):123–136, Janaury 1989.

[17] Z. Xie, C.K. Rushforth, and R.T. Short. Multiuser signal detection using sequential decoding. *IEEE Transactions on Communications*, 38(5):578–583, May 1990.

[18] S. L. Miller. Training analysis of adaptive interference suppression for direct sequence code-division multiple access. *IEEE Trans. Commun.*, 44(4):488–495, April 1996.

[19] S. Haykin. *Adaptive Filter Theory.* Prentice Hall, 1996.

[20] M.L. Honig, U. Madhow, and S. Verdu. Blind adaptive multiuser detection. *IEEE Transactions on Information Theory*, 41(4):944–960, July 1995.

[21] A.J. Viterbi. Very low rate convolutional codes for maximum theoretical performance of Spread-Spectrum Multiple-Access channels. *IEEE Journal on Selected Areas in Communications*, 8(4):641–649, May 1990.

[22] P. Patel and J. Holtzman. Analysis of a simple successive interference cancellation scheme in a DS/CDMA system. *IEEE J. Select. Areas Commun.*, 12(5):796–807, June 1994.

[23] A. DuelHallen. On suboptimal detection for aysnchronous Code-Division Multiple-Access channels. In *Proceedings of the 26th Annual Conference on Information Sciences and Systems*, pages 838–843, March 1992.

[24] A. Duel-Hallen. Decorrelating decision-feedback multiuser detector for synchronous Code-Division Multiple-Access channel. *IEEE Transactions on Communications*, 41(2):285–290, February 1993.

[25] M. K. Varanasi and B. Aazhang. Multistage detection in asynchronous Code-Division Multiple Access communications. *IEEE Trans. Commun.*, 38(4):509–519, April 1990.

[26] R. Kohno, H. Imai, M. Hatori, and S. Pasupathy. An adaptive canceller of cochannel interference for spread-spectrum multiple-access communication networks in a power line. *IEEE Journal on Selected Areas in Communications*, 8(4):691–699, May 1990.

[27] S. Striglis, A. Kaul, N. Yang, and B. D. Woerner. A multistage RAKE receiver for improved capacity of CDMA systems. In *IEEE Vehicular Technology Conference*, pages 789–793, June 1994.

[28] D. Divsalar and M. Simon. Improved CDMA performance using parallel interference cancellation. Technical Report 95-21, JPL, October 1995.

[29] Neiyer S. Correal, R. Michael Buehrer, and Brian D. Woerner. Improved CDMA performance through bias reduction for parallel interference cancellation. In *IEEE International Symposium on Personal, Indoors and Mobile Radio Communications*, pages 565–569, 1997.

[30] D. Divsalar, M.K. Simon, and D. Raphaeli. Improved parallel interference cancellation for CDMA. *IEEE Trans. Commun.*, 46(2):258–268, February 1998.

[31] C. Boulanger and L. Ouvry. Multistage linear DS-CDMA receivers. In *Proc., IEEE Int. Symp. on Spread Spectrum Techniques and Applications*, 1998.

[32] K.S. Gilhousen and et. al. On the capacity of a CDMA system. *IEEE Transactions on Vehicular Technology*, 40(2):303–312, May 1991.

[33] R. Kohno, M. Hatori, and H. Imai. Cancellation techniques of co-channel interference in asynchronous spread spectrum multiple access systems. *Electronics and Commuincations in Japan*, 66-A(5):20–29, 1983.

[34] M. J. Juntti, B. Aazhang, and J. O. Lilleberg. Iterative implementation of linear multiuser detection for dynamic asynchronous CDMA systems. *IEEE Trans. Commun.*, 46(4):503–508, April 1998.

[35] S. Verdu. Adaptive multiuser detection. In *IEEE International Symposium on Spread Spectrum Techniques and Applications*, pages 43–50, July 1994.

[36] P. Patel and J.M. Holtzman. Analysis of a DS-CDMA successive interference cancellation scheme using correlations. *IEEE Global Telecommunications Conference*, pages 76–80, June 1993.

[37] Wang Zhaocheng, Ge Ning, Yao Yan, and Qiang Wang. A reduced state Viterbi algorithm for multiuser detection in DS/CDMA systems. In *ICCT International Conference on Communication Technology*, volume 2, pages 1102–1105, 1996.

[38] B. Aazhang, B.P. Paris, and G.C. Orsak. Neural networks for multiuser detection in Code-Division Multiple-Access communications. *IEEE Transactions on Communications*, 40(7):1212–1222, July 1992.

[39] U. Mitra and H.V. Poor. Neural network techniques for adaptive multiuser demodulation. *IEEE Journal on Selected Areas in Communications*, 12(9):1460–1470, December 1994.

[40] R. B. Ward and K. P. Yiu. Acquisition of pseudonoise signals by recursion-aided sequential estimation. *IEEE Trans. Commun.*, CT-13:475–483, December 1995.

[41] R. B. Ward. Acquisition of pseudonoise signals by sequential estimation. *IEEE Trans. Commun.*, COM-25:784–794, August 1977.

[42] K. K. Chawla and D. V. Sawrwate. Parallel acquisition of PN sequences in DS/SS systems. *IEEE Trans. Commun.*, 42(5):2155–2164, May 1994.

[43] M. Srinivasan and D. V. Sawrwate. Simple schemes for parallel acquisition of spreading sequences in DS/SS systems. *IEEE Trans. Commun.*, 45(3):593–598, August 1996.

[44] R. R. Rick and L. B. Milstein. Parallel acquisition in mobile DS-CDMA systems. *IEEE Trans. Commun.*, 45(11):1466–1476, November 1997.

[45] A. Polydoros and C. Weber. A unified approach to serial search spread spectrum code acquisition: Part II. a matched filter receiver. *IEEE Trans. Commun.*, COM-32(5):550–560, May 1984.

[46] M. K. Simon. Noncoherent pseudonoise code tracking performance of spread spectrum receivers. *IEEE Trans. Commun.*, COM-25(3):327–345, March 1997.

[47] R. C. Dixon. *Spread Spectrum Systems*. John Wiley & Sons, 1984.

[48] R. L. Peterson, R. E. Ziemer, and D. E. Borth. *Introduction to Spread-Spectrum Communications*. Prentice-Hall, 1995.

[49] Z. L. Shi, P. F. Driessen, and W. Du. PN code acquisition in spread spectrum packet radio communications. *Proceedings IEEE Pacific Rim Conference*, pages 778–781, 1993.

[50] Z. L. Shi and P. F. Driessen. Automatic threshold control for acquisition in spread spectrum packet radio communication. In *Proc., IEEE Int. Conf. on Commun.*, May 1993.

[51] M. Latva-aho and J. Lilleberg. Parallel interference cancellation in multiuser CDMA channel estimation. *Wireless Personal Communications*, Kluwer Academic Press. In Press., 1998.

[52] R.A. Cameron. *Fixed Point Implementation of a Multistage Receiver*. PhD thesis, Virginia Polytechnic Institute and State University, 1997.

[53] P. S. Kumar and J. M. Holtzman. Power control for a spread spectrum system with multiuser receivers. In *Proc., IEEE PIMRC*, pages 155–159, 1995.

[54] S. D. Gray, M. Kocic, and D. Brady. Multiuser detection in mismatched multiple-access channels. *IEEE Trans. Commun.*, 43(12):3080–3089, December 1995.

[55] E. G. Strom, S. Parkvall, S. L. Miller, and B. E. Otterson. The impact of timing errors on the performance of linear DS-CDMA receivers. *IEEE J. Select. Areas Commun.*, 14(8):1660–1668, October 1996.

[56] F. Heeswyk, D. D. Falconer, and A. U. Sheikh. A delay independent decorrelating detector for quasi-synchronous CDMA. *IEEE Journal on Selected areas in Communications*, 14:1619–1626, October 1996.

[57] F. Cheng and J. M. Holtzman. Effect of tracking error on DS/CDMA successive interference cancellation. In *Proc., IEEE GLOBECOM, Communication Theory Mini-Conference*, pages 166–170, 1994.

[58] R. M. Buehrer, A. Kaul, S. Striglis, and B. D. Woerner. Analysis of DS-CDMA parallel interference cancellation with phase and timing errors. *IEEE J. Select. Areas Commun.*, 14(8):1522–1535, October 1996.

[59] R. M. Buehrer. *The Application of Multiuser Detection to Cellular CDMA*. PhD thesis, Virginia Polytechnic Institute and State University, 1996.

[60] Y. Miki, H. Andoh, and M. Sawahashi. Coherent interference canceller system with pilot symbol-aided data estimation for forward-link and reverse link channels of DS-CDMA. *Proceedings Wireless 95*, 1995.

[61] M.K. Varanasi. Noncoherent detection in asynchronous multiuser channels. *IEEE Trans. Inform. Theory*, 39(1):157–176, January 1993.

[62] Z. Zvonar and D. Brady. Coherent and differentially coherent multiuser detectors for asynchronous CDMA frequency-selective fading channels. In *Proc., IEEE MILCOM*, pages 442–446, 1992.

[63] EIA/TIA. *Wideband Spread Spectrum Digital Cellular System Dual-Mode Mobile Station-Base Station Compatibility Standard*. TIA, April 1992.

[64] S. Verdu. *Optimum Multi-user Signal Detection*. PhD thesis, Univ. Illinois, Urbana-Champaign, 1984.

[65] Z. Xie, C.K. Rushforth, R.T. Short, and T.K.Moon. Joint signal detection and parameter estimation in multiuser communications. *IEEE Trans. Commun.*, 41(7):1208–1215, August 1993.

[66] T.K. Moon, Z. Xie, C.K. Rushfort, and R.T.Short. Parameter estimation in a multiuser communication system. *IEEE Trans. Commun.*, 42(8):2553–2560, August 1994.

[67] Y. Steinberg and H. V. Poor. Sequential amplitude estimation in multiuser communications. *IEEE Trans. Inform. Theory*, 40(1):11–20, January 1994.

[68] F. Mazzenga and F. Vatalaro. Parameter estimation in CDMA multiuser detection using cyclostationary statistics. *Electronics Letters*, 32(2):179–181, February 1996.

[69] T. J. Lim and L. K. Rasmussen. Adaptive symbol and parameter estimation in asynchronous multiuser CDMA detectors. *IEEE Trans. Commun.*, 45(2):213–220, February 1997.

[70] U. Fawer and B. Aazhang. A multiuser receiver for code division multiple access communications over multipath channels. *IEEE Trans. Commun.*, 43(2), 1995.

[71] B. P. Paris. Finite precision decorrelating receivers for multiuser CDMA communication systems. *IEEE Trans. Commun.*, 44(4):496–507, April 1996.

[72] K. Yasukawa and L. B. Milstein. Finite word length effects on the performance of the MMSE receiver for DS-CDMA systems. In *Proc., IEEE PIMRC*, pages 724–728, 1997.

[73] C. Chien, P. Duncan, and E. Cohen. A CAD approach to the performance evaluation and IC implementation of communication systems. *Proceedings of the 1995 DSPX Technical Program*, pages 648–659, 1995.

[74] A. Kaul and B.D. Woerner. An analysis of adaptive multistage interference cancellation for CDMA. *Proc., IEEE Veh. Tech. Conf.*, pages 82–26, 1994.

[75] P. G. Renucci and B.D. Woerner. Optimization of soft cancellation for DS-CDMA. *IEE Electronics Letters*, 34(8):731–733, April 1998.

[76] R. M. Buehrer and B.D. Woerner. Analysis of adaptive multistage interference cancellation for CDMA using an improved gaussian approaximation. *IEEE Trans. Commun.*, 44(10):1308–1320, October 1996.

[77] J.S. Lehnert and M.B. Pursley. Error probabilities for binary direct-sequence spread-spectrum communications with random sequences. *IEEE Trans. Commun.*, 37(10):1052–1061, October 1989.

[78] R.K. Morrow and J. S. Lehnert. Bit-to-bit error dependence in slotted DS/SSMA packet systems with random signature sequences. *IEEE Trans. Commun.*, 37(10):1052–1061, October 89.

[79] M. B. Pursley. Performance evaluation for phase-coded spread-spectrum multiple-access communication - part i: System analysis. *IEEE Trans. Commun.*, COM-25(8):795–799, August 1977.

[80] S. Moshavi. Multi-user detection for DS-CDMA communications. *IEEE Commun. Magazine*, pages 124–136, October 1996.

[81] T.S. Rappaport, S.Y. Seidel, and R. Singh. 900-mhz multipath propagation measurements for U.S. digital cellular radiotelephone. *IEEE Trans. Veh. Tech.*, 39(2):132–139, February 1990.

[82] D.F. Breslin. Adaptive antenna arrays applied to position location. Master's thesis, Virginia Polytechnic Institute and State University, August 1997.

[83] B.M. Leiner, R.J. Ruth, and A.R. Sastry. Goals and challenges of the DARPA GloMo program. *IEEE Personal Commun.*, 3(6):34–43, December 1996.

[84] A. Duel-Hallen, J. Holtzman, and Z. Zvonar. Multiuser detection for CDMA systems. *IEEE Personal Commun.*, 2(2):46–58, April 1995.

[85] P. Lapsley, J. Bier, S. Shoham, and E.A. Lee. *DSP Processor Fundamentals: Architectures and Features*. IEEE Press, 1995.

[86] R. Baines. The DSP bottleneck. *IEEE Commun. Magazine*, 33(5):46–54, May 1995.

[87] R. Kerr. CDMA digital cellular, an ASIC overview. *Applied Microwave and Wireless*, pages 30–41, October 1993.

[88] J.A. Wepman. Analog and digital converters and their applications in radio receivers. *IEEE Commun. Magazine*, 33(5):39–54, May 1995.

[89] M.E. Frerking. *Digital Signal Processing in Communication Systems*. Chapman and Hall, New York, 1994.

[90] C. Olmstead and M. Petrowski. Digital IF processing. *RF Design*, pages 34–40, September 1994.

[91] R.Cameron and B.D. Woerner. Synchronization of CDMA systems employing interference cancellation. *Proc., IEEE Veh. Tech. Conf.*, pages 178–182, 1996.

[92] S.F. Swanchara. An FPGA-based multiuser receiver employing parallel interference cancellation. Master's thesis, Virginia Polytechnic Institute and State University, July 1998.

[93] K.I. Pedersen, T.E. Kolding, I. Seskar, and J.M. Holtzman. Practical implementation of successive interference cancellation in DS/CDMA systems. *Proc., IEEE Int. Conf. on Universal Personal Commun.*, pages 321–325, 1996.

[94] J. R. Lequepeys, N. Danielle, D. Lattard, B. Piaget, D. Varreau, L. Ouvry, and C. Boulanger. CESSIUM: a single component for implementing high data rates DSSS/CDMA interference cancellation receivers. In *Proc., IEEE Int. Symp. on Spread Spectrum Techniques and Applications*, 1998.

[95] D. Dalhaus, R. Heddergott, and M. Pesce. A concept of a two-user CDMA hardware demonstrator for wireless outdoor communications. *Proc. of the ACTS Mobile Communication Summit*, October 1997.

[96] H. Kaufmann, R. Kung, and U. Fawer. Digital spread-spectrum multipath diversity receiver for indoor communications. In *Proc., IEEE Veh. Tech. Conf.*, pages 1038–1041, 1992.

[97] S. Kubota, S. Kato, and K. Feher. Inter-channel interference cancellation technique for CDMA mobile/personal communication systems. In *Proc., IEEE PIMRC*, pages 112–117, 1992.

[98] J. Huang. Study of a feed-backward CDMA interference cancellation receiver to combat the near-far problem. In *Proc., Virginia Tech Symp. on Wireless Personal Commun.*, pages 9.1–9.11, June 1997.

[99] D. Divsalar and M. K. Simon. Multiple symbol differential detection of mpsk. *IEEE Trans. Commun.*, 38(3):300–308, March 1990.

[100] D. Makrakis and K. Feher. Optimal noncoherent detection of PSK signals. *Electronics Letters*, 26(6):398–400, March 1990.

[101] S. Stein. Unified analysis of certain coherent and non-coherent binary communication systems. *IEEE Trans. Inform. Theory*, pages 43–51, January 1964.

[102] M. K. Simon and M-S. Alouini. A unified approach to the performance analyisis of digital communications overgeneralized fading channels. *Proc. IEEE*, 86(9):1860–1877, September 1998.

[103] G.D. Forney Jr. The Viterbi algorithm. *Proc. IEEE*, 61(3):268–278, March 1973.

[104] F. Adachi and M. Sawahashi. Viterbi-decoding differential detection of DPSK. *Electronics Letters*, 28(23):2196–2198, November 1992.

[105] B. Sklar. Rayleigh fading channels in mobile digital communication systems, Part II: Mitigation. *IEEE Commun. Magazine*, 35(9):148–155, September 1997.

[106] P. Jung and J. Blanz. Joint detection with coherent receiver antenna diversity in CDMA mobile radio systems. *IEEE Trans. Veh. Tech.*, 44(1):76–88, February 1995.

[107] Z. Zvonar. Combined multiuser detection and diversity reception for wireless CDMA systems. *IEEE Trans. Veh. Tech.*, 45(1):205–211, February 1996.

[108] W. L. Stutzman. *Polarization in Electromagnetic Systems*. Artech House, 1993.

[109] A. M. D. Turkmani, A. A. Arowojolu, P. A. Jefford, and C.J. Kellett. An experimental evaluation of the performance of two-branch space and polarization diversity schemes at 1800 MHz. *IEEE Trans. Veh. Tech.*, 44(2):318–326, May 1995.

[110] S. Kozono, T. Tsuruhara, and M. Sakamoto. Base station polarization diversity reception for mobile radio. *IEEE Trans. Veh. Tech.*, VT-33(4):301–306, November 1984.

[111] W .C. Y. Lee and Y. S. Yeh. Polarization diversity systems for mobile radio. *IEEE Trans. Commun.*, COM-20(5):912–923, October 1972.

[112] J. M. Holtzman and L. M. Jalloul. Rayleigh fading effect reduction with wideband DS/CDMA signals. *IEEE Trans. Commun.*, 42(2):1012–1017, February 1994.

[113] Rappaport T.S. Characterization of UHF multipath radio channels in factory buildings. *IEEE Transaction on Antennas and Propagation*, 37(8):1058–1069, August 1989.

[114] T.B.Sorensen, A.O. Nielsen, P.E. Morgensen, M. Tolstrup, and K Steffensen. Performance of two-branch polarizarion antenna diversity in operational GSM network. In *Proc., IEEE Veh. Tech. Conf.*, pages 741–743, 1998.

[115] R.M. Buehrer and B.D. Woerner. The asymptotic multiuser efficiency of m-stage interference cancellation receivers. In *IEEE International Symposium on Personal, Indoors and Mobile Radio Communications*, pages 570–574, 1997.

Vita

Neiyer S. Correal was born in Bogota, Colombia on November 26, 1968. He received the B.S. degree in Electronics Engineering from the Pontifical Javeriana University, Colombia in 1992, and the M.S. degree in Electrical Engineering from Old Dominion University, VA in 1994, where he was involved with real-time automatic speech recognition at the Speech Communications and Signal Processing Laboratory.

In 1995, he joined the Mobile and Portable Radio Research Group (MPRG) at Virginia Polytechnic Institute and State University (Virginia Tech), where he pursued his Doctoral degree. His research interests include spread spectrum communications, multiuser detection, real-time signal processing and implementation of advanced digital radio transceivers. Mr. Correal is a member of Eta Kappa Nu and Tau Beta Pi.